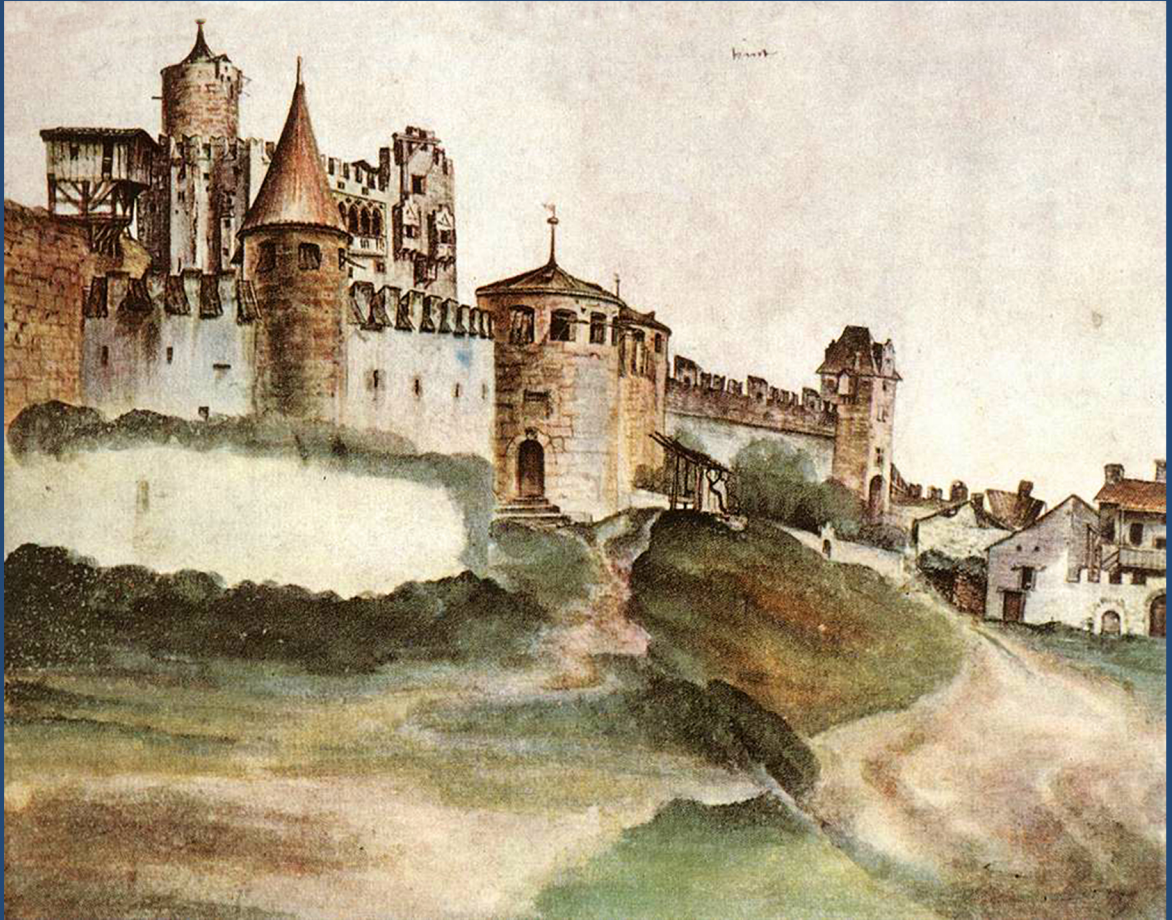# INFN ISTITUTO NAZIONALE DI FISICA NUCLEARE
Laboratori Nazionali di Frascati
FRASCATI PHYSICS SERIES

LFC19: Strong Dynamics for Physics within and beyond the Standard Model at LHC and Future Colliders

ECT*, Trento, Italy, September 9-13, 2019

Editors:

Gennaro Corcella, Stefania De Curtis, Stefano Moretti,

Giulia Pancheri, Roberto Tenchini, Marcel Vos

FRASCATI PHYSICS SERIES

Series Editor
　　Paola Gianotti

Technical Editor
　　Lia Sabatini

Cover by Claudio Federici

_____

Volume LXX

_____

LFC19

**Strong Dynamics for Physics within and beyond the
Standard Model at LHC and Future Colliders**

September 2019

PREFACE

The workshop 'LFC19: Strong dynamics for physics within and beyond the Standard Model at LHC and Future Colliders' took place at the European Center for Theoretical Physics (ECT*), Villazzano (TN), Italy, on September 9-13, 2019. It was the ninth edition of a series of meetings which were first organized to discuss the physics case of electron-positron Linear Colliders and lately became regular forums gathering theorists and experimentalists, with a relevant fraction of graduate students and untenured researchers, active on the physics of future accelerators. Such workshops were held at ECT* in 2011, 2013, 2015 and 2017, whereas the previous editions were in Florence (2007), Perugia (2009) and twice in the INFN Frascati National Laboratories (2008 and 2010).

The general structure of the workshop is well consolidated: general talks on physics and detectors of future facilities were scheduled on the first and last day, while the other days featured topical sessions on perturbative and non-perturbative Quantum Chromodynamics, top-quark phenomenology, electroweak symmetry breaking and physics Beyond the Standard Model (BSM). In particular, through all the sessions, much focus was on the role of strong interactions, within and beyond the Standard Model, in both perturbative and non-perturbative regimes.

The opening general talks featured a presentation on the European Stategy for Particle Physics, whose further update is expected later in 2020, as well as talks on the perspectives of the High-Luminosity LHC, the circular colliders FCC-hh, FCC-ee and CEPC, and the linear ones such as CLIC and ILC. Concerning the leptonic colliders, the prospects for a muon collider were explored and the challenges in Higgs, top and BSM phenomenology reviewed. Given the workshop emphasis on QCD and strongly-interacting physics, overview talks on QCD measurements at LHC and opportunities at future machines were scheduled as well. Furthermore, we had presentations reviewing the state of the art and the perspectives for the fits of the Standard Model parameters, on flavour physics from present to future colliders, on the connection between observations at low (GeV scales) and high (TeV scales) energies.

The perturbative QCD session featured reviews of hard QCD results at LHC and parton distributions, with a talk devoted to transverse-momentum parton densities. Furthermore, we discussed improvements in the implementation of parton-shower simulations, higher-order corrections to the Higgs

transverse-momentum spectrum, multi-parton scattering and even heavy ions, with some emphasis on heavy-flavour production in nuclear collisions. Moreover, the LHCb Collaboration presented measurements on spectroscopy and exotic hadrons, while, still for the purpose of low-energy QCD, we had presentations on perturbative aspects of soft QCD dynamics and AdS/CFT correspondence and its application to thermalization.

The top-quark session was indeed pretty lively, as it featured first an experimental overview of the main top-related results at LHC, on behalf of ATLAS and CMS Collaborations, and then higher-order calculations, including both QCD and electroweak corrections, and recent studies on the role played by infrared renormalons in top-mass observables and on the top-quark Yukawa coupling at future e^+e^- accelerators.

The session on physics beyond the Standard Model included a number of interesting talks discussing several scenarios of New Physics. In detail, we listened to presentations on hidden sectors, exotic top-quark partners, vector-like quarks, heavy composite resonances, composite Higgs models, composite and strongly-interacting Dark Matter, supervised learning and novelty detection, non-perturbative mechanisms to give mass to fermions and weak bosons, Minimal Supersymmetric Standard Model (MSSM) and the current bounds in the MSSM parameter space.

A good fraction of the contributions to the LFC19 workshop are included in these proceedings, which could hence be a useful collection, especially for young researchers willing to undertake exploration onthe physics of future colliders. More details and the slides of the talks can be found at:

https://www.ectstar.eu/node/4448;

https://indico.ectstar.eu/event/55/.

Committees

Organizers:

Gennaro Corcella, INFN LNF (chair)
Stefania De Curtis, INFN Florence
Stefano Moretti, University of Sounthampton
Giulia Pancheri INFN LNF
Roberto Tenchini, INFN Pisa
Marcel Vos, IFIC & CSIC & University of Valencia

Conveners:

Aldo Deandrea, University of Lyon & CNRS/IN2P3 (Electroweak Symmetry Breaking)
Giancarlo Ferrera, University of Milan & INFN Milan (Perturbative QCD)
Roberto Franceschini, University of Rome 3 & INFN Rome 3 (Beyond the Standard Model)
Francesco Tramontano, University of Naples & INFN Naples (Top Quark Physics)

CONTENTS

PHYSICS AT THE HIGH-LUMINOSITY LHC

Andreas B. Meyer
DESY, Notkestr. 85, Hamburg, Germany

Abstract

The High-Luminosity LHC (HL-LHC) is scheduled to start operation in 2027. By the end of the 2030s it is expected to deliver to upgraded LHC experiments a factor 20 more data than collected so far. To further refine the expectations of the physics potential of the HL-LHC, the Workshop on the Physics of the HL-LHC and Perspectives for the HE-LHC took place from October 2017 to December 2018. The whole LHC community, theorists and experimentalists, collaborated closely and produced detailed studies of HL-LHC measurements towards ultimate precision, and of searches for new phenomena. The updated experimental projections are generally based on recent publications of the LHC Run-2 data. The results are presented in a comprehensive document [1]. An executive summary of the report was also submitted to the European Particle Physics Strategy Group [2]. Here, a small selection of the projections of the physics at the HL-LHC is presented.

1 Introduction

For the HL-LHC, the ATLAS and CMS collaborations are preparing a major upgrade, with significantly improved detector resolutions, larger acceptance, enhanced triggering capabilities and increased recording rate. The tracking detectors cover an enhanced acceptance up to a pseudo-rapidity $|\eta| < 4$ and are complemented by extended or new muon systems and calorimeters, as well as novel precision timing detectors. Detector upgrades for the experiments LHCb and Alice are taking place during the current shutdown.

Two examples for the improved detector performance of ATLAS and CMS are shown in Fig. 1. Due to the improvements in tracking, the expected resolution for the reconstruction of the Higgs boson mass in the decay into two muons is significantly improved (Fig. 1a), leading to better signal significance
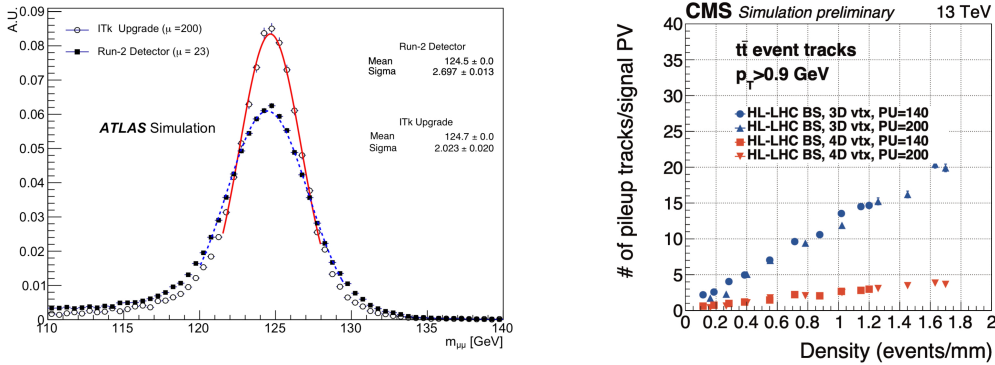
Figure 1: *a) Signal resolution for $H \to \mu\mu$ signal events. The Run-2 resolution is compared to that at the HL-LHC (from [3]), b) Rate of tracks from pileup vertices, incorrectly associated with the primary vertex of the hard interaction, normalized to the total number of tracks in the vertex (from [4]).*

and smaller statistical uncertainties for the measurement of the invariant mass. The high instantaneous luminosity at the HL-LHC, will produce up to 200 proton–proton collisions per bunch crossing (pile-up), and consequently very high densities of the collision vertices. The fraction of pile-up tracks associated with the primary vertex is expected to increase proportionally (Fig. 1b). With additional timing layers around the tracker volume, precision measurements of the track timing, with target resolution 30 ps, become possible. Including the time information as a fourth dimension the number of pile-up tracks associated to the primary vertex is substantially reduced, almost to the level of Run-2.

In addition to better detectors and large luminosity, significant improvements over current LHC results are also expected from the continuous refinement of analysis techniques and theory calculations. To determine the physics yield of the HL-LHC as precisely as possible, a main goal of the workshop was to produce projections of the uncertainties of the future measurements that are as realistic as possible. ATLAS and CMS agreed on the following common approach [5, 4]: statistical uncertainties are expected to scale as $1/\sqrt{L}$; theory uncertainties are assumed to be reduced by a factor of two; and Monte Carlo simulations are expected to give no uncertainty. For the experimental uncertainties, the statistical component of such systematics is naturally expected to scale with $1/\sqrt{L}$. In contrast, systematic components of the uncertainties may be hard, and ultimately impossible, to overcome. ATLAS and CMS estimated these 'floors' individually for each experimental input. Good general agreement was found.

The relevance on the assumptions for the evolution of the systematic uncertainties is illustrated in

Figure 2: *Expected significance of a search for 4-top production with CMS at HL-LHC. The expected significance of the 4-top signal over a background-only hypothesis in standard deviations is given for various HL-LHC systematic uncertainty scenarios (from [6]).*
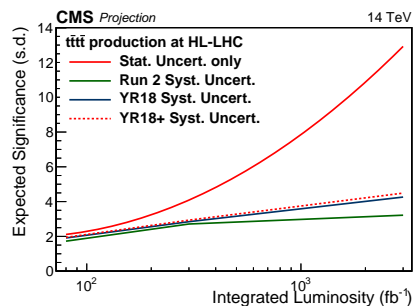
Fig. 2, using the example of the 4-top analysis. With current uncertainties, additional signal statistics would barely lead to further improvements. In contrast, if the total uncertainty was purely statistical, a measurement with very high significance would become possible. It is worth noting that, in many areas, the actual results from LHC Run-2 data proved to be significantly better than original expectations prior to Run-2. Beyond-design detector performance could be achieved, theory uncertainties could be constrained and refined analysis techniques were developed, e.g. using novel machine learning approaches. The coming two decades are likely to bring about further improvements beyond current projections.

2   Standard Model Physics

Due to much better detectors and refined analysis techniques, measurements of standard model (SM) processes are expected to improve significantly beyond the already precise results from the LHC. Such measurements are key to determining SM parameters, such as the masses of the top quark and the W boson, as well as the strong coupling constant α_s and the proton structure functions, just to name a few. In electroweak and QCD fits, rigorous consistency tests of the SM will be performed. Ultimately, the W boson mass is expected to be measured with an uncertainty as small as 5 MeV. For the measurement of the top quark mass, a precision of better than 200 MeV is expected. For a theoretically well-defined interpretation of such top quark mass measurements, theory developments are ongoing. At the HL-LHC, a precision of 1% is envisaged for the measurement of the integrated luminosity, a crucial input to cross section measurements, which are also used to determine the parton distribution functions. Due to the large statistics, jet cross sections can be measured up to transverse jet momenta of 4 TeV. In addition to SM physics at medium and high energy scales, better detectors will also open a new realm of forward physics as well as hadron spectroscopy.

3   Higgs Physics

Since the discovery of a scalar boson at 125 GeV in 2012, the precision determination of its properties is a primary target of the LHC and the HL-LHC. A guiding question is whether the boson is identical to the one expected in the SM or whether it carries signs of new physics. The Higgs program at the HL-LHC comprises measurements of the discovered particle in all accessible production and decay channels. In the κ-framework, scale factors quantifying the agreement of the measured Higgs Yukawa couplings with expectations are determined (assuming SM structure). In Fig. 3a) the expectations for the achievable precision are presented. In combination, the ATLAS and CMS measurements are expected to reach a precision as low as 1 to 1.5% for the most precise channels. Within the κ-framework, contributions from non-SM couplings can be constrained at the level of 2.5%.

Differential measurements are expected to achieve a precision that allows to constrain the couplings of the Higgs boson also from shape analysis. The direct measurement of the coupling to charm depends directly on the efficiency to disentangle charm quarks and b quarks in the experiments. Already now LHC experiments are exceeding original expectations by a large amount. In Fig. 3b) a summary of the expectations for the HL-LHC for the coupling to light quarks is presented.

Inclusive and differential measurements of vector boson scattering (VBS) processes involving triple and quartic gauge couplings, are going to probe the Higgs boson as virtual particle, providing insight into the Higgs mechanism. While electroweak multiboson production involving W, such as WW, WZ and WWW, are expected to be measured at uncertainties as low as 6%, the measurements of electroweak ZZ, WWZ and WZZ processes will be much less precise. However, better analysis techniques, e.g. for the
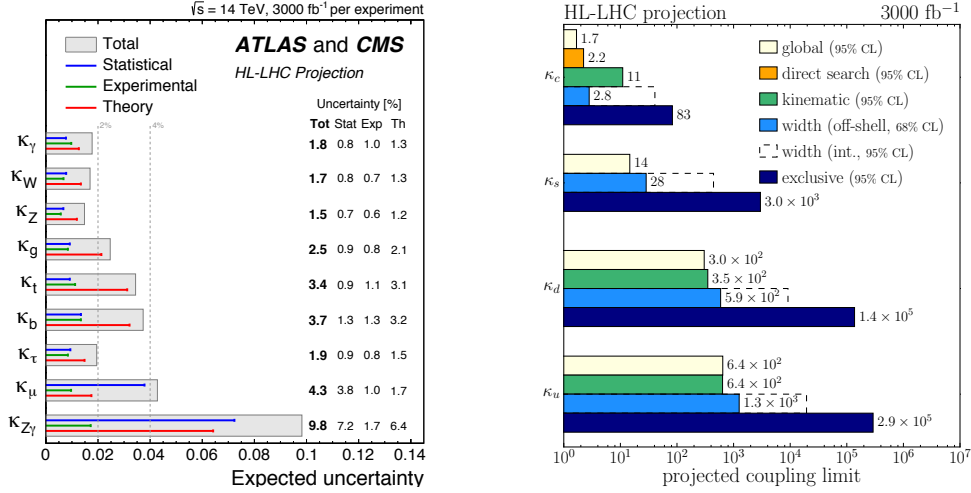
Figure 3: *a) Projected uncertainties on κ_i, combining ATLAS and CMS (from [2]), b) Summary of the projected HL-LHC limits on the quark Yukawa couplings (from [2]).*

reconstruction of forward jets, could possibly improve future measurements beyond current projections.

One important goal of Higgs physics is to measure the self-coupling of the Higgs as predicted in the SM. At the HL-LHC, about 120k events with two Higgs bosons (HH) will be produced per experiment. The HH cross section is driven by a negative interference between the Higgs self-coupling diagram and a diagram involving a top-quark box. Direct measurements of HH production have been performed using a combination of several final states. Best sensitivity is expected for events where one H decays into bb (large branching ratio) and the other one decays into a pair of photons (clear signature), as shown in Fig. 4a), or τ-leptons. Other final states have also been investigated [1]. Current projections indicate that CMS and ATLAS will be able to measure the cross section with a significance of 4 standard deviations. The expected likelihood profile of the self-coupling modifier κ_λ is shown in Fig. 4b).

4   Direct Searches

The potential of the HL-LHC to directly observe physics beyond the standard model has been studied for a large variety of scenarios. Only a very small selection of the studies can be presented here. Arguably the simplest approach is to look for high-mass resonances. In Fig. 5a) the upper limit is shown for a heavy vector boson Z', as predicted e.g. in the Sequential SM or the E_6 GUT model, decaying into a pair of leptons. At the HL-LHC, a Z' with a mass of about 6 TeV can be excluded. For this, as for many other resonance searches, the HL-LHC extends the reach in mass by typically 2 TeV w.r.t. current limits.

New physics could also occur in a dark sector of new particles, connected with standard model particles through a portal described by a kinetic mixing parameter ϵ. In Fig. 5b), a summary of searches for dark photons from Higgs decays is presented. If ϵ is very small, dark photons can be long-lived, with a lifetime between a few millimeters up to several meters.
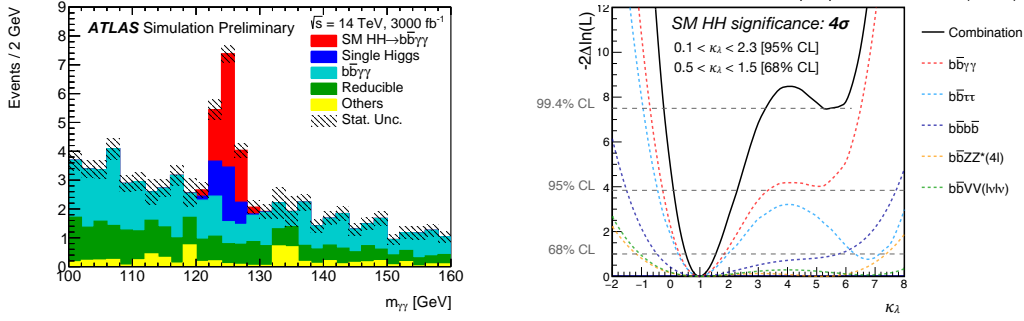
Figure 4: *a) Distribution of $m_{\gamma\gamma}$ following the BDT response cut (from [1]), b) Projected combined HL-LHC sensitivity to Higgs trilinear coupling from direct search channels (from [2]).*
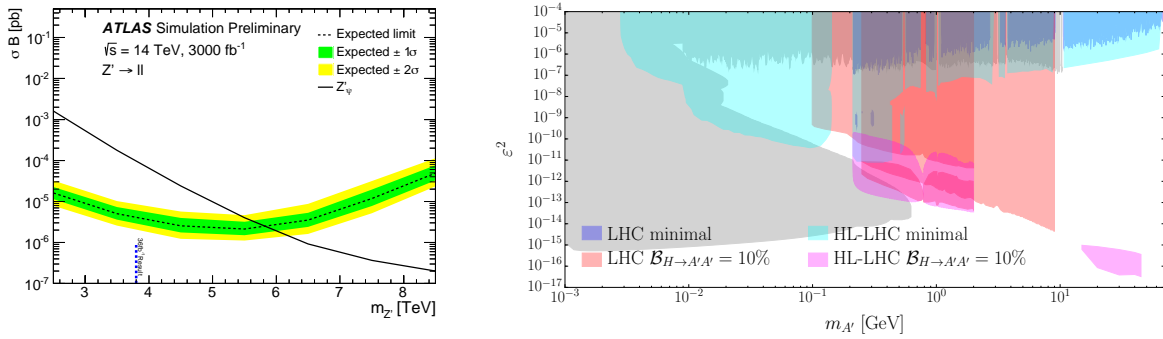
Figure 5: *a) Expected upper limit for a Z', and the prediction for a Z'_ψ in the E_6 model (from [2]), b) Projections for dark photons from Higgs decays, assuming a branching ratio of 10% (from [1]).*

Long-lived particles could also arise when phase space is small, e.g. in scenarios of mass-degenerate supersymmetric particles. While SUSY particles produced in strong interactions have largely been excluded up to masses of 1 TeV or above, the cross sections for supersymmetric particles produced via electro-weak processes are too small for current LHC data to have sensitivity. Scenarios involving electroweakinos with masses above about 500 GeV are still consistent with current data, and compatible with SUSY naturalness. In Fig. 6a), limits are shown for the search of pairs of higgsino-like electroweakinos.

The search for leptoquarks (LQ) involving 2nd or 3rd generation particles has recently received enhanced interest, as their existence is suggested in models addressing the tensions observed in B-factory data, often referred to as 'flavour anomalies'. It is expected that LHCb and Belle II experiments will clarify the situation in the next few years. ATLAS and CMS can also have an impact at low momenta, in final states with muons, and also exploiting new track trigger systems that are able to reconstruct tracks, vertices and invariant masses at first trigger level. If deviations from standard model expectations in low-momentum flavour physics persist at high significance, ATLAS and CMS provide complementarity at high mass scales, as they are able to discover, or exclude, exotic heavy particles, such as LQ. In Fig. 6b) upper limits on the LQ pair-production cross section at 95% CL as a function of the LQ mass and the branching fraction are shown for LQ decaying into a top quark and a muon or τ-lepton. With HL-LHC,
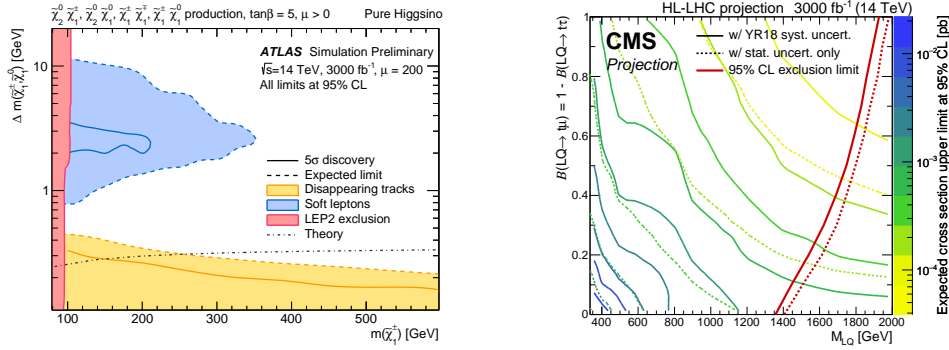
Figure 6: *a) Expected 95% CL exclusion / discovery reach from disappearing-track and low-momentum lepton pair searches in higgsino-like electroweakino models (from [1]), b) Expected upper limits on the LQ pair-production cross section at 95% CL as function of LQ mass and branching fraction (from [1]).*

the presence of such LQ can be excluded up to almost 2 TeV.

5 Conclusions

In conclusion, upgraded machine and detectors at the HL-LHC are expected to produce an excellent and diverse physics yield. With the expected statistics and precision, stringent tests will be performed of the Standard Model and of the properties of the Higgs boson. In searches for heavy resonances, the HL-LHC increases the reach in mass by typically 2 TeV w.r.t. current limits. With the greatly improved HL-LHC detectors, exotic signatures, e.g. of long-lived particles, can be studied in much more detail. Possible indirect discoveries in the flavour sector could turn out to be complementary to findings at high mass scales. Using collisions with heavy ions (HI), the LHC and the HL-LHC also pursue a comprehensive and rich program for the study of QCD in media, not covered in this report.

References

1. A. Dainese et al., "Physics of the HL-LHC, and perspectives at the HE-LHC", CERN Yellow Reports: Monographs Vol 7 (2019) doi:http://dx.doi.org/10.23731/CYRM-2019-007

2. A. Dainese et al,, "The physics potential of HL-LHC", Input to the European Particle Physics Strategy Update 2018-2020, https://indico.cern.ch/event/765096/contributions/3295995/

3. The ATLAS Collaboration, "Technical Design Report for the ATLAS Inner Tracker Strip Detector", ATLAS-TDR-025, https://cds.cern.ch/record/2257755

4. CMS Collaboration, "Expected performance of the physics objects with the upgraded CMS detector at the HL-LHC", Technical Report CMS-NOTE-2018-006, https://cds.cern.ch/record/2650976

5. ATLAS Collaboration, "Expected performance of the ATLAS detector at the High-Luminosity LHC", ATL-PHYS-PUB-2019-005, http://cds.cern.ch/record/2655304

6. CMS Collaboration, "Projections of sensitivities for 4-top production at HL-LHC and HE-LHC", CMS PAS-FTR-18-031, http://cds.cern.ch/record/2650211

FUTURE CIRCULAR e$^+$e$^-$ COLLIDERS

Franco Bedeschi

INFN - Sezione di Pisa, Largo B. Pontecorvo 3, I-56127 Pisa, Italy

Abstract

As the process to update of the European strategy for particle physics gets close to its conclusion, electron-positron Higgs factories are gathering more and more consensus as the the highest priority for the next global machine. In this paper we present the motivations and the physics program of the currently proposed circular e$^+$e$^-$ accelerators, FCC [1] and CEPC [2]. Comparisons with the performance of colliders based on linear accelerators, ILC [3] and CLIC [4], are also given for several key measurements.

1   Physics motivations

The discovery of the Higgs boson [5, 6] at the CERN LHC [7] accelerator in 2012 has been one of the greatest successes of HEP, confirming the last missing block of the Standard Model (SM) of particle physics. Additional work by the LHC experimental collaborations have proved that the Higgs boson properties match well those expected from the SM although with rather large uncertainties. Indeed the couplings of the Higgs to different fermions and vector bosons are currently measured with a precision ∼10% percent or larger [8, 9]. Projections to the final accuracy attainable after the completion of the High Luminosity LHC program [10], with 3000 fb^{-1} delivered to the experiments, indicate that a maximum precision in the order of a couple of percents is possible for the most favorable Higgs decay modes [11]. A significant part of this error is related to theory uncertainties, as a direct measurement of the Higgs total width is not possible at a hadron collider.

Intensive direct searches for new particles have also been made at the LHC testing a comprehensive variety of new physics models (BSM). These searches are presently excluding new particles up to mass scales in the order of 1 TeV or above in most cases. Projections with an integrated luminosity of 3000

fb^{-1} indicate the possibility to exclude mass scales up to 2-3 times higher, depending on the search target, by the end of the complete LHC program.

Indirect sensitivity to new physics processes is possible by studying deviations from the SM expectations, in particular the couplings of the Higgs boson to fermions and vector bosons. Furthermore the pattern of these deviations is strongly related to the specific model as shown in the examples of fig.1, taken from a study done for ILC [12]. The study of Higgs couplings at the future e$^+$e$^-$ colliders can
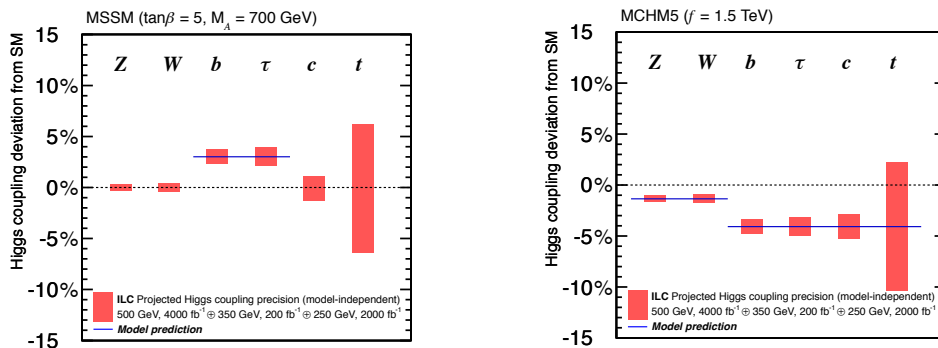
Figure 1: *(left) Pattern of deviations of Higgs couplings for a MSSM Supersymmetry model, (right) pattern for a composite Higgs model.*

thus explore new physics at mass scales at scales not reachable by direct searches at LHC and also points us to a potential explanation. The exploration of multi TeV mass scales however requires sub-per-cent resolutions on the couplings. This is a level of precision not possible at the LHC and indeed at any hadron collider unless a dedicated electron-positron collider provides a measurement of the Higgs total width or a reference branching ratio to avoid most of the theory error. There is by now a general consensus that at least one such machine should be built in the world.

Several e$^+$e$^-$ machines capable of a detailed study of the Higgs boson properties have been developed and studied. Their expected performance has been carefully analyzed to prepare for the update of the European strategy for particle physics, which is due to be completed in mid-2020. In the following sections we shall outline the main features of these machines with a primary focus on the circular colliders.

2   The e$^+$e$^-$ colliders

Linear electron-positron colliders have been considered for many years as a natural way to extend the center-of-mass energy for these types of collisions. Two main technologies have been developed to contain the cost and total power: superconducting or high frequency radio frequency (RF) cavities. The former is used for the proposed ILC collider [3, 13], while the latter for the proposed CLIC collider [4] with the addition of a novel strategy for generating the RF. The ILC is designed to cover the energy range 90 - 1000 TeV with a a staging plan [13] starting at 250 GeV and then upgrading first to 500 and then to 1000 GeV. In the case of CLIC the staging [14] would involve starting with 380 GeV and then upgrading first to 1500 and then to 3000 GeV.

The discovery of a Higgs boson with a mass of only 125 GeV/c^2 has revived the interest in circular electron-positron colliders. Indeed, as shown in fig.2, the highest cross section for associated ZH production peaks at 250 GeV, not too far from the maximum energy reached by the LEP accelerator [15]. If the decrease of luminosity with increasing energy is taken into account 240 GeV is the energy that provides

the highest rate of Higgs boson production. Two very similar proposals are currently being studied both
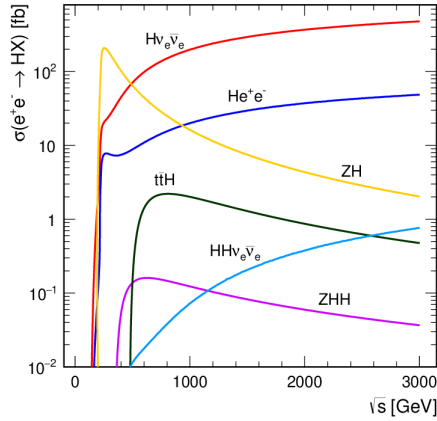
Figure 2: $e^+e^- \to H + X$ cross sections.

involving a 100 km circular tunnel: FCC-ee [1] at CERN and CEPC [2] in China. The CEPC version is assuming less sinchrotron radiation power from the beams, thus lowering the luminosity as well as the operation costs, and does not foresee at the moment running at 350 GeV. A comparison of the luminosity performance at each interaction point is shown in fig.3. Unlike linear colliders the circular colliders
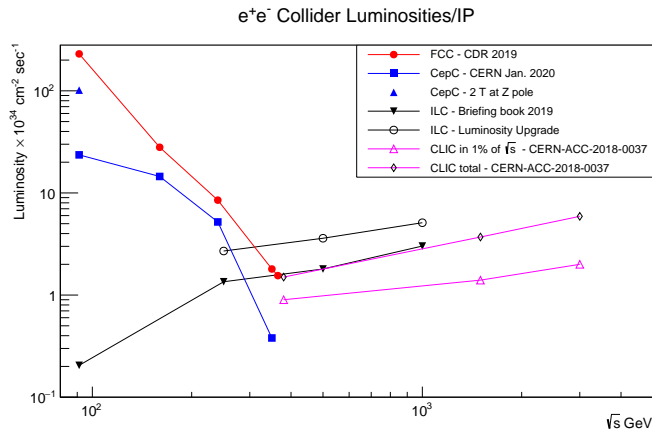
Figure 3: Comparison of linear and circular e^+e^- collider luminosities.

provide the option of having two or four interaction points increasing the combined collected luminosity accordingly. The figure shows clearly that circular colliders are superior to linear machines in the region 90 to 240 GeV, while above 350 GeV the linear colliders are more performant. The 100 km tunnel used by circular colliders can be "recycled" at later stage to house a proton-proton collider with center of mass energy in the 100 TeV scale once the needed magnet technology has been developed.

3 The FCC-ee physics program

The main motivation of FCC-ee is the detailed study of the Higgs boson, however the huge luminosity increase of these circular colliders relative to LEP at the Z pole ($\times 10^4$) and the WW pair production threshold ($\times 10^3$) makes them also a powerful tool to significantly improve the measurements of all electroweak observables and to complement the results of Belle2 [16] and LHCb after all upgrades [17] on heavy flavors. Direct searches for several new physics processes are also considered. Running in the range 350 - 365 GeV is foreseen to measure accurately the top quark properties.

3.1 Higgs

The goal is is to collect $\sim 10^6$ ZH events in about three years. Additional Higgs bosons are collected during the 350 GeV operation, including a component from vector boson fusion (VBF). The total ZH cross section can be measured by selecting events with a Z boson, measuring its momentum and then calculating the mass of everything that recoils against the Z using the constraint of the collision energy. An example of the recoil mass distribution that can be obtained experimentally is given in fig.4, where a clear Higgs boson peak can be observed even without any selection cuts. The coupling of the Higgs to the Z can be extracted from this cross section. The additional selection of Higgs boson decays to two Z's allows the measurement of the total Higgs boson width. Additional precision can be obtained including W fusion Higgs production from the runs at higher energy. In any case, once the total H cross sections are determined all Higgs branching ratios and couplings can be determined in a model independent way. The
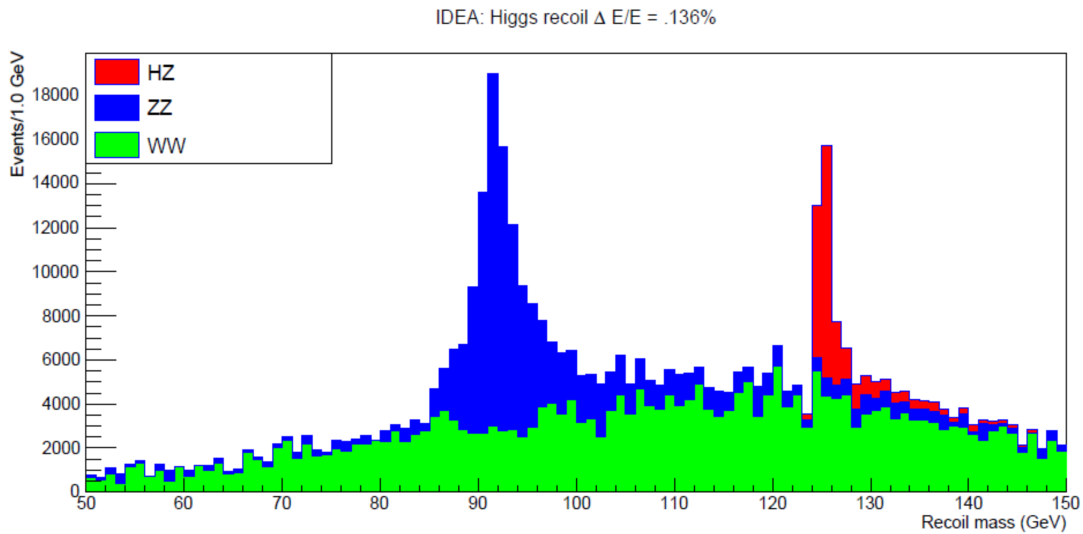
Figure 4: $Z \to \mu^+\mu^-$ recoil mass distribution assuming 0.136% center of mass energy spread with the IDEA detector concept [1] with 5 fb^{-1} of data. No selection cuts have been applied.

sensitivity on potential discrepancies between the SM predictions and measurements can be expressed in terms of the relative error on the Higgs couplings. A comparison of the precision attainable at circular and linear colliders is shown in table 1 as determined in [18]. These results are obtained with a fit based on an Effective Field Theory parameterization as described in the given reference. In this approach it's important to have improved precision on many electro-weak observables, precise measurements in

di-boson production and in the top EW sector. To achieve this one needs to operate at several center-of-mass energies (Z-pole, 240 GeV, above the ttbar threshold to do top and VBF Higgs production and break degeneracies in the fit).

Table 1: Precision on the Higgs boson couplings for the four low-energy Higgs factories (ILC, CLIC, CEPC, and FCC-ee). All numbers are in % and indicate 68% C.L. sensitivities. They include current projected parametric uncertainties, and are combined with the projected HL-LHC precision. Running times beyond initial configuration include upgrade period. Only the first two planned operation energies are shown.

Collider	HL-LHC	ILC		CLIC		CEPC	FCC-ee	
Energy (GeV)	14,000	250	500	380	1,500	240	240	365
Lumi (ab^{-1})	3	2	+4	1	+3	5.6	5	+1.7
Years		11.5	+10.5	8	+9	7	3	+6
g_{HZZ} (%)	3.6	0.39	0.22	0.50	0.20	0.45	0.47	**0.26**
g_{HWW} (%)	3.2	0.41	0.22	0.50	0.19	0.43	0.46	**0.27**
g_{Hbb} (%)	5.3	0.78	0.52	0.99	0.44	0.63	0.71	**0.56**
g_{Hcc} (%)	SM	1.8	1.2	4.0	1.8	1.8	1.4	**1.2**
g_{Hgg} (%)	2.3	1.1	0.79	1.3	0.96	0.76	0.95	**0.82**
$g_{H\tau\tau}$ (%)	3.4	0.81	0.59	1.3	0.93	0.66	0.70	**0.57**
$g_{H\mu\mu}$ (%)	5.5	4.1	3.9	4.4	4.1	3.8	4.0	**3.8**
$g_{H\gamma\gamma}$ (%)	3.6	1.3	1.2	1.4	1.3	1.3	1.3	**1.2**
$g_{HZ\gamma}$ (%)	11.	9.6	6.8	9.7	4.6	6.3	9.8	**9.3**
g_{Htt} (%)	3.5	3.2	2.9	3.2	2.2	3.1	3.1	**3.1**
g_{HHH} (%)	52.	49.	27.	50.	36.	49.	49.	**33.**
Γ_H (%)	SM	2.2	1.1	2.5	1.7	1.7	1.8	**1.1**
BR$_{inv}$ (%)	1.9	0.26	0.23	0.63	0.62	0.27	0.22	**0.19**
BR$_{EXO}$ (%)	SM (0.0)	1.8	1.4	2.7	2.4	1.1	1.2	**1.0**

The last coupling shown in this table, g_{HHH}, refers to the Higgs coupling with itself even if the energies considered in the table are too low for producing two real Higgs bosons. This is possible since there is sensitivity to Higgs self-coupling in the virtual loop correction to the coupling to the Z in pair production or to the W in VBF. The best precision, at the level of 33% of the SM value, is attained by the full FCCee program. Measurements by direct production of two Higgs bosons with ILC at 500 GeV or CLIC at 1500 GeV obtain comparable resolution. CLIC at 3 TeV can reach slightly less than 10% accuracy and one needs the full electron-positron and proton-proton FCC program to reach 5% precision.

4   Current status and plans

All proposed circular colliders have by now completed their CDRs and are preparing for the next steps of the approval process. This is a delicate operation since the cost of these machines is rather high: 10.5 billion CHF for FCCee (11.6 with the 365 GeV upgrade) and $\sim$ 6 BCHF for CEPC, mostly due to the cheaper cost of the tunnel in China. In comparison linear colliders costs are around 6 BCHF for their first stage and require an additional 4-5 BCHF for their first energy step (500 GeV for ILC and 1500

GeV for CLIC). In the case of FCC a critical point will be the endorsement by the CERN council in the context of the update of the European strategy for particle physics in May 2020. In this case the proposed schedule would involve getting all necessary funding and administrative processes completed in about six years, followed by getting all permissions and then executing the construction of the tunnel, the technical infrastructure and the accelerator, that is planned to be completed by the end of the decade starting in 2030. The plan would be to run the electron-positron machine for ∼15 years and then upgrade to a very high energy proton-proton collider.

The critical point for the Chinese CEPC is the approval as a "Big Science cultivation" project that would allow a significant step up of the R&D toward an accelerator TDR in 2021. In case of a subsequent final approval civil construction could start in 2023 and the accelerator would be complete by 2030.

5   Conclusions

The future circular electron-positron colliders would allow a deep study of the Higgs boson as well as a major improvement in the precision of most electro-weak observables. They also have a large potential for heavy flavor studies complementary to both LHC and SuperKEKB. Construction completion times could be fast, as in the case of CEPC, and in any case not later then the end of the high luminosity LHC program, since there are no outstanding technical issues that need to be resolved. The infrastructure developed for these machine, tunnel and services, could be reused for an extreme energy proton-proton collider that would provide additional precision in the study of Higgs boson properties as well as an outstanding discovery potential. The sequential implementation of the e$^+$e$^-$ and pp colliders represents a great plan for HEP in this century.

References

1. A. Abada *et al.* [FCC Collaboration], Eur. Phys. J. ST **228**, no. 2, 261 (2019).

2. [CEPC Study Group], arXiv:1809.00285 [physics.acc-ph].

3. T. Behnke *et al.*, arXiv:1306.6327 [physics.acc-ph].

4. M. Aicheler *et al.*, doi:10.5170/CERN-2012-007, P. N. Burrows *et al.* , CERN Yellow Rep. Monogr. **1802**, 1 (2018) doi:10.23731/CYRM-2018-002 [arXiv:1812.06018 [physics.acc-ph]].

5. G. Aad *et al.* [ATLAS Collaboration], Phys. Lett. B **716**, 1 (2012) [arXiv:1207.7214 [hep-ex]].

6. S. Chatrchyan *et al.* [CMS Collaboration], Phys. Lett. B **716**, 30 (2012) [arXiv:1207.7235 [hep-ex]].

7. O. S. Bruning, P. Collier, P. Lebrun, S. Myers, R. Ostojic, J. Poole and P. Proudlock, doi:10.5170/CERN-2004-003-V-1

8. A. M. Sirunyan *et al.* [CMS Collaboration], Eur. Phys. J. C **79**, no. 5, 421 (2019).

9. G. Aad *et al.* [ATLAS Collaboration], Phys. Rev. D **101**, no. 1, 012002 (2020).

10. G. Apollinari, I. Bjar Alonso, O. Brning, P. Fessia, M. Lamont, L. Rossi and L. Tavian, CERN Yellow Rep. Monogr. **4**, 1 (2017). doi:10.23731/CYRM-2017-004

11. M. Cepeda *et al.*, CERN Yellow Rep. Monogr. **7**, 221 (2019) doi:10.23731/CYRM-2019-007.221 [arXiv:1902.00134 [hep-ph]].

12. K. Fujii *et al*, arXiv: 1506.05992 (2015).

13. P. Bambade *et al.*, arXiv:1903.01629 [hep-ex].

14. M. J. Boland *et al.* [CLIC and CLICdp Collaborations], doi:10.5170/CERN-2016-004 arXiv:1608.07537 [physics.acc-ph].

15. C. Wyss, CERN-AC/96-01.

16. I. Adachi *et al.* [sBelle Design Group], arXiv:0810.4084 [hep-ex].

17. R. Aaij *et al.* [LHCb Collaboration], arXiv:1808.08865.

18. J. de Blas *et al.*, arXiv:1905.03764 [hep-ph].

QUANTUM CHROMODYNAMICS AT THE LHC

Jennifer Roloff
Brookhaven National Laboratory, Upton, NY

Abstract

The LHC physics program aims to both perform some of the most precise measurements of Standard Model processes and search for physics beyond the Standard Model in phase space that has never been accessible before. This ambitious program requires a deep understanding of a broad array of phenomena. Central to all of this is our understanding of quantum chromodynamics (QCD), which affects everything from precision calculations of hard processes to the modeling of jets. I summarize a selection of measurements which further our understanding of parton distribution functions, the strong coupling constant, and jet modeling, and discuss the implications of such measurements for the high-luminosity LHC physics program.

1 Introduction

Our understanding of QCD directly impacts the quality of the entire physics program at the LHC. Jet-related systematics are frequently the limiting experimental systematic uncertainty, both searches and measurements struggle to estimate multijet backgrounds accurately, and precision measurements Higgs processes are becoming more sensitive to the uncertainty on the strong coupling constant α_s as the statistical precision improves. Even analyses without jets still rely on our understanding of perturbative QCD through our ability to model parton distribution functions (PDFs). In many cases, searches are limited by the PDF uncertainties as they probe challenging phase space. Despite its importance, precision understanding of QCD has remained elusive due to its complexity; high-order calculations are difficult to produce, meaningful observables are not always apparent, and accurate models do not exist for all relevant scales.

There are three specific ways in which QCD is relevant to a broad set of analyses at the LHC: parton distribution functions, the strong coupling constant, and jet modeling. Each of these topics poses unique

challenges and provides specific opportunities for extending the reach of the LHC physics program. The high-luminosity LHC is expected to produce around 3000 fb^{-1} of data, around 20 times the existing dataset. In studies of the expected sensitivity to various phenomena [1], ATLAS and CMS provide a few different scenarios for expected reduction in uncertainties at the HL-LHC, Most of these studies assume the scenario where all three of these uncertainties improve by approximately a factor of two. Some of these improvements are fairly concrete, such as increased statistical accuracy and the inclusion of more recent measurements in PDF fits, while others are more speculative, such as assumptions about improved methodology and improvements in jet modeling. These assumptions are only feasible through measurements that improve our understanding of QCD across all scales. I highlight a few representative examples of innovative measurements which are being used to further our understanding of QCD.

2 Parton Distribution Functions

Cross-section calculations at the LHC are factorized into two parts: the calculation of a hard process and the probability of the incoming partons existing at a given momentum within the colliding protons. While hard processes may often be calculated from first principles, the internal structure of a proton cannot be calculated due to the non-perturbative interactions of its partons. Instead, these are determined experimentally using PDFs, which describe the probability of finding a particular parton which carries a fraction x of a proton with energy Q. As searches push the mass limits for new particles higher, they become increasingly sensitive to high-x PDFs. Since these PDFs tend to be poorly constrained, the PDF uncertainties are becoming increasingly relevant to enabling us to find physics beyond the Standard Model. This is particularly relevant for searches for physics beyond the Standard Model. While the HL-LHC will provide more data for rare parameter space, its usefulness will be limited by the ability to predict the cross-sections for these distributions using PDFs.

PDFs are determined from a combination of perturbative QCD calculations and analytical parameterizations using measurements from experiments across a wide range of energy scales to fit the functional forms of different partons. Much of this is best-constrained by measurements of deep inelastic scattering, but particularly for the high-x regions, LHC data is crucial for constraining PDFs. Fig. 1b demonstrates this with the example of a measurement of the dijet cross-section at $\sqrt{s} = 8$ TeV, where this measurement is able to provide significant constraints on the high-x gluon PDF compared to a PDF produced using only measurements from HERA. This is further demonstrated in Fig. 1, which shows that dijet measurements from ATLAS and CMS are the most constraining measurements for the high-x gluon PDF for the CT18 NNLO fits. These fits only consider measurements from $\sqrt{s} = 7$ and 8 TeV, and with the large dataset that has already been produced at 13 TeV, further improvements can be expected both from the increased statistics and higher energy.

3 The Strong Coupling Constant

The strong coupling constant α_s has long been a challenging parameter to measure. Currently, α_s is only known with a precision around 1%, and significant tensions exist among the values extracted from different measurements, as seen in Fig. 2. While this could be explained, at least in part, by the underestimation of uncertainties for some of these measurements, this motivates the development of other uncorrelated measurements to be included in the world average while also improving our understanding of existing measurement techniques. This is challenging for a couple reasons. It is difficult to find observables which are both sensitive to α_s but fairly insensitive to various non-perturbative effects. In addition, at
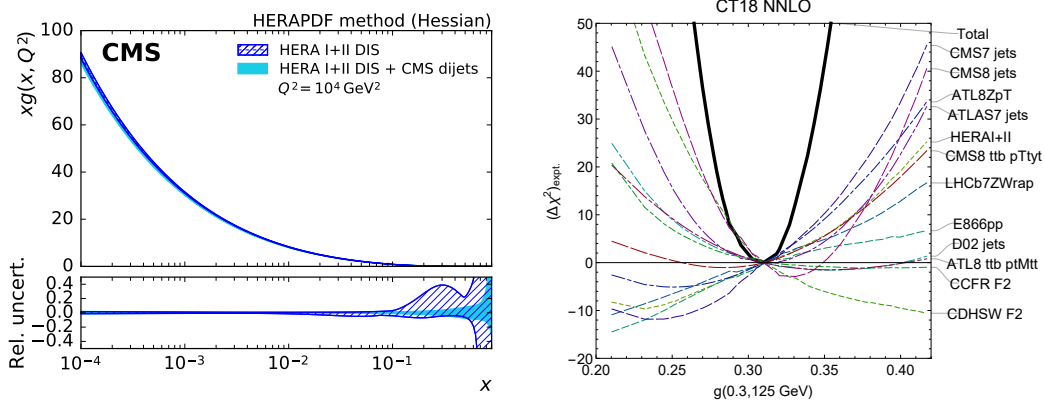
Figure 1: *a) The gluon PDF at $Q^2 = 10^4$ GeV^2 as a function of x as derived from HERA inclusive DIS data alone, and in combination with CMS dijet data* [3]*, and b) The Lagrange Multiplier scan of gluon PDF at Q=125 GeV and x = 0.3, for the CT18 NNLO fits.* [2]*.*

a hadron collider, calculations must be available at NNLO in order for them to be included in the world average. Currently, the only measurement from a hadron collider which has been used to extract α_s using NNLO predictions is the measurement of the $t\bar{t}$ cross-section. Even so, there are many observables at the LHC sensitive to α_s, and since there has been significant theoretical progress towards creating predictions, there is strong motivation to perform measurements of sensitive observables. The precision of such measurements is still unknown, but extractions of α_s at NLO at the LHC demonstrate precision which is competitive with other methods which are already being used [7, 8, 9].

Measurements of α_s at the LHC are not only useful for understanding the world average; they uniquely provide access to high scales, and also enable measurements across a wide range of scales within a single measurement. Measurements of the running of α_s can be used to provide indirect constraints on physics beyond the SM in a model-independent way [5, 6]. While the $t\bar{t}$ measurement does provide an important insight into α_s at high scales, it is currently not possible to probe the running of the coupling using this measurement. However, several other observables that have been calculated at NLO accuracy have been measured at the LHC. These observables include the inclusive jet cross section, the ratio of the 3-jet to 2-jet cross sections, transverse energy-energy correlations, the 3-jet mass, and angular correlations. Several of these measurements are shown in Fig. 3, which shows the broad range of scales which can be accessed by any single one of these measurements. As theoretical predictions become available at higher order, these types of measurements will test the limits of our understanding of QCD by accessing scales that have not yet been carefully explored.

4 Jet Modeling

Most analyses at the LHC – both searches and measurements – rely on accurate modeling of jets, either by using them directly, or through a jet veto. Jets are notoriously difficult to model, since jet observables are affected not only by perturbative effects such as the parton shower, but also nonperturbative effects like hadronization. First principle calculations of jets across all relevant scales are difficult, and Monte Carlo generators are necessary for providing predictions for these effects. Several Monte Carlo generators exist using different models for the parton shower and hadronization, and their parameters are tuned to
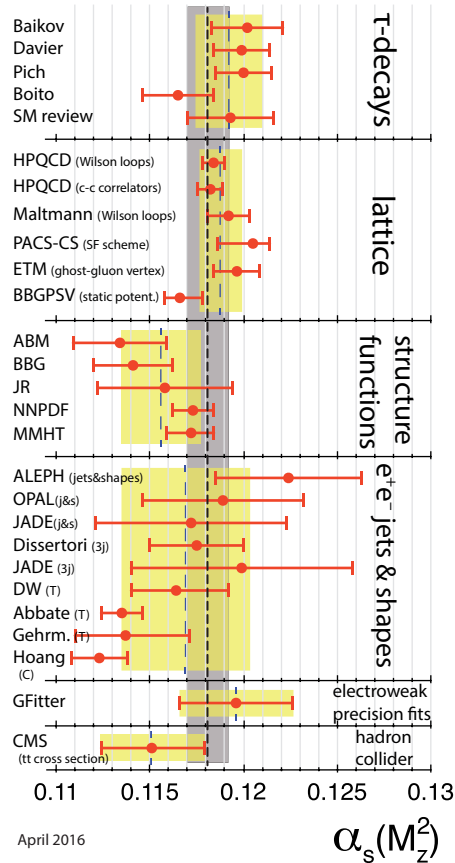
Figure 2: *Summary of determinations of $\alpha_s(M_Z^2)$ from different sub-fields. The yellow (light shaded) bands and dotted lines indicate the pre-average values of each sub-field. The dashed line and blue (dark shaded) band represent the final world average value of $\alpha_s(M_Z^2)$* [4].

measured data in order to provide accurate descriptions of jets.

ATLAS and CMS both produce their own individual Monte Carlo tunes using their own measurements, using a variety of measurements of jet substructure observables, multijet observables, and distributions of individual jet properties. These measurements are sometimes sensitive to multiple effects, and since not all tunable parameters have a clear physical meaning, it can be challenging to select the optimal observables for tuning. These challenges may be visualized in looking at several Monte Carlo predictions for jet substructure observables, which demonstrate clear differences between the predictions [11, 12, 13, 14].

This can be improved by providing more and better inputs to the tuning procedure, which would better constrain the tuned parameters. Ideally, to reduce the complexity of the fitting procedure, measurements would be sensitive to a single effect or parameter, though in practice such observables are hard to find. Recently, a new jet observable was proposed, which builds upon years of understanding of how to describe jets. This observable is called the Lund jet plane [15], and it approximates the emissions of a parton as a series of emissions from the core of a jet, parameterized by the fraction of momentum carried by the emission z and the angle of the emission ΔR. This simple characterization of a jet is extremely

Figure 3: *Comparison of the values $\alpha_s(Q)$ obtained from fits from several experiments with the uncertainty band from the global fit (orange full band) and the 2016 world average (green hatched band). Determinations from other experiments are also shown as data points. The errorbars, as well as the orange full band, include all experimental and theoretical sources of uncertainty. The strong coupling constant is assumed to run according to the two-loop solution of the RGE* [7].
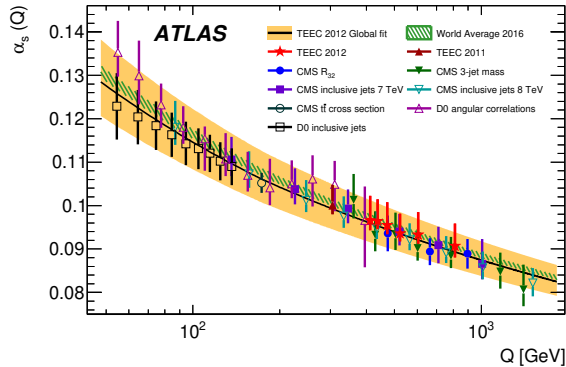
powerful, as it factorizes different effects into different regions of this two-dimensional space, which is represented in Fig. 4a.

The Lund Jet plane was measured in dijet events by the ATLAS experiment. Fig. 4b shows a single slice of the plane, where the left side of the distribution is sensitive to effects from the parton shower, while the right side of the distribution is sensitive to hadronization effect. It demonstrates the factorization predicted, since differences between similar generators are only seen in the regions predicted. While it remains to be seen how this will impact Monte Carlo tuning, the demonstration of the factorization of effects indicates that this could be a powerful tool.

5   Summary

Continuing to measure observables sensitive to various QCD effects will enable us to study rare processes, perform precision measurements, and searches for physics beyond the Standard Model. Analyses frequently probe processes where the relevant PDFs are poorly constrained, making LHC measurements relevant. Measurements of proceses such as the dijet cross section are already being used to constrain PDFs and will continue to be important in preparation for the HL-LHC. ATLAS and CMS have laid the foundations for measuring α_s using a variety of observables, and theoretical progress will enable these to be used to study QCD at high scales, testing the limits of our understanding. Even analyses that are not limited by PDFs or α_s are often reliant on jet modeling, which impacts the multijet background modeling and jet energy scale uncertainties. Only by studying QCD will we be able to use the full power of the data that will be collected by the HL-LHC.

References

1. ATLAS and CMS Collaborations [ATLAS and CMS Collaborations], CERN Yellow Rep. Monogr. **7** (2019) Addendum doi:10.23731/CYRM-2019-007.Addendum

2. T. J. Hou *et al.*, arXiv:1908.11394 [hep-ph].
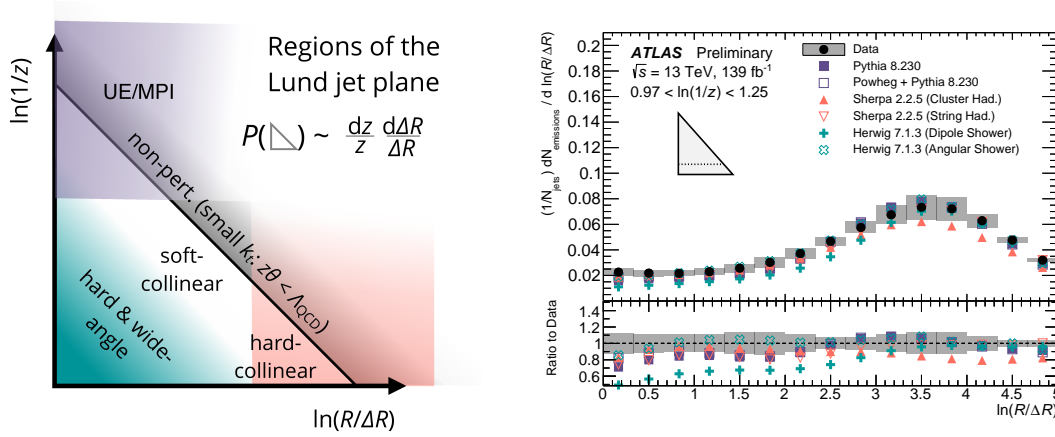
Figure 4: *a) Diagram of the Lund jet plane, highlighting regions where different effects are dominant. b) Representative horizontal slice through the Lund jet plane. Unfolded data are compared to particle-level simulation from several Monte Carlo generators. The uncertainty band includes all sources of systematic and statistical uncertainty. The inset triangle illustrates which slice of the plane is depicted [14].*

3. A. M. Sirunyan *et al.* [CMS Collaboration], Eur. Phys. J. C **77**, no. 11, 746 (2017) doi:10.1140/epjc/s10052-017-5286-7

4. M. Tanabashi *et al.* [Particle Data Group], Phys. Rev. D **98** (2018) no.3, 030001. doi:10.1103/PhysRevD.98.030001

5. D. Becciolini, M. Gillioz, M. Nardecchia, F. Sannino and M. Spannowsky, Phys. Rev. D **91** (2015) no.1, 015010 Addendum: [Phys. Rev. D **92** (2015) no.7, 079905] doi:10.1103/PhysRevD.91.015010, 10.1103/PhysRevD.92.079905

6. J. Llorente and B. P. Nachman, Nucl. Phys. B **936** (2018) 106 doi:10.1016/j.nuclphysb.2018.09.008

7. M. Aaboud *et al.* [ATLAS Collaboration], Eur. Phys. J. C **77**, no. 12, 872 (2017) doi:10.1140/epjc/s10052-017-5442-0

8. S. Chatrchyan *et al.* [CMS Collaboration], Eur. Phys. J. C **73** (2013) no.10, 2604 doi:10.1140/epjc/s10052-013-2604-6

9. V. Khachatryan *et al.* [CMS Collaboration], JHEP **1703** (2017) 156 doi:10.1007/JHEP03(2017)156 [arXiv:1609.05331 [hep-ex]].

10. G. Aad *et al.* [ATLAS Collaboration], arXiv:1912.09837 [hep-ex].

11. M. Aaboud *et al.* [ATLAS Collaboration], JHEP **1908** (2019) 033 doi:10.1007/JHEP08(2019)033

12. A. M. Sirunyan *et al.* [CMS Collaboration], JHEP **1811** (2018) 113 doi:10.1007/JHEP11(2018)113

13. A. M. Sirunyan *et al.* [CMS Collaboration], Phys. Rev. D **98** (2018) no.9, 092014 doi:10.1103/PhysRevD.98.092014

14. The ATLAS Collaboration, (2019) https://cds.cern.ch/record/2683993

15. F. A. Dreyer, G. P. Salam, G. Soyez, JHEP **12**, 064 (2018).

QCD CHALLENGES AT PRESENT AND FUTURE COLLIDERS

Andrea Banfi
Department of Physics and Astronomy, University of Sussex,
Sussex House, Brighton, BN1 9RH, U.K.

Abstract

I give a personal view of three important challenges that QCD practitioners face when dealing with the physics of present and future high-energy colliders. I will discuss in particular the quest for precision in inclusive cross sections, differential distributions, and the role played by hadronisation corrections.

1 Introduction

Despite not having yet provided any striking signal of new physics beyond the Standard Model (SM), the LHC is playing a crucial role in constraining extensions of the SM, hence giving us important clues in understanding the phenomenon of electroweak symmetry breaking. Projections for the high-luminosity phase of the LHC (HL-LHC) indicate the possibility of constraining anomalous Higgs couplings at the percent level [1]. In order to establish whether any deviations can be genuinely attributed to new physics, SM theoretical predictions need to be pushed at a comparable level of accuracy. This has fostered an impressive progress in our understanding of strong interactions, in particular the high-order structure of QCD.

At hadron colliders, cross sections can be written as convolutions of parton-distribution functions, which are universal and encode the long-range dynamics of partons (quarks and gluons) in the proton, and process-dependent, short-distance partonic cross sections, that can be computed as perturbative expansions in the strong coupling α_s. The lowest order

in α_s is called leading order (LO), next-to-LO (NLO) contributions are suppressed by an extra power of α_s with respect to LO ones, and so on. Fixed-order perturbative contributions are generally calculated from the appropriate Feynman diagrams, taking care that infrared singularities cancel between real and virtual corrections. Such a cancellation can be achieved more easily for inclusive cross sections than for differential distributions. This is why the former, discussed in section 2, enjoy a better accuracy than differential distributions, the topic of section 3. The last section deals with the fact that we measure hadronic, and not partonic cross sections. Given the current level of precision, it is now important to reconsider the modelling of the transition from parton to hadron level.

2 Inclusive cross sections

Perturbative QCD expansions converge quite slowly, hence it is important to reach high orders to have a satisfactory theoretical accuracy. This is particularly true for the Higgs cross section, which starts to show satisfactory convergence starting at NNLO. The new state of the art for inclusive cross sections is an impressive N³LO, in the limit of an infinitely heavy top [2]. In fact, only by taking into account N³LO corrections is it possible to push the theoretical accuracy for the Higgs cross section at the percent level. Notably, all integrals for relevant $2 \to 1$ processes at N³LO are known [2]. This gives access to further important total cross sections, such as that for Higgs production through bottom-quark fusion [3], and for the Drell-Yan process, whose calculation is in progress and gives promise to reach sub-percent accuracy. Using a systematic expansion around threshold it is also possible to compute the Higgs rapidity distribution at N³LO [4]. Finally, approximating Higgs production in vector-boson fusion (VBF) as the combination of two independent deep-inelastic-scattering (DIS) processes, it has been possible to compute the VBF cross section at N³LO [5]. It is known that this approximation breaks down at NNLO due to gluon exchanges between the two DIS lines. These contributions are at the permille level [6], the same size as the N³LO ones [5]. The main message here is that the VFB cross section is well under control, and NNLO is sufficient to achieve percent accuracy.

3 Differential distributions

Theoretical control of differential cross sections is particularly important when large invariant masses are probed. In fact, this regime could give access to quantum corrections involving new physics contributions that are inaccessible at low invariant masses. At HL-LHC, data for interesting high-energy regions will reach percent accuracy [1], so it will be crucial to match the same accuracy on the theoretical side.

At fixed-order, percent accuracy can be reached in most cases only through NNLO calculations. There is plenty of evidence that, when they exist, NNLO calculations agree much better with data than the corresponding NLO ones (see e.g. the comparison of theory and experiment for WZ production [7]). In recent years, there has been an explosion of new NNLO results, so that at the moment all relevant SM $2 \to 2$ processes are

known at NNLO. These results have been driven by an impressive progress in the techniques used to perform the cancellation of infrared singularities between real and virtual corrections [8, 9, 10, 11, 12, 13]. In the following, instead of listing all these results, I will focus on a couple of examples of the benefit of having fully differential information on the final state.

The first example is the azimuthal correlation between leptons in top-antitop events. This observable is sensitive to physics beyond the SM. For instance, if the tops were originated from the decay of scalar stops, one would observe a different pattern of spin correlations in top decay. In fact, a fully differential NNLO calculation [14] of this observable in top-antitop production shows a much better agreement with data than the corresponding NLO prediction, with a substantial change in the shape of the distribution with respect to NLO.

One of the most important examples of a $2 \to 2$ process with jets in the final state is Higgs production with an additional jet. There, the tail of the transverse momentum distribution of the Higgs is sensitive to physics beyond the SM [15, 16, 17]. At LO, this process needs already a loop of quarks, with the top quark playing the dominant contribution. An NLO calculation requires the evaluation of two-loop diagrams with an internal mass, which have been computed only very recently using semi-numerical methods [18]. The most remarkable finding of this calculation is that the K-factor NLO/LO is about 2, of the same size as that of the Higgs total cross section, and basically independent of the Higgs transverse momentum.

For Higgs characterisations, it is also crucial to compute NNLO corrections to $2 \to 3$ processes, especially to Higgs production in association with a top-antitop pair, which gives direct access to the top Yukawa coupling. Here progress is needed in the evaluation of the corresponding two-loop amplitudes. In this respect, we mention the first analytic calculation of a $2 \to 3$ two-loop amplitude, the full-colour five-gluon all-plus helicity amplitude [19]. Also, the recent calculation of NNLO corrections to three-photon production at the LHC [20] constitutes the first NNLO QCD calculation of a $2 \to 3$ process.

A general problem of fixed-order calculations for processes characterised by two disparate scales is the occurrence of large logarithms L of the ratio of the two scales. This happens for instance whenever we impose a jet-veto in the production of a heavy object (e.g. Higgs decaying to WW) to suppress some large irreducible background (e.g. top-antitop). These large logarithms need to be resummed at all orders to obtain meaningful predictions. For most observables, such resummation consists in a reorganisation of the perturbative series in the region $\alpha_s L \sim 1$. The leading logarithms (LL) build up an exponential function $\exp[Lg_1(\alpha_s L)]$, next-to-LL (NLL) factorise in a function of $\alpha_s L$, next-to-NLL (NNLL) contributions, for $\alpha_s L$ fixed, are suppressed by a power of α_s with respect to NLL ones, and so on.

Jet-veto resummations have reached a remarkable accuracy (NNLL for the production of a colour singlet [21]). Predictions are now fully differential in the decay products of the colour singlet (e.g. a Higgs or a vector boson) with a jet-veto, and we now have an implementation of such NNLL jet-veto resummations in soft-collinear effective theory (SCET) in MADGRAPH (MADGRAPH_MC@NLO_SCET [22]), and in QCD in MCFM

(MCFM-RE [23]).

The highest resummation accuracy (N^{3}LL) has been reached for the transverse momentum distribution of a colour singlet, both in QCD with the RadISH formalism [24], and in SCET [25]. Notably, RadISH is able to provide a double differential distribution in the transverse momentum of the colour singlet and the leading accompanying jet, being simultaneously fully differential in the decay products of the colour singlet [26].

4 Hadronisation

In view of the precision of present and future calculations, precise measurements of α_s start to play a role. Until very recently, the determination of α_s from jet observables in e^+e^- annihilation was mainly affected by perturbative QCD uncertainties [27]. The precision of current calculations [28, 29, 30] is such that the dominant uncertainty is due to poorly understood hadronisation effects. These are either determined with Monte Carlo event generators [30], or with analytic models of the leading hadronisation corrections [28, 29]. Note that hadronisation corrections, suppressed by inverse powers of the e^+e^- centre-of-mass energy, become smaller with increasing energy. Therefore, at future e^+e^- colliders, different Monte Carlo hadronisation models might have less impact on the determination of α_s than perturbative QCD uncertainties. Also, considering only leading hadronisation corrections might be appropriate. This might foster improvements in analytic models of hadronisation, for instance their extension to a larger set of observables. Also, hadronisation effects in three-jet events at future e^+e^- colliders will be of the same order as in two-jet events at LEP1 [31]. This will give the opportunity to perform further non-trivial tests of the features of leading hadronisation corrections.

5 Conclusions

To conclude, present and future colliders offer many exciting possibilities to reinforce our understanding of QCD dynamics. The precision of experimental data, especially at the HL-LHC, pushes theory at least to NNLO accuracy, and requires fully differential predictions, both fixed-order and resummed. Future e^+e^- colliders give promise to provide better determinations of the strong coupling due to smaller hadronisation corrections. This in turn might positively affect the accuracy of theoretical predictions for the LHC. We hope that all these improvements will help give access to hints of new physics that could explain the unsolved puzzles of the SM.

6 Acknowledgements

References

1. M. Cepeda *et al.*, CERN Yellow Rep. Monogr. **7** (2019) 221 doi:10.23731/CYRM-2019-007.221 [arXiv:1902.00134 [hep-ph]].

2. B. Mistlberger, JHEP **1805** (2018) 028 doi:10.1007/JHEP05(2018)028 [arXiv:1802.00833 [hep-ph]].

3. C. Duhr, F. Dulat and B. Mistlberger, arXiv:1904.09990 [hep-ph].

4. F. Dulat, B. Mistlberger and A. Pelloni, Phys. Rev. D **99** (2019) no.3, 034004 doi:10.1103/PhysRevD.99.034004 [arXiv:1810.09462 [hep-ph]].

5. F. A. Dreyer and A. Karlberg, Phys. Rev. Lett. **117** (2016) no.7, 072001 doi:10.1103/PhysRevLett.117.072001 [arXiv:1606.00840 [hep-ph]].

6. T. Liu, K. Melnikov and A. A. Penin, Phys. Rev. Lett. **123** (2019) no.12, 122002 doi:10.1103/PhysRevLett.123.122002 [arXiv:1906.10899 [hep-ph]].

7. M. Aaboud *et al.* [ATLAS Collaboration], Phys. Lett. B **762** (2016) 1 doi:10.1016/j.physletb.2016.08.052 [arXiv:1606.04017 [hep-ex]].

8. A. Gehrmann-De Ridder, T. Gehrmann and E. W. N. Glover, JHEP **0509** (2005) 056 doi:10.1088/1126-6708/2005/09/056 [hep-ph/0505111].

9. S. Catani and M. Grazzini, Phys. Rev. Lett. **98** (2007) 222002 doi:10.1103/PhysRevLett.98.222002 [hep-ph/0703012].

10. M. Czakon, Nucl. Phys. B **849** (2011) 250 doi:10.1016/j.nuclphysb.2011.03.020 [arXiv:1101.0642 [hep-ph]].

11. R. Boughezal, X. Liu and F. Petriello, Phys. Rev. D **91** (2015) no.9, 094035 doi:10.1103/PhysRevD.91.094035 [arXiv:1504.02540 [hep-ph]].

12. M. Cacciari, F. A. Dreyer, A. Karlberg, G. P. Salam and G. Zanderighi, Phys. Rev. Lett. **115** (2015) no.8, 082002 Erratum: [Phys. Rev. Lett. **120** (2018) no.13, 139901] doi:10.1103/PhysRevLett.115.082002, 10.1103/PhysRevLett.120.139901 [arXiv:1506.02660 [hep-ph]].

13. V. Del Duca, C. Duhr, A. Kardos, G. Somogyi and Z. Trcsnyi, Phys. Rev. Lett. **117** (2016) no.15, 152004 doi:10.1103/PhysRevLett.117.152004 [arXiv:1603.08927 [hep-ph]].

14. A. Behring, M. Czakon, A. Mitov, A. S. Papanastasiou and R. Poncelet, Phys. Rev. Lett. **123** (2019) no.8, 082001 doi:10.1103/PhysRevLett.123.082001 [arXiv:1901.05407 [hep-ph]].

15. A. Banfi, A. Martin and V. Sanz, JHEP **1408** (2014) 053 doi:10.1007/JHEP08(2014)053 [arXiv:1308.4771 [hep-ph]].

16. A. Azatov and A. Paul, JHEP **1401** (2014) 014 doi:10.1007/JHEP01(2014)014 [arXiv:1309.5273 [hep-ph]].

17. C. Grojean, E. Salvioni, M. Schlaffer and A. Weiler, JHEP **1405** (2014) 022 doi:10.1007/JHEP05(2014)022 [arXiv:1312.3317 [hep-ph]].

18. S. P. Jones, M. Kerner and G. Luisoni, Phys. Rev. Lett. **120** (2018) no.16, 162001 doi:10.1103/PhysRevLett.120.162001 [arXiv:1802.00349 [hep-ph]].

19. S. Badger *et al.*, Phys. Rev. Lett. **123** (2019) no.7, 071601 doi:10.1103/PhysRevLett.123.071601 [arXiv:1905.03733 [hep-ph]].

20. H. A. Chawdhry, M. L. Czakon, A. Mitov and R. Poncelet, arXiv:1911.00479 [hep-ph].

21. A. Banfi, P. F. Monni, G. P. Salam and G. Zanderighi, Phys. Rev. Lett. **109** (2012) 202001 doi:10.1103/PhysRevLett.109.202001 [arXiv:1206.4998 [hep-ph]].

22. T. Becher, R. Frederix, M. Neubert and L. Rothen, Eur. Phys. J. C **75** (2015) no.4, 154 doi:10.1140/epjc/s10052-015-3368-y [arXiv:1412.8408 [hep-ph]].

23. L. Arpino, A. Banfi, S. Jger and N. Kauer, JHEP **1908** (2019) 076 doi:10.1007/JHEP08(2019)076 [arXiv:1905.06646 [hep-ph]].

24. P. F. Monni, E. Re and P. Torrielli, Phys. Rev. Lett. **116** (2016) no.24, 242001 doi:10.1103/PhysRevLett.116.242001 [arXiv:1604.02191 [hep-ph]].

25. X. Chen *et al.*, Phys. Lett. B **788** (2019) 425 doi:10.1016/j.physletb.2018.11.037 [arXiv:1805.00736 [hep-ph]].

26. P. F. Monni, L. Rottoli and P. Torrielli, arXiv:1909.04704 [hep-ph].

27. G. Dissertori, A. Gehrmann-De Ridder, T. Gehrmann, E. W. N. Glover, G. Heinrich, G. Luisoni and H. Stenzel, JHEP **0908** (2009) 036 doi:10.1088/1126-6708/2009/08/036 [arXiv:0906.3436 [hep-ph]].

28. T. Gehrmann, G. Luisoni and P. F. Monni, Eur. Phys. J. C **73** (2013) no.1, 2265 doi:10.1140/epjc/s10052-012-2265-x [arXiv:1210.6945 [hep-ph]].

29. A. H. Hoang, D. W. Kolodrubetz, V. Mateu and I. W. Stewart, Phys. Rev. D **91** (2015) no.9, 094018 doi:10.1103/PhysRevD.91.094018 [arXiv:1501.04111 [hep-ph]].

30. A. Verbytskyi *et al.*, JHEP **1908** (2019) 129 doi:10.1007/JHEP08(2019)129 [arXiv:1902.08158 [hep-ph]].

31. L. Arpino, A. Banfi and B. K. El-Menoufi, arXiv:1912.09341 [hep-ph].

HIGHER-ORDER QCD CORRECTIONS TO HIGGS BOSON TRANSVERSE-MOMENTUM DISTRIBUTION

Fabrizio Caola
Rudolf Peierls Centre for Theoretical Physics, Oxford University, Oxford, UK
Kirill Kudashkin
Department of Physics, University of Milan, Milan, Italy
Jonas M. Lindert
Department of Physics and Astronomy, Sussex University, Falmer, UK
Kirill Melnikov
Institute for Theoretical Particle Physics (TTP), KIT, Karlsruhe, Germany
Pier F. Monni
Theoretical Physics Department, CERN, Geneva, Switzerland
Lorenzo Tancredi
Rudolf Peierls Centre for Theoretical Physics, Oxford University, Oxford, UK
Chris Wever
Physik-Department T31, Technische Universität München, Garching, Germany

Abstract

We present up-to-date Standard Model theory predictions for the Higgs transverse-momentum ($p_\perp$) distribution. In the region of intermediate values of transverse momenta we present the NNLL+NLO QCD predictions including both top and bottom quark contributions. At very large $p_\perp \gg 2m_t$ we show the next-to-leading order QCD corrections to the production of the Higgs boson at the LHC.

1 Introduction

Detailed exploration of the Higgs boson is one of the central tasks of the particle physics program at the LHC. Since the majority of the Higgs bosons is produced by gluon fusion, it is only natural to study Higgs coupling to gluons as precisely as possible. Incidentally, the Higgs-gluon coupling is very interesting phenomenologically. Indeed, since the Higgs coupling to gluons is loop-induced, and since contributions of heavy particles whose masses are generated by the Higgs mechanism do not decouple, the ggH interaction vertex becomes an intriguing probe of the TeV-scale physics. The goal of this proceeding is to present the Higgs $p_\perp$ spectrum in the moderate [1] $m_b \lesssim p_\perp \lesssim m_H$ as well as the large [2] $p_\perp \gg 2m_t$ range.

In the moderate $p_\perp$ range we present results that involve the top and bottom-quark contributions at next-to-leading order combined with next-to-next-to-leading logarithmic transverse momentum resummation (NLO+NNLL), presented originally in Ref. [1]. Although the contributions of bottom and charm loops to the ggH coupling and direct production of a Higgs boson in quark fusion $q\bar{q} \to H$, $q \in \{c, b\}$ are small in the Standard Model, if the Yukawa couplings differ from their Standard Model values, these light-quark effects in Higgs production become much more important. In fact, it was pointed out in Refs. [3, 4] that studies of kinematic distributions of Higgs bosons produced in hadron collisions may lead to interesting constraints on light quark Yukawa couplings, especially at the high-luminosity LHC.

On the other hand, to disentangle the effective one-loop ggH coupling induced through heavy BSM particles from that induced through the SM top quark running in the loop, one has to consider the Higgs boson transverse momentum distribution at very large Higgs $p_\perp$. [5] The two-loop amplitudes for the production of the Higgs boson at high-$p_\perp$ were computed in Ref. [6] and enabled the calculation of the Higgs boson transverse momentum distribution for $p_\perp > 2m_t$ at NLO QCD presented originally in Ref. [2], that we report in the second half of the proceedings.

2 Results

We discuss here our main result for the Higgs transverse momentum distribution. We separate the discussion for the case where the Higgs transverse momentum is below and above the top-mass threshold, i.e. $p_\perp \sim 2m_t \sim 350$ GeV. In section 2.1, results are shown for moderate $p_\perp \lesssim 100$ GeV values, while in section 2.2 our results for very large $p_\perp \gtrsim 350$ GeV values are presented. We refer to Refs. [1, 2] for the details of the computations.

2.1 Higgs transverse-momentum distribution below the top-mass threshold

Our results for the fixed-order and matched distributions below the top-mass threshold are shown in Fig. 1. Let us consider first the left plot that shows our result for the top-bottom interference contribution. In order to make a conservative estimate of the uncertainty for the matched interference distribution we took the envelope of the following uncertainties: the usual scale variations of μ_R, μ_f; the variation of half and twice the central scale $Q_t = Q_b = m_H/2$ at fixed central scales $\mu_R = \mu_f$; the difference between the on-shell and $\overline{\text{MS}}$ bottom-mass scheme; matching scheme difference between additive and multiplicative cases; finally the difference between resummation scale choice of $Q_b = 2m_b$ and $Q_b = m_H/2$. The effect of the resummation in this case is larger than in the full spectrum shown in the right plot, as was already observed in Fig. 1 of Ref. [8]. The qualitative features of the fixed order result are unchanged by the resummation, which however has a noticeable effect. The resummation prescription tames the fixed order result down to 10 GeV $\lesssim p_\perp$, while at the same time keeping the errors under control at the order of at most $\sim 20\%$ throughout the range of 10 GeV $\lesssim p_\perp \lesssim 70$ GeV.

In the right plot of Fig. 1 we present our main results for the full spectrum. The plot shows the fixed-order result in orange and the total top and bottom resummed result in blue. The uncertainty band for the resummed result contains in this case only the scale variations of μ_R, μ_f and $Q_t = Q_b$, since as we have seen above the effects of the bottom-mass scheme and different resummation scales for the bottom are already well captured by these variations. At large values of the Higgs $p_\perp \gtrsim 40$ GeV, the fixed-order result is contained in the error band of the resummed result. However, at smaller values $p_\perp \lesssim 40$ GeV, we observe a marked difference between the two results. The error for the full matched result is well under control and contained to about 5-10% in this range, increasing to about $\sim 20\%$ at larger $p_\perp$, where the effect of the resummation prescription is reduced and the fixed order NLO result is approached. At the same time, the effect of the bottom contribution on the central value is small though still noticeable, while its effect on the error-band widths is negligible.

This final result constitutes the best theoretical prediction up till now for the Higgs transverse momentum distribution for moderate values of the Higgs $p_\perp$ and is to be compared with current experimental measurements. From our discussion above it becomes clear that further improvement of our results is appreciated in the region of Higgs $p_\perp \gtrsim m_h/2$, where the collinear approximation breaks down and the resummation is turned off. This improvement would require matching to higher fixed-order NNLO result.
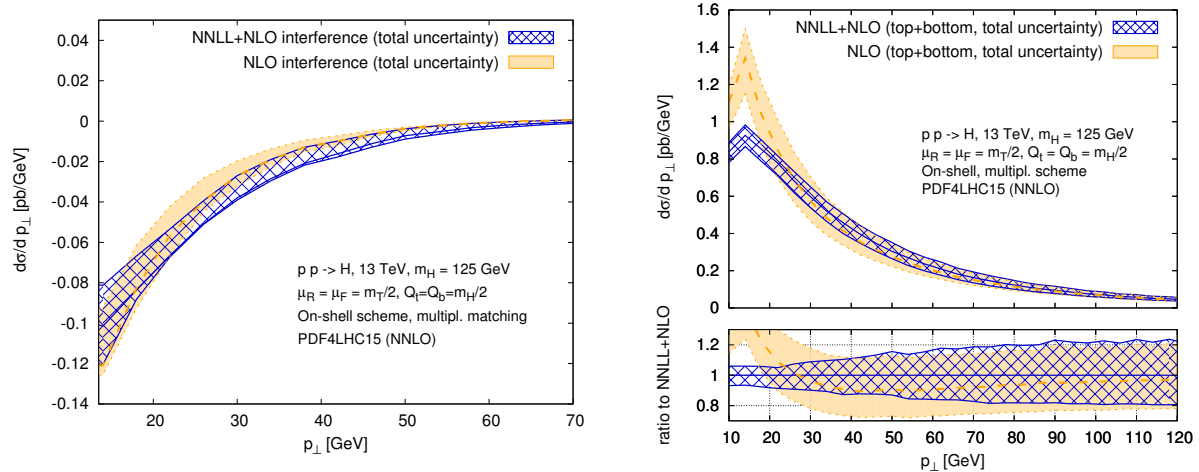
Figure 1: The distributions for the top-bottom interference contribution (left) and the full NNLL matched result (right), using the multiplicative scheme with resummation scale $Q_b = Q_t = m_h/2$ as central values. See text for details.

2.2 Higgs transverse momentum distribution at very large $p_\perp$

For the results in this range we use the amplitudes in Ref. [6] expanded in the small ratio $4m_t^2/p_\perp$, keeping sub-leading terms in the expansion. We start by illustrating how well our mass expansion of the amplitude works at LO. In the left plot of Fig. 2, we compare the exact leading-order $p_\perp$ distribution of the Higgs boson with its various expansions. We see that the amplitude expanded to $\mathcal{O}(m_H^0, m_t^2)$ terms gives the result that tracks the leading-order amplitude all the way down to the top-quark threshold; on the contrary, if the sub-leading top-quark mass terms are not retained, the expanded and exact cross sections have $\mathcal{O}(20\%)$ difference at $p_\perp \sim 800$ GeV.

We employ the five-flavor scheme and consider the bottom quark as a massless parton in the proton. We use the NNPDF3.0 set of parton distribution functions [9] at the respective perturbative order and employ the strong coupling constant α_s that is provided with these PDF sets. We choose renormalization and factorization scales to be equal and take as the central value

$$\mu_0 = \frac{H_T}{2}, \quad H_T = \sqrt{m_H^2 + p_\perp^2} + \sum_j p_{\perp,j} \,. \tag{1}$$

The inclusive cross sections are computed for both the point-like Higgs-gluon coupling, obtained by integrating out the top quark, and for the physical Higgs-gluon coupling with a proper dependence on m_t. We will refer to the two cases as HEFT and SM, respectively.

The Higgs-boson transverse-momentum distribution for $p_\perp > 350$ GeV is shown in the right plot of Fig. 2. The results show that both the SM and the HEFT K-factors are flat over the entire range of $p_\perp$. For the central scale $\mu = \mu_0$ (see Eq. (1)), the differences between the two K-factors is about 5%. The scale dependence of HEFT and SM results are also similar. The residual theoretical uncertainty related to perturbative QCD computations remains at the level of 20%, as estimated from the scale variation. Such an uncertainty is typical for NLO QCD theoretical description of many observables related to Higgs boson production in gluon fusion. Further improvements in theory predictions are only possible if the proximity of the HEFT and SM K-factors is taken seriously and postulated to occur even at higher
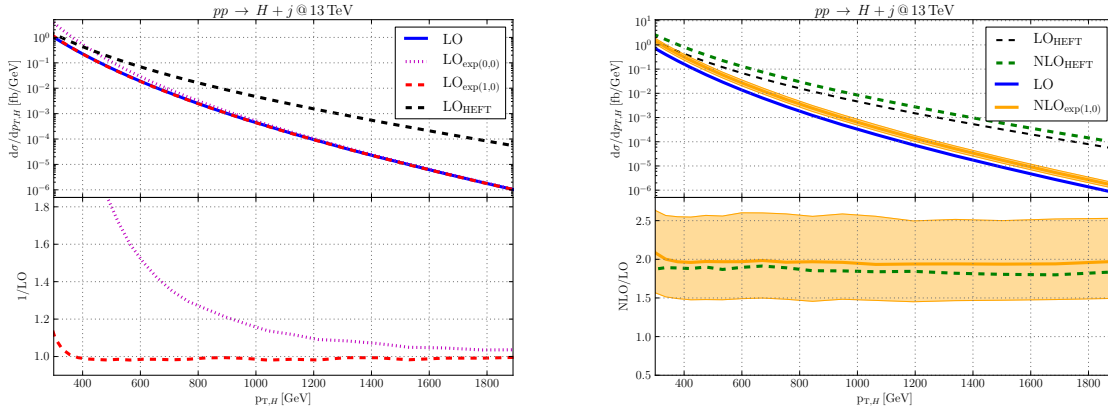
Figure 2: Left: Ratio of approximate to exact leading order cross sections. By retaining $\mathcal{O}(m_t^2/p_\perp^2)$ corrections in scattering amplitudes (red line), we obtain an excellent approximation to the exact LO result. Right: Transverse momentum distribution of the Higgs boson at the LHC with $\sqrt{s}$=13 TeV. The upper panel shows absolute predictions at LO and NLO in the full SM and in the infinite top-mass approximation (HEFT). The lower panel shows respective NLO/LO correction factors. The bands indicate theoretical errors of the full SM result due to scale variation.

orders. In this case, one will have to re-weight the existing HEFT $H + j$ computations [10, 11, 12] with the exact leading-order cross section for producing the Higgs boson with high $p_\perp$. In fact, such a reweighting can now be also performed at the NLO level.

3 Summary

We presented accurate theory predictions to the Higgs boson transverse momentum distribution. In the region of intermediate values of transverse momenta, $m_b \lesssim p_\perp \lesssim m_H$, we presented a description of the Higgs $p_\perp$ spectrum at NNLL+NLO QCD including both top and bottom quark contributions. We found that the uncertainty on the top-bottom interference is $\mathcal{O}(20\%)$ in the region of interest $m_b \lesssim p_\perp \lesssim m_H$. Given the intrinsic ambiguities from scale dependence and, in particular, from the choice of the bottom-mass renormalization scheme and matching scheme, any improvement in this description will inevitably require the computation of the NNLO QCD corrections to the bottom-quark contribution to $gg \to H$ and $gg \to H + jet$.

In the range of very large $p_\perp$ values, we presented the NLO QCD corrections to the Higgs boson transverse momentum distribution. To compute them, we employed the calculation of the two-loop scattering amplitudes for all relevant partonic channels [6] where an expansion in $m_t/p_\perp$ was performed. The real-emission corrections were computed with the `Openloops` [7] program. We have found that the QCD corrections to the Higgs-boson transverse-momentum distribution increase the leading order result by almost a factor of two. However, their magnitude appears to be quite similar to the QCD corrections computed in the approximation of a point-like Higgs-gluon vertex; the difference of the two result is close to 5%. Our computation removes the major theoretical uncertainty in the description of the Higgs boson transverse momentum distribution at high $p_\perp$ and opens a way to a refined analysis of the sensitivity of this observable to BSM contributions, using existing [13] and forthcoming experimental measurements.

References

1. F. Caola, J. M. Lindert, K. Melnikov, P. F. Monni, L. Tancredi and C. Wever, JHEP **09** (2018) 035.

2. J. M. Lindert, K. Kudashkin, K. Melnikov and C. Wever, Phys. Lett. B **782** (2018) 210.

3. F. Bishara, U. Haisch, P. F. Monni and E. Re, Phys. Rev. Lett. **118** (2017) 121801.

4. Y. Soreq, H. X. Zhu and J. Zupan, JHEP **12** (2016) 045.

5. C. Arnesen, I. Z. Rothstein and J. Zupan, Phys. Rev. Lett. **103** (2009) 151801.

6. K. Kudashkin, K. Melnikov, and C. Wever, JHEP **02** (2018) 135.

7. F. Cascioli, P. Maierhöfer and S. Pozzorini, Phys. Rev. Lett. **108**, 111601 (2012).

8. A. Banfi, P. F. Monni and G. Zanderighi, JHEP **01** (2014) 097.

9. R. D. Ball *et al.* [NNPDF Collaboration], JHEP **1504**, 040 (2015).

10. R. Boughezal *et al.*, Phys. Rev. Lett. **115** (2015) no.8, 082003.

11. R. Boughezal, C. Focke, W. Giele, X. Liu and F. Petriello, Phys. Lett. B **748** (2015) 5.

12. X. Chen, T. Gehrmann, E. W. N. Glover, and M. Jaquier, Phys. Lett. B **740** (2015) 147.

13. **CMS** Collaboration, (2017) CMS-PAS-HIG-17-010.

IMPACT OF THE RECOIL SCHEME ON THE ACCURACY OF ANGULAR-ORDERED PARTON SHOWERS

Silvia Ferrario Ravasio, Gavin Bewick

Institute for Particle Physics Phenomenology, Department of Physics, Durham University, Durham DH1 3LE, United Kingdom

Abstract

In these proceedings we present three possible interpretations of the ordering variable implemented in the `Herwig7` angular-ordered parton shower. Each interpretation determines a different recoil-scheme prescription and we show how it can impact the logarithmic accuracy of the algorithm. We also present comparisons with LEP data.

1 Introduction

General Purpose Monte Carlo (GPMC) generators are fundamental tools for collider phenomenology, as they are able to simulate fully realistic collider events, describing both inclusive and exclusive distributions with high accuracy. GPMC involve several components. The event generation starts with the computation of the scattering process at some hard scale, Q, at a fixed order in perturbation theory (usually at least NLO QCD). The event is then fed to a Parton Shower (PS) algorithm, which handles the emissions of soft and collinear partons. The PS thus evolves the system from the hard scale, Q, down to a soft scale, Λ. At this point we enter the non-perturbative regime: QCD interactions are so strong that the coloured partons are forced to form colour singlets, *i.e.* they hadronize. To properly simulate hadron colliders, we also need to provide a model of the *underlying event*, *i.e.* secondary interactions between initial-state partons that do not participate in the hard interaction.

In these proceedings we will focus on the PS component, which provides a bridge between the perturbative and non-perturbative regimes of QCD and allows the multiplicity of particles in the event to increase, which is a key requirement for performing realistic simulations of collider data. To achieve this task, the PS exploits the factorisation properties of QCD in the soft and collinear limits. When a

soft-collinear gluon is emitted from a parton i, the cross section is enhanced and behaves like

$$d\sigma_{n+1} = d\sigma_n \frac{\alpha_s}{\pi} 2C_i \frac{d\epsilon}{\epsilon} \frac{dp_T}{p_T}, \tag{1}$$

where $d\sigma_n$ is the differential cross-section for the production of n particles, C_i is the colour factor associated with the emission from parton i (C_A if i is a gluon, C_F if it is a quark), ϵ is the energy fraction carried by the gluon and p_T is its transverse momentum with respect to the emitter. From eq. (1) we clearly see that we can have two sources of logarithmic divergence: one associated with $\epsilon \to 0$ and one with $p_T \to 0$. Thus, when we generate m emissions we can have at most $2m$ logarithms: these are the leading logarithms (LL). It is a common belief that all of the available PS are able to resum such logarithms since the splitting kernels that are employed to mimic the emission of a gluon always approach eq. (1) in the soft-collinear limit. Many efforts have been made towards reaching next-to-leading log (NLL) accuracy, *i.e.* $2m-1$ logarithms for m powers of α_s. For example, the use of quasi-collinear splitting functions [1] gives the first subleading collinear logarithms. If one also adopts the two-loop expression for the running of α_s and the CMW scheme [2], then all the LL and NLL are included, except for those arising from soft wide-angle gluon emissions.

Due to the increasing precision of experimental measurements, the determination of the formal accuracy of a PS is becoming a serious issue which must be addressed. A recent work [3] introduced an approach to evaluate the logarithmic accuracy based on the ability of the PS to reproduce the singularity structure of multi-parton matrix elements, and the logarithmic resummation results. The authors focus on the process of double gluon emission in $e^+e^- \to q\bar{q}$ events, where the quark, q, is massless and the two gluons are well separated in rapidity so that the emission probability reduces to

$$dP_2 = \frac{1}{2} \prod_{i=1}^{2} \left(\frac{\alpha_s}{\pi} 2C_F \frac{dp_{T,i}}{p_{T,i}} \frac{d\epsilon_i}{\epsilon_i} \right) = \frac{1}{2} \prod_{i=1}^{2} \left(\frac{\alpha_s}{\pi} 2C_F \frac{dp_{T,i}}{p_{T,i}} dy_i \right), \tag{2}$$

where y_i is the rapidity of the gluon. The analysis is restricted to dipole showers, specifically the `Pythia` [4] one, which is the default option of the `Pythia8` [5] generator, and the `Dire` [6] one, available in both `Pythia8` and `Sherpa` [7]. The authors identified regions of phase space where the second gluon emission probability is generated with the wrong colour factor, namely $C_A/2$ instead of C_F.[1] This happens when the second gluon, g_2, is closest in angle to the first gluon, g_1, in the rest frame of the qg_1 (or $\bar{q}g_1$) dipole but closest to q (or $\bar{q}$) in the original $q\bar{q}$ frame. Another consequence is that the first gluon must absorb the transverse-momentum recoil

$$\vec{p}_{T,1} \to \vec{p}_{T,1} - \vec{p}_{T,2}. \tag{3}$$

This also breaks the factorisation of the two emissions, as $p_{T,1}$ can vary quite significantly after the generation of another branching.

Although it is clear that the coherent formalism [8] implemented in the `Herwig7` [9] angular-ordered parton shower prevents the aforementioned subleading colour issue, the impact of the recoil scheme on the accuracy of the algorithm must be investigated. In these proceedings we summarise the findings of Ref. [10], restricting ourselves to the case of a massless final-state parton shower in $e^+e^- \to q\bar{q}$ events.

2 Interpretation of the Ordering Variable

In this section we present the main features of the `Herwig7` angular-ordered (final-state) parton shower, focusing on several possible interpretations of the ordering variable.

---

[1] This is a subleading colour issue, as $C_F \to C_A/2$ in the large-number-of-colours limit.
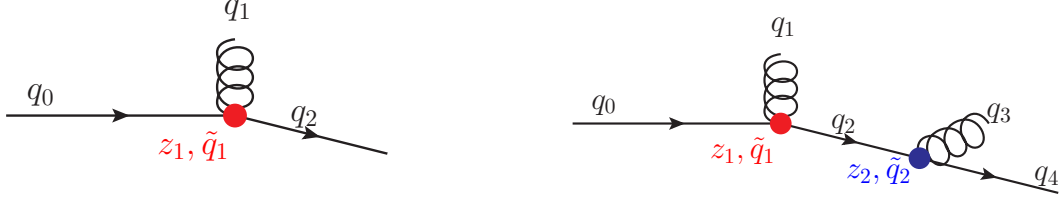
Figure 1: Single (left pane) and double (right pane) gluon emission from a quark line.

2.1 One Emission

We want to generate an emission collinear to the quark, as shown in the left pane of Fig. 1. We denote with p the quark momentum and with n a light-like vector parallel to the momentum of the anti-quark, which is colour connected to the quark in the original two-body configuration. The ordering variable can be equivalently expressed in terms of the transverse momentum ($p_{T,1}$), the virtuality of the emitting quark or the dot-product of the momenta of the emitted partons,

$$\tilde{q}^2 = \frac{p_{T,1}^2}{z_1^2(1-z_1)^2} = \frac{q_0^2}{z_1(1-z_1)} = \frac{2q_1 \cdot q_2}{z_1(1-z_1)}, \tag{4}$$

where z_1 is the light-cone momentum fraction carried by the emitted quark. If we define $\epsilon_1 = 1 - z_1$ we see that in the soft limit, $i.e.$ $\epsilon_1 \to 0$

$$|p_{T,1}| \approx \epsilon_1 \tilde{q}_1, \qquad y_1 \approx -\log \frac{\tilde{q}_1}{Q}, \tag{5}$$

where Q is the centre-of-mass energy, and the `Herwig7` emission probability approaches the correct limit

$$dP_{\text{Hw7}} = \frac{\alpha_s}{2\pi} \frac{d\tilde{q}^2}{\tilde{q}} C_F \frac{1 + z_1^2}{1 - z_1} dz_1 \to 2C_F \frac{\alpha_s}{\pi} \frac{d|p_{T,1}|}{|p_{T,1}|} dy_1. \tag{6}$$

2.2 Double Emission

We now want to generate the second gluon emission. If the second gluon is parallel to the anti-quark, the `Herwig7` algorithm identifies the $\bar{q}$ as the emitter, the auxiliary vector n is then chosen to be parallel to the original quark momentum and the generation of the emission is completely independent to the cascade originating from the quark.

If both gluons are collinear to the quark, then the requirement that they have a large rapidity separation suppresses the contribution arising from the $g \to gg$ splitting and both gluons will be generated from the quark line with colour factor C_F. The angular-ordering condition $\tilde{q}_2 < z_1 \tilde{q}_1$ dictates that the gluon with the smallest rapidity is emitted first, as shown in the right pane of Fig. 1. The first emitted quark now becomes off-shell gaining a virtuality $q_2^2 = z_2(1 - z_2)\tilde{q}_2^2$ and the relations in eq. (4) are no longer valid, as it is impossible to preserve simultaneously $p_{T,1}$, q_0^2 and $q_1 \cdot q_2$. The quantity that we preserve determines the recoil-scheme prescription.

2.2.1 Transverse-Momentum-Preserving Scheme

The original choice [11] was to preserve the transverse momentum so that we can always write

$$p_{T,i} = z_i(1 - z_i)\tilde{q}_i. \tag{7}$$

In the soft-collinear limit, the transverse momentum and the rapidity of each gluon always reproduce eq. (5). Thus, two gluons that are well separated in rapidity are effectively emitted independently as required.

To preserve the transverse momentum, the virtuality of the previous emitter must increase

$$q_0^2 = z_1(1 - z_1)\tilde{q}_1^2 \rightarrow z_1(1 - z_1)\tilde{q}_1^2 + \frac{z_2(1 - z_2)\tilde{q}_2^2}{z_1}. \tag{8}$$

This tends to produce too much hard radiation in the non-logarithmically-enhanced region of phase space, overpopulating the tail of certain distributions.

2.2.2   Virtuality-Preserving Scheme

It was then suggested that the virtuality should be preserved [12]: the transverse momentum of the first emission is then reduced

$$p_{T,1}^2 = (1 - z_1)\left[z_1^2(1 - z_1)\tilde{q}_1^2 - z_2(1 - z_2)\tilde{q}_2^2\right]. \tag{9}$$

This choice does not guarantee the existence of a positive solution. It is easy to see that, even if both emissions are soft, if the first one is much softer than the second one then there will be a negative solution, thus breaking the factorisation of multiple gluon emissions that are well separated in rapidity.

However, it was found that by setting the transverse momentum to 0 whenever a negative solution was encountered, the agreement with the experimental data is much better than in the p_T-preserving scheme.

2.2.3   Dot-Product-Preserving Scheme

Motivated by the desire to implement a scheme that is able to produce independent soft gluon emissions but does not overpopulate the non-logarithmically-enhanced regions, the last recoil scheme implemented [10] preserves the dot-product of the emitted partons and features intermediate properties between the p_T- and q^2-preserving schemes. After n emissions, the transverse momentum of the first gluon is modified to

$$p_{T,1}^2 = (1 - z_1)^2 \left[z_1^2\tilde{q}_1^2 - \sum_{i=2}^{n}(1 - z_i)\tilde{q}_i^2\right]. \tag{10}$$

Using the angular-ordering condition $z_i\tilde{q}_i > \tilde{q}_{i+1}$ it can be proven that $p_{T,1}$ cannot became negative. Furthermore, if all the emissions are soft

$$p_{T,1}^2 \rightarrow \epsilon_1^2(\tilde{q}_1^2 - \sum_{i=2}^{n}\epsilon_i\tilde{q}_i^2) \approx \epsilon_1^2\tilde{q}_1^2, \tag{11}$$

i.e. subsequent soft emissions do not affect the transverse momentum of the previous ones.

The virtuality of the first emitter still increases, however,

$$q_0^2 = z_1(1 - z_1)\tilde{q}_1^2 + \sum_{i=2}^{n} z_i(1 - z_i)\tilde{q}_i^2, \tag{12}$$

thus leading, again, to a poor description of the tails of certain distributions, although better than that provided by the p_T-preserving scheme.

To prevent the virtuality of the original quark and anti-quark from becoming too large, we can accept the event with a probability given by

$$r = \sqrt{1 - 2\left(\frac{q_q^2 + q_{\bar{q}}^2}{s}\right) + \left(\frac{q_q^2 - q_{\bar{q}}^2}{s}\right)^2}, \tag{13}$$

where $\sqrt{s}$ is the centre-of-mass energy, q_q^2 is the virtuality developed by the quark and $q_{\bar{q}}^2$ by the anti-quark. The factor r comes from the fact that the original underlying two-body phase space is reduced when the particles increase their mass. With the inclusion of this factor, the phase-space factorisation becomes exact. We can easily see that for soft-collinear emissions $r \rightarrow 1$, thus this veto does not affect the logarithmically-enhanced contributions but it can introduce, at most, power corrections.

3 LEP results

In this section we present the results of our simulations obtained with the `Herwig7` generator and compare them with data from LEP.

We begin by showing the thrust distribution (Fig. 2), which can be considered as a proxy for all shape distributions. The p_T- and dot-product preserving schemes overpopulate the tail of the distribution, which corresponds to the non-logarithmically-enhanced region of the phase space. Conversely, the q^2-preserving scheme leads to a worse description of the data for $1 - T \leq 1/3$. When we apply the phase space veto (*i.e.* we accept the event with probability given by eq. (13)), the behaviour of the dot-product scheme improves in the tail, leading the best overall agreement with the data.

The jet-resolution-parameter distribution is shown in the left panel of Fig. 3. As in the previous case, the q^2 scheme is the most accurate in the non-logarithmically-enhanced region (that corresponds to small values of $-\log(y_{23})$), while the p_T scheme provides the best description in the opposite limit, but gives the worst overall agreement. The dot-product scheme with the veto is similar to the q^2 scheme, while without the veto it leads to the best overall agreement with data.

From the right panel of Fig. 3 it can bee seen that none of the schemes are able to reproduce the bottom quark fragmentation function for large values of x_B. Issues related to multiple emissions from heavy quarks, as well as gluons splitting into heavy quarks, are currently subjects of further investigation.

4 Summary and Outlook

Motivated by Ref. [3)] we have investigated the impact that the choice of recoil scheme has on the accuracy of the `Herwig7` angular-ordered PS. We found that although the p_T-preserving recoil scheme ensures the independence of successive soft-collinear emissions well separated in rapidity, it produces too much radiation in the non-logarithmically-enhanced region of phase space. The q^2-preserving scheme, on the other hand, avoids overpopulating this region of phase space but breaks the independence of successive emissions and therefore loses logarithmic accuracy. We introduced the dot-product-preserving scheme as an attempt to retain the best features of both schemes, but it still somewhat overpopulates non-logarithmically-enhanced region of phase space. To ameliorate this we went on to introduce a phase-space veto that suppresses events with large-virtuality partons. In these proceedings we did not mention the effect of quark masses, although this is considered to some extent in Ref. [10)] and is an ongoing area of research we hope to address further in future publications.
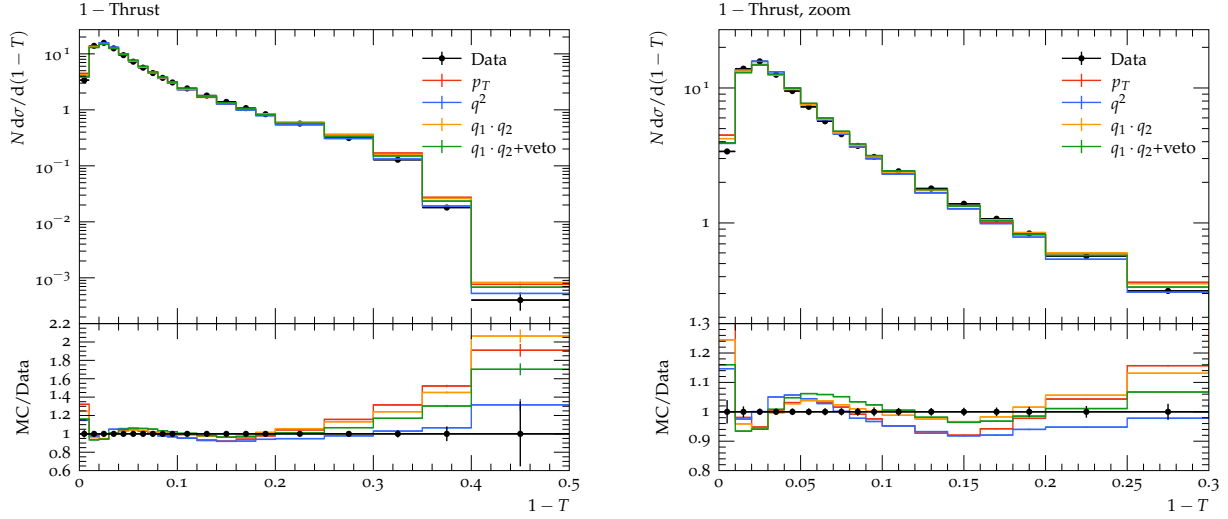
Figure 2: The thrust distribution at the Z-pole compared with data from the DELPHI [13] experiment. The right panel gives an expanded view of the same for small values $1 - T$.
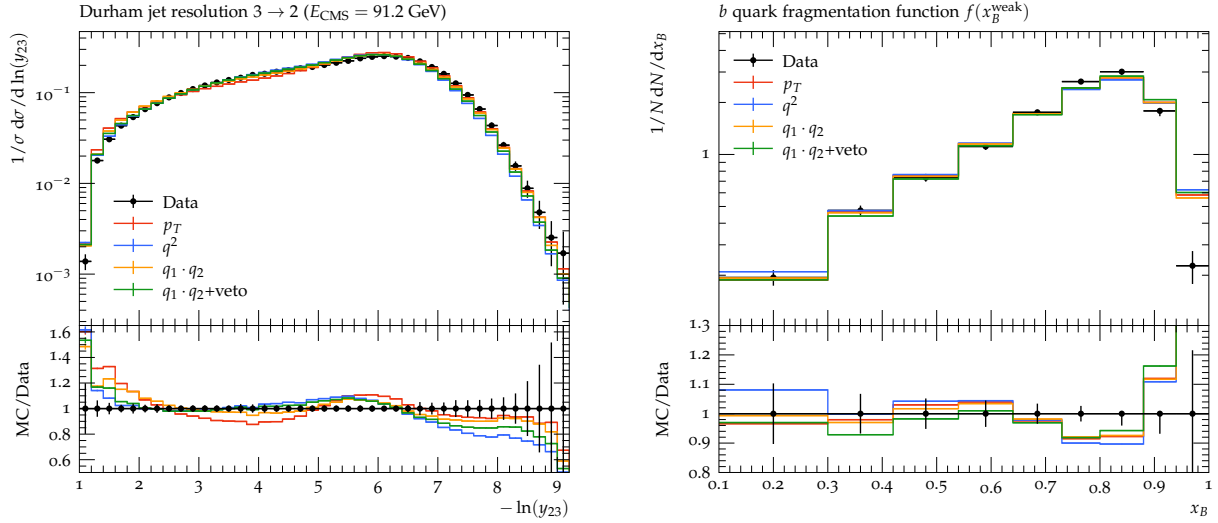

Figure 3: In the left panel the 3-to-2 jet resolution parameter for the Durham algorithm at the Z-pole compared with data from the ALEPH [14] experiment. In the right panel the fragmentation function of weakly-decaying B-hadrons compared with data from DELPHI [15].

5   Acknowledgements

studentship.

References

1. S. Catani, S. Dittmaier and Z. Trocsanyi, Phys. Lett. B **500** (2001) 149 doi:10.1016/S0370-2693(01)00065-X [hep-ph/0011222].

2. S. Catani, B. R. Webber and G. Marchesini, Nucl. Phys. B **349** (1991) 635. doi:10.1016/0550-3213(91)90390-J

3. M. Dasgupta, F. A. Dreyer, K. Hamilton, P. F. Monni and G. P. Salam, JHEP **1809**, 033 (2018) doi:10.1007/JHEP09(2018)033 [arXiv:1805.09327 [hep-ph]].

4. T. Sjöstrand and P. Z. Skands, Eur. Phys. J. C **39** (2005) 129 doi:10.1140/epjc/s2004-02084-y [hep-ph/0408302].

5. T. Sjöstrand *et al.*, Comput. Phys. Commun. **191** (2015) 159 doi:10.1016/j.cpc.2015.01.024 [arXiv:1410.3012 [hep-ph]].

6. S. Höche and S. Prestel, Eur. Phys. J. C **75** (2015) no.9, 461 doi:10.1140/epjc/s10052-015-3684-2 [arXiv:1506.05057 [hep-ph]].

7. T. Gleisberg, S. Hoeche, F. Krauss, M. Schonherr, S. Schumann, F. Siegert and J. Winter, JHEP **0902**, 007 (2009) doi:10.1088/1126-6708/2009/02/007 [arXiv:0811.4622 [hep-ph]].

8. G. Marchesini and B. R. Webber, Nucl. Phys. B **238** (1984) 1. doi:10.1016/0550-3213(84)90463-2

9. M. Bahr *et al.*, Eur. Phys. J. C **58** (2008) 639 doi:10.1140/epjc/s10052-008-0798-9 [arXiv:0803.0883 [hep-ph]].

10. G. Bewick, S. Ferrario Ravasio, P. Richardson and M. H. Seymour, arXiv:1904.11866 [hep-ph].

11. S. Gieseke, P. Stephens and B. Webber, JHEP **0312**, 045 (2003) doi:10.1088/1126-6708/2003/12/045 [hep-ph/0310083].

12. D. Reichelt, P. Richardson and A. Siodmok, Eur. Phys. J. C **77** (2017) no.12, 876 doi:10.1140/epjc/s10052-017-5374-8 [arXiv:1708.01491 [hep-ph]].

13. P. Abreu *et al.* [DELPHI Collaboration], Z. Phys. C **73** (1996) 11. doi:10.1007/s002880050295

14. A. Heister *et al.* [ALEPH Collaboration], Eur. Phys. J. C **35** (2004) 457. doi:10.1140/epjc/s2004-01891-4

15. J. Abdallah *et al.* [DELPHI Collaboration], Eur. Phys. J. C **71** (2011) 1557 doi:10.1140/epjc/s10052-011-1557-x [arXiv:1102.4748 [hep-ex]].

MODELING DOUBLE PARTON SCATTERING AT LHC

Giulia Pancheri

INFN Frascati National Laboratories, 00044 Frascati, Italy

Agnes Grau

Departamento de Fisica Teorica y del Cosmos, Universidad de Granada, 18071 Granada, Spain

Simone Pacetti and Yogendra N. Srivastava

Department of Physics & Geology, University of Perugia, 06123 Perugia, Italy

Abstract

We examine present data for double parton scattering at LHC and discuss their energy dependence from its earliest measurements at the Intersecting Storage Rings (ISR). Different models for the effective cross-section are considered and their behavior studied for a variety of selected final states. We point out that data for $pp \rightarrow 4\ jets$ or $pp \rightarrow\ quarkonium\ pair$ indicate σ_{eff} to increase with energy. We compare this set of data with different models, including one inspired by our soft gluon resummation model for the impact parameter distribution of partons.

1 Introduction

Double parton scattering in hadron collisions has been searched for and measured since more than 30 years. Recently, the ATLAS collaboration [1] has examined all existing data for Double Parton Scattering events, from ISR to LHC 13 TeV, and a value for the effective cross-section has been extracted. For a process of the type $pp \rightarrow A + B + X$ the following expression was used

$$\sigma_{DPS}^{AB} = \frac{k}{2}\frac{\sigma_{SPS}^A\sigma_{SPS}^B}{\sigma_{eff}} \tag{1}$$

with k a symmetry factor to indicate identical or different final states, and σ_{eff} interpreted as the overlap area (in the transverse plane) between the interacting partons.

In this note, the energy dependence of σ_{eff} will be discussed in light of a few models and a rather general theorem. We shall start by presenting in Sect. 2 the general framework for multi-parton scattering as recently presented by D'Enterria in [2] and then apply this formalism to show that, in general, σ_{eff} cannot be asymptotically a constant.

In Sect. 3 and Sect. 4 we consider various strategies for the calculation of σ_{eff}: a geometrical one in which σ_{eff} is interpreted as the area occupied by the partons involved in the collision and thus obtain it from modelling the impact parameter distribution of partons, another one in which the area is directly obtained as the Fourier transform of the scattering amplitude. These different strategies may lead to different energy dependence, as we shall see.

2 Matter distribution in a hadron

Theoretically multi-parton scattering (MPS) has been of great interest [3, 4, 5, 6, 7, 8, 9]. A key element in an analysis of an n-parton process (NPS) with final particle states $(a_1, a_2, ...a_n)$ in terms of the single-parton processes (SPS) is the role played by an *effective parton cross-section* defined as follows:

$$\sigma^{NPS}_{h_1 h_2 \to a_1, a_2, ... a_n} = \left[\frac{m}{\Gamma(n+1)} \frac{\sigma^{SPS}_{h_1 h_2 \to a_1} \sigma^{SPS}_{h_1 h_2 \to a_2} ..... \sigma^{SPS}_{h_1 h_2 \to a_n}}{(\sigma_{eff, NPS})^{n-1}} \right]. \tag{2}$$

As Eq. (2) deals with *probabilities* rather than *probability amplitudes*, it is clear that the description is *semi-classical* and ignores any correlation between production of particles. On the other hand, the degeneracy factor m in these equations, to be defined momentarily, does distinguish between identical and non-identical particle states and thus must be thought as of quantum-mechanical origin. For a two-parton process (DPS) (say, a_1, a_2), $m = 1$ if the two particle states are identical $(a_1 = a_2)$ and $m = 2$ if they are different $(a_1 \neq a_2)$. For a three particle process (TPS), $m = 1$ if $a_1 = a_2 = a_3$; $m = 3$ if $a_1 = a_2$, $m = 6$ if $a_1 \neq a_2 \neq a_3$ and so on.

Under a set of *reasonable* hypothesis of factorization of parallel and transverse momenta, the quantity of interest σ^{NPS}_{eff} is approximated in terms of the normalized *single* parton distribution or, generally a matter distribution $T(\mathbf{b})$ inside a hadron in impact-parameter space, as follows

$$\int (d^2 \mathbf{b}) \, T(\mathbf{b}) = 1; \quad \Sigma^{(n)} \equiv \int (d^2 \mathbf{b}) \, T^n(\mathbf{b}); \quad \sigma^{NPS}_{eff} = [\Sigma^{(n)}]^{-1/(n-1)} \tag{3}$$

Before turning our attention to the crucial input of the single-parton *overlap function* we present here an argument as to why σ_{eff} cannot - in general, i.e., for all types of final states in DPS or MPS scattering - be a constant.

In particular, we shall now show that, if $\sigma_{eff}(s)$ approaches a constant as $s \to \infty$, then *all*, multi-parton cross-sections $\sigma^n_{a_1; ... a_n}(s)$ must also approach some constants asymptotically, under the very mild hypothesis that $\sigma^{n+1}_{a_1; ... a_{n+1}}(s) < \sigma^n_{a_1; ... a_n}(s)$ for $a_i \neq a_j$. Consider in fact Eq.(9) of [2]:

$$\sigma^{(2)}_{a_1; a_2}(s) = \left(\frac{m}{2} \right) \frac{\sigma^{(1)}_{a_1}(s) \sigma^{(1)}_{a_2}(s)}{\sigma_{eff}(s)}; \quad m = 2 \text{ if } a_1 \neq a_2; \quad m = 1 \text{ if } a_1 = a_2, \tag{4}$$

in an obvious notation. Let

$$(i) \; \sigma_{a_i}(s) \to L_i(s), \text{ where } L_i(s) \text{ increase with } s; \quad \text{and} \;\; (ii) \; \sigma_{eff}(s) \to \text{a constant.} \tag{5}$$

Then, it follows from (i) and (ii) that

$$\text{for } a_1 \neq a_2: \; \sigma^{(2)}_{a_1; a_2}(s) \propto L_1(s) L_2(s), \text{ but then } \left[\frac{\sigma^{(2)}_{a_1; a_2}(s)}{\sigma^{(1)}_{a_1}(s)} \right] \propto L_2(s) \text{ increases with } s \tag{6}$$

and thus it is not bounded by a constant, thereby violating the initial hypothesis. Hence, $L_2(s)$ cannot increase with s, but must be bounded by a constant. We can repeat the proof by exchanging $a_1 \leftrightarrow a_2$

and show that also $L_1(s)$ must be a constant. Ergo, also $\sigma^{(2)}_{a_1;a_2}(s)$ must go to a constant as $s \to \infty$. Extensions of the above result to the identical case $(a_1 = a_2)$ and for $n = 3, 4, ...$ are left as exercises to the reader. The proof is especially easy if Eqs.(3) and (7) of [2] are recalled. In the next section, we turn our attention to $T(\mathbf{b})$.

3   The BN model for σ_{eff}

In this section we examine a model for σ_{eff}, in which the impact-parameter distribution of partons is obtained from soft-gluon resummation. As we shall see later, this model reproduces the order of magnitude of σ_{eff} but bears different energy trends depending on the parton distribution function (PDF) used. A suitable model for a normalized $T(\mathbf{b})$ - albeit with a different name $A(\mathbf{b})$ - has been the object of our attention for over two decades and detailed references can be found in our review [10]. We start with a model in which the area occupied by the partons involved in parton scattering can be related to soft-gluon resummation. In this model for the total cross-section, the energy behaviour of the total and inelastic cross-sections are obtained in the eikonal formalism, with *mini-jets*, i.e. partons with $p_t > p_{tmin} \approx 1.1$-1.5 GeV, to drive the rise and soft-gluon resummation to tame it. The impact-parameter distribution is determined by the Fourier transform of the k_t distribution of soft gluons emitted during semi-hard parton scattering. Namely, the normalized matter distribution in impact-parameter space, $T(\mathbf{b})$ in this model, is given by:

$$A(b, s) = N(s)\mathcal{F}[\Pi(\mathbf{K}_t)] = N(s) \int d^2\mathbf{K}_t \int d^2\mathbf{b} \, e^{i\mathbf{K}_t \cdot \mathbf{b}} e^{-h(b,s)}; \quad h(b,s) = \int_0^{qmax} d^3\bar{n}(k)[1 - e^{-i\mathbf{k_t} \cdot \mathbf{b}}], \quad (7)$$

where the overall distribution $\Pi(\mathbf{K}_t)$ is obtained by the resummation of soft gluons emitted with average number $\bar{n}(\mathbf{k})$. The above expressions are semi-classical and can be obtained by summing all the gluons emitted with momentum $\mathbf{k}_t$ in a Poisson-like distribution. The effect of imposing energy-momentum conservation on all possible distributions results in the factor among square brackets in Eq. (7). Such a factor allows to integrate in k_t down to zero, if $\bar{n}(k)$ is no more singular than an inverse power. While this is true in QED, for gluons this is not possible. In our model for the total cross-section, which is related to the large-distance behaviour of the interaction, the impact-parameter distribution is related to very small k_t values. This implies including very small values of k_t, even lower than Λ_{QCD}, usually not included in the resummation or "lumped" into an intrinsic transverse momentum. In order to evaluate $h(b, s)$ down to such low values, we proposed a phenomenological approximation for $\alpha_s(k_t \to 0)$, namely our phenomenological choice is

$$\alpha_s(k_t \to 0) \propto \left[\frac{k_t}{\Lambda_{QCD}}\right]^{-2p}; \quad \alpha_s(k_t \gg \text{QCD scale}) = \alpha_s^{asym-free}(k_t) = \frac{1}{b_0 \ln\left(k_t^2/\Lambda_{QCD}^2\right)} \quad (8)$$

with $1/2 < p < 1$. Our model for σ_{eff}, using $A(b, s)$ from Eq. (7) is given by:

$$\sigma_{eff}(s) = \frac{\left[\int d^2\mathbf{b} \, e^{-h(b,s)}\right]^2}{\int d^2\mathbf{b} e^{-2h(b,s)}} \quad (9)$$

We have indicated that function $h(b, s)$ depends upon the c.m.s energy of the collision, which will then be true also for $A(b, s)$. Because of the minimum transverse momentum p_{tmin} allowed to the minijet cross-section, q_{max} will depend also on p_{tmin}. Through an averaging procedure [11], one can obtain $\langle q_{max} \rangle$ as a function of $\sqrt{s}$, PDF and p_{tmin}. The results from this resummation can then be used to model the eikonal function and calculate inclusive quantities such as total and inelastic cross-sections. In
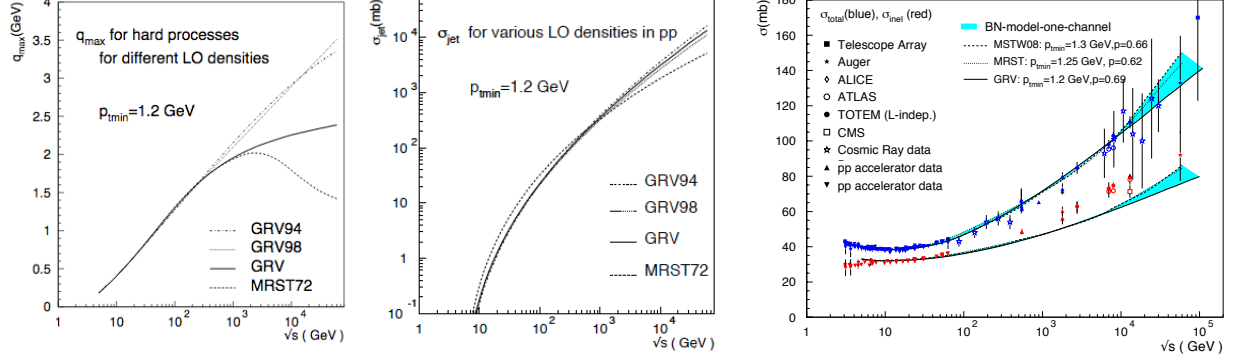
Figure 1: For a given set of PDFs with corresponding p_{tmin}, left and center plots respectively show the maximum transverse momentum allowed to soft gluons emitted by partons participating to a semi-hard collision and the behaviour of the minijet cross-section used in the model from [12]. The figure at right shows the corresponding description of total and Non Single Diffractive inelastic cross-section with appropriate choices of the singularity parameter p.

our model, soft and semi-hard gluons contribute to the observed rise of the total cross-section with soft gluons tempering the fast rise (with energy) due to the mini-jet cross section. In Fig. 1 results for $\langle q_{max} \rangle$ and $\sigma_{jet}(\sqrt{s}, p_{tmin})$ are shown for different LO PDFs, together with the total or inelastic cross-section corresponding to the indicated parameter choice, including updated PDFs, such as MSTW. One should notice that the energy behaviour of $\langle q_{max} \rangle$ is different for different densities, as the one of σ_{jet}, but they compensate in the predicted behaviour of the total cross-sections, which both smoothly rise in accordance with the Froissart bound, as shown in [13]. This will not be true for σ_{eff}, as the model produces an energy dependence of σ_{eff} which correlates only with the energy dependence of q_{max}, i.e. the upper limit of the integration over the soft-gluon spectrum, so that if q_{max} increases with $\sqrt{s}$, then σ_{eff} decreases with $\sqrt{s}$ and vice-versa.

4   The elastic amplitude and σ_{eff} energy dependence

According to [2] and following the summary presented in Sec. 2:

$$\int (d^2\mathbf{b})\, T(\mathbf{b}) = 1; \quad \Sigma^{(2)} \equiv \int (d^2\mathbf{b})\, T^2(\mathbf{b}); \quad \sigma_{eff}^{DPS} = \frac{1}{\Sigma^{(2)}} \tag{10}$$

The above equation is obtained considering factorization between the hard jet cross-sections and the impact parameter distribution of the involved partons, whose $\mathcal{F}$-transform gives the transverse momentum of partons involved in the hard cross-section. This model has a theoretical basis, but one needs an expression for $T(\mathbf{b})$ to use. The derivation in D'Enterria gives the following expression for T($\mathbf{b}$):

$$T(\mathbf{b}) = \int d^2\mathbf{b_1}\, f(\mathbf{b_1}) f(\mathbf{b} - \mathbf{b_1}), \tag{11}$$

where $f(\mathbf{b})$ describes the transverse parton density of the hadron.

Apart from phenomenological fits of the type $\exp[-(b/\text{scale})^m]$, which have problems with analyticity if $m < 1$ [13], let us consider what is at the root of the formalism being considered regarding the transverse-spatial (in short, the b) distribution adopted in Eq.(11). Also, we can recall the lessons learnt

from analyticity of hadronic form factors and the elastic amplitudes.

One begins with $f(\mathbf{b})$, a normalized b-density function and its Fourier transform, namely the transverse-momentum distribution $\hat{f}(\mathbf{q})$ for a single parton, as follows:

$$f(\mathbf{b}) = \int \frac{d^2\mathbf{q}}{(2\pi)^2} \, e^{i\mathbf{b}\cdot\mathbf{q}} \, \hat{f}(\mathbf{q}); \quad \hat{f}(\mathbf{q}) = \int (d^2\mathbf{b}) \, e^{-i\mathbf{b}\cdot\mathbf{q}} \, f(\mathbf{b}); \quad \hat{f}(\mathbf{q}=\mathbf{0}) = \int (d^2\mathbf{b}) \, f(\mathbf{b}) = 1. \tag{12}$$

Let us consider this parton distribution first in momentum space and then in b-space. The simplest case to start with is that of collinear partons. The probability density that two partons are at the same momentum transfer is given by:

$$\hat{T}(\mathbf{q}) \equiv [\hat{f}(\mathbf{q})]^2, \quad \text{with} \quad \hat{T}(\mathbf{q}=\mathbf{0}) = 1, \tag{13}$$

whose Fourier transform $T(\mathbf{b})$ reads

$$T(\mathbf{b}) \equiv \int \frac{d^2\mathbf{q}}{(2\pi)^2} e^{i\mathbf{b}\cdot\mathbf{q}} \hat{T}(\mathbf{q}) = \int \frac{d^2\mathbf{q}}{(2\pi)^2} e^{i\mathbf{b}\cdot\mathbf{q}} [\hat{f}(\mathbf{q})]^2 = \int (d^2\mathbf{b}_1) \, f(\mathbf{b}_1) f(\mathbf{b}-\mathbf{b}_1), \tag{14}$$

which exactly reproduces Eq.(11). Also, by virtue of Eqs.(12) and (13), $T(\mathbf{b})$ is properly normalized, viz.,

$$\int (d^2\mathbf{b}) \, T(\mathbf{b}) = \int d^2(\mathbf{b}) \int (d^2\mathbf{b}_1) \, f(\mathbf{b}_1) f(\mathbf{b}-\mathbf{b}_1) = [\int (d^2\mathbf{b}) \, f(\mathbf{b})]^2 = 1; \quad \hat{T}(\mathbf{q}=\mathbf{0}) = \int (d^2\mathbf{b}) T(\mathbf{b}) = 1. \tag{15}$$

Now to some considerations about the effective cross-section $\sigma_{eff}(s)$, which for this simple identical parton model shall be taken to be (with a factor of a $1/2$)

$$2\sigma_{eff}(s) = \left[\frac{1}{\int (d^2\mathbf{b}) T^2(\mathbf{b})} \right], \tag{16}$$

but, by virtue of Eqs.(13) *et sec*, it follows that

$$\int (d^2\mathbf{b}) T^2(\mathbf{b}) = \int \frac{d^2\mathbf{q}}{(2\pi)^2} [\hat{f}(\mathbf{q})]^2 [\hat{f}(-\mathbf{q})]^2 = \int \frac{d^2\mathbf{q}}{(2\pi)^2} [\hat{f}(\mathbf{q})]^4 \tag{17}$$

Since, $\hat{f}(\mathbf{q}=\mathbf{0}) = 1$, at first sight, it may appear reasonable to assume that it is the elastic form factor. So, for this form factor assuming the dipole form, we have

$$\hat{f}(\mathbf{q}) = \frac{1}{[1+(q^2/t_o(s))]^2}; \quad \sigma_{eff}^{(el)}(s) = \frac{1}{\int \frac{d^2\mathbf{q}}{(2\pi)^2} \frac{1}{[1+(q^2/t_o(s))]^8}} = \left[\frac{14\pi}{t_o(s)} \right]. \tag{18}$$

To get a simple estimate, we can employ the result from a fit to the elastic differential cross-section, discussed in [14]. At 13 TeV, our estimate for the elastic scattering form-factor value (work in preparation) is $t_o(13 \text{ TeV}) \approx 0.6 \text{ GeV}^2$, leading to

$$\sigma_{eff}^{(el)}(13 \text{ TeV}) \approx 28.6 \text{ mb}. \tag{19}$$

We notice that the value predicted for σ_{eff} appears large compared to present data [1]. Of course, what the above naive calculation might be telling us is that $\hat{f}(\mathbf{q})$ is related not so much to the elastic, but to an "inelastic form factor". Counting four protons being present in elastic events, whereas only two (initial) protons being present in a true "break up" inelastic event, we expect only the second power and not the fourth power of the elastic form factor to appear in Eq. (18). If so,

$$\sigma_{eff}^{(inel)}(s) = \frac{1}{\int \frac{d^2\mathbf{q}}{(2\pi)^2} \frac{1}{[1+(q^2/t_o(s))]^4}} = \frac{6\pi}{t_o(s)}; \quad \sigma_{eff}^{inel}(13 \text{ TeV}) \approx 12.3 \text{ mb}, \tag{20}$$
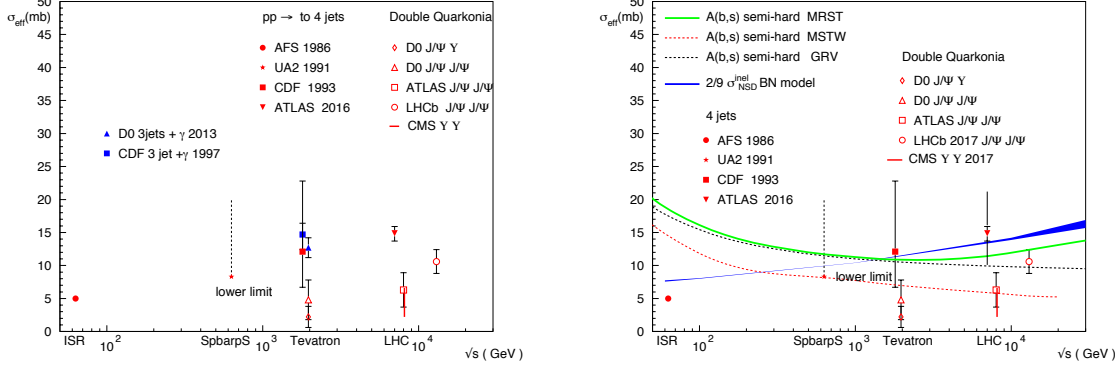
Figure 2: In the left panel, existing DPS data as described in the text from Axial Field Spectrometer (AFS), [15], UA2 [16], CDF 1993 [17] for $\bar{p}p \to 4\ jets$ and ATLAS at $\sqrt{s} = 7$ TeV [18] for $pp \to 4\ jets$. We also have plotted CDF 1997 [19] and D0 [20] for $\bar{p}p \to \gamma\ 3\ jets$, D0 [21] for $\bar{p}p \to J/\Psi\ J/\Psi$, ATLAS [22] and LHCb for $pp \to J/\Psi\ J/\Psi$ [23], CMS for $pp \to \Upsilon\ \Upsilon$ [24], D0 for $\bar{p}p \to J/\Psi\ \Upsilon$ [25]. At right, comparison of $\bar{p}/p\ p \to 4\ jets$ or with $\bar{p}/p\ p \to quarkonia\ pair$ with two models described in the text.

a bit closer to the phenomenological value estimated by exploration of the ATLAS compilation [1].

In this model the energy dependence of σ_{eff} proceeds from that of the parameter $t_0(s)$. We notice here that in [14] we have shown that the presently available data for the differential elastic cross-section as well as the total cross-section, i.e. the imaginary part of the forward elastic amplitude, can be described rather accurately through an expression which includes an energy-dependent form factor. In this model, $t_0(s)$ decreases with energy, hence this model would predict $\sigma_{eff}(s)$ increasing with $\sqrt{s}$. We now turn to a discussion of the data and a comparison with the models we have just illustrated.

5 About data and models

Available data not only span a very large energy range, but, as compiled by ATLAS, refer to very different types of final states. This may indeed generate confusion since parton distributions, hence the calculation of σ_{eff}, differ according to whether the initial state be mostly driven by gluon-gluon scattering or imply valence quarks as well. Thus we have focused on similarly homogenous final states and show them in the left panel of Fig. 2. The figure may indicate the following trends:

- for processes dominated by gluon-gluon scattering, such as $\bar{p}/p\ p \to 4$ jets and $\bar{p}/p\ p \to J/\Psi\ J/\Psi$, $\sigma_{eff}(\sqrt{s})$ grows with $\sqrt{s}$, although the scale is different, with $\sigma_{eff}^{singlet}(\sqrt{s}) \approx \frac{1}{3}\sigma_{eff}(\sqrt{s})^{all}$

- for processes in which at least one of the final state particles must originate from a valence quark, as in 3 jets $+ \gamma$, the effective cross-section appears to be decreasing, as seen in the left panel of Fig. 2 (full blue symbols).

In the right-hand panel we have compared the selected sets of data *vs.* two models: the BN-inspired soft-gluon resummation model described in Sect. 3, and a model based on the ansatz that all inclusive cross-sections rise. This model would be adequate to describe the case of gluon-initiated processes, less so when valence quarks initiate the process, as it is likely to be the case for the 3 jets $+ \gamma$ final state. Our

ansatz, to describe σ_{eff} for $\bar{p}/p\ p \to 4$ jets, is the following:

$$\sigma_{eff} \propto \sigma_{inel}^{NSD} \tag{21}$$

We then use the description of σ_{inel}^{NSD} from the model of [14] and plot it as a blue band in the right hand panel of Fig. 2, with an arbitrarily chosen factor 2/9 for normalization to the data.. We consider the two different cases of GRV or MSTW densities (MRST densities for total and inelastic cross-section are in good agreement with results from MSTW, as shown in the right hand panel of Fig. 1).

For the model which uses $A(b)$ from soft-gluon resummation (Sect.3) we see that at LHC energies the model gives good agreement with data, but the trend with energy is different.

In summary for $pp \to 4$ jets:

- the impact parameter description as from Sect. 3 (green, red and dotted curves in Fig. 2) gives an absolute overall normalization of LHC data in good agreement with the plotted data, but is inconclusive as far as the energy dependence is concerned;

- the scattering amplitude *cum* form factor model from Sect. 4 would also reproduce the correct order of magnitude at LHC, and may indicate a rising σ_{eff} from ISR to LHC;

- an empirical description from the NSD inelastic cross-section of [26] would reproduce a rising energy trend from ISR to LHC.

References

1. Morad Aaboud et al. Study of the hard double-parton scattering contribution to inclusive four-lepton production in pp collisions at $\sqrt{s} = 8$ TeV with the ATLAS detector. *Phys. Lett.*, B790:595–614, 2019.

2. David d'Enterria and Alexander Snigirev. Double, triple, and n-parton scatterings in high-energy proton and nuclear collisions. *Adv. Ser. Direct. High Energy Phys.*, 29:159–187, 2018.

3. N. Paver and D. Treleani. Multiple Parton Interactions and Multi - Jet Events at Collider and Tevatron Energies. *Phys. Lett.*, 146B:252–256, 1984.

4. L. Ametller, N. Paver, and D. Treleani. Possible Signature of Multiple Parton Interactions in Collider Four Jet Events. *Phys. Lett.*, 169B:289–292, 1986.

5. Torbjorn Sjostrand and Maria van Zijl. A Multiple Interaction Model for the Event Structure in Hadron Collisions. *Phys. Rev.*, D36:2019, 1987.

6. Mark Strikman and Werner Vogelsang. Multiple parton interactions and forward double pion production in pp and dA scattering. *Phys. Rev.*, D83:034029, 2011.

7. Michael H. Seymour and Andrzej Siodmok. Extracting $\sigma_{\text{effective}}$ from the LHCb double-charm measurement. 2013.

8. Paolo Bartalini and Jonathan Richard Gaunt. Multiple Parton Interactions at the LHC. *Adv. Ser. Direct. High Energy Phys.*, 29:pp.1–450, 2018.

9. Markus Diehl and Jonathan R. Gaunt. Double parton scattering theory overview. *Adv. Ser. Direct. High Energy Phys.*, 29:7–28, 2018.

10. Giulia Pancheri and Y. N. Srivastava. Introduction to the physics of the total cross-section at LHC. *Eur. Phys. J.*, C77(3):150, 2017.

11. R. M. Godbole, A. Grau, G. Pancheri, and Y. N. Srivastava. Soft gluon radiation and energy dependence of total hadronic cross-sections. *Phys. Rev.*, D72:076001, 2005.

12. D. A. Fagundes, A. Grau, G. Pancheri, Y. N. Srivastava, and O. Shekhovtsova. Soft edge of hadron scattering and minijet models for the total and inelastic pp cross sections at LHC and beyond. *Phys. Rev.*, D91(11):114011, 2015.

13. Agnes Grau, Rohini M. Godbole, Giulia Pancheri, and Yogendra N. Srivastava. Soft Gluon k(t)-Resummation and the Froissart bound. *Phys. Lett.*, B682:55–60, 2009.

14. Daniel A. Fagundes, Agnes Grau, Simone Pacetti, Giulia Pancheri, and Yogendra N. Srivastava. Elastic pp scattering from the optical point to past the dip: An empirical parametrization from ISR to the LHC. *Phys. Rev.*, D88(9):094019, 2013.

15. T. Akesson et al. Double Parton Scattering in pp Collisions at $\sqrt{s}$ = 63-GeV. *Z. Phys.*, C34:163, 1987.

16. J. Alitti et al. A Study of multi - jet events at the CERN anti-p p collider and a search for double parton scattering. *Phys. Lett.*, B268:145–154, 1991.

17. F. Abe et al. Study of four jet events and evidence for double parton interactions in $p\bar{p}$ collisions at $\sqrt{s}$ = 1.8 TeV. *Phys. Rev.*, D47:4857–4871, 1993.

18. Morad Aaboud et al. Study of hard double-parton scattering in four-jet events in pp collisions at $\sqrt{s}$ = 7 TeV with the ATLAS experiment. *JHEP*, 11:110, 2016.

19. F. Abe et al. Double parton scattering in $\bar{p}p$ collisions at $\sqrt{s}$ = 1.8TeV. *Phys. Rev.*, D56:3811–3832, 1997.

20. Victor Mukhamedovich Abazov et al. Double Parton Interactions in $\gamma + 3$ Jet and $\gamma + b/cjet + 2$ Jet Events in $p\bar{p}$ Collisions at $\sqrt{s}$ = 1.96 TeV. *Phys. Rev.*, D89(7):072006, 2014.

21. Victor Mukhamedovich Abazov et al. Observation and Studies of Double J/ψ Production at the Tevatron. *Phys. Rev.*, D90(11):111101, 2014.

22. Morad Aaboud et al. Measurement of the prompt J/ ψ pair production cross-section in pp collisions at $\sqrt{s}$ = 8 TeV with the ATLAS detector. *Eur. Phys. J.*, C77(2):76, 2017.

23. Roel Aaij et al. Measurement of the J/ψ pair production cross-section in pp collisions at $\sqrt{s}$ = 13 TeV. *JHEP*, 06:047, 2017. [Erratum: JHEP10,068(2017)].

24. Vardan Khachatryan et al. Observation of Υ(1S) pair production in proton-proton collisions at $\sqrt{s}$ = 8 TeV. *JHEP*, 05:013, 2017.

25. Victor Mukhamedovich Abazov et al. Evidence for simultaneous production of J/ψ and Υ mesons. *Phys. Rev. Lett.*, 116(8):082002, 2016.

26. Andrea Achilli, Rohini M. Godbole, Agnes Grau, Giulia Pancheri, Olga Shekhovtsova, and Yogendra N. Srivastava. Total and inelastic cross-sections at LHC at $sqrts = 7 - TeV$ and beyond. *Phys. Rev.*, D84:094009, 2011.

HEAVY FLAVOURS IN RELATIVISTIC NUCLEAR COLLISIONS: RECENT DEVELOPMENTS

Andrea Beraudo
INFN - Sezione di Torino, Via Pietro Giuria 1 - 10125 Torino

Abstract

Transport calculations represent the major tool to simulate the modifications induced by the presence of a hot-deconfined medium on the production of heavy-flavour particles in high-energy nuclear collisions. After a brief description of the approach and of the major achievements in its phenomenological applications we discuss some recent developments. In particular we focus on observables arising from event-by-event fluctuations in the distribution of deposited energy (odd flow harmonics, event-shape engineering) and from the tilting of the initial geometry with respect to the beam axis (directed flow), with a possible role played by the strong magnetic field generated by the spectator nucleons.

1 Introduction

Heavy-flavour particles play a peculiar role in probing the hot-deconfined matter produced in relativistic heavy-ion collisions. Soft observables (light hadrons of low transverse momentum) provide information on the collective behaviour of the medium formed after the collision; they are nicely described by hydrodynamic calculations, assuming as a working hypothesis to deal with a system close to local thermal equilibrium. The suppression of the production of jets and high-p_T particles tells us that a quite opaque medium is formed in the collisions: its description requires to model the energy loss of high-energy partons in the hot plasma. Heavy-flavour particles, arising from the hadronization of heavy quarks produced in initial hard events and having crossed the fireball during its whole evolution, require to employ a more general tool, allowing one to model their asymptotic approach to local thermal equilibrium with the medium: such a tool is represented by transport calculations, which we are going to briefly describe. Actually, since the fireball undergoes a rapid expansion and has a finite lifetime, one does not expect charm and beauty quarks to reach full kinetic equilibrium with the medium: this fact, however, has

the potential to provide an estimate of the value of the transport coefficients of the medium, for which otherwise one would just get a lower/upper bound.

2 Transport calculations

The starting point of any transport calculation is the relativistic Boltzmann equation. Actually, in most numerical implementations, the latter is approximated as a more tractable Langevin equation, assuming that the heavy-quark interaction with the medium is dominated by multiple uncorrelated soft scatterings. One has then

$$\Delta \vec{p}/\Delta t = -\eta_D(p)\vec{p} + \vec{\xi}(t). \tag{1}$$

Eq. (1) provides a recipe to update the heavy quark momentum in the time-step Δt through the sum of a deterministic friction force and a random noise term specified by its temporal correlator

$$\langle \xi^i(\vec{p}_t)\xi^j(\vec{p}_{t'})\rangle = b^{ij}(\vec{p}_t)\delta_{tt'}/\Delta t \quad \text{with} \quad b^{ij}(\vec{p}) \equiv \kappa_{\parallel}(p)\hat{p}^i\hat{p}^j + \kappa_{\perp}(p)(\delta^{ij} - \hat{p}^i\hat{p}^j). \tag{2}$$

Following the heavy-quark dynamics in the medium requires then the knowledge of three transport coefficients representing the transverse/longitudinal ($\kappa_{\perp/\parallel}$) momentum broadening and the drag (η_D) received from the medium. Actually, the above coefficients are not independent, but are related by the Einstein fluctuation-dissipation relation, which ensures the asymptotic approach of the heavy quarks to thermal equilibrium.

Various transport calculations applied to heavy-flavour production in nuclear collisions can be found in the literature, essentially differing in the choice of transport coefficients to insert into Eq. (1). The challenge for the above models is to consistently reproduce various experimental observables, like the momentum and angular distributions of the produced heavy-flavour hadrons. The latter display sizable modifications with respect to proton-proton collisions. In particular, important medium effects are captured by two quantities, the nuclear modification factor R_{AA} and the elliptic-flow coefficient v_2, defined as

$$R_{\mathrm{AA}} \equiv \frac{(dN/dp_T)_{\mathrm{AA}}}{\langle N_{\mathrm{coll}}\rangle (dN/dp_T)_{\mathrm{AA}}} \quad \text{and} \quad v_2 \equiv \langle \cos[2(\phi - \Psi_{\mathrm{RP}})]\rangle. \tag{3}$$

R_{AA} is the ratio of the momentum distribution measured in A-A and p-p collisions normalized to the average number of independent binary nucleon-nucleon collisions in an A-A event. Deviations from unity signal the presence of medium effects: at high p_T one gets $R_{\mathrm{AA}} < 1$, due to the energy-loss of charm and beauty quarks; instead, its rise at low-moderate p_T may come from the collective radial flow of the fireball, boosting particles from very low to higher transverse momenta. The v_2 coefficient quantifies the azimuthal anisotropy of the angular distribution of final particles and is interpreted as arising from the elliptic asymmetry of the initial condition in non-central collisions, with the larger pressure gradients along the reaction plane ψ_{RP} giving rise to a larger acceleration of the fluid along this direction. The challenge for the models is to consistently reproduce these and other observables. A snapshot of the results of different transport calculations [2, 3, 4, 5] compared to ALICE data [1] is given in Fig. 1. Notice that, in all cases, in order to reproduce the experimental data, it is important to include the possibility for heavy quarks to hadronize via recombination with the light thermal partons from the medium.

3 Recent developments

The finite impact parameter of a nucleus-nucleus collision leads, on average, to an elliptic deformation of the produced fireball. Pressure gradients map this initial geometric asymmetry into a final momentum
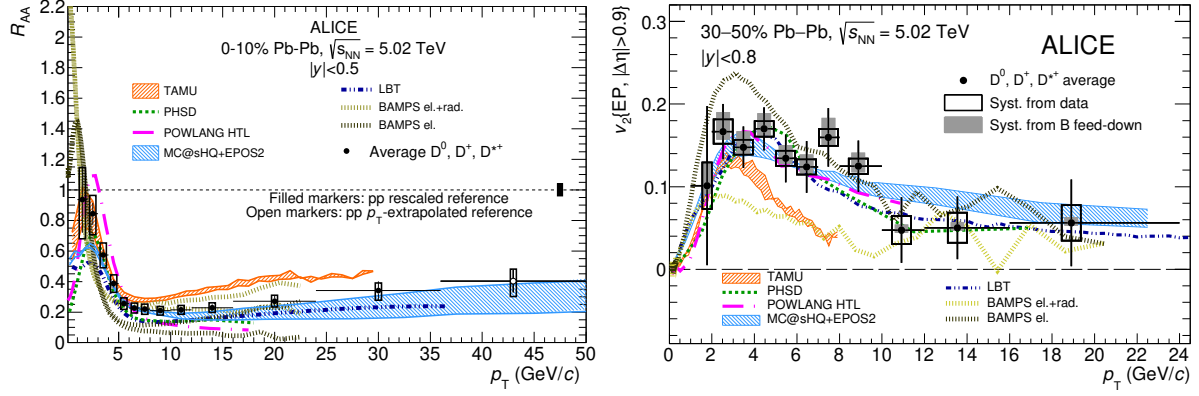
Figure 1: Recent results by the ALICE collaboration for the average D-meson R_{AA} and v_2 [1] compared to the predictions of various transport calculations.
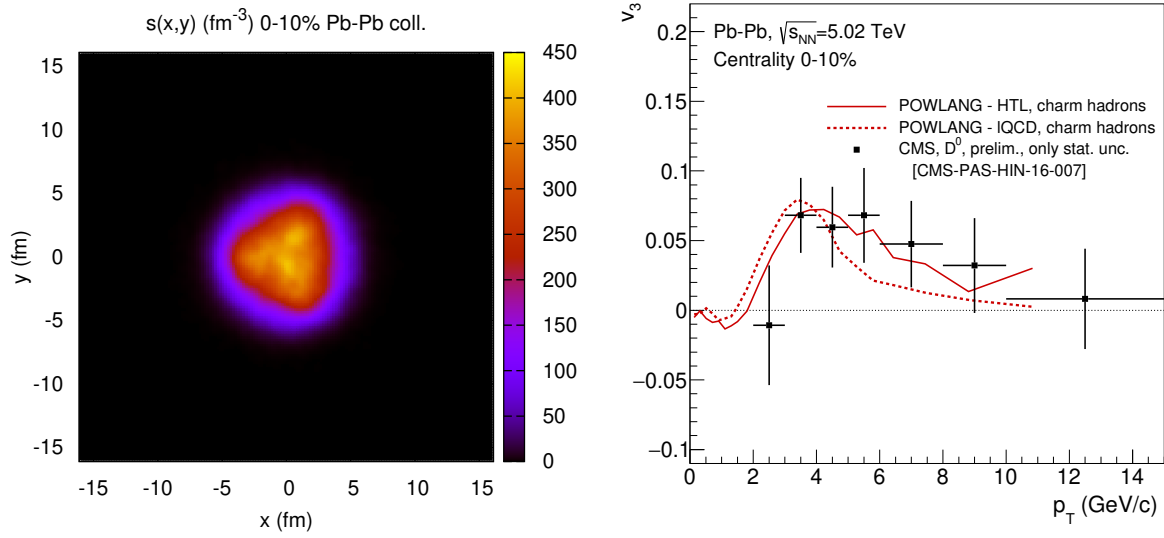
Figure 2: Initial condition for a central Pb-Pb collision at the LHC displaying a triangular eccentricity (left panel) and the resulting v_3 coefficient (right panel) of the azimuthal distribution of D-mesons for different choices of the transport coefficients [6].

anisotropy of the particles decoupling from the medium, giving rise to the elliptic flow v_2 shown for instance in the right panel of Fig. 1. However, event-by-event fluctuations (e.g. in the nucleon positions) can give rise to more complicated initial geometries, quantified by higher order eccentricity coefficients

$$\epsilon_m = \frac{\sqrt{\left[r_\perp^2 \cos(m\phi)\right]^2 + \left[r_\perp^2 \sin(m\phi)\right]^2}}{r_\perp^2} \qquad (4)$$

which lead to higher harmonics in the final hadron distributions $v_m \equiv \langle \cos[m(\phi - \Psi_m)] \rangle$. In Fig. 2 we show the result of a one-shot hydro+transport simulation starting from an average initial condition with

a triangular deformation referring to the 0-10% most central Pb-Pb collisions at $\sqrt{s_{NN}} = 5.02$ TeV. The final D-meson angular distribution is then characterized by a non-vanishing triangular flow v_3, as shown in the right panel of the figure where we compare the results of our transport simulations [6] to CMS data [7].
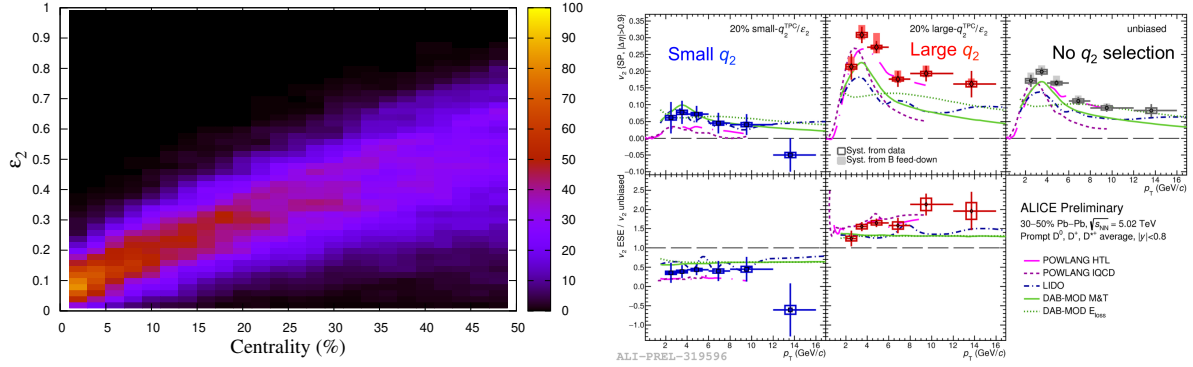
Figure 3: Left panel: (elliptic) eccentricity-vs-centrality correlations in Pb-Pb collisions at the LHC from event-by-event Glauber-MC simulations of the initial condition [8]. Right panel: D-meson elliptic flow after selecting events, within a given centrality class, with high/low eccentricity. ALICE data [9] are compared to the predictions of various transport models.
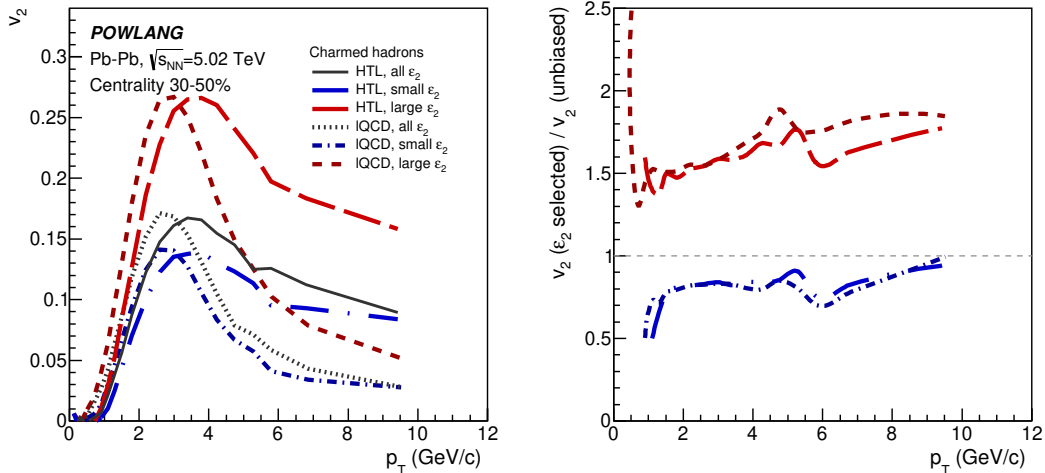
Figure 4: D-meson elliptic flow in the 30-50% centrality class for events with high/low initial eccentricity compared to an unbiased selection of events [8]. The ratio to the unbiased result (right panel) turns out to be independent of the choice of the transport coefficients.

Furthermore, due to event-by-event fluctuations, events belonging the same centrality class – usually identified by some estimator like the number of binary nucleon-nucleon collisions (in numerical simulations) or the multiplicity of produced particles (in actual experiments) – can be characterized by quite

different initial eccentricities, as shown in the left panel of Fig. 3. It is then of interest to study, for a given centrality, the elliptic (or triangular) flow of subsamples of events of high/low eccentricity, comparing the result to the unbiased case. This technique, known as *event-shape-engineering*, was first introduced for light hadrons [10] and later applied also to study of the flow of D-mesons [9]. Results obtained by the ALICE collaboration, compared to various transport calculations, are displayed in the right panel of Fig. 3. In Fig. 4 we show the results of the transport model of Ref. [8] for the D-meson elliptic flow in Pb-Pb collisions, in the 30-50% centrality class, for the 0-20% highest and 0-60% lowest-eccentricity subsamples. Notice how the ratio to the unbiased result does not depend on the choice of the transport coefficients, reflecting only the initial geometry. This holds quite generally also for beauty-hadrons and for different centrality classes.
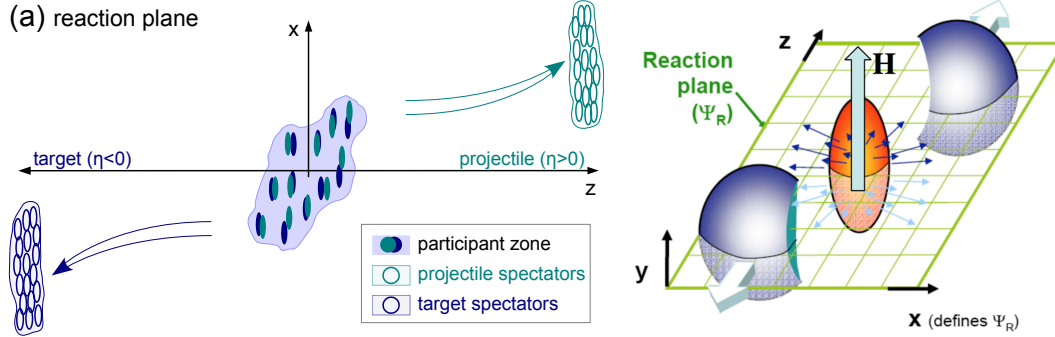
Figure 5: Schematic picture of a non-central heavy-ion collision, showing the tilting of the initial condition with respect to the beam axis (left panel) and the magnetic field orthogonal to the reaction plane arising from the spectator nucleons.
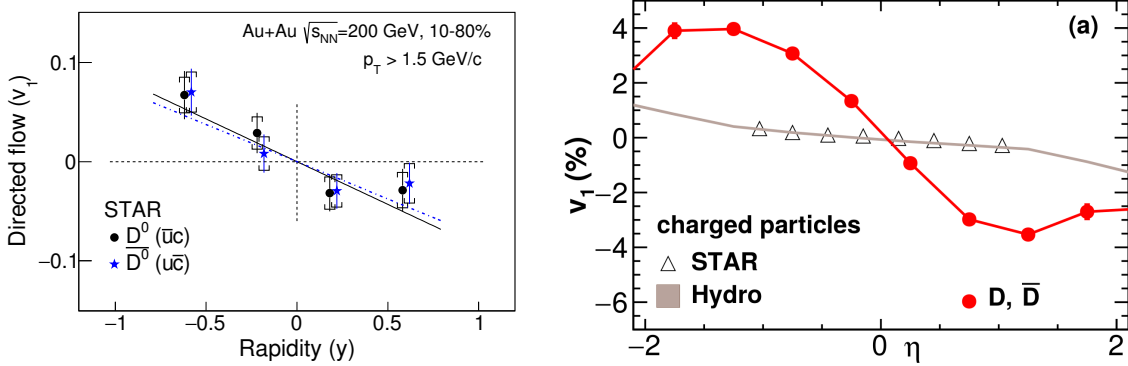
Figure 6: The directed flow v_1 of $D^0/\overline{D}^0$ mesons in Au-Au collisions at $\sqrt{s_{NN}} = 200$ GeV as a function of rapidity measured by the STAR collaboration [11] and predicted by a transport calculation [12].

Recently, a strong interest is growing also for the study of the directed flow $v_1 \equiv \langle \cos(\phi - \Psi_{RP}) \rangle$. Since participant nucleons of the colliding nuclei tend to deposit more energy along their direction of motion, in non-central collisions the fireball is characterized by an initial tilted geometry (see left panel of Fig. 5) and by a sizable orbital angular momentum (of order 1000 $\hbar$) and vorticity [13]. Experimentally,

this can give rise to a negative/positive directed flow v_1 of charged hadrons at forward/backward rapidity and possibly to other effects like the polarization of Λ hyperons [14]. Interestingly, one expects a stronger v_1 signal (quite small for light hadrons) in the case of charmed particles. On top of the directed flow of the background medium, an important contribution to the final signal arises in fact from the mismatch between the tilted geometry of the medium and the initial position of the $c\bar{c}$ pairs, symmetrically distributed around the beam axis. Predictions for the D-meson v_1 of the transport calculation of Ref. [12] are shown in the right panel of Fig. 6. The comparison with experimental data should allow one to probe the three-dimensional distribution of matter in heavy-ion collisions. Recently, some authors [15, 16] have also proposed that the difference between the v_1 of D^0 and $\overline{D^0}$ mesons can be a unique probe of the huge electromagnetic fields present in the fireball during the deconfined phase; however, current experimental data [11] do not allow yet to draw firm conclusions.

4 Conclusions and perspectives

The study of heavy-flavour observables in nucleus-nucleus collisions has the potential to provide information on charm and beauty transport coefficients in the quark-gluon plasma, describing their spatial diffusion and their approach to kinetic equilibrium. For the moment several theoretical calculations allow one to get a quite satisfactory description of the data, leading then to a substantial theoretical uncertainty on the value of the above coefficients. In-medium hadronization plays a role at least as important as the one of the transport in the partonic phase; furthermore, so far, one has experimental access to a kinematic window where the heavy-quark dynamics can not be captured simply by one non-relativistic transport coefficient. We expect the situation to improve as soon as measurements of beauty at low transverse-momentum will get available.

Besides the transport coefficients, the study of heavy-flavour observables provides information on other non-trivial features of nuclear collisions, like the event-by-event fluctuations and the initial three-dimensional distribution of deposited energy and, possibly, on the effect of the initial huge magnetic field arising from the spectator nucleons. In this connection, we tried to give an overview of the most recent theoretical studies and experimental analyses.

References

1. Acharya S *et al.* (ALICE) 2018 *JHEP* **10** 174 (*Preprint* `1804.09083`)

2. Beraudo A, De Pace A, Monteno M, Nardi M and Prino F 2015 *Eur. Phys. J.* **C75** 121 (*Preprint* `1410.6082`)

3. He M, Fries R J and Rapp R 2014 *Phys. Lett.* **B735** 445–450 (*Preprint* `1401.3817`)

4. Cao S, Luo T, Qin G Y and Wang X N 2018 *Phys. Lett.* **B777** 255–259 (*Preprint* `1703.00822`)

5. Nahrgang M, Aichelin J, Gossiaux P B and Werner K 2014 *Phys. Rev.* **C89** 014905 (*Preprint* `1305.6544`)

6. Beraudo A, De Pace A, Monteno M, Nardi M and Prino F 2018 *JHEP* **02** 043 (*Preprint* `1712.00588`)

7. Sirunyan A M *et al.* (CMS) 2018 *Phys. Rev. Lett.* **120** 202301 (*Preprint* `1708.03497`)

8. Beraudo A, De Pace A, Monteno M, Nardi M and Prino F 2019 *Eur. Phys. J.* **C79** 494 (*Preprint* `1812.08337`)

9. Acharya S *et al.* (ALICE) 2019 *JHEP* **02** 150 (*Preprint* 1809.09371)

10. Adam J *et al.* (ALICE) 2016 *Phys. Rev.* **C93** 034916 (*Preprint* 1507.06194)

11. Adam J *et al.* (STAR) 2019 *Phys. Rev. Lett.* **123** 162301 (*Preprint* 1905.02052)

12. Chatterjee S and Bozek P 2018 *Phys. Rev. Lett.* **120** 192301 (*Preprint* 1712.01189)

13. Becattini F, Inghirami G, Rolando V, Beraudo A, Del Zanna L, De Pace A, Nardi M, Pagliara G and Chandra V 2015 *Eur. Phys. J.* **C75** 406 [Erratum: Eur. Phys. J.C78,no.5,354(2018)] (*Preprint* 1501.04468)

14. Adamczyk L *et al.* (STAR) 2017 *Nature* **548** 62–65 (*Preprint* 1701.06657)

15. Das S K, Plumari S, Chatterjee S, Alam J, Scardina F and Greco V 2017 *Phys. Lett.* **B768** 260–264 (*Preprint* 1608.02231)

16. Chatterjee S and Bozek P 2019 *Phys. Lett.* **B798** 134955 (*Preprint* 1804.04893)

HOLOGRAPHIC THERMALISATION OF STRONGLY-COUPLED SYSTEMS

Floriana Giannuzzi
University of Bari, via Orabona 4, Bari, Italy

Abstract

The thermalisation of a strongly-coupled plasma is studied through the AdS/CFT correspondence. The system starts behaving as in viscous hydrodynamics shortly after the end of the perturbation. Local and nonlocal probes are used to characterise the process towards equilibrium.

1 Introduction

One of the challenges of the ALICE experiment is the study of ultrarelativistic heavy ion collisions (HIC) at LHC with the aim of understanding what happens to matter under extreme conditions, similar to those just after the Big Bang, and what the features of the system are. It has been stated that almost 1 fm/c after the collision the system enters a local equilibrium phase, known as quark-gluon plasma (QGP), and subsequently it expands and cools down until its temperature falls below the QCD transition to the hadronic phase [1, 2]. The QGP contains deconfined partons and behaves as a nearly perfect fluid in which matter flows collectively, hence it can be described by hydrodynamics at low viscosity. However, the description of the system immediately after the collision is much more difficult, since it involves the study of an out-of-equilibrium problem. Recently, the AdS/CFT correspondence has been applied to such issues [3], with the aim of understanding how equilibrium is reached and how much time is needed, and of identifying some features of the medium produced in HIC experiments [4, 5, 6, 7]. The AdS/CFT correspondence, unlike other nonperturbative approaches, can be straightforwardly applied to systems under extreme conditions and far from equilibrium. It has predicted a very small value for the ratio of shear viscosity over entropy density (η/s), *i.e.* $\eta/s = 1/(4\pi)$, a general result that holds for any strongly-coupled gauge theory having a gravity dual [8]. Experiments at RHIC and LHC have indeed found out that η/s should be small in the QGP phase, at odds with predictions of models based on perturbative

calculations, thus showing that the AdS/CFT correspondence could capture the strong-coupling features of the system. Moreover, we expect that the results obtained through the correspondence for $\mathcal{N} = 4$ super Yang-Mills theory may be relevant to the QGP since it is deconfined and strongly interacting.

2 AdS/CFT correspondence in a nutshell

The AdS/CFT correspondence establishes a duality between a superstring theory in $AdS_5 \times S_5$ and a gauge theory, namely $\mathcal{N} = 4$ super Yang-Mills theory, living in a four-dimensional ($4d$) Minkowski space [9]. An interesting aspect of the correspondence is its weak version, according to which the supergravity limit is dual to the large-N and strong-coupling limit of the gauge theory, and this suggests that the nonperturbative regime of the gauge theory can be studied by a semiclassical theory.

The $5d$ AdS (anti-de Sitter) space has a boundary, which is equivalent to a $4d$ Minkowski space (plus a point at infinity), so the dual gauge theory can be built on the boundary of the AdS space. The metric of the AdS_5 space in Eddington-Finkelstein coordinates is:

$$ds^2 = 2drdt - r^2dt^2 + r^2d\vec{x}^2 \,, \tag{1}$$

where r is the fifth coordinate, and the boundary is reached in the limit $r \to \infty$.

A specific dictionary has been introduced to relate the two theories [10, 11]. It states that there is a correspondence between a local gauge-invariant operator of the gauge theory and a field in the $5d$ theory, whose mass is related to the conformal dimension Δ of the operator. The boundary value of the field is identified with the source of the operator. Finally, the generating functional of the correlators of the gauge theory is equal to the partition function of the gravity theory.

Finite temperature effects can be achieved by introducing a black hole in the $5d$ metric as follows:

$$ds^2 = 2drdt - r^2(1 - r_H^4/r^4)dt^2 + r^2d\vec{x}^2 \,, \tag{2}$$

where r_H represents the position of the horizon of the black hole, which is related to the temperature by

$$T = \frac{r_H}{\pi} \,. \tag{3}$$

It turns out that at small temperatures the horizon of the black hole is far from the boundary, while at high temperatures the horizon comes close to the boundary.

3 Out-of-equilibrium nonabelian conformal plasma

Let us exploit the AdS/CFT correspondence to study the thermalisation process of an out-of-equilibrium system, as the one produced in HIC. We require: boost invariance along the collision axis (x_3), translation invariance and $O(2)$ rotation invariance in the orthogonal plane $x_\perp = \{x_1, x_2\}$. It is thus convenient to change coordinates and define the proper time (τ) and the rapidity (y) from the time t and x_3 by $t = \tau \cosh y$ and $x_3 = \tau \sinh y$. In this approach, a system can be taken out of equilibrium by perturbing the $4d$ metric [4]:

$$ds^2 = -d\tau^2 + e^{\gamma(\tau)}dx_\perp^2 + \tau^2 e^{-2\gamma(\tau)}dy^2 \,. \tag{4}$$

The metric now contains a factor, $\gamma(\tau)$, which modifies the Minkowski metric for a short time interval until it vanishes or becomes constant.

Once the $4d$ metric is fixed, Einstein equations have to be solved to fix the corresponding $5d$ metric, which, in general form, can be written as:

$$ds^2 = 2drd\tau - A(\tau, r)d\tau^2 + \Sigma(\tau, r)^2 e^B(\tau, r)dx_\perp^2 + \Sigma(\tau, r)^2 e^{-2B(\tau,r)}dy^2 \,. \tag{5}$$

As a boundary condition, the $5d$ metric must coincide with the $4d$ perturbed metric (4) on the boundary, *i.e.* in the limit $r \to \infty$. At initial time we require that the metric matches the unperturbed AdS one.

After solving Einstein equations (for the numerical procedure see Ref. [12]), a general result has been obtained: for any considered $\gamma(\tau)$, the $5d$ metric contains a black hole, so, as soon as the perturbation starts, a horizon appears in the $5d$ space.

The analysis of thermalisation is put forward by means of two kinds of $4d$ observables, *i.e.* local and nonlocal probes. To this aim, an interesting local probe is the energy-momentum tensor, gathering information on energy density and pressure of the system, while nonlocal probes are the equal-time two-point correlation function, and the expectation value of Wilson loops of different shapes, rectangular and circular. By comparing such observables with their values foreseen in viscous hydrodynamics, it is possible to study thermalisation as the onset of the hydrodynamic regime.

3.1 Local probes

The boundary energy-momentum tensor is obtained as the operator dual to the metric tensor

$$T^\mu_\nu = \frac{N_c^2}{2\pi^2} \operatorname{diag}(-\epsilon, p_\perp, p_\perp, p_\parallel) . \tag{6}$$

Its components are the energy density, pressure in the transverse direction with respect to the collision axis, and longitudinal pressure. It can be computed following a recipe based on holographic renormalisation [12, 13, 14]. We have also defined an effective temperature using Eq. (3).

These observables have been computed both with the perturbed metric (5) and with a metric describing a setup governed by viscous hydrodynamics. In particular, viscous effects have been included up to second order in an expansion at late time [15, 16], obtaining:

$$\epsilon_H(\tau) = \frac{3\pi^4 \Lambda^4}{4(\Lambda\tau)^{4/3}} \left[1 - \frac{2c_1}{(\Lambda\tau)^{2/3}} + \frac{c_2}{(\Lambda\tau)^{4/3}} + \mathcal{O}\left((\Lambda\tau)^{-2}\right) \right], \tag{7}$$

$$p_{\parallel,H}(\tau) = \frac{\pi^4 \Lambda^4}{4(\Lambda\tau)^{4/3}} \left[1 - \frac{6c_1}{(\Lambda\tau)^{2/3}} + \frac{5c_2}{(\Lambda\tau)^{4/3}} + \mathcal{O}\left((\Lambda\tau)^{-2}\right) \right], \tag{8}$$

$$p_{\perp,H}(\tau) = \frac{\pi^4 \Lambda^4}{4(\Lambda\tau)^{4/3}} \left[1 - \frac{c_2}{(\Lambda\tau)^{4/3}} + \mathcal{O}\left((\Lambda\tau)^{-2}\right) \right], \tag{9}$$

$$T_{eff,H}(\tau) = \frac{\Lambda}{(\Lambda\tau)^{1/3}} \left[1 - \frac{1}{6\pi(\Lambda\tau)^{2/3}} + \frac{(-1+\log 2)}{36\pi^2(\Lambda\tau)^{4/3}} + \mathcal{O}\left((\Lambda\tau)^{-2}\right) \right], \tag{10}$$

with $c_1 = 1/(3\pi)$, $c_2 = (1 + 2\log 2)/(18\pi^2)$; the effective temperature in Eq. (10) has been defined from the relation $\epsilon_H = (3/4)\pi^4 T_{eff,H}^4$. The parameter Λ can be fixed by matching the hydrodynamic temperature with the one computed in the perturbed model at late times.

3.2 Nonlocal probes

Nonlocal observables can probe deeper into the bulk spacetime, since they are sensitive to a wide range of energy scales in the boundary field theory, giving a scale dependence of thermalisation.

The equal-time two-point correlation function of an operator with large conformal dimension can be computed from the length $\mathcal{L}$ of the extremal string connecting the points on the boundary [17, 18]:

$$\langle \mathcal{O}(t, \boldsymbol{x}) \mathcal{O}(t, \boldsymbol{x}') \rangle \simeq e^{-\Delta \mathcal{L}} . \tag{11}$$

The expectation value of a spatial Wilson loop can be computed from the Nambu Goto action $\mathcal{S}_{NG}$, which is the area of the surface spanned by the extremal string attached to the contour $\mathcal{C}$ [17, 18]:

$$\langle W_{\mathcal{C}} \rangle \sim e^{-\mathcal{S}_{NG}} \,. \tag{12}$$

Details on the definition of these quantities can be found in [18]. Nonlocal probes can have different sizes, corresponding to the distance between the two points on the boundary for the correlation function and to the size of the loop $\mathcal{C}$. It is worth emphasising that the strings from which Eqs. (11)-(12) are computed start on the boundary of the $5d$ space and then get into the bulk, to smaller and smaller values of r according to their size: observables with a large size on the boundary can probe deeper into the bulk. Nonlocal probes have been computed both with the nonequilibrium metric (5) and with a $5d$ metric reproducing, through holographic renormalisation, the energy-momentum tensor in Eqs. (7)-(9).

4 Results

Let us adopt the following profile for the function $\gamma(\tau)$ appearing in the $4d$ metric (4) [12]:

$$\gamma(\tau) = \frac{2}{5} \tanh^7 \left(\frac{\tau - 0.25}{1.2} \right) + [1 - (\tau - 4)^2]^6 e^{-1/[1-(\tau-4)^2]} \Theta[1 - (\tau - 4)^2] \,. \tag{13}$$

It is characterised, as shown in Fig. 1, by one peak plus a slow deformation, becoming at $\tau_f = 5$ almost constant (end of the perturbation). The results obtained for the energy-momentum tensor in the whole time interval are shown in the left panel of Fig. 1, while the results for nonlocal probes after the end of the perturbation are in the right panel. It emerges that nonlocal probes with larger sizes thermalise later.

It is interesting to look more in detail at what happens to the energy-momentum tensor after the end of the perturbation, as shown in Fig 2. One can notice that the energy density starts following the hydrodynamic behaviour as soon as the perturbation ends, while longitudinal and transverse pressures are, for a short time interval, quite different from hydrodynamics.

Let us define an equilibration time τ^* from the relation:

$$\left| \frac{\epsilon(\tau^*) - \epsilon_H(\tau^*)}{\epsilon(\tau^*)} \right| = 0.05 \,, \tag{14}$$

and an isotropisation time τ_p from:

$$\left| \frac{p_{\parallel}(\tau_p)/p_{\perp}(\tau_p) - p_{\parallel,H}(\tau_p)/p_{\perp,H}(\tau_p)}{p_{\parallel}(\tau_p)/p_{\perp}(\tau_p)} \right| = 0.05 \,. \tag{15}$$

It turns out that the equilibration time coincides with the end of the perturbation ($\tau^* = 5$), while the isotropisation time gets a higher value, $\tau_p = 6.74$. If we fix an energy scale requiring that the temperature at the end of the perturbation is equal to 500 MeV, we find that complete thermalisation is reached almost 0.42 fm/c after the end of the perturbation.

The calculation was repeated with different choices of $\gamma(\tau)$, getting the same qualitative results and a time delay for thermalisation of almost 1 fm/c in all the considered cases [12].

In conclusion, by exploiting the AdS/CFT correspondence we have been able to study an out-of-equilibrium process, finding some common features in all the considered models [12, 18], meaning that the response of the system to perturbation seems to be general. A first observation is that thermal equilibration and isotropisation are not simultaneous, the former occurring before the latter. Full
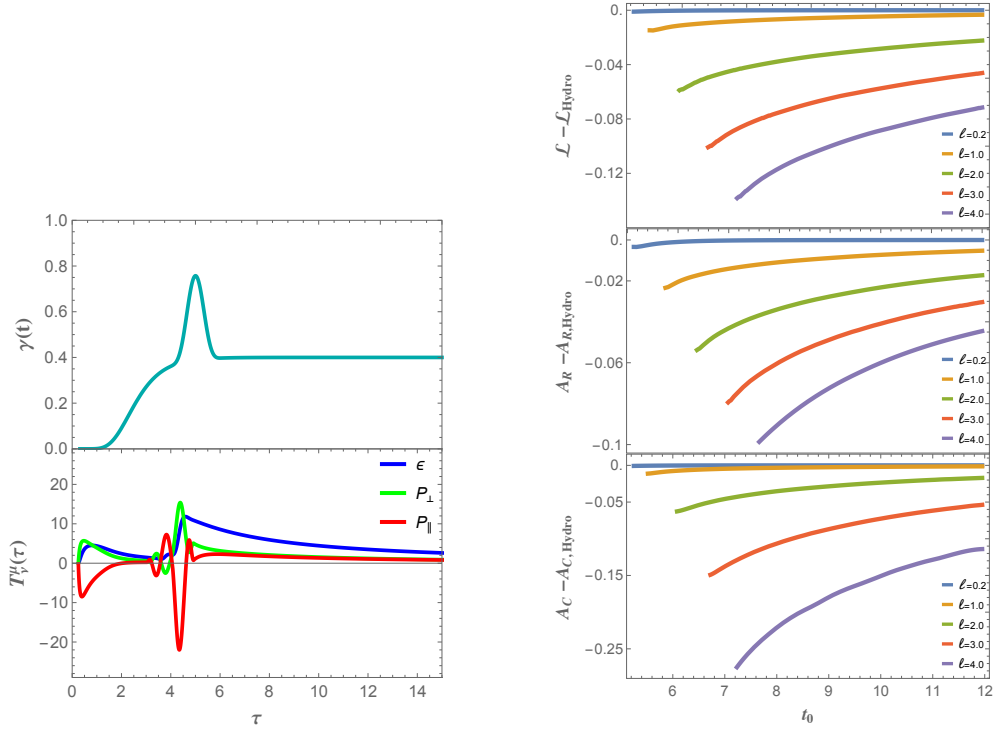
Figure 1: Left panel: $\gamma(\tau)$ (top), energy-momentum tensor in the out-of-equilibrium model (bottom). Right panel: geodesic length (top), area of the extremal surface for the rectangular Wilson loop (middle), area of the extremal surface for the circular Wilson loop (bottom), computed in the out-of-equilibrium model minus the same quantity in the viscous hydrodynamic model. In the hydrodynamic model the value $\Lambda = 1.12$ has been used.
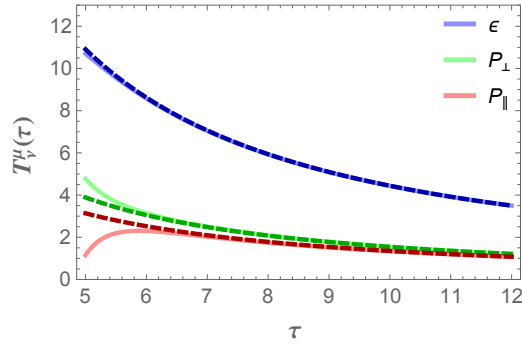
Figure 2: Comparison between the energy-momentum tensor in the out-of-equilibrium model (plain curves) and Eqs. (7)-(9) with $\Lambda = 1.12$ (dashed curves).

hydrodynamic behaviour is reached after a time of a few fm/c, in agreement with the experimental results. Another evidence is that local modes equilibrate first, so they need a lower time to thermalise with respect to nonlocal observables with large sizes, confirming that the considered system is strongly coupled. This approach has been also used to compute other quantities characterising the QGP, like, for example, the energy loss of a heavy quark moving in the plasma [19] and the dissociation time of a heavy quark-antiquark pair [20].

5 Acknowledgements

References

1. U. W. Heinz, AIP Conf. Proc. **739**, no. 1, 163 (2004).

2. E. Shuryak, Rev. Mod. Phys. **89**, 035001 (2017).

3. V. E. Hubeny *et al*, Adv. High Energy Phys. **2010**, 297916 (2010).

4. P. M. Chesler *et al*, Phys. Rev. Lett. **102**, 211601 (2009).

5. M. P. Heller *et al*, Phys. Rev. Lett. **108**, 201602 (2012).

6. M. P. Heller *et al*, Phys. Rev. Lett. **108**, 191601 (2012).

7. B. Wu *et al*, Int. J. Mod. Phys. C **22**, 1317 (2011).

8. G. Policastro *et al*, Phys. Rev. Lett. **87**, 081601 (2001).

9. J. M. Maldacena, Int. J. Theor. Phys. **38**, 1113 (1999).

10. E. Witten, Adv. Theor. Math. Phys. **2**, 253 (1998).

11. S. S. Gubser *et al*, Phys. Lett. B **428**, 105 (1998).

12. L. Bellantuono *et al*, JHEP **1507**, 053 (2015).

13. S. de Haro *et al*, Commun. Math. Phys. **217**, 595 (2001).

14. S. Kinoshita *et al*, Prog. Theor. Phys. **121**, 121 (2009).

15. M. P. Heller *et al*, Phys. Rev. D **76**, 025027 (2007).

16. R. Baier *et al*, JHEP **0804**, 100 (2008).

17. V. Balasubramanian *et al.*, Phys. Rev. D **84**, 026010 (2011).

18. L. Bellantuono *et al*, Phys. Rev. D **94**, no. 2, 025005 (2016).

19. P. M. Chesler *et al*, JHEP **1310**, 013 (2013).

20. L. Bellantuono *et al*, Phys. Rev. D **96**, no. 3, 034031 (2017).

OVERVIEW ON RECENT TOP-QUARK MEASUREMENTS AT THE LHC

Davide Melini
Technion, Department of Physics, Haifa 3200003, Israel

Abstract

The top-quark was the last quark to be discovered, in 1995, and since then its production and decay mechanisms as well as its properties have been studied. In the latest years in particular, the Large Hadron Collider (LHC) produced a huge quantity of top-quarks, which allowed experiments to measure the behaviour of top-quarks with a precision never seen before. In these proceedings a selection of the latest results on top-quark physics produced by the LHC experiments is presented.

1 Introduction

The top-quark is the heaviest particle in the Standard Model (SM) and its detailed study is of paramount importance for testing high energy particle physics theories. The Large Hadron Collider (LHC) is the best machine available at the moment to study top-quarks, since such particles are produced in abundance in high energy pp collisions. Since the beginning of its operations in 2011, the LHC produced roughly 10^9 top-quarks, 95% of which produced from 2015 to 2018 when the LHC was colliding protons at a centre of mass energy of 13 TeV. This massive amount of top-quarks allowed LHC experiments such as ATLAS and CMS to study with a never seen before accuracy the properties of the top-quark and its behaviour in various regions of its phase space. In the following the latest top-quark results are presented, from recent measurements of cross sections to determinations of top-quark properties.

2 Top-quark cross sections

Top-quarks at the LHC are mostly produced in $t\bar{t}$ pairs, with a predicted cross section of roughly 820 pb^{-1} in 13 TeV pp collisions, for top-quarks with a mass of 172.5 GeV. It corresponds to an increase in cross section of roughly four times in comparison to the 8 TeV predictions.

2.1 Inclusive cross sections

Inclusive cross sections are usually measured by experiments in a particular final state and then extrapolated to the full phase space considering the chosen final state probability..

A recent analysis [1] measured for the first time the $t\bar{t}$ inclusive cross section in a final state where one τ lepton decaying to hadrons (τ_h) is present. Such a channel is difficult to measure given the fact that the τ lepton does not leave a signal in detectors as clean as the one left by electrons and muons. The analysis measured $\sigma_{t\bar{t}} = 781 \pm 66$ pb^{-1}, in agreement with the theoretical predictions and previous measurements. Its uncertainty was dominated by systematic uncertainties, in particular related to the τ_h reconstruction. Measuring the $t\bar{t}$ cross section in such final state also proved that lepton flavour universality is preserved and that partial widths ratio are in agreement with the expectations.

Top-quark production modes which have a much smaller cross section have also been measured: two recent analyses measured the $t\bar{t}b\bar{b}$ inclusive cross section, which is important to constraint experimentally, given it is a large and irreducible background in $t\bar{t}H(b\bar{b})$ measurements. Final states with at least one lepton [2] (semileptonic $t\bar{t}$ decay) and fully hadronic [3] final states were considered. The measured cross section in all the different final states were found to be slightly larger than the SM theoretical predictions at Next-to-Leading-Order (NLO) plus Parton Shower (PS) in Quantum-Chromo-Dynamic (QCD) , but consistent within two standard deviations.

Other processes still are too elusive to be measured. That is the case for the $pp \rightarrow t\bar{t}t\bar{t}$ production, which is predicted by the SM to have a NLO cross section $\sigma_{t\bar{t}t\bar{t}} \sim 12$ fb^{-1}. Such cross section is very challenging to measure experimentally given the complexity of its final state. Three different recent analyses [4, 5, 6] looked for four top-quarks production in final states with one or more leptons, but did not find any evidence for it. The most stringent limits to date on $t\bar{t}t\bar{t}$ production were set and constraints on anomalous four-top-quark coupling deriving from potential new physics effects were given.

2.2 Differential cross sections

The large amount of statistics also benefits top-quark differential cross sections measurements.
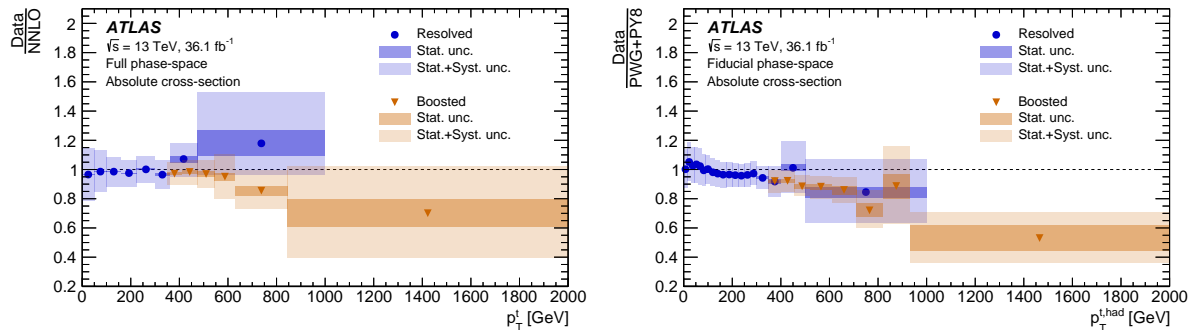
Figure 1: *Comparison between theoretical predictions and measured data of the hadronic top-quark p_T distribution. Data is measured in the resolved and boosted regime and then corrected to parton level (left) and particle level (right), where it is compared to theoretical calculations at NNLO QCD and NLO+PS respectively.*

A recent measurement of the kinematic distributions of semileptonic $t\bar{t}$ events [7] was published. A number of differential distributions were measured and then corrected for detector effects only (particle

level), and also for hadronisation and top-quark decay effects (parton level). Two different kinematic regimes were studied and found to give compatible results in their overlap region: the resolved channel, where the decay products of the hadronic decaying top-quark are contained inside three separated jets, and the boosted channel, where the top-quark hadronic decays are contained within a single jet of large radius. The large statistics used to perform the measurement allowed also the extraction of two dimensional differential distributions. It was found that the theoretical predictions slightly overestimate the measured data in the high energy tails of various distributions, such as the hadronic top-quark transverse momentum (p_T^{had}) shown in fig.1. The tension is more evident at particle level, where the uncertainties on the measurement are around 10-15% and the comparison to the theory is done with MC simulations at NLO+PS. At parton level the systematic uncertainties were larger since data had to be corrected for more effects, and the total uncertainty ranges from 10% to 30%. Such uncertainty fully covers the tension between NNLO predictions and the measured corrected data.

Another recent measurement [8] focused on measuring the leptonic distributions in $t\bar{t}$ events with two leptons (dileptonic $t\bar{t}$ decay) with different flavours and opposite electromagnetic charges in their final state . Such channel has a very clean experimental signature and allow to extract differential distributions at particle level with percent-level precision. The measured distributions were found to agree well, within uncertainties, with the available NNLO theoretical predictions which also included Next-to-Leading-Logarithm (NNLL) accuracy . On the other hand a slight mismodelling was found for MC simulations, which could not reproduce the data spectra of the lepton p_T above ~ 130 GeV and of the dilepton invariant mass below 50 GeV.

3 Properties

A number of interesting quantities related to the top-quark have been measured at the LHC. New recent measurements reduce the uncertainties on previous results, taking advantage of up to $\sim 140\mathrm{fb}^{-1}$ of collected data and the development of new techniques and approaches.

3.1 Asymmetries

Top-quarks in $t\bar{t}$ event produced in pp collisions are predicted in the SM to behave slightly asymmetrically: while t quarks are produced more along the the beam axis, the $\bar{t}$ are more perpendicular to it. To test such fact the number N of $t\bar{t}$ events where the top-quarks are produced with higher/lower absolute rapidity y than the anti-top-quarks is considered. A measurement of the so-called *charge asymmetry*

$$A_C = \frac{N_{|y_t|>|y_{\bar{t}}|} - N_{|y_t|<|y_{\bar{t}}|}}{N_{|y_t|->|y_{\bar{t}}|} + N_{|y_t|<|y_{\bar{t}}|}} \tag{1}$$

was recently performed [9] in semileptonic $t\bar{t}$ events, in both resolved and boosted topologies. A 4σ evidence for A_C was found, compatible to the SM expectations, but not significant enough to claim the discovery of such effect. The distribution of A_C as a function of the invariant mass of the $t\bar{t}$ system ($m_{t\bar{t}}$) was also measured and corrected to parton level, where it was found to agree to MC simulations and an advanced SM theoretical prediction which includes NNLO QCD and NLO electro-weak (EW) effects.

Another effect predicted to happen in $t\bar{t}$ production is that the spins of the top-quark and anti-top-quark are correlated. Such prediction can be tested by experiments since the top-quark lifetime is shorter than the hadronisation and spin decorrelation time scales, hence allowing the top-quark spin information to pass to its decay products. Two recent measurements [10, 11] evaluated spin correlations in dileptonic $t\bar{t}$ events using very different approaches.
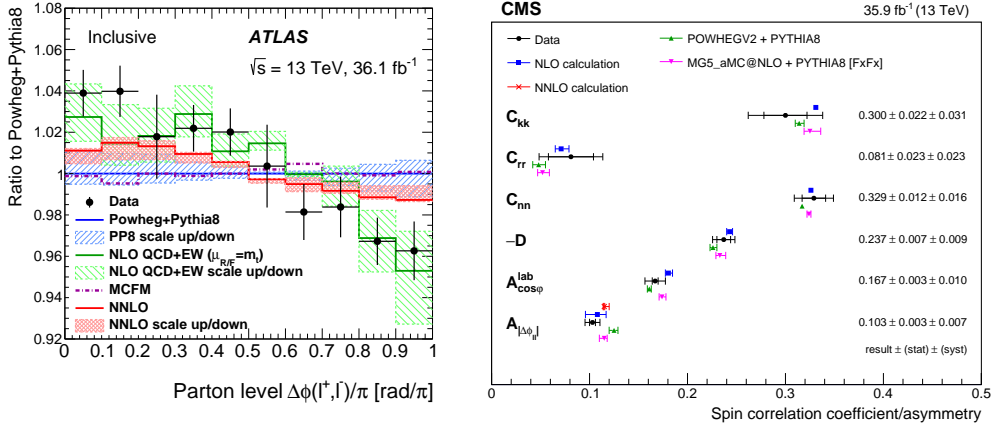
Figure 2: *Summary of recent results on spin correlation measurements. On the left, differences in the distribution of the angular distance $\Delta(\phi)$ between two leptons from $t\bar{t}$ decay. Data is corrected to parton level where it is compared to different available theoretical calculations. On the right, measurements of various coefficients responsible for spin correlations in $t\bar{t}$ production.*

Spin correlations affect the angular distances $\Delta\eta$ and $\Delta\phi$ between the two leptons and one method [10] measured such distributions. The $\Delta\phi$ distribution, corrected to parton level, was found to be in slight tension with NLO and NNLO QCD predictions, but in good agreement with NLO QCD+EW calculations as can be seen in fig. 2. This result showed that EW correction in certain region of the phase space can be very important and cannot be neglected.

In an alternative approach all the 15 coefficients which can be used to parametrise the spin dependent part of the $t\bar{t}$ production were constrained through the measurement of 15 different observables [11]. In this case a good agreement was found between the values of the coefficients as extracted from data and the NLO QCD predictions from the SM, as shown in fig. 2.

3.2 Width and mass

One of the most peculiar properties of the top-quark is its short lifetime, which is due to its very high mass, m_t and strictly connected to the value of its decay width Γ_t. The SM predicts at NNLO QCD a value $\Gamma_t^{\mathrm{SM}} = 1.322$ GeV for a top-quark with a mass of 172.5 GeV, with a small 6% theoretical uncertainty.

In a recent article [12] the top-quark decay width was measured in $t\bar{t}$ dileptonic events. The analysis employed the invariant mass of the lepton and b+jet system, which was found to be quite sensitive to changes of the top-quark width. A fit at detector level of MC predictions to data yielded $\Gamma_t = 1.94 \pm 0.50$ GeV, where systematics uncertainties where included in the fit and constrained through a simultaneous fit to the $b\bar{b}$ system invariant mass.

The top-quark mass is, contrary to Γ_t, a free parameter of the SM and its direct determination is therefore of great importance. Top-quark mass measurements have a long tradition and experimental uncertainties are usually very well under control. In fact, the evaluation of the theoretical uncertainties associated to m_t determinations started to play a key role, since such uncertainties are becoming the dominant ones with values estimated to be around 0.5-1 GeV. In this direction, the extraction of m_t may benefit from using fixed order calculations beyond the LO. Such calculations are computed in a well defined renormalisation scheme and allow for precise definition of the parameters of the Lagrangian,

including the top-quark mass. This makes possible the determination of quantities such as the pole mass (m_t^{pole}) and the running mass $(m_t(\mu))$ with a theoretical uncertainty estimated with a few hundreds MeV precision.

One analysis [13] exploiting this direction studied $t\bar{t}+1$ jet events produced in pp collisions at 8 TeV, with exactly one lepton in their final state. The cross section as a function of the invariant mass of the $t\bar{t}+1$ was measured and corrected to the parton level, as shown in fig.3. A fit to NLO QCD calculations estimated the best value of the top-quark pole mass to be $m_t^{\mathrm{pole}} = 171.1 \pm 1.1$ GeV, where the reported uncertainty includes statistical and systematic experimental uncertainties as well as theoretical uncertainties covering the choice of parton distribution functions (PDFs), the choice of the value of α_s and the impact of missing higher orders not included in the theoretical calculation. Even though only the 8 TeV dataset was used in this measurement, its precision was found to be competitive with other mass measurements at 13 TeV, due to the high sensitivity of the chosen observable on the top-quark mass.
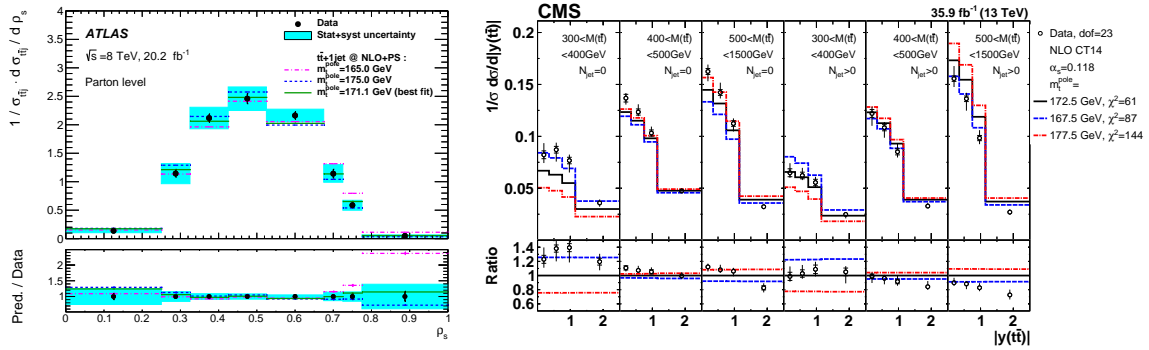

Figure 3: *Observables used in recent m_t^{pole} measurements. On the left, the normalised differential cross section of $t\bar{t}+1$ jet as a function of $\rho_s = 340~GeV/m_{t\bar{t}+1~jet}$. On the right the triple differential cross section of $t\bar{t}$ events as a function of the number of extra jets (N_{jet}) and invariant mass ($M_{(t\bar{t})}$) and absolute pseudo-rapidity ($|y_{(t\bar{t})}|$) of the $t\bar{t}$ system. Both observables are present at parton level and compared to NLO QCD predictions.*

A second analysis [14] used $t\bar{t}$ events at 13 TeV, with two opposite sign leptons in the final state, and measured the triple differential cross section as function of number of jets and invariant mass and rapidity of the $t\bar{t}$ system. A fit to NLO QCD theoretical predictions at parton level was developed which simultaneously extracted the best values of $m_t^{\mathrm{pole}}, \alpha_s$ and constrained the PDF choice. It resulted in a top-quark pole mass value of $m_t^{\mathrm{pole}} = 170.5$ GeV with a total experimental and theoretical uncertainty of ± 0.8 GeV. In this case the theoretical uncertainty only covered the impact of perturbative terms not included in the calculation, given that the α_s and PDF dependencies were constrained by the fit.

Both these recent m_t measurements were found to prefer a central value for the top-quark mass which is slightly lower than other previous mass measurements which extracted top-quark mass from a direct comparison of data to MC simulations. More tension exists if comparing these new results to recent global EW fits [15], which predict $m_t^{\mathrm{pole}} \sim 176.5 \pm 2$ GeV. On the other hand, good agreement is found with the m_t determination from a NNLO QCD global fit [16].

Finally, two new measurements strictly related to the top-quark mass were published for the first time. One analysis [17] measured directly the Yukawa coupling of the top-quark (Y_t), proportional to m_t in the SM. The measurement took advantage of the fact that EW corrections to $t\bar{t}$ production depends on Y_t. Using a profile likelihood fit, the analysis found $Y_t \sim 1.1 \pm 0.4$ where the large uncertainty comes from

the limited sensitivity of the method. Another study [18] looked for the running of the top-quark mass parameter, as defined in the modified minimal subtraction ($\overline{MS}$) scheme. To do so $\overline{m}_t(\mu)$ was extracted in four different $m_{t\bar{t}}$ intervals, which were setting the scale of the process, i.e. $\mu = m_{t\bar{t}}$. Comparing data corrected to parton level to NLO QCD calculations produced in the $\overline{MS}$ scheme, a slight evidence of the running of $\overline{m}_t(\mu)$ was found.

4   Summary and conclusions

Top-quark physics is an important part of the scientific program of the LHC experiments. The successful operation of the LHC allowed experiments to collect an unprecedented amount of data which allowed to deepen the knowledge of top-quark behaviour. Recent analyses provided results for inclusive and differential cross sections, as well as top-quark properties, setting a new standard of precision for top-quark measurements. Overall good agreement was found between the measured data and the available theoretical predictions. Few tensions and non significant disagreements were also found between data and theory, which motivate an even deeper study of the top-quark physics and a further improvements in top-quark modelling.

References

1. CMS Collaboration, CMS-PAS-TOP-18-005

2. CMS Collaboration, CMS-PAS-TOP-18-002

3. CMS Collaboration CMS-PAS-TOP-18-011

4. ATLAS Collaboration, Phys. Rev. **D 99** (2019) 052009

5. CMS Collaboration, CMS-PAS-TOP-17-019

6. CMS Collaboration, CMS-PAS-TOP-18-003

7. ATLAS Collaboration, Eur. Phys. J. **C 79** (2019) 2018

8. ATLAS Collaboration, arXiv:1910.08819

9. ATLAS Collaboration, ATLAS-CONF-2019-026

10. ATLAS Collaboration, arXiv:1903.07570,

11. CMS Collaboration, Phys. Rev. **D 100** (2019) 7 072002

12. ATLAS Collaboration, ATLAS-CONF-2019-038

13. ATLAS Collaboration, JHEP 11 (2019) 150

14. CMS Collaboration, arXiv:1904.05237

15. J. Haller *et al*, Eur. Phys. J. **C 78** (2018) 675

16. S. Alekhin *et al*, PRD **96** (2017) 014011

17. CMS Collaboration, CMS-PAS-TOP-17-004

18. CMS Collaboration, CMS-PAS-TOP-19-007

RENORMALON EFFECTS IN TOP-MASS SENSITIVE OBSERVABLES

Silvia Ferrario Ravasio
Institute for Particle Physics Phenomenology, Department of Physics, Durham University, Durham
DH1 3LE, United Kingdom

Abstract

A precise determination of the top mass is one of the key goals of the LHC and future colliders. Since power corrections are now becoming a source of worry for top-mass measurements, in these proceedings I discuss the impact of linear infrared renormalons, which plague the definition of the top pole-mass m, on observables expressed in terms of m and in terms of a short-distance mass.

1 Introduction

The top quark is one of the most peculiar particles predicted by the Standard Model and its phenomenology is entirely driven by the large value of its mass m_t. The most precise measurements of m_t are based on the use of Monte Carlo (MC) event generations and the current errors are of the order of several hundreds of MeV. Thus, linear power corrections arising from the pole mass ambiguity, which is estimated to be of the order of 110-250 MeV [1, 2], are becoming a major worry in top-mass measurements at hadron colliders. Furthermore, even if the perturbative calculations implemented in the MC generators adopt the pole-mass scheme, there is still no consensus in the theoretical community regarding the interpretation of such measurements, due to the complicated interplay of hadronization and parton shower dynamics [3]. The purpose of these proceedings is not to investigate the relation between the pole and the MC mass (see *e.g.* [4]), but instead to investigate the asymptotic behaviour of quantities calculated in terms of the pole mass and of the $\overline{\text{MS}}$ mass (that we can consider as a proxy of all the short-distance mass schemes) in a simplified theoretical frameworks where we understand some aspects concerning the non perturbative corrections to the pole mass. We focus upon the case of single top production and we look at the total cross section, which is known to be free from physical linear renormalons, the reconstructed-top mass, which is highly sensitive to the value of m_t, and leptonic observables, which are assumed to be independent from non-perturbative QCD effects. More details can be found in Refs. [5, 6].

2 QCD infrared renormalons

In gauge theories in general, and in QCD in particular, there is a certain class of Feynman graphs whose number grows as the factorial of the order of the perturbative expansion in the strong coupling constant. The resulting perturbative series is then divergent and it is typically treated as an asymptotic series. As a consequence, there is an uncertainty in the value of the sum of the series of the order $(\Lambda_{\mathrm{QCD}}/Q)^p$, being Q the scale of the process, Λ_{QCD} the infrared scale at which the validity of perturbative QCD breaks down and p a positive integer. This is the so-called renormalon ambiguity [7].

Indeed, when we perform all-orders calculations, some contributions can be thought as NLO corrections where the fixed-scale coupling is replaced with the running one. After the removal of the UV and IR divergencies, the perturbative series will take the form

$$Q^{-p} \int_0^Q d\ell \, \ell^{p-1} \, \alpha_s(\ell) \approx Q^{-p} \sum_{i=0}^{\infty} \alpha_s^{n+1}(Q) \int_0^Q \ell^{p-1} d\ell \left(b_0 \log \left(\frac{Q^2}{\ell^2} \right) \right)^n = \sum_{i=0}^{\infty} \frac{n!}{p} \left(\frac{2b_0}{p} \right)^n \alpha_s^{n+1}(Q), \quad (1)$$

where ℓ is the (real or virtual) gluon momentum, p is a positive integer and b_0 is the one-loop QCD β function

$$b_0 = \frac{11 C_A}{12\pi} - \frac{n_l T_R}{3\pi}, \quad (2)$$

with n_l being the number of light flavours. Since b_0 is positive, the series in eq. 1 is not even Borel resummable. The terms in the series will first decrease until

$$\frac{n!}{p} \left(\frac{2b_0}{p} \right)^n \approx \frac{(n+1)!}{p} \left(\frac{2b_0}{p} \right)^{n+1} \alpha_s(Q) \quad \Rightarrow \quad n \approx \frac{p}{2b_0 \alpha_s(Q)}. \quad (3)$$

At this point, if we want to interpret the series as an asymptotic one, we need to truncate the expansion and the size of the last term, which is also an indication of the ambiguity in our result, will be of the order $(\Lambda_{\mathrm{QCD}}/Q)^p$. The dominant ambiguities are the ones corresponding to $p = 1$, *i.e.* the linear renormalons, and those affect the definition of the pole mass.

Performing all-order calculations is however not possible for any non-trivial gauge theory. To overcome this task, we can imagine that the number of flavours n_f is large and the dominant corrections arise from $g \to q\bar{q}$ splittings. Thus, everytime we encounter a gluon line, we replace the free propagator with the dressed one

$$\frac{-i g^{\mu\nu}}{\ell^2 + i\eta} \to \frac{-i g^{\mu\nu}}{\ell^2 + i\eta} \times \frac{1}{1 + \Pi(\ell^2 + i\eta, \mu^2) - \Pi_{\mathrm{ct}}}, \quad (4)$$

where μ^2 is the renormalization scale, Π is the fermionic contribution to the vacuum polarization and Π_{ct} is the counterterm we introduce to renormalize the strong coupling. In $D = 4 - 2\epsilon$ dimensions we can write

$$\Pi(\ell^2 + i\eta, \mu^2) - \Pi_{\mathrm{ct}} = -\alpha_s(\mu) \frac{n_f T_R}{3\pi} \left[\log \frac{|\ell^2|}{\mu^2} - i\pi\theta(\ell^2) + C \right] + \mathcal{O}(\epsilon), \quad (5)$$

where C is a renormalization-scheme dependent constant ($C = -5/3$ in the $\overline{\mathrm{MS}}$ scheme). To recover the non-abelian behaviour of QCD, we can imagine that n_f is large and negative. At the end of the computation we match the fictitious number of flavours n_f with the real number of light flavours n_l

$$n_f \to n_l - \frac{11 C_A}{4} = -\frac{3\pi b_0}{T_R}, \quad (6)$$

so that the vacuum polarization appearing in the dressed gluon propagator takes the desired form

$$\Pi(\ell^2 + i\eta, \mu^2) - \Pi_{\mathrm{ct}} = \alpha_s(\mu) \, b_0 \left[\log \frac{|\ell^2|}{\mu^2} - i\pi\theta(\ell^2) + C \right] + \mathcal{O}(\epsilon). \quad (7)$$
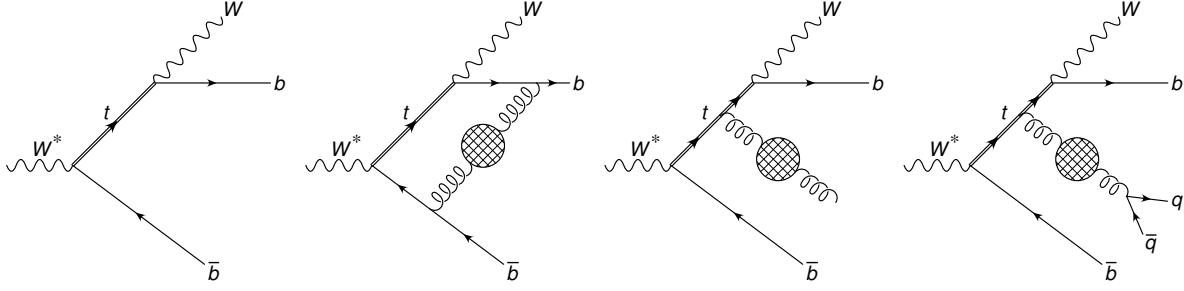
This is the so-called large-b_0 approximation [8, 9].

Figure 1: Feynman diagram for Born $W^* \to Wb\bar{b}$ process, and samples of Feynman diagrams for the virtual and the real-emission contributions and for the $W^* \to Wb\bar{b}q\bar{q}$ production. The bubble denotes the insertion of the vacuum polarization of eq. (7) in the gluon propagator.

3 Single-top production at all orders

We now calculate the process of single-top production and decay, $W^* \to t\bar{b} \to Wb\bar{b}$, at all-orders in the large-b_0 approximation. Explicative examples of the diagrams that must be considered are illustrated in Fig. 1. We stress that together with the virtual and real corrections where the gluon line has been dressed, we also need to include the contribution arising from a real $g \to q\bar{q}$ splitting.

The expression for the total-cross section[1] in presence of selection cuts (that we denote with $\Theta(\Phi)$, being Φ a phase space point) is given by

$$\sigma = \int d\Phi \frac{d\sigma}{d\Phi} \Theta(\Phi) = \sigma^{(0)} - \frac{1}{\pi b_0} \int_0^\infty d\lambda \frac{d}{d\lambda} \left[\frac{T(\lambda)}{\alpha_s(\mu)} \right] \arctan \left[\pi b_0 \alpha_s (\lambda e^{-C/2}) \right] \tag{8}$$

where $\sigma^{(0)}$ is the Born cross section, C is the renormalization-scheme dependent constant that we choose in such a way that

$$\alpha_s(\lambda e^{-C/2}) = \alpha_s(\lambda) + \alpha_s^2(\lambda) b_0 C + \mathcal{O}(\alpha_s^3) \equiv \alpha_s(\lambda) + \frac{\alpha_s^2(\lambda)}{2\pi} \left[\left(\frac{67}{18} - \frac{\pi^2}{6} \right) C_A - \frac{5}{2} n_l \right] = \alpha_s^{\text{CMW}}(\lambda), \tag{9}$$

where CMW denotes the Catani-Marchesini-Webber renormalization scheme for the strong coupling [11], also known as the Monte Carlo scheme. The function $T(\lambda)$ is given by

$$T(\lambda) = \sigma^{(1)}(\lambda) + \frac{3\lambda^2}{2T_R \alpha_s(\mu)} \int d\Phi_{g^*} d\Phi_{\text{dec}} \frac{d\sigma_{q\bar{q}}^{(2)}(\Phi)}{d\Phi} \left[\Theta(\Phi) - \Theta(\Phi_{g^*}) \right], \tag{10}$$

where $\sigma^{(1)}(\lambda)$ is the $\mathcal{O}(\alpha_s)$ cross section calculated with a gluon of mass λ, $\sigma_{q\bar{q}}^{(2)}$ is the leading-order cross section for the process $W^* \to Wb\bar{b}q\bar{q}$, Φ_{g^*} is the phase-space for the production of a heavy gluon of mass λ, Φ_{dec} the phase-space for its decay into a $q\bar{q}$ pair (so that the total phase space Φ can be written as $d\Phi = \frac{d\lambda^2}{2\pi} d\Phi_{g^*} d\Phi_{\text{dec}}$). Thus we see that the factor $T(\lambda) - \sigma^{(1)}(\lambda)$ takes into account the fact that the event in which the $q\bar{q}$ pair has been clustered in a massive gluon g^* can lead to different kinematics with respect to the full event. This term is closely related to the Milan factor [10].

It is easy to check that the $\mathcal{O}(\alpha_s)$ expansion of eq. 8 is given by $\sigma^{(0)} + \sigma^{(1)}(0)$, as expected. From eq. 8 we also see that we have a linear renormalon if

$$\frac{dT(\lambda)}{d\lambda} \bigg|_{\lambda=0} \neq 0, \tag{11}$$

---

[1]We can obtain the expression of the average value of an observable O from the one of the total cross-section replacing $\Theta(\Phi)$ with $\frac{\Theta(\Phi)}{\sigma^{(0)}} \left[O(\Phi) - \langle O \rangle^{(0)} \right]$ in $T(\lambda)$, where $\langle O \rangle^{(0)}$ is the Born prediction.
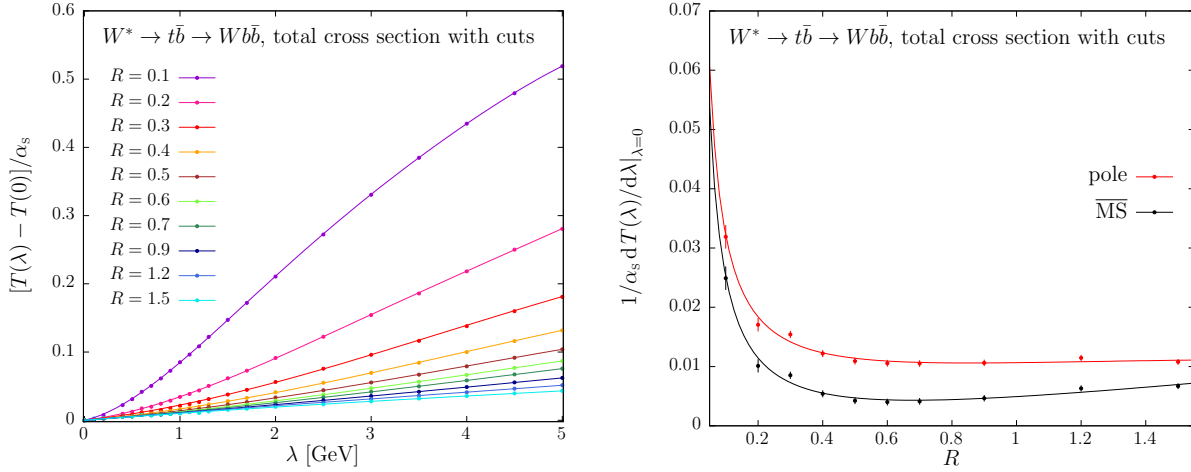
Figure 2: In the left pane the small-λ behaviour for $T(\lambda)$ for the total cross section with cuts calculated in the pole scheme for several jet radii. In the right panel the slope of $T(\lambda)$ at $\lambda = 0$ for the pole and the $\overline{\text{MS}}$ scheme.

so we will focus our attention on the small-λ behaviour of the function $T(\lambda)$ to assess the presence of linear renormalons.

4   Results

In this section we present the most relevant phenomenological results of Ref. [5]. The center-of-mass energy is chosen to be $E = 300$ GeV, the W mass is set to 80.4 GeV and the bottom mass is set to 0. We choose the complex pole scheme for a consistent treatment of top-offshell effect

$$m^2 = m_0^2 - im_0\Gamma_t, \tag{12}$$

where $m_0 = 172.5$ GeV, $\Gamma_t = 1.3279$ GeV. We choose m_0 as renormalization scale. We use the e^+e^- version of the anti-k_T algorithm to reconstruct the b and $\bar{b}$ jets. If not specified, we require the b and the $\bar{b}$ jets to be separated and to have a minimum transverse momentum of 25 GeV.

4.1   Cross section

For the total cross section without cuts the function $T(\lambda)$ reduces to $\sigma^{(1)}(\lambda)$. For small values of λ, the linear λ term is due to the pole-mass counterterm and is equal to

$$\left.\frac{dT(\lambda)}{d\lambda}\right|_{\lambda=0} = \alpha_s(\mu)\frac{C_F}{2}\frac{\partial\sigma^{(0)}(m, m^*)}{\partial\text{Re}(m)}, \tag{13}$$

where $\text{Re}(m)$ denotes the real part of the top mass. By expanding eq. (8) in series of $\alpha_s(\mu)$, we find that the minimal term is reached at the 8th order and leads an ambiguity of relative order 5×10^{-4}.

When the $\overline{\text{MS}}$ scheme is employed, such linear renormalon disappears and the behaviour of the perturbative series improves, no visible minimum arises considering the first 10th orders and the relative corrections are smaller then 10^{-5} already from the 4th order.

However, when selections cuts to identify the final state are introduced, the benefit of using the $\overline{\text{MS}}$ scheme is reduced. The requirement that the b and the $\bar{b}$ jets are separated and have a minumum
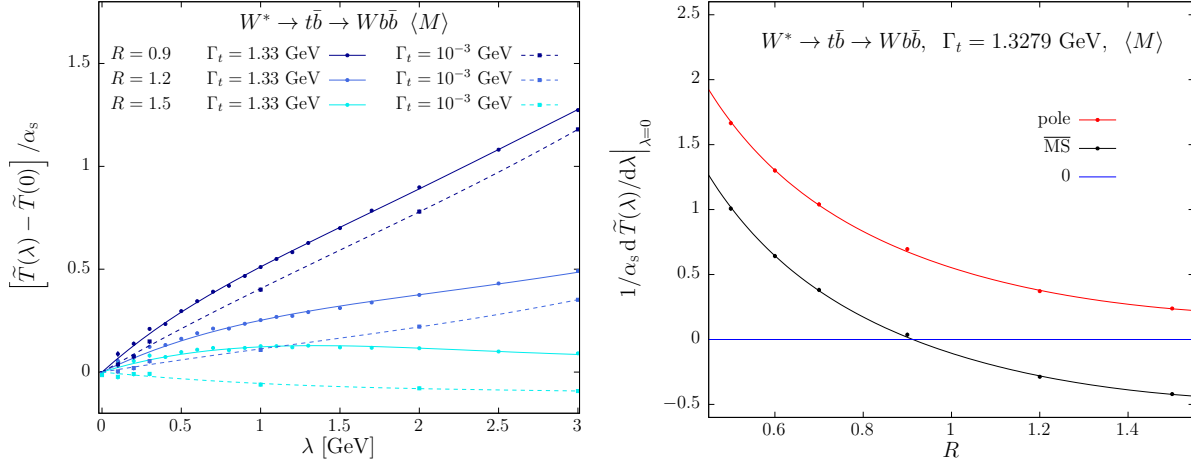
Figure 3: In the left pane the small-λ behaviour for $T(\lambda)$ for the reconstructed-top mass calculated in the pole scheme for several jet radii using $\Gamma_t = 1.3279$ GeV (solid lines) and $\Gamma_t = 10^{-3}$ GeV (dashed lines). In the right panel the slope of $T(\lambda)$ at $\lambda = 0$ for the pole and the $\overline{\text{MS}}$ scheme.

transverse momentum of 25 GeV introduces a linear term whose magnitude grows with the inverse of the jet radius, as was found in other contexts as well [12, 13]. This behaviour is illustrated in Fig 2.

4.2 Reconstructed-top mass

We define the reconstructed-top mass M as the mass of the system comprising the final-state W boson and the b-jet. As for the case of the cross section, selection cuts introduce a linear-λ term in the function $T(\lambda)$, whose magnitude is proportional to the inverse of the jet radius.

For vanishing top width, M approaches the pole mass when a large jet radius is adopted, thus reducing the renormalon ambuiguity. On the other hand, the use of a short distance scheme like the $\overline{\text{MS}}$ would introduce a term of the form

$$\frac{1}{\alpha_s(\mu)} \frac{dT(\lambda)}{d\lambda}\bigg|_{\lambda=0} = -\frac{C_F}{2} \frac{\partial M(m, m^*)}{\partial \text{Re}(m)} \approx -\frac{C_F}{2} = -0.667, \tag{14}$$

and thus have a worse perturbative expansion. This behaviour is due to the fact that this observable contains a physical renormalon that cancels with the pole renormalon if the pole scheme is adopted.

The inclusion of finite-width effects slightly modifies the slope of the function $T(\lambda)$ in the range $\lambda < \Gamma_t$, as can be seen from the left panel of Fig. 3. In the right panel of the same figure we see that for large jet radii there is still a large cancellation between the physical renormalon present in the definition of M and the one in the pole mass. In the $\overline{\text{MS}}$ scheme we do observe a cancellation between the jet renormalon and the one in M for jet radii of the order of 0.9. However, conversely to the previous case, this cancellation is accidental and cannot be taken as indication of a small overall ambiguity as the two effects should be considered independent source of errors.

4.3 Leptonic observables

The last observable we consider is the average value of the energy of the final-state W boson, $\langle E_W \rangle$, which can be considered as a proxy of all leptonic observables. For this analysis we do not impose any selection cuts to avoid to be contaminated by jet renormalons.

We find that in the narrow-width approximation, $\langle E_W \rangle$ has a linear renormalon both in the pole and in the $\overline{\text{MS}}$ scheme. Conversely to the case of the total cross section, if we compute E_W in the laboratory frame the calculation cannot be factorized between production and decay, thus spoiling the cancellation of the linear λ term in $\langle E_W \rangle$. This cancellation takes place only if E_W is computed in the top frame.

When a finite width is employed, the top can never be on-shell as p_t^2 is real, thus a linear λ term can develop only if the pole mass counterterm is used. However, this is also telling us that we can start appreciating the good convergence of the $\overline{\text{MS}}$ scheme at orders $n = 1 + \log(m/\Gamma_t) \approx 6$, as it can be seen from Tab. 1.

	$\langle E_W \rangle$ [GeV]			
	pole scheme		$\overline{\text{MS}}$ scheme	
i	c_i	$c_i\,\alpha_s^i$	c_i	$c_i\,\alpha_s^i$
1	$-1.435\,(0) \times 10^1$	$-1.552\,(0) \times 10^0$	$-7.192\,(0) \times 10^0$	$-7.779\,(0) \times 10^{-1}$
2	$-4.97\,(4) \times 10^1$	$-5.82\,(4) \times 10^{-1}$	$-3.88\,(4) \times 10^1$	$-4.54\,(4) \times 10^{-1}$
3	$-1.79\,(5) \times 10^2$	$-2.26\,(6) \times 10^{-1}$	$-1.45\,(5) \times 10^2$	$-1.84\,(6) \times 10^{-1}$
4	$-6.9\,(4) \times 10^2$	$-9.4\,(6) \times 10^{-2}$	$-5.7\,(4) \times 10^2$	$-7.8\,(6) \times 10^{-2}$
5	$-2.9\,(3) \times 10^3$	$-4.4\,(5) \times 10^{-2}$	$-2.4\,(3) \times 10^3$	$-3.5\,(5) \times 10^{-2}$
6	$-1.4\,(3) \times 10^4$	$-2.2\,(4) \times 10^{-2}$	$-1.0\,(3) \times 10^4$	$-1.7\,(4) \times 10^{-2}$
7	$-8\,(2) \times 10^4$	$-1.3\,(4) \times 10^{-2}$	$-5\,(2) \times 10^4$	$-8\,(4) \times 10^{-3}$
8	$-5\,(2) \times 10^5$	$-9\,(4) \times 10^{-3}$	$-2\,(2) \times 10^5$	$-4\,(4) \times 10^{-3}$
9	$-3\,(2) \times 10^6$	$-7\,(4) \times 10^{-3}$	$-1\,(2) \times 10^6$	$-2\,(4) \times 10^{-3}$
10	$-3\,(2) \times 10^7$	$-6\,(5) \times 10^{-3}$	$0\,(2) \times 10^6$	$-1\,(5) \times 10^{-4}$

Table 1: Coefficients of the perturbative expansion of the average W-boson energy in the pole and $\overline{\text{MS}}$-mass schemes.

The last undesirable feature connected to the use of this observable is the reduced sensitivity to the top mass. Indeed, for our choice of the center-of-mass energy $d\langle E_W \rangle / dm \approx 0.1$, while in the top frame $d\langle E_W \rangle / dm \approx 0.4$.

5   Conclusions

In these proceedings we have summarized the method introduced in Ref. [5] to evaluate all-orders corrections in the large-b_0 approximation. When the method is applied to processes involving a decaying top quark, we can predict which observables are affected by linear renormalons if the pole or a short-distance mass scheme is adopted. This method is also sensitive to linear corrections associated with jets.

The total cross section does not display linear renormalons related to the top mass if a short distance scheme is adopted. This is the case for leptonic observables only if a finite width Γ_t is employed, unless such observables are computed in the top frame. This also implies that the good convergence of leptonic-observables predictions will manifest only at high orders ($n \geq 1 + \log(m/\Gamma_t) \approx 6$). The reconstructed-top mass is affected by a physical renormalon that partially cancels with the one contained in the pole mass definition. This cancellation is almost exact for $\Gamma_t \to 0$ if the jet radius is large enough.

6 Acknowledgements

The work summarized here has been carried out in collaboration with Paolo Nason and Carlo Oleari. I also want to thank the organisers of LFC19 for the invitation, particularly Gennaro Corcella, Giancarlo Ferrera and Francesco Tramontano, the STRONG-2020 network for the financial support and Tomáš Ježo for useful comments on the manuscript.

References

1. M. Beneke, P. Marquard, P. Nason and M. Steinhauser, Phys. Lett. B **775** (2017) 63 doi:10.1016/j.physletb.2017.10.054 [arXiv:1605.03609 [hep-ph]].

2. A. H. Hoang, C. Lepenik and M. Preisser, JHEP **1709** (2017) 099 doi:10.1007/JHEP09(2017)099 [arXiv:1706.08526 [hep-ph]].

3. M. Butenschoen, B. Dehnadi, A. H. Hoang, V. Mateu, M. Preisser and I. W. Stewart, Phys. Rev. Lett. **117** (2016) no.23, 232001 doi:10.1103/PhysRevLett.117.232001 [arXiv:1608.01318 [hep-ph]].

4. A. H. Hoang, S. Plätzer and D. Samitz, JHEP **1810** (2018) 200 doi:10.1007/JHEP10(2018)200 [arXiv:1807.06617 [hep-ph]].

5. S. Ferrario Ravasio, P. Nason and C. Oleari, JHEP **1901** (2019) 203 doi:10.1007/JHEP01(2019)203 [arXiv:1810.10931 [hep-ph]].

6. S. Ferrario Ravasio, arXiv:1902.05035 [hep-ph].

7. M. Beneke, Phys. Rept. **317** (1999) 1 doi:10.1016/S0370-1573(98)00130-6 [hep-ph/9807443].

8. M. Beneke and V. M. Braun, Phys. Lett. B **348** (1995) 513 doi:10.1016/0370-2693(95)00184-M [hep-ph/9411229].

9. P. Ball, M. Beneke and V. M. Braun, Nucl. Phys. B **452** (1995) 563 doi:10.1016/0550-3213(95)00392-6 [hep-ph/9502300].

10. Y. L. Dokshitzer, A. Lucenti, G. Marchesini and G. P. Salam, Nucl. Phys. B **511** (1998) 396 Erratum: [Nucl. Phys. B **593** (2001) 729] doi:10.1016/S0550-3213(97)00650-0, 10.1016/S0550-3213(00)00646-5 [hep-ph/9707532].

11. S. Catani, B. R. Webber and G. Marchesini, Nucl. Phys. B **349** (1991) 635. doi:10.1016/0550-3213(91)90390-J

12. G. P. Korchemsky and G. F. Sterman, Nucl. Phys. B **437** (1995) 415 doi:10.1016/0550-3213(94)00006-Z [hep-ph/9411211].

13. M. Dasgupta, L. Magnea and G. P. Salam, JHEP **0802** (2008) 055 doi:10.1088/1126-6708/2008/02/055 [arXiv:0712.3014 [hep-ph]].

Z PORTAL TO A CONFINING HIDDEN SECTOR

Ennio Salvioni

Physik-Department, Technische Universität München, Garching, Germany
Theoretical Physics Department, CERN, Geneva, Switzerland

Abstract

Motivated by Neutral Naturalness we consider hidden QCD with one light flavor, which confines at a scale Λ in the range $0.1 \lesssim \Lambda/\text{GeV} \lesssim 10$. The hidden and visible sectors interact through both the Higgs and Z portals. The latter dominates the phenomenology, making exotic Z decays a powerful probe of the hidden mesons. This talk is based on Ref. [1], with some additional comments.

1 Introduction

The existence of a hidden sector, which interacts weakly with the Standard Model (SM), is an important possible manifestation of New Physics. Given the enormous range of options for such theories, motivations from addressing open questions of the SM, such as the Higgs naturalness and Dark Matter problems, provide key guidance. A central example is given by theories of Neutral Naturalness, where a *confining* hidden sector, or "hidden valley," [2] is generically expected.

The name Neutral Naturalness (NN) defines a broad set of symmetry-based solutions to the little hierarchy problem, where the top partners are neutral under the SM strong interactions, thus reconciling the lightness of the Higgs with the strong LHC bounds on new colored particles. While the quantum numbers and properties of the top partners vary greatly (see Refs. [3, 4, 5, 6, 7] for a partial list of proposals), these particles are always charged under a hidden color $SU(3)'$ symmetry. The cancellation of the largest (i.e., quadratic) one-loop corrections to the Higgs mass is achieved even if $SU(3)'$ is a global symmetry, but two-loop effects are quantitatively relevant and suggest gauging $SU(3)'$, with coupling approximately equal to the SM QCD coupling at the ultraviolet scale (of $O(10)$ TeV) where the NN theory requires completion. [8] As a consequence, hidden color is generically expected to confine at a scale

Λ within the typical range $0.1 \lesssim \Lambda/\text{GeV} \lesssim 10$, since the hidden sector often contains fewer light matter states than the visible sector. The light hidden hadrons can provide crucial signatures of NN.

Several factors determine the detailed phenomenology of NN-motivated confining hidden sectors, among which we should mention: the mass spectrum of hidden matter; the portals that connect the hidden and visible sectors, always including at least the Higgs portal; as well as the possible presence of additional interactions within the hidden sector (such as, e.g., hidden electroweak forces). A clear path to progress is, then, to identify representative cases with distinct phenomenology, in order to set targets for experimental searches. In this talk we consider a new type of confining hidden sector, where some of the hidden matter fields are light compared to Λ, and both the Higgs and Z portals couple the hidden sector to the SM. This setup arises as the low-energy limit of a Tripled Top model for supersymmetric NN, [1] which provided motivation for this work. Nonetheless, we emphasize that the necessary ingredients are fairly common in NN, and in what follows we remain agnostic about the ultraviolet (UV) completion, by phrasing our discussion within an effective field theory (EFT) for the SM plus the light hidden fields.

2　The setup

We consider a hidden sector containing one Dirac fermion ψ in the fundamental representation of the local $SU(3)'$, with mass $m_\psi \ll \Lambda$. ψ is a full singlet under the SM, but couples to the visible sector according to the effective Lagrangian

$$\mathcal{L}_6 = \frac{y_t^2}{2M^2}\Big(|H|^2\,\overline{\psi}_R i\slashed{D}\psi_R + \text{h.c.} + i(D_\mu H)^\dagger H\,\overline{\psi}_R\gamma^\mu\psi_R + \text{h.c.} + c_g\,\frac{\hat{\alpha}_s}{12\pi}|H|^2\hat{G}^a_{\mu\nu}\hat{G}^{a\,\mu\nu}\Big), \qquad (1)$$

where M is the mass of heavy fermions charged under both the SM electroweak interactions and $SU(3)'$, which are expected in several UV-complete NN models. The appearance of the top Yukawa y_t in Eq. (1) is specific to the Tripled Top (TT) model, but we note that it simply fixes our normalization for M. c_g is a dimensionless parameter, and $\hat{\alpha}_s$ is the fine structure constant of $SU(3)'$. The EFT description encoded by $\mathcal{L}_6$ is valid at energies $\Lambda \ll E \ll M$.

In unitary gauge the second operator of Eq. (1) yields a small coupling of ψ to the Z boson, and thus a branching ratio for Z decays to the hidden sector,

$$\frac{g_Z}{2}\frac{y_t^2 v^2}{2M^2}\overline{\psi}_R\gamma^\mu\psi_R Z_\mu \quad \rightarrow \quad \text{BR}(Z \to \overline{\psi}\psi) \approx 2.2 \times 10^{-5}\left(\frac{2\,\text{TeV}}{M}\right)^4, \qquad (2)$$

where $g_Z \equiv \sqrt{g^2 + g'^2}$. The first operator in Eq. (1) can be rewritten as $y_t^2|H|^2 m_\psi\overline{\psi}\psi/(2M^2)$ by applying the equation of motion for ψ, hence it plays a negligible role under our assumption of small m_ψ. Therefore, the couplings of the Higgs to the hidden sector are mediated by the last operator in Eq. (1),

$$\frac{y_t^2 v^2}{2M^2}\frac{h}{v}c_g\,\frac{\hat{\alpha}_s}{12\pi}\hat{G}^a_{\mu\nu}\hat{G}^{a\,\mu\nu} \quad \rightarrow \quad \text{BR}(h \to \hat{g}\hat{g}) \approx 2.0 \times 10^{-4}\left(\frac{\hat{\alpha}_s}{0.18}\right)^2\left(\frac{2\,\text{TeV}}{M}\right)^4\left(\frac{c_g}{4}\right)^2, \qquad (3)$$

where $\hat{g}$ denotes the hidden gluons, and we chose as reference some typical expectations for $\hat{\alpha}_s$ and c_g. [1] Taking into account that the statistics attainable for Z production at current and future colliders is much larger than for h production, we find that Z decays have a far superior reach in probing the hidden sector. For example, at the 13 TeV LHC we have $\sigma_Z \approx 55$ nb, $\sigma_h \approx 49$ pb, leading to $N(Z \to \overline{\psi}\psi)/N(h \to \hat{g}\hat{g}) \approx 120\,(0.18/\hat{\alpha}_s)^2(4/c_g)^2$. Looking ahead to future e^+e^- colliders, a Z factory could produce between 10^9 and 10^{12} Z bosons, whereas a Higgs factory would be limited to between 10^6 and 10^7 Higgses. Thus we focus on Z decays to the hidden sector, a topic that has received relatively little attention in the literature. [9, 10]
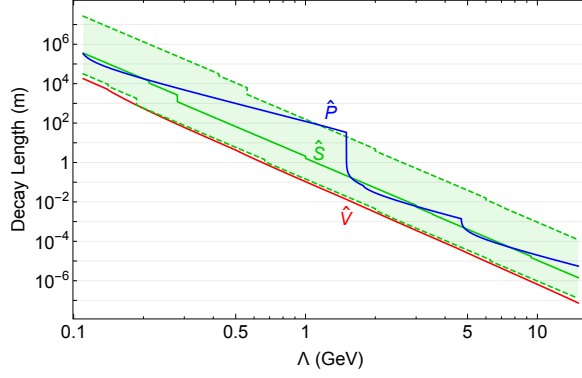
Figure 1: *Decay length of the lightest hidden mesons as a function of Λ, for $M = 2$ TeV. We assume $m_{\hat{P},\hat{V}} = 2\Lambda$ and vary $\Lambda/2 < \Delta m < 3\Lambda/2$ (green band). The solid green line corresponds to $\Delta m = \Lambda$.*

We assume the hidden QCD has one light flavor because this is expected in the TT model. [1)] The distinctive aspect of one-flavor QCD is that it does not predict any light pseudo-Nambu-Goldstone bosons (pNGBs), since the anomaly removes all chiral symmetries. [11)] The only existing lattice study [12)] found that the mesons are nevertheless lighter than the baryons. [1] The lightest meson is the pseudoscalar $\hat{P}$, while the scalar meson is heavier by a factor $m_{\hat{S}}/m_{\hat{P}} \approx 1.5$. Unfortunately, no information is presently available about the vector meson $\hat{V}$, which plays a major role in the phenomenology, as we will see. The lightest baryon $\hat{\Delta}$ (of spin $N_c/2 = 3/2$) is significantly heavier, sitting at $m_{\hat{\Delta}}/m_{\hat{P}} \approx 2.5$-3. Therefore we neglect the effects of baryons, limiting ourselves to note that $\hat{\Delta}$ could also be a candidate for asymmetric Dark Matter, as previously studied in the Fraternal Twin Higgs with light twin bottom, where the low-energy description is one-flavor QCD, too. [13)]

In the one-flavor theory, several among the lightest mesons play an important phenomenological role: here we consider the $\hat{P}, \hat{V}$, and $\hat{S}$. [2] In the absence of any information on $m_{\hat{V}}$ from the lattice, we assume $m_{\hat{P}}, m_{\hat{V}} = 2\Lambda$ and $\Delta m \equiv m_{\hat{S}} - m_{\hat{V}} = \Lambda$ as benchmark, but we also consider departures from this. The mesons decay back to the SM through the Z and Higgs portals in Eq. (1). The $\hat{P}$ decays to the heaviest kinematically available $f\bar{f}$ pair through mixing with the longitudinal Z, whereas the $\hat{V}$ decays "democratically" to fermions via mixing with the transverse Z. For the $\hat{S}$, a detailed analysis [1)] shows that the dipole-type $\hat{S} \to \hat{V} f\bar{f}$ dominates over the Higgs-mediated $\hat{S} \to f\bar{f}$, unless $\Delta m \ll \Lambda$. In summary, all meson decays proceed dominantly through the Z portal. Then the phenomenology is determined by two main parameters: the confinement scale Λ and the mediation scale M. The decay length of the mesons is shown in Fig. 1 as a function of Λ, for $M = 2$ TeV (for different M, the decay length scales as M^4 for all mesons). The green band shows the impact on the $\hat{S}$ decay length of varying $\Lambda/2 < \Delta m < 3\Lambda/2$, stemming from the dependence $\Gamma(\hat{S} \to \hat{V} f\bar{f}) \propto (\Delta m)^7$.

---

[1]This can be partly explained by observing that the pseudoscalar meson $\hat{P}$ is the η', whose mass is $m_{\eta'}^2 = 2N_f\chi_t/f_\pi^2 \propto N_f/N_c$, where χ_t is the topological susceptibility of the pure gauge theory. [14)] Therefore, in the one-flavor case the η' is parametrically lighter than in QCD.

[2]This is in contrast to the multi-flavor scenario, where the pNGBs dominate the signatures. The study of the multi-flavor phenomenology is ongoing. [15)]

3 Phenomenology

An indirect constraint on the setup comes from electroweak precision data, since diagrams contaning two insertions of the Z portal operator give a correction $\widehat{T} = \kappa N_c y_t^4 v^2 / (32\pi^2 M^2)$ to the T parameter, where κ is a model-dependent $O(1)$ coefficient. Taking the TT model as example we have $\kappa = 4/3$, corresponding to a current limit $M \gtrsim 0.9$ TeV, and a projected $M \gtrsim 2.7$ TeV at future e^+e^- colliders. [16] As we illustrate in the remainder of this section, *direct* probes of the hidden sector have the potential to strongly increase the reach on M. A variety of signatures were analyzed in Ref. [1]. Due to space limitations, here we focus only on two representative regions of parameter space.

3.1 $\Lambda \sim 10$ GeV, $M \sim$ few TeV: $Z \to 2$ mesons, prompt decays

In this region the hidden mesons have masses of 10 to 30 GeV, hence Z decays to the hidden sector yield primarily two-meson final states. Among them, we focus here on $Z \to \hat{P}\hat{S}$, which we suspect to be dominant. [1] The most promising final state is $Z \to \hat{P}\hat{S} \to \hat{P}\hat{V}f\bar{f} \to (b\bar{b})(\mu\mu) + X$, where the $b\bar{b}$ and $\mu\mu$ pairs reconstruct $m_{\hat{P}}$ and $m_{\hat{V}}$, respectively.

At the LHC no search for this process has been performed yet, but we can learn from the existing analyses of $h \to aa \to (b\bar{b})(\mu\mu)$, where a is a light pseudoscalar. We find that the CMS selection, [17] which requires $p_T^{\mu 1,2} > 20, 9$ GeV and $p_T^{b1,2} > 20, 15$ GeV, has ~ 10 times smaller efficiency on our signal compared to $h \to aa$. This is due to the smaller total energy, m_Z versus m_h, which is shared among the final-state objects. Softening the cuts, even by moderate amounts, would have a big impact: we have checked that requiring $p_T^{\mu 1,2} > 17, 8$ GeV (corresponding to the CMS dimuon trigger threshold) and $p_T^b > 15$ GeV gives a factor ~ 2 increase in signal efficiency. Conversely, the mildly stronger cuts adopted in the ATLAS analysis [18] yield negligible sensitivity. We encourage the LHC collaborations to undertake a study of this process, which could fill an important coverage gap. The distribution of the $b\bar{b}\mu\mu$ invariant mass after basic cuts is in Fig. 2(a), for two benchmark meson spectra denoted I and II.

At a future GigaZ factory, the same final state is background free ($N_B < 0.1$ events) after a set of dedicated cuts. Normalized distributions of the $b\bar{b}\ell\ell$ invariant mass after the initial selection are shown for both signal and background in Fig. 2(b). The 95% CL projected limits on the mediation scale are
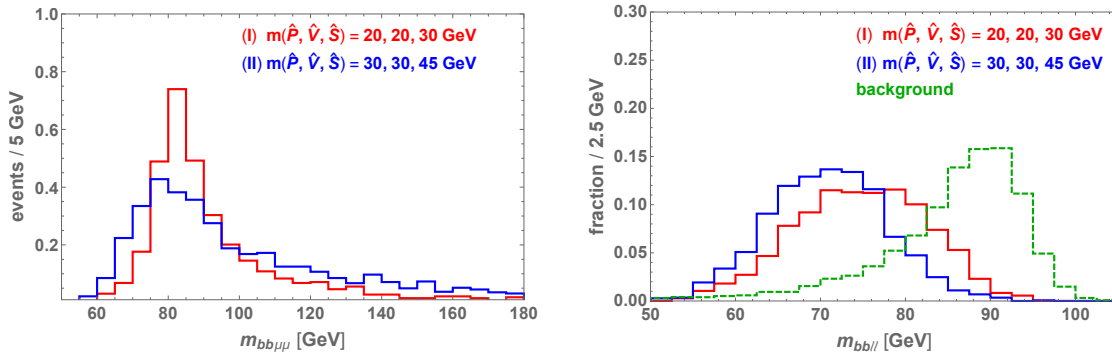

Figure 2: *a) LHC 13 TeV, 35.9 fb^{-1}: distribution of the invariant mass of the $b\bar{b}\mu\mu$ system for the $Z \to \hat{P}\hat{S} \to \hat{P}\hat{V}f\bar{f} \to (b\bar{b})(\mu\mu) + X$ signal, after basic cuts. b) Future Z factory: normalized distribution of the $b\bar{b}\ell\ell$ invariant mass ($\ell = e$ or μ) for the $Z \to \hat{P}\hat{S} \to \hat{P}\hat{V}f\bar{f} \to (b\bar{b})(\ell\ell) + X$ signal and the background, after basic cuts.*

$M \gtrsim 5.4$ [5.2] TeV $(\mathcal{B}_{\hat{P}\hat{S}}/1)^{1/4}$ for benchmark I [II], where $\mathcal{B}_{\hat{P}\hat{S}}$ is the fraction of Z decays to the hidden sector that result in the $\hat{P}\hat{S}$ final state. We have estimated that LEP1 had a limited sensitivity to this signature, due to the smaller statistics and low b-tagging efficiency.

3.2 $\Lambda \lesssim$ 2-3 GeV: $Z \to$ hidden jets, long-lived mesons

For sufficiently small Λ, the Z decays to the hidden sector result in parton showering and formation of hidden jets. These objects share some similarities with emerging [19] and semi-visible [20] jets, but are characterized by the softer production mode and by the democratic decay of the vector meson $\hat{V}$ to SM fermions. We find that the best sensitivity can be obtained at LHCb, by resolving a single $\hat{V} \to \mu\mu$ decay within the Vertex Locator, [21] while $\hat{P}$ is assumed to be collider-stable. The reach, shown in Fig. 3(a) for representative parameters, is optimal for $c\tau_{\hat{V}} = O(1)$ cm. Including the expected background, the projected 95% CL limits are $M \gtrsim 1.6$ (2.0) TeV for an integrated luminosity $L = 15$ (300) fb^{-1}.

For $m_{\hat{V}} \lesssim$ GeV the vector meson can also be produced through other mechanisms, including bremsstrahlung, meson decays, and Drell-Yan. In this regime the $\hat{V}$ behaves as a composite dark photon, which however couples to the SM neutral current but not to the electromagnetic current. In the absence of a dedicated study of this case, we draw a crude picture of the current and future sensitivity by neglecting the differences between the weak and electromagnetic charges of the SM fermions. In this way we obtain an "effective kinetic mixing parameter" $\varepsilon \approx 10^{-7}(m_{\hat{V}}/\text{GeV})^2(2\,\text{TeV}/M)^2$ that allows us to place our $\hat{V}$ on the standard dark photon parameter space, as shown in Fig. 3(b). The promising sensitivity expected at planned experiments motivates a detailed analysis of this scenario, which is left for future work.

4 Concluding remarks

We have shown that the Z portal, which had not been considered before in the hidden valley literature, can dramatically improve the prospects to detect the hidden sector. Here we have highlighted only a few among the possible signatures, and we refer the reader to Ref. [1] for a thorough analysis. We conclude by
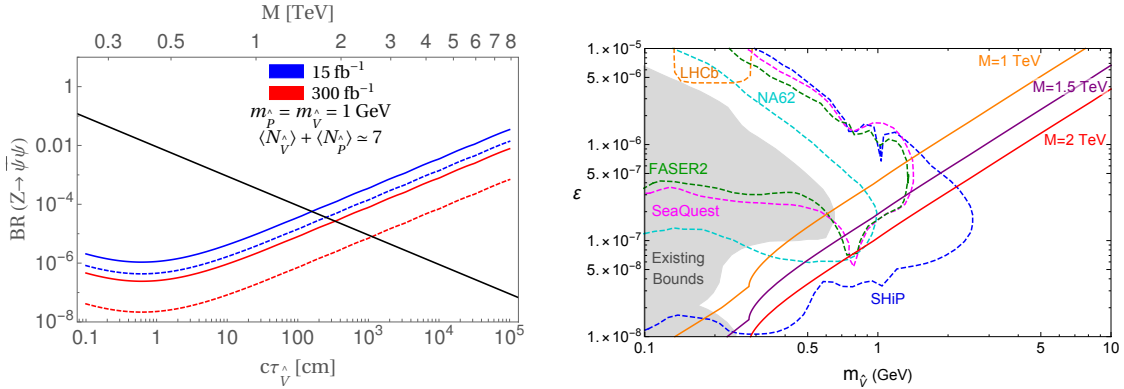

Figure 3: a) Projected limits on the Z branching ratio to the hidden sector, derived from the search for a single $\hat{V} \to \mu\mu$ displaced vertex within a hidden jet at LHCb. Solid (dashed) lines correspond to the standard background prediction (a background-free hypothesis). The straight black line corresponds to the theory prediction. b) Solid lines illustrate where our $\hat{V}$ lies in the dark photon parameter space, for three M benchmarks. The bending at small $m_{\hat{V}}$ is due to the inclusion of BR($\hat{V} \to \nu\bar{\nu}$). Current exclusions are shaded in gray, while the projected reach of future experiments is shown by dashed curves.

stressing that the lack of non-perturbative results for one-flavor QCD (beyond the partial ones given in the pioneering Ref. [12]) is a real limitation for beyond-the-SM phenomenology, and we hope that studies like the one presented in this talk will provide motivation for further lattice work. [3]

References

1. H.-C. Cheng, L. Li, E. Salvioni and C. Verhaaren, JHEP **1911** 031 (2019), arXiv:1906.02198 [hep-ph].

2. M.J. Strassler and K.M. Zurek, PLB **651** 374 (2007), arXiv:hep-ph/0604261.

3. Z. Chacko, H.S. Goh and R. Harnik, PRL **96** 231802 (2006), arXov:hep-ph/0506256.

4. G. Burdman, Z. Chacko, H.S. Goh and R. Harnik, JHEP **0702** 009 (2007), arXiv:hep-ph/0609152.

5. H. Cai, H.-C. Cheng and J. Terning, JHEP **0905** 045 (2009), arXiv:0812.0843 [hep-ph].

6. H.-C. Cheng, L. Li, E. Salvioni and C. Verhaaren, JHEP **1805** 057 (2018), arXiv:1803.03651 [hep-ph].

7. T. Cohen, N. Craig, G.F. Giudice and M. McCullough, JHEP **1805** 091 (2018), arXiv:1803.03647 [hep-ph].

8. N. Craig, A. Katz, M. Strassler and R. Sundrum, JHEP **1507** 105 (2015), arXiv:1501.05310 [hep-ph].

9. N. Blinov, E. Izaguirre and B. Shuve, PRD **97** 015009 (2018), arXiv:1710.07635 [hep-ph].

10. J. Liu, L.T. Wang, X.P. Wang and W. Xue, PRD **97** 095044 (2018), arXiv:1712.07237 [hep-ph].

11. M. Creutz, Annals Phys. **322** 1518 (2007), arXiv:hep-th/0609187.

12. F. Farchioni *et al.*, EPJ C **52** 305 (2007), arXiv:0706.1131 [hep-lat].

13. I. García García, R. Lasenby and J. March-Russell, PRL **115** 121801 (2015), arXiv:1505.07410 [hep-ph].

14. E. Witten, Nucl. Phys. B **156** 269 (1979); G. Veneziano, Nucl. Phys. B **159** 213 (1979).

15. H.-C. Cheng, L. Li, E. Salvioni and C. Verhaaren, in progress.

16. J. Fan, M. Reece and L.T. Wang, JHEP **1509** 196 (2015), arXiv:1411.1054 [hep-ph].

17. CMS Collaboration, PLB **795** 398 (2019), arXiv:1812.06359 [hep-ex].

18. ATLAS Collaboration, PLB **790** 1 (2019), arXiv:1807.00539 [hep-ex].

19. P. Schwaller, D. Stolarski and A. Weiler, JHEP **1505** 059 (2015), arXiv:1502.05409 [hep-ph].

20. T. Cohen, M. Lisanti and H.K. Lou, PRL **115** 171804 (2015), arXiv:1503.00009 [hep-ph].

21. A. Pierce, B. Shakya, Y. Tsai and Y. Zhao, PRD **97** 095033 (2018), arXiv:1708.05389 [hep-ph].

22. T. DeGrand and E.T. Neil, arXiv:1910.08561 [hep-ph].

---

[3]A recent, excellent effort to bridge the gap between lattice and composite phenomenology is Ref. [22].

EXOTIC TOP-PARTNER DECAYS: SEARCH GAPS AND OPPORTUNITIES

Thomas Flacke

Center for Theoretical Physics of the Universe, Institute for Basic Science (IBS), Daejeon, 34126, Korea

Abstract

Current LHC searches for vector-like quarks (VLQs) mostly focus on VLQ decays into electroweak gauge bosons and a top or bottom quark. However, many Standard Model extensions with VLQs which address the hierarchy problem also contain potentially light BSM scalars, which allow for additional VLQ decay channels. We present several theoretically well motivated "exotic" top partner decays, determine the sensitivity of current LHC searches for them and discuss possible new search channels and strategies. As one example, we point out that the VLQ decay $T \to ta \to tgg$ is only weakly constrained. As another example, we show that exotic decays of charge 5/3 top partners are constrained by same-sign lepton searches, but simple extensions can substantially increase the discovery potential for some decays. As a framework, we use underlying models of a composite Higgs with top partners, but our phenomenological studies are performed in terms of effective models and applications to other models with VLQs. These proceedings are mainly based on the following articles: [1, 2, 3, 4)

1 Introduction

Top partners, i.e. vector-like quarks (VLQs) which dominantly couple to the Standard Model top and bottom quarks, are a crucial part of many Standard Model extensions which address the hierarchy problem, including composite Higgs models with top partial compositeness, Little-Higgs models, or models with extra-dimensions, and have also been studied as extensions of supersymmetric models and two-Higgs-doublet models. Many of these models contain BSM resonances beyond the top partner(s) to which it can decay (which in the following we refer to as "exotic" decays). The ATLAS and CMS collaborations run active search programs for top partners, which so far have mainly focused on QCD pair production of top partners with subsequent decay into an electroweak boson (W, Z, h) and a 3rd generation quark

(t, b).[1] Under the assumption that no exotic VLQ decays occurs, VLQs with charge 5/3, 2/3, -1/3, and -4/3 are excluded up to a mass of 1.35 TeV [8], 1.3-1.45 TeV [9], 1.0-1.35 TeV [9], and 1.35 TeV [9].[2]

How do these bounds change if (theoretically well-motivated) exotic VLQ decays are present? Are there search gaps and (how) can they be closed? And are there new "golden channels"?

To address these questions, we first give a brief theoretical motivation for exotic VLQ decays in underlying models of a composite Higgs in Sec. 2. We then present results on exotic decays for charge 2/3 VLQs (T) into either tgg or $tb\bar{b}$ through a neutral scalar resonance [1] in Sec. 3, showing that VLQ mass bounds can be substantially relaxed. In Sec. 4, we present results on exotic decays for charge 5/3 VLQs, [2] which show that existing same-sign lepton (SSL) searches provide a good coverage for most decay channels. We also show projections for HL-LHC and discuss in more detail the decay $X_{5/3} \to t\phi^+ \to t\gamma W^+$ for which the sensitivity can be substantially increased by simple means.

We conclude in Sec. 5.

2 A theory motivation for exotic VLQ decays: underlying models of a composite Higgs

Vector-like quarks commonly emerge as top partners in composite Higgs models where the top acquires a mass via a linear mixing in the partial compositeness mechanism. [10] Underlying models in which the Higgs and the top partnerx arise as bound states of underlying fermions which are charged under a confining hyper-color gauge group have been classified. [11, 12] The models contain two types of underlying fermions (ψ, χ). The Higgs is realized as a pseudo-Nambu-Goldstone boson (pNGB) $\psi\psi$, of the global ψ-family symmetry which is spontaneously broken when hyper-color gets strongly coupled at a scale of $\mathcal{O}(10 \text{ TeV})$, and the electroweak gauge group is embedded into the unbroken subgroup. The (colored) top partners are $\chi\psi\psi$ or $\chi\chi\psi$ bound states, and $SU(3)_c$ is embedded in the unbroken subgroup of the χ-family symmetry. All models yield an additional anomaly free SM-neutral pNGB (a) (and an anomalous and thus potentially heavy η') as well as additional electroweakly charged and colored pNGBs, which are listed in Table 1.

Table 1: *Goldstone bosons in underlying models of a composite Higgs with partial top compositeness, depending on the global symmetry pattern.* [12]

Electroweak coset	$SU(2)_L \times U(1)_Y$
$SU(5)/SO(5)$	$\mathbf{3}_{\pm 1} + \mathbf{3}_0 + \mathbf{2}_{\pm 1/2} + \mathbf{1}_0$
$SU(4)/Sp(4)$	$\mathbf{2}_{\pm 1/2} + \mathbf{1}_0$
$SU(4) \times SU(4)'/SU(4)_D$	$\mathbf{3}_0 + \mathbf{2}_{\pm 1/2} + \mathbf{2}'_{\pm 1/2} + \mathbf{1}_{\pm 1} + \mathbf{1}_0 + \mathbf{1}'_0$
Color coset	$SU(3)_c \times U(1)_Y$
$SU(6)/SO(6)$	$\mathbf{8}_0 + \mathbf{6}_{(-2/3 \text{ or } 4/3)} + \bar{\mathbf{6}}_{(2/3 \text{ or } -4/3)}$
$SU(6)/Sp(6)$	$\mathbf{8}_0 + \mathbf{3}_{2/3} + \bar{\mathbf{3}}_{-2/3}$
$SU(3) \times SU(3)'/SU(3)_D$	$\mathbf{8}_0$

While colored pNGBs are excluded for masses below ~ 1 TeV, [12, 13] electroweak and SM neutral pNGBs are far less constrained by experiment. As an example, we show bounds on the SM neutral

---

[1] Single-produced VLQs have a high discovery potential, [5, 6] and several searches by ATLAS and CMS are available, but bounds are more model-dependent as the production depends on a BSM coupling. Searches for VLQ decays into electroweak bosons and light quarks are also possible, [7] but less explored, experimentally.

[2] T, B have three "standard" decay channels and precise bounds depend on the branching ratio.

pseudo-scalars a and η' in Fig. 1. a and η' are linear combinations of $\chi\chi$ and $\psi\psi$ bound states, and their couplings to gauge bosons within a model are fixed by anomaly coefficients, while couplings to SM fermions are proportional to their mass. Thus, in a given model, all branching ratios of a and η' are fixed, and the only free parameters are their mass, which originates from explicit symmetry breaking, and their decay constant, which is related to the composite Higgs decay constant f_ψ.[3, 12] Hence, for a given model and masses, resonance search bounds can be translated into a bound on f_ψ.

Figure 1 shows these bounds and future projections[14] for one sample model ("M7").[3] For "M7", like for all other models, f_ψ is very weakly constrained for (theoretically expected) light a and heavy η'. This shows that a light a is still experimentally viable and can be tested at future LHC runs.[14]
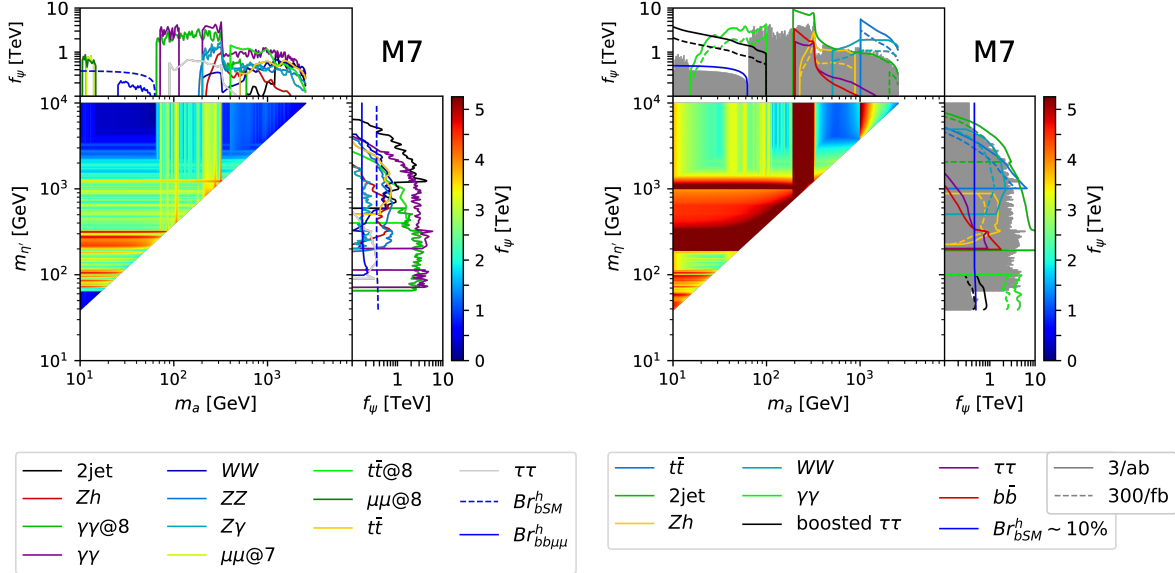

Figure 1: *Bounds on the Higgs decay constant f_ψ from resonance searches for a and η' pNGBs in the m_a vs. $m_{\eta'}$ mass plane.*[3] *Left: Bounds from current searches. Right: Projected bounds for HL-LHC (including proposed searches for light a*[14, 15]*).*

In underlying models, the hyper-fermion content of VLQs (and pNGBs) is determined, which allows to classify their couplings, showing that VLQ decays into the pNGB a and those listed in Table 1 are the rule rather than the exception.[4]

3 Exotic charge 2/3 VLQ decays: mind the search gap

The presence of new VLQ decay channels can substantially alter bounds on VLQs. As a first example, we consider QCD pair production of a top partner T with the dominant decay $T \to ta$, with either $a \to gg$ or $a \to b\bar{b}$ (which in underlying models are the dominant a decays for $m_a < 2m_t$).[1] The new final states are thus $(t(jj))(\bar{t}(jj))$ and $(t(b\bar{b}))(\bar{t}(b\bar{b}))$, where resonances are indicated by brackets, and the tops can either decay leptonically or hadronically. The former final state is not well-covered by VLQ searches, and we found the 8 TeV RPV SUSY search[16] and the 13 TeV excited top search[17] to be most sensitive.

---

[3]Results for all models of the classification[11] are available.[3]

For the latter final state, regions of the broad-band VLQ search for $T \to th$ [18] have some sensitivity. Fig.2 shows the resulting bounds which are obtained by recasting the above cited searches.[4] As can be seen, in particular the $T \to ta \to tgg$ decay is only very weakly constrained. This is not surprising, as $t\bar{t} + jets$ is a background for VLQ searches, but in the case of $(t(jj))(\bar{t}(jj))$ (with a resonance structure), it is also the signal.
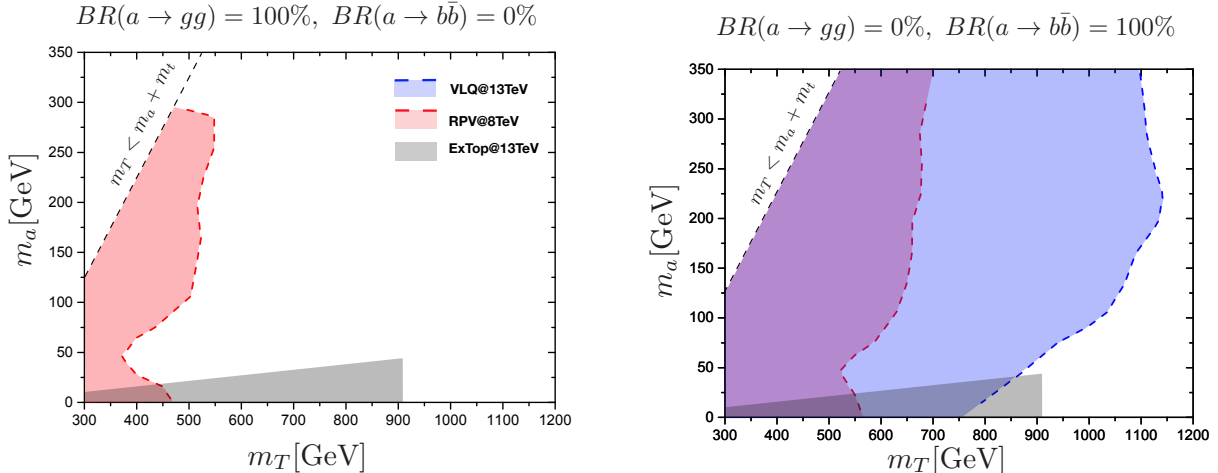

Figure 2: *Direct search limits on the m_T vs. m_a plane for different branching ratios of a to gg and $b\bar{b}$.* [1] *Grey: Exclusion from the excited top search. Red: Exclusion from the RPV SUSY search. Blue: Exclusion from the VLQ search.*

4 Exotic charge 5/3 VLQ decays: reinterpreting same-sign lepton searches

As a second example, we consider pair production and exotic decays of a charge 5/3 top partner $X_{5/3}$.[2] The "standard" decay is $X_{5/3} \to tW^+$, but, with the pNGBs listed in Table 1 present, additional decays into a charged ϕ^+ or doubly charged ϕ^{++}, or a color-sextet charge 4/3 π_6 are possible, which themselves have several possible decay channels. However, all decays can yield same-sign leptons.

Fig.3 shows the bounds which we obtain for various decay channels (which are motivated from underlying models) by recasting the VLQ same-sign lepton search [19]. For reference, the bound on $M_{X_{5/3}}$ for the "standard" decay is shown in green. Dashed lines indicate an estimate of the exclusion reach at HL-LHC with 3 ab^{-1} luminosity.[5] As can be seen, the bounds for exotic decays are in most cases comparable to those obtained for $X_{5/3} \to tW^+$. Only in case of longer cascade decays, the bounds are weaker, as the resulting leptons have lower p_T. The SSL search is relatively robust, as it is performed as a cut-and-count analysis. The final state kinematics of standard and exotic decays differ substantially [2] and would be distinguishable if an excess was observed, but it does not have a large impact on the current bounds.

---

[4] See Ref. [1] for details on the recasting and for bounds with other branching ratios of T.

[5] As a by-product, recasting the same-sign lepton search also yields a direct bound on the mass of the color-sextet M_{π_6}, indicated in red in the top-left plot.

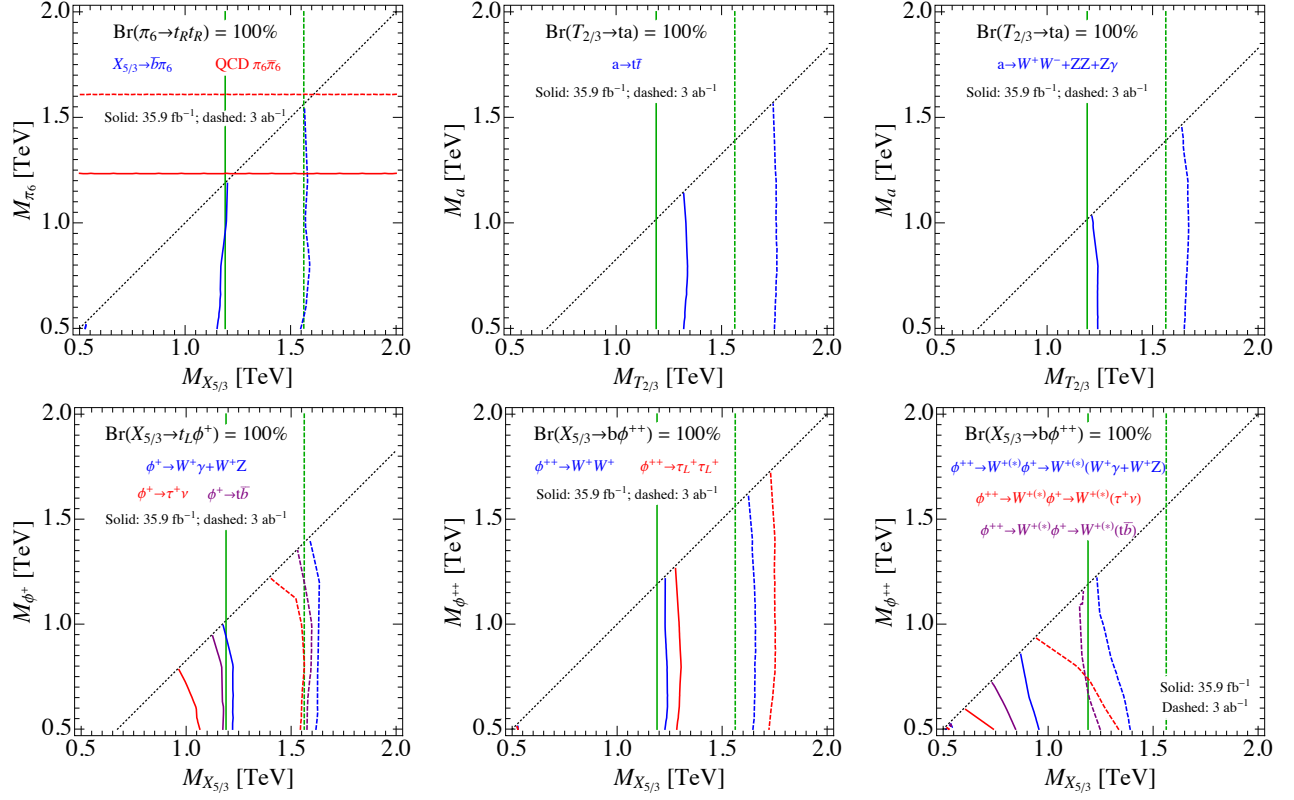Figure 3: *Bounds and projected LHC-HL bounds for various exotic VLQ decays from same-sign lepton searches in the M_{VLQ} vs. M_{pNGB} mass plane.* [2]
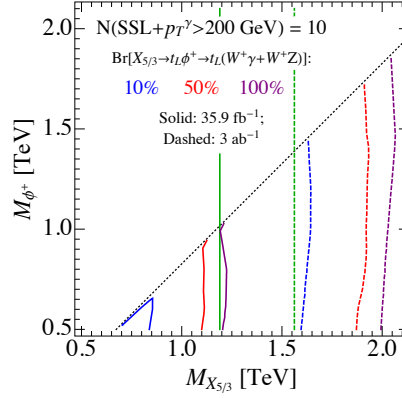

Figure 4: *Contours of 10 signal events for LHC with 35.9 fb^{-1} and for HL-LHC with 3 ab^{-1} after demanding SSL search cuts and a hard photon cut in the $M_{X_{5/3}}$ vs. M_{ϕ^+} mass plane for various $BR(X_{5/3} \to t\phi^+ \to tW^+\gamma)$.* [2]

Several final states of exotic decays offer features which could be explored to suppress the background further. As an example, the $X_{5/3} \to t\phi^+ \to tW^+\gamma$ decay yields a high-p_T photon in addition to same-sign leptons. Fig. 4 shows the parameter space in which we expect 10 signal events with the SSL cuts applied before, with the addition of demanding one hard photon ($p_T > 200$ GeV). For SSL background, event-rates with an additional high-p_T photon are very suppressed. Thus checking for high p_T photons provides a very efficient handle to search for the $X_{5/3} \to t\phi^+ \to tW^+\gamma$ decay.

5 Conclusions and outlook

Many models with VLQs also contain additional, lighter BSM states into which VLQs decay, as demonstrated in the context of underlying models with a composite Higgs and partial top compositeness. These common exotic VLQ decays yield a plethora of novel final states which are not explicitly targeted by current VLQ searches at the LHC. As a first example, we demonstrated that, for the decay $T \to ta \to tgg$, reinterpretations of existing searches yield a very weak bound, as low as $M_T \gtrsim 400\text{-}550$ GeV (depending on m_a), while for the channel $T \to ta \to t b\bar{b}$ bounds are $M_T \gtrsim 900\text{-}1100$ GeV, and thus not substantially weaker than for standard VLQ decay channels. As a second example, we showed that same-sign lepton searches yield a good coverage of $X_{5/3}$ decays, and that the discovery potential can be improved for some decay channels.

These examples show how much exotic decays can alter the VLQ phenomenology, bounds, and opportunities. A comprehensive analysis of theoretically well-motivated VLQ decays and their collider phenomenology is needed to maximize the LHC search reach and coverage, to leave no stone unturned.

References

1. G. Cacciapaglia, T. Flacke, M. Park and M. Zhang, "Exotic decays of top partners: mind the search gap," Phys. Lett. B **798** (2019) 135015, [arXiv:11908.07524 [hep-ph]].

2. K. P. Xie, G. Cacciapaglia and T. Flacke, "Exotic decays of top partners with charge 5/3: bounds and opportunities," JHEP **1910** (2019) 134, [arXiv:11907.05894 [hep-ph]].

3. G. Cacciapaglia, G. Ferretti, T. Flacke and H. Serdio, "Light scalars in composite Higgs models," Front. in Phys. **7** (2019) 22, [arXiv:1902.06890 [hep-ph]].

4. N. Bizot, G. Cacciapaglia and T. Flacke, "Common exotic decays of top partners," JHEP **1806** (2018) 065, [arXiv:1803.00021 [hep-ph]].

5. M. Backovi, T. Flacke, S. J. Lee and G. Perez, "LHC Top Partner Searches Beyond the 2 TeV Mass Region," JHEP **1509** (2015) 022, [arXiv:1409.0409 [hep-ph]].

6. M. Backovic, T. Flacke, J. H. Kim and S. J. Lee, "Search Strategies for TeV Scale Fermionic Top Partners with Charge 2/3," JHEP **1604** (2016) 014, [arXiv:1507.06568 [hep-ph]].

7. C. Delaunay, T. Flacke, J. Gonzalez-Fraile, S. J. Lee, G. Panico and G. Perez, "Light Non-degenerate Composite Partners at the LHC," JHEP **1402** (2014) 055, [arXiv:1311.2072 [hep-ph]].

8. M. Aaboud *et al.* [ATLAS Collaboration], "Search for pair production of heavy vector-like quarks decaying into high-p_T W bosons and top quarks in the lepton-plus-jets final state in pp collisions at $\sqrt{s} = 13$ TeV with the ATLAS detector," JHEP **1808** (2018) 048, [arXiv:1806.01762 [hep-ex]].

9. M. Aaboud *et al.* [ATLAS Collaboration], "Combination of the searches for pair-produced vector-like partners of the third-generation quarks at $\sqrt{s} = 13$ TeV with the ATLAS detector," Phys. Rev. Lett. **121** (2018) no.21, 211801, [arXiv:1808.02343 [hep-ex]].

10. D. B. Kaplan, "Flavor at SSC energies: A New mechanism for dynamically generated fermion masses," Nucl. Phys. B **365** (1991) 259.

11. G. Ferretti and D. Karateev, "Fermionic UV completions of Composite Higgs models," JHEP **1403** (2014) 077, [arXiv:1312.5330 [hep-ph]].

12. A. Belyaev, G. Cacciapaglia, H. Cai, G. Ferretti, T. Flacke, A. Parolini and H. Serodio, "Di-boson signatures as Standard Candles for Partial Compositeness," JHEP **1701** (2017) 094, Erratum: [JHEP **1712** (2017) 088], [arXiv:1610.06591 [hep-ph]].

13. G. Cacciapaglia, H. Cai, A. Deandrea, T. Flacke, S. J. Lee and A. Parolini, "Composite scalars at the LHC: the Higgs, the Sextet and the Octet," JHEP **1511** (2015) 201, [arXiv:1507.02283 [hep-ph]].

14. G. Cacciapaglia, G. Ferretti, T. Flacke and H. Serodio, "Revealing timid pseudo-scalars with taus at the LHC," Eur. Phys. J. C **78** (2018) no.9, 724, [arXiv:1710.11142 [hep-ph]].

15. A. Mariotti, D. Redigolo, F. Sala and K. Tobioka, "New LHC bound on low-mass diphoton resonances," Phys. Lett. B **783** (2018) 13, [arXiv:1710.01743 [hep-ph]].

16. G. Aad *et al.* [ATLAS Collaboration], "Search for massive supersymmetric particles decaying to many jets using the ATLAS detector in pp collisions at $\sqrt{s} = 8$ TeV," Phys. Rev. D **91** (2015) no.11, 112016, Erratum: [Phys. Rev. D **93** (2016) no.3, 039901], [arXiv:1502.05686 [hep-ex]].

17. A. M. Sirunyan *et al.* [CMS Collaboration], "Search for pair production of excited top quarks in the lepton + jets final state," Phys. Lett. B **778** (2018) 349, [arXiv:1711.10949 [hep-ex]].

18. M. Aaboud *et al.* [ATLAS Collaboration], "Search for pair production of up-type vector-like quarks and for four-top-quark events in final states with multiple b-jets with the ATLAS detector," JHEP **1807** (2018) 089, [arXiv:1803.09678 [hep-ex]].

19. A. M. Sirunyan *et al.* [CMS Collaboration], "Search for top quark partners with charge 5/3 in the same-sign dilepton and single-lepton final states in proton-proton collisions at $\sqrt{s} = 13$ TeV," JHEP **1903** (2019) 082, [arXiv:1810.03188 [hep-ex]].

RECONSTRUCTING MSSM PARAMETERS FROM HIGGS SEARCHES

Farvah Mahmoudi

Université de Lyon, Université Claude Bernard Lyon 1, CNRS/IN2P3,
Institut de Physique des 2 Infinis de Lyon, UMR 5822, F-69622, Villeurbanne, France

Theoretical Physics Department, CERN, CH-1211 Geneva 23, Switzerland

Abstract

We present some highlights on the complementarity of the Higgs and SUSY searches at the LHC, using the 8 and 13 TeV results. In particular, we discuss the constraints that can be obtained on the MSSM parameters by the determination of the Higgs boson mass and couplings. In addition, we investigate the interplay with heavy Higgs searches, and evaluate how higher LHC luminosities and a future linear collider can help probing the pMSSM Higgs sector and reconstructing the underlying parameters.

1 Introduction

The discovery of the Higgs boson at the LHC has marked a major step for our understanding of particle physics, and for the construction of the Higgs sector of new physics scenarios. Direct searches for new particles are currently actively pursued at the LHC, in particular in the context of supersymmetry (SUSY). No new physics signal has been discovered so far, implying that new physics should be subtle or heavy. Therefore, indirect constraints are at the moment of utmost importance. The measurements of the properties of the Higgs boson can provide in this respect very strong constraints on new physics scenarios. The measurement of its mass at 125 GeV [1] is very constraining for supersymmetry, because the Higgs mass can receive large corrections from the stop sector, and has a large impact on the SUSY parameter space [2]. In the following, we will discuss the status of the Higgs sector of the phenomenological MSSM. To do so, we perform random scans on the 19 parameters of the pMSSM, following the procedures detailed in [3]. In particular, we use a master program based on SuperIso [4], generate the MSSM spectra with SOFTSUSY [5] and compute the Higgs boson decay widths and couplings with HDECAY [6]. We keep only the parameter points for which the lightest supersymmetric particle is a neutralino (constituting a dark matter candidate) and with a light Higgs mass of 125 ± 3 GeV.

2 Higgs coupling measurements and SUSY direct searches

We first study the interplay of the measurement of the Higgs boson properties and of the results of the SUSY direct searches. We impose the LEP constraints on the SUSY masses [1]. To assess the constraints from SUSY searches at the LHC, we generate events with PYTHIA [7], simulate the detector with Delphes [8] and obtain constraints from ATLAS and CMS results with a luminosity between 36 and 139 fb^{-1} [9], for gluino and squark, neutralino and chargino, stop and sbottom, and monojet searches. For the Higgs measurements, we consider that there are 6 independent effective Higgs couplings, to the photons κ_γ, gluons κ_g, vector bosons κ_V, tops κ_t, bottoms κ_b and taus κ_τ. We use the combined ATLAS measurements of the Higgs couplings at 7, 8 and 13 TeV [10]. In order to verify whether a point is consistent with these measurements, we use a χ^2 test and keep only the points which are in agreement with the data at 95% C.L. In Figure 1, we present the photon, gluon and bottom squared coupling distributions as a function of M_A, applying different sets of constraints: First we apply the Higgs mass constraint, then the LEP constraints on superpartner masses, followed by the LHC direct search constraints, and finally the constraints from Higgs coupling measurements. We can see that all the shown couplings are sensitive to M_A, in addition to other SUSY parameters which modify the couplings

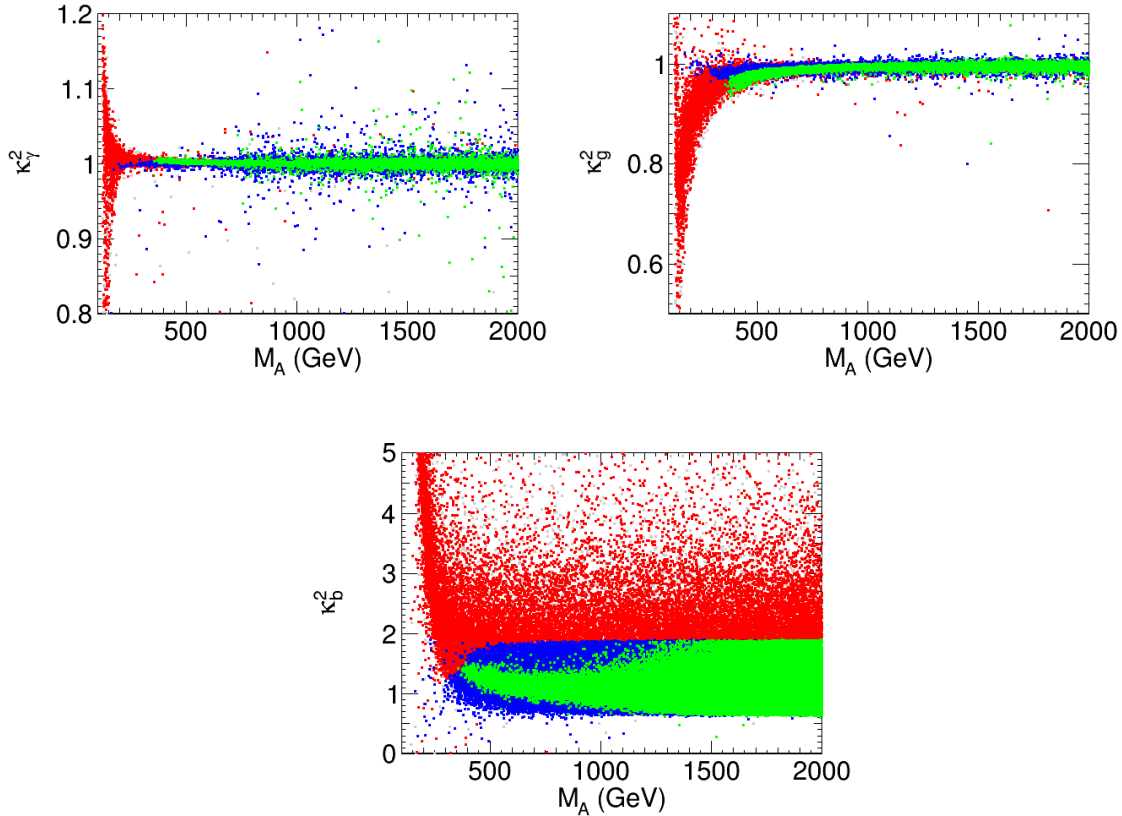Figure 1: *Distributions of the squared light scalar Higgs couplings to photons (upper left), gluons (upper right) and bottoms (lower), as a function of M_A in the pMSSM. The gray points correspond to all points with $M_h \sim 125$ GeV, the red points pass in addition the constraints from LEP, the blue points are also consistent with LHC SUSY direct searches and the green points are compatible with Higgs coupling measurements.*

at loop level. In particular, the photon and gluon couplings are sensitive to the stop and sbottom masses. The bottom coupling is modified by the Δ_b corrections [11]. It is clear that the combination of the direct searches and Higgs measurements strongly restricts the coupling values to be close to 1. Since the different couplings are related to SUSY masses, these results can be used to obtain constraints on the pMSSM parameters.

3 Heavy Higgs direct searches and Higgs coupling measurements

The Higgs sector can be constrained directly through searches for heavier Higgs states and the light Higgs coupling measurements. To compute the Higgs decay rates and production cross-sections we use HDECAY [6] and SusHi [12], respectively, and apply ATLAS and CMS heavy Higgs search limits [13]. We compare the exclusion from the Higgs coupling measurements to the one from heavy Higgs searches in Figure 2, which reveals the important interplay between the light Higgs coupling measurements and the heavy Higgs search limits. We consider three parameter planes: $(M_A, \tan\beta)$ which are the two main parameters for the couplings of the Higgs bosons; $(M_{\tilde{b}_1}, X_b)$ which can enter the Higgs mass calculation and can affect Δ_b; (M_2, μ) which are the main parameters for the electroweakino sector. As can be expected the $(M_A, \tan\beta)$ parameter plane is constrained by both the Higgs coupling measurements and very strongly by heavy Higgs searches, and in particular the $H/A \to \tau^+\tau^-$ searches. The $(M_{\tilde{b}_1}, X_b)$ and (M_2, μ) parameter planes are rather uniformly probed by heavy Higgs searches with a small exclusion power, as these parameters only weakly affect the heavy Higgs production cross-sections. On the contrary, the Higgs couplings are sensitive to light charginos, neutralinos and sbottoms, leading to strong exclusions in some regions of both parameter planes.

4 Prospects for the MSSM Higgs sector

As we have seen in the previous sections, the Higgs couplings are affected by pMSSM parameters, and an important question is whether it can be possible to determine these parameters indirectly through the exploitation of Higgs coupling measurements and direct searches. While it is now impossible with the data at hand, we study here the prospects for the high-luminosity LHC (HL-LHC) run and ILC [14], by considering the possibility of reconstructing specific scenarios using the Higgs coupling measurements. We test two categories of scenarios: the first one where only M_A and $\tan\beta$ are varied, and the second one where $\mu\tan\beta$ is modified. We assume the accuracy reached when the ILC collects 1 ab^{-1} of luminosity at energies between 350 and 800 GeV. We consider the following method: Within our large sample of pMSSM parameter points, we choose a particular scenario in agreement with the current data. We then use, as prospective central experimental values, the Higgs decay rates and cross-sections of this specific point considering the prospective experimental uncertainties for HL-LHC and ILC. We finally search in our sample for the points that are compatible with those data, and find the mean values and standard deviations for M_A and $\tan\beta$, or $\mu\tan\beta$. Table 1 summarizes our results for several example scenarios (some at the limit of being excluded by current searches). We can conclude that the HL-LHC alone would allow us to reconstruct CP-odd Higgs masses up to 500 GeV. For higher masses, or for scenarios with modified $\mu\tan\beta$, the ILC will be necessary to identify the underlying parameters of the scenario.

5 Conclusions

In this study, we have considered the MSSM Higgs sector, and demonstrated how it can be probed by both the light Higgs coupling measurements and heavy Higgs searches. We showed that indirect signals
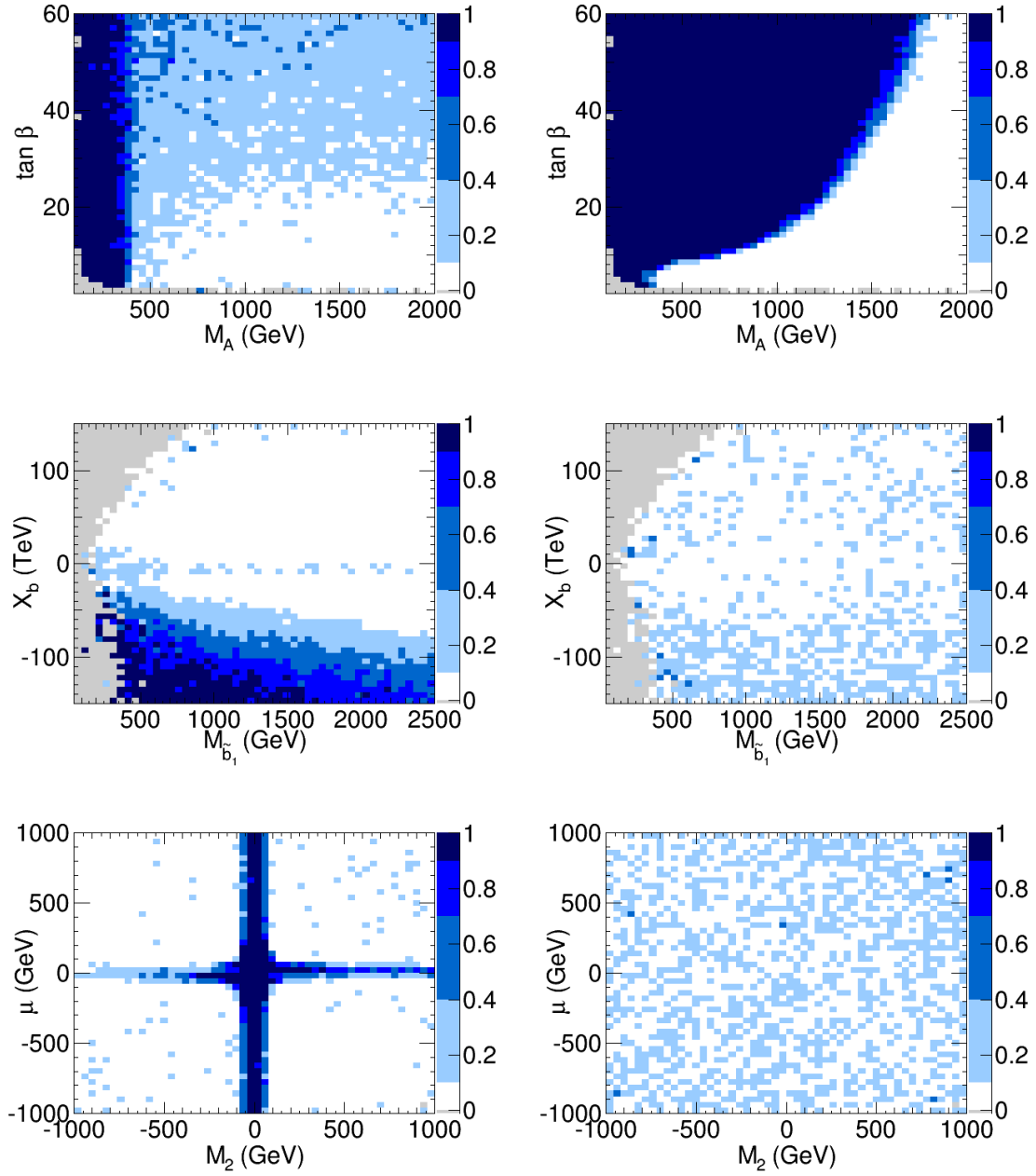
Figure 2: *Fraction of points excluded by Higgs coupling measurements (left) and heavy Higgs searches (right), in the $(M_A, \tan\beta)$ (top), $(M_{\tilde{b}_1}, X_b = A_b - \mu \times \tan\beta)$ (middle) and (M_2, μ) (bottom) parameter planes.*

	M_A(GeV)	$\tan\beta$	M_A(GeV)	$\tan\beta$	M_A(GeV)	$\tan\beta$
Original parameters	334.9	9.9	427.3	5.7	657.2	12.7
HL-LHC reconstruction	394±40	9.6±4.0	471^{+341}_{-56}	-	-	-
ILC reconstruction	351±23	9.2±1.9	460^{+54}_{-45}	10.4^{+6}_{-4}	747.7^{+302}_{-97}	10.2^{+20}_{-4}

Original $\mu\tan\beta$ (TeV)	−149.9	−86.6	0	79.6	108.6
ILC reconstruction	-76.3^{+28}_{-39}	-124.6^{+46}_{-60}	-2.2 ± 22	67.2^{+39}_{-22}	82.5^{+40}_{-22}

Table 1: *Reconstruction potential of different pMSSM scenarios with HL-LHC and ILC projections.*

of supersymmetry can be revealed at the LHC, even in the case no superparticle is directly observed. In addition, precision measurements of the light Higgs properties enables the extraction of the relevant SUSY parameters, if deviations from the SM are observed.

References

1. M. Tanabashi *et al.* [Particle Data Group], Phys. Rev. D **98** (2018) no.3, 030001.

2. A. Arbey *et al.*, Phys. Lett. B **708** (2012) 162 [arXiv:1112.3028]; Eur. Phys. J. C **72** (2012) 1906 [arXiv:1112.3032]; JHEP **1209** (2012) 107 [arXiv:1207.1348]; Phys. Lett. B **720** (2013) 153 [arXiv:1211.4004]; Annalen Phys. **528** (2016) 179 [arXiv:1504.05091].

3. A. Arbey, M. Battaglia and F. Mahmoudi, Eur. Phys. J. C **72** (2012) 1847 [arXiv:1110.3726]; Phys. Rev. D **89** (2014) no.7, 077701; Phys. Rev. D **94** (2016) no.5, 055015 [arXiv:1506.02148].

4. F. Mahmoudi, Comput. Phys. Commun. **180** (2009) 1579 [arXiv:0808.3144]; A. Arbey and F. Mahmoudi, Comput. Phys. Commun. **181** (2010) 1277 [arXiv:0906.0369].

5. B. C. Allanach, Comput. Phys. Commun. **143** (2002) 305 [hep-ph/0104145].

6. A. Djouadi, J. Kalinowski and M. Spira, Comput. Phys. Commun. **108** (1998) 56 [hep-ph/9704448]; A. Djouadi, J. Kalinowski, M. Muehlleitner and M. Spira, arXiv:1801.09506 [hep-ph].

7. T. Sjstrand *et al.*, Comput. Phys. Commun. **191** (2015) 159 [arXiv:1410.3012].

8. J. de Favereau *et al.* [DELPHES 3 Collaboration], JHEP **1402** (2014) 057 [arXiv:1307.6346].

9. A. Ventura [ATLAS and CMS], Int. J. Mod. Phys. Conf. Ser. **46** (2018) 1860006 [arXiv:1711.00152].

10. G. Aad *et al.* [ATLAS Collaboration], Phys. Rev. D **101** (2020) no.1, 012002 doi:10.1103/PhysRevD.101.012002 [arXiv:1909.02845 [hep-ex]].

11. A. Djouadi, Phys. Rept. **459** (2008) 1 [hep-ph/0503173]; M. Spira, Prog. Part. Nucl. Phys. **95** (2017) 98 [arXiv:1612.07651].

12. R. V. Harlander, S. Liebler, H. Mantler, Comput. Phys. Commun. **184** (2013) 1605 [arXiv:1212.3249].

13. J. Schaarschmidt [ATLAS Collaboration], Int. J. Mod. Phys. Conf. Ser. **46** (2018) 1860056; C. Asawatangtrakuldee [CMS Collaboration], PoS EPS-HEP2017 (2017) 254.

14. G. Moortgat-Pick *et al.*, Eur. Phys. J. C **75** (2015) no.8, 371 [arXiv:1504.01726].

ON THE SPECTRUM OF COMPOSITE RESONANCES

Michele Frigerio
Laboratoire Charles Coulomb (L2C), University of Montpellier, CNRS, Montpellier, France

Abstract

I discuss the infrared mass spectrum of strongly-coupled gauge theories, that induce the Higgs as a composite pseudo-Nambu-Goldstone boson. The set of composite states accompanying the Higgs is determined by the symmetries of the theory. Here we estimate their mass spectrum by non-perturbative techniques inspired by QCD, as well as by exploiting gauge-gravity duality.

1 Composite Higgs: motivations and relevant energy scales

As the Large Hadron Collider (LHC) did not find new states significantly coupled to the Standard Model (SM) below the TeV scale, any SM extension by such heavy states suffers from a little hierarchy problem, as the mass of the scalar Higgs boson lies close to the 100 GeV scale. Still, some SM extensions have the potential to address the big hierarchy between the TeV scale and the Planck scale. One possibility is to avoid elementary scalar fields, and assume the observed Higgs is a composite object, with a compositeness scale $f \gtrsim 1$ TeV. This scenario requires a strongly-coupled sector, whose spectrum generically includes several additional composite states besides the Higgs. The mass of the lowest-lying states cannot exceed $\sim 4\pi f$, and some could be significantly lighter and within the LHC reach. Definite predictions for the mass spectrum require to specify the strongly-coupled theory in the ultraviolet (UV). Here we will assume it is a gauge theory of fermions, that confines in the infrared. We will estimate its mass spectrum in some well-defined approximations, by employing non-perturbative techniques inspired by QCD [1], as well as gauge-gravity duality techniques [2].

In models where the Higgs is a pseudo-Nambu-Goldstone boson (pNGB) the electroweak scale, $v \simeq 246$ GeV, is induced in two steps. The theory has a global (flavour) symmtry G_F, that is spontaneously broken to a subgroup H_F at the scale f. The electroweak symmetry $SU(2)_L \times U(1)_Y$ is embedded in

H_F, and the set of NGB includes the SM Higgs doublet. Weak sources of explicit symmetry breaking – typically loops involving the top-quark Yukawa coupling – misalign the vacuum, inducing an effective potential for h, whose minimum determines v. The electroweak precision parameters as well as the Higgs couplings receive corrections of order v^2/f^2, and present data already imply $f \gtrsim 1$ TeV.

If the scale f is induced by strong dynamics, it is protected from large radiative corrections from UV physics, and the pNGB Higgs is a composite object. [3] The spectrum of composite resonances has typical mass gap $m_* \sim g_* f$, where $1 \lesssim g_* \lesssim 4\pi$ is the generic inter-resonance coupling. Since only resonances significantly lighter than $\sim 4\pi f$ have chances to be discovered at the LHC, our aim is to investigate the strong dynamics in order to find a rationale for the lightness of some composite states, besides the pNGB Higgs. In some instances light states are also welcome to minimise the fine-tuning in the Higgs potential.

2 UV-complete composite-Higgs models

A prototypical strongly-coupled sector is provided by an asymptotically-free gauge theory, with a hyper-colour gauge group G_C and fermion matter fields only (no scalars). We will assume that the theory enters a strongly-coupled, walking (approximately scale-invariant) regime at some UV scale Λ_{UV}, and eventually develops a mass gap at some IR scale m_*. A large walking region, that is, a hierarchy $m_* \ll \Lambda_{UV}$, is required to induce the SM Yukawa couplings and to suppress flavour violation at the same time.

The choice of the appropriate gauge theory of fermions requires some exercise in group theory. In order to correctly describe electroweak symmetry breaking and preserve the SM custodial symmetry to a good approximation, the flavour-symmetry-breaking pattern should satisfy $G_F \to H_F \supset SU(2)_L \times SU(2)_R$, and the associated set of NGBs should include the Higgs transforming as $h \sim (2_L, 2_R)$. A generic gauge theory of fermions has flavour symmetry $G_F = SU(N_1) \times \cdots \times SU(N_k) \times U(1)^{k-1}$, where N_i is the number of Weyl fermions in the representation R_i of the gauge group G_C. The minimal possibility satisfying the above requirements is provided by $G_F = SU(4) \to H_F = Sp(4)$, that corresponds to four Weyl fermions in a pseudoreal representation of G_C. The simplest pseudoreal representation is the fundamental of a group $Sp(2n)$. Thus, we are led to choose as hypercolour group $G_C = Sp(2N_C)$, with Weyl fermions $\psi^a \sim \square_{Sp(2N_C)}$, where $a = 1, 2, 3, 4$ is the flavour index.

Once the hypercolour theory confines, the constituent degrees of freedom, ψ^a and the hypergluons, are replaced by composite, hypercolour-singlet states. They are associated to operators constructed out of the constituent fields, in given Lorentz and flavour representations. Let us limit ourselves to fermion-bilinear operators, which excite several spin-0 and spin-1 composite states, including the NGB Higgs, as illustrated in table 1. Scalars organise into a flavour-singlet $\sigma \sim 1_{Sp(4)}$ and a flavour-multiplet $S^{\hat{A}} \sim 5_{Sp(4)}$, where $\hat{A}$ runs over the five broken generators. Pseudoscalars sit in the same representations, $\eta' \sim 1_{Sp(4)}$ and $G^{\hat{A}} \sim 5_{Sp(4)}$. The latter is the NGB multiplet, that is massless in the chiral limit, $G = \{h, \eta\} \sim \{(2_L, 2_R), (1_L, 1_R)\}$: note that the Higgs doublet is accompanied by an electroweak singlet state. On the other hand η' is expected to be massive, because the associated flavour symmetry, an axial $U(1)_\psi$, is anomalous with respect to G_C, in analogy with the axial $U(1)$ in QCD. Coming to spin-one states, vectors organise in a multiplet $V_\mu^A \sim 10_{Sp(4)}$, where A runs over the ten unbroken generators. Axial vectors transform as $a_\mu \sim 1_{Sp(4)}$ and $A_\mu^{\hat{A}} \sim 5_{Sp(4)}$. It is also possible to establish spectral sum rules [1], that relate the masses and decay constants of the various states.

Before discussing the dynamics, let us generalise the model to the case of a large number of flavours N_F. In fact, in a realistic model the group G_F should contain several other symmetries besides $SU(2)_L \times SU(2)_R$. Firstly, in order to induce the SM Yukawa couplings, one needs to mix the SM fermions with composite operators. The latter should have the same colour and electroweak charges as the various SM

	Lorentz	$Sp(2N_C)$	$SU(4)$	$Sp(4)$
ψ_i^a	$(1/2,0)$	$\square_i$	4^a	4
$\overline{\psi}_{ai} \equiv \psi_{aj}^\dagger \Omega_{ji}$	$(0,1/2)$	$\square_i$	$\overline{4}_a$	4^*
$M^{ab} \sim (\psi^a \psi^b)$	$(0,0)$	1	6^{ab}	$5+1$
$\overline{M}_{ab} \sim (\overline{\psi}_a \overline{\psi}_b)$	$(0,0)$	1	$\overline{6}_{ab}$	$5+1$
$a^\mu \sim (\overline{\psi}_a \overline{\sigma}^\mu \psi^a)$	$(1/2,1/2)$	1	1	1
$(V^\mu, A^\mu)_a^b \sim (\overline{\psi}_a \overline{\sigma}^\mu \psi^b)$	$(1/2,1/2)$	1	15_b^a	$10+5$

Table 1: The transformation properties of the constituent fermions, and of the spin-0 and spin-1 fermion bilinears, in the $N_F = 2$ model. The hypercolour $Sp(2N_C)$ indexes $i, j, \ldots$ are contracted by the antisymmetric invariant tensor Ω_{ij}, and brackets stand for hypercolour-invariant contractions. Spinor indexes are understood, and $a, b, \ldots$ are flavour $SU(4)$ indexes.

fermions, therefore the whole $SU(3)_c \times SU(2)_L \times U(1)_Y$ needs to be embedded within G_F. Secondly, the SM global symmetries, such as baryon and lepton number, or custodial, should be also included in G_F, to avoid that hypercolour dynamics violates these symmetries too strongly. Thus, one is led to introduce additional constituent fermions, $\psi^a \sim \square_{Sp(2N_C)}$, with $a = 1, \ldots, 2N_F$, corresponding to the flavour-symmetry-breaking pattern $G_F = SU(2N_F) \to H_F = Sp(2N_F)$, with $N_F \gtrsim 5$ depending on the model details. [2] One also needs [4, 1] to introduce constituents fermions X in larger representation of $Sp(2N_C)$, in order to build hypercolour-singlet trilinear operators such as $(\psi\psi X)$, that interpolate fermionic composite states, such as top-quark partners. We argue that, to preserve asymptotic freedom, it is preferable to minimise the number of X flavours, and rather assign the required SM charges to the $2N_F$ copies of ψ. Here we will neglect the X sector, and discuss only the spectrum of ψ-bilinear operators.

To go beyond the symmetry considerations above, and derive a quantitative estimate of the mass spectrum, one needs to model the hypercolour dynamics, either numerically on the lattice, or by some analytical approximations in the large-N_C limit. We will show that the latter provide relatively rapid and general estimates for the spectrum, complementarily to lattice computations, which are currently limited to $Sp(2N_C)$ theories with $N_C = 1, 2$. [5] In order to determine the spectrum of composite states associated to a given operator, one has to determine the poles of the associated two-point correlation function. Let us consider, for illustration, the case of vector currents,

$$i \int d^4x \, e^{iq \cdot x} \langle \text{vac} | T\{\mathcal{J}_\mu^A(x) \mathcal{J}_\nu^B(0)\} | \text{vac} \rangle = \Pi_V(q^2) \delta^{AB} (q_\mu q_\nu - \eta_{\mu\nu} q^2) \tag{1}$$

where $\mathcal{J}_\mu^A = \overline{\psi} \overline{\sigma}_\mu T^A \psi$. In the large-$N_C$ limit one expects the form factor to behave as a sum over narrow resonances, $\Pi_V(q^2) \simeq \sum_n f_{Vn}^2 (q^2 - m_{Vn}^2)^{-1}$. Our aim is to estimate the position of the poles, m_{Vn}^2, and similarly for other two-point correlators. We will discuss two methods that provide an analytic approximation for such correlators.

3   Spectrum of mesons à la Nambu-Jona Lasinio

The Nambu-Jona Lasinio (NJL) model approximates strong dynamics by effective four-fermion interactions. This corresponds to give a dynamical mass to the gauge bosons and decouple them, writing an effective Lagrangian for the constituent fermions only. For the $Sp(2N_C)$ hypercolour theory, the

$SU(2N_F)$-invariant Lagrangian for $N_F = 2$ reads [4]

$$\mathcal{L}_{scalar} = \frac{\kappa_A}{2N_C}(\psi^a \psi^b)(\overline{\psi}_a \, \overline{\psi}_b) - \frac{\kappa_B}{8N_C}\left[\epsilon_{abcd}(\psi^a \psi^b)(\psi^c \psi^d) + h.c.\right] , \tag{2}$$

where for simplicity we included only scalar-scalar operators. The κ_A operator is induced by a tree-level hypergluon exchange, while the κ_B operator accounts for the anomaly of the axial $U(1)_\psi$ symmetry. One can show [4, 1] that this NJL Lagrangian can describe spontaneous breaking $SU(4) \to Sp(4)$, by inducing a non-zero mass gap, $N_C M_\psi = (\kappa_A + \kappa_B)\langle\psi\psi\rangle \neq 0$, where M_ψ is the dynamical mass for the fermions.

To estimate two-point correlators, one can resum massive fermion loops, at leading order in $1/N_C$:

Here ϕ is the meson associated with a given fermion bilinear, K_ϕ is the corresponding four-fermion coupling, and the resummation describes the composite meson propagator,

$$\overline{\Pi}_\phi(q^2) \equiv \frac{\tilde{\Pi}_\phi(q^2)}{1 - 2K_\phi\tilde{\Pi}_\phi(q^2)} , \tag{3}$$

where $\tilde{\Pi}_\phi$ is the one-loop function. The resummation of the geometric series induces a pole in the composite propagator $\overline{\Pi}_\phi$, for some specific value of q^2, that defines the meson mass in the NJL approximation.

In fig.1 we show our results for the pole of each meson correlator, as a function of the dimensionless four-fermion coupling $\xi \equiv (\kappa_A+\kappa_B)\Lambda^2/(4\pi^2)$, where Λ is the cutoff of the fermion loops. One can check [1] that $\xi \geq 1$ is needed to induce a non-zero M_ψ and global symmetry breaking, while $\xi \leq (1 - \ln 2)^{-1}$ is needed for the mass gap not to exceed the cutoff, $M_\psi \leq \Lambda$. The NGB decay constant f can also be computed [1] as a function of ξ: in fig.1 the meson masses are given in units of f. Note the pole positions do not scale with N_C, however $f \sim N_C^{1/2}$, therefore the physical masses decrease with the number of colours if $f \simeq$ TeV is kept fixed. The only exception is the η' pole, that scales as $N_C^{-1/2}$, as the axial anomaly vanishes in the large-N_C limit.

Assuming the dynamics is dominated by a current-current operator (corresponding to a single hypergluon exchange), one can relate the scalar-scalar and vector-vector operators by using Fierz identities: this fixes the relative size of spin-zero and spin-one meson masses. The latter are always heavy, $\gtrsim 5f$, while spin-zero mesons can become light in several cases. First, NGBs are massless, $M_h = M_\eta = 0$, as we neglected possible sources of $SU(4)$ explicit breaking. Second, the singlet pseudoscalar η' also becomes light in the large-N_C limit. Third, the singlet scalar σ becomes light as the four-fermion coupling approaches the critical value $\xi = 1$. This lightness indicates that the four-fermion operator becomes marginal as $\xi \to 1$, that is, the explicit breaking of scale invariance vanishes, and σ can be interpreted as an approximate dilaton.

4 Spectrum of mesons via gauge-gravity duality

If the hypercolour sector is close to a fixed point, it behaves as an approximately Conformal Field Theory (CFT). The CFT in the limit of large number of colours, N_C, and large 't Hooft coupling, $\lambda \equiv g_C^2 N_C$, has a holographic description in terms of a five-dimensional (5d) theory of gravity in the classical and weakly-coupled regime, with Anti-de Sitter (AdS) metric, $ds^2 = dr^2 + e^{2A(r)}dx_{1,3}^2$ with warp factor $A(r) = r$. [6] Holography implications for composite Higgs scenarios are reviewed in Ref. [7].
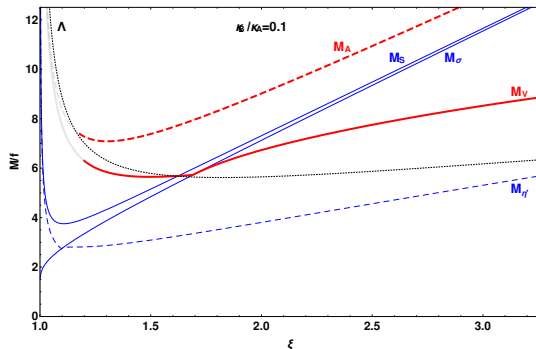
Figure 1: The masses of the spin-zero (blue) and spin-one (red) mesons in units of the Goldstone decay constant f, as a function of the dimensionless four-fermion coupling $\xi \equiv (\kappa_A + \kappa_B)\Lambda^2/(4\pi^2)$, for $\kappa_B/\kappa_A = 0.1$ and $N_C = 4$. The Goldstone multiplet (not shown) is massless, $M_G = 0$, and the two axial-vector multiplets are degenerate, $m_a = M_A$. See Ref. [1] for more details.

According to the holographic dictionary, the CFT global symmetry corresponds to a 5d gauge symmetry G_F, and CFT operators O_Φ are associated to 5d fields Φ, in the same G_F representation and with the same spin. Moreover, CFT correlators correspond to 5d correlators built from the bulk action on-shell, $S_{bulk}^{on-shell}$, in particular they scale in the same way with N_C and N_F. [2] For example, the glue-glue correlator $\langle G_{ij} G_{ij} \rangle \sim N_C^2$ can be extracted from a 5d gravity action, $S_{bulk}[R] \propto N_C^2$, with R the Ricci scalar. On the other hand, the fermion-fermion correlator $\langle \psi_i^a \psi_j^a \Omega_{ij} \rangle \sim N_C N_F$ is associated to a 5d scalar action, $S_{bulk}[\mathrm{Tr}\,\Phi^{ab}] \propto N_C N_F$, with a 5d scalar Φ^{ab} dual to the operator $(\psi^a \psi^b)$.

The CFT departure from scale invariance in the IR with a mass gap m_* can be described by adding a 5d scalar field with non-flat profile, $\sigma(r)$. The latter back-reacts on the metric, inducing a warp factor $A(r) \neq r$, that is, a departure from AdS. Let us consider the case $\sigma(r) \equiv \mathrm{Tr}\,[\Phi^{ab}(r)]/N_F$, that is, the scalar associated to flavour-symmetry breaking. The gravity-scalar interplay is described by

$$ S_{bulk} \supset N_C^2 \int d^5x \sqrt{-g} \left[\frac{R}{4} - \frac{\Lambda_c}{2} - x_F \left(\frac{1}{2} g^{MN} \partial_M \sigma \partial_N \sigma + V(\sigma) \right) \right] \tag{4} $$

where $x_F \equiv N_F/N_C$ and Λ_c a cosmological constant. We are interested in the large N_F case, to accommodate all the required SM global symmetries. Thus, we are led to consider the Veneziano limit, with large N_C and constant $x_F \sim 1$. This implies that the back-reaction of the flavour sector on the 5d geometry is an order-one effect. Indeed, for some appropriate choice of the potential $V(\sigma)$, motivated by string theory compactifications, the equations of motion imply [2] that $A(r)$ and $\sigma(r)$ have a singularity at some finite value $r = r_{IR}$, which corresponds to the dynamical generation of a mass gap, $m_* \neq 0$. This opens the possibility to relate m_* and the G_F spontaneous-breaking scale f, that is associated to $\langle O_\sigma \rangle$.

The nature of scale-invariance breaking is determined by the UV behaviour of $\sigma(r)$,

$$ \sigma(r) \underset{r \to \infty}{\simeq} \left(\sigma_- e^{-\Delta_- r} + \sigma_+ e^{-\Delta_+ r} \right), \quad \Delta_\pm = 2 \pm \sqrt{4 + m_\sigma^2}, \tag{5} $$

where the bulk mass m_σ as well as the values of $\sigma_\pm$ depend on the choice of $V(\sigma)$. We are interested in the regime $-4 \leq m_\sigma \leq 0$, corresponding to a departure from scale-invariance in the IR. The dual operator $\mathcal{O}_\sigma$ has scaling dimension Δ_+. A non-zero σ_- corresponds to a relevant deformation of the CFT, $\Delta \mathcal{L}_{CFT} = \sigma_- \mathcal{O}_\sigma$. This amounts to explicit breaking of scale invariance and G_F: the CFT couplings acquire non-zero β-functions, and there are no massless dilaton nor exact NGBs. A non-zero σ_+ corresponds to a vacuum
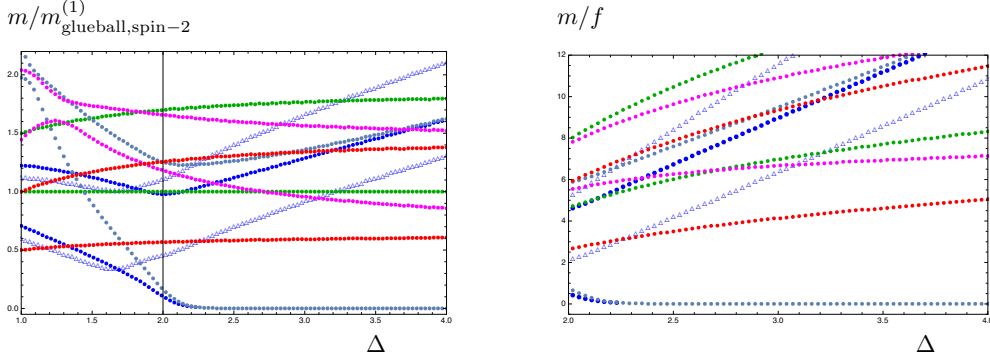
Figure 2: The masses of the flavour-singlet scalars (blue), flavour-multiplet scalars (blue triangles), pseudoscalars (cyan), vectors (red), axial vectors (magenta) and spin-two glueballs (green), in units of the lightest spin-two mass (left panel) and in units of the Goldstone decay constant f (right panel), as a function of the anomalous dimension Δ.

expectation value, $\langle \mathcal{O}_\sigma \rangle \sim \sigma_+$, that controls spontaneous breaking of scale invariance and G_F. In models with $\sigma_- \to 0$ one then finds a massless dilaton as well as massless NGBs.

In order to estimate the composite mass spectrum, let us extract the poles of two-point correlators using the gauge-gravity duality. The solution of the equations of motion for $A(r)$ and $\sigma(r)$ fixes the 5d background. One can expand S_{bulk} around such background, to quadratic order in the field fluctuations, for any 5d field ϕ_i, dual to the CFT operator of interest $\mathcal{O}_i$. Solving the equations of motion linear in the fluctuations, one can compute S_{bulk} on shell. The latter determines the CFT correlators, according to

$$\langle \mathcal{O}_1 \mathcal{O}_2 \rangle = \lim_{r \to \infty} \frac{\delta^2 S_{bulk}^{on-shell}[\phi_i]}{\delta \phi_1 \delta \phi_2} \ . \tag{6}$$

Let us consider the CFT correlator in momentum space, and call the 4d momentum q. The 5d field fluctuations satisfy appropriate boundary conditions [2] only for discrete values of q^2, that correspond to the mass of the composite states. For example, the axial-vector transverse correlator takes the form

$$\langle J^\mu(q) J^\nu(-q) \rangle = - \lim_{r \to \infty} \frac{\delta^2 S_{bulk}^{on-shell}}{\delta A_\mu(-q,r) \delta A_\nu(q,r)} \sim \lim_{r \to \infty} \left[e^{2A(r)} (\eta^{\mu\nu} - q^\mu q^\nu / q^2) \frac{\partial_r A_\rho(q,r)}{A_\rho(q,r)} \right] \ . \tag{7}$$

In this case the poles are given by the values of q^2 where the 5d gauge field vanishes asymptotically, $\lim_{r \to \infty} A_\rho(q,r) = 0$. Moreover, the value of f^2 is given by the residue of this correlator at $q^2 = 0$.

In the left panel of fig.2 we show our preliminary result for the spectrum of bosonic resonances (spin 0, 1 and 2), as a function of the parameter Δ, defined by $\sigma(r) \sim e^{-\Delta r}$ for $r \to \infty$, in units of the smallest spin-two mass. The dilaton and NGBs remain massless for $2 < \Delta < 4$ (spontaneous symmetry breaking), while they are lifted for $0 < \Delta < 2$ (explicit symmetry breaking). With the given choice of model parameters the dilaton mass grows faster than the pNGB one. Scale invariance may be broken explicitly by additional flavour-singlet sources, that raise the mass of the dilaton only. [2] From the phenomenological perspective, one should include radiative corrections from SM couplings, in particular the top quark Yukawa, before comparing the pNGB mass with the 125 GeV scalar observed at the LHC. An even lighter dilaton cannot be excluded, as its couplings to the SM are suppressed. [8] In the spontaneous breaking regime, one can estimate f and display the spectrum in units of f, see the

right panel of fig.2. We remark that the exact value of f is determined by the overall normalisation of the gauged-G_F kinetic term. [2] While the f scaling with N_C and N_F is generic, the order-one normalisation can be predicted only in a complete top-down model coming e.g. from a specific string theory.

5 Perspective

We showed that, in UV-complete models for the Higgs compositeness, a plethora of composite states are expected to accompany the Higgs boson. We focused on the composite bosons of the hypercolour theory, associated to fermion-bilinear operators. Similarly, one can consider composite fermions, associated to fermion-trilinear operators, relevant to induce Yukawa couplings, especially the large top-quark one. In order to study the strongly-coupled sector, one needs to model non-perturbative effects, making radical assumptions to simplify the dynamics. We considered the NJL model and a gauge-gravity duality model, showing that they catch several essential features of the mass spectrum, and thus provide an important guidance for future searches, even though quantitative estimates are model-dependent. The crucial phenomenological question is whether some new states could be significantly lighter than the compositeness scale, $m_* \sim 10$ TeV. The rationale for light spin-zero states is to realise a hierarchically large (small) spontaneous (explicit) breaking scale for global symmetries. Light spin-one-half states may occur in the case of approximate chiral symmetries of the hypercolour theory. Our models provide exploratory tools to characterise such composite physics at the high energy frontier.

Acknowledgements

References

1. N. Bizot, M. Frigerio, M. Knecht and J. L. Kneur, Phys. Rev. D **95** (2017) no.7, 075006 [arXiv:1610.09293 [hep-ph]].

2. D. Elander, M. Frigerio, M. Knecht and J. L. Kneur, *in preparation*.

3. G. Panico and A. Wulzer, Lect. Notes Phys. **913** (2016) [arXiv:1506.01961 [hep-ph]].

4. J. Barnard, T. Gherghetta and T. S. Ray, JHEP **1402** (2014) 002 [arXiv:1311.6562 [hep-ph]].

5. R. Arthur, V. Drach, A. Hietanen, C. Pica and F. Sannino, arXiv:1607.06654 [hep-lat]. E. Bennett *et al.*, arXiv:1912.06505 [hep-lat].

6. O. Aharony, S. S. Gubser, J. M. Maldacena, H. Ooguri and Y. Oz, Phys. Rept. **323** (2000) 183 [hep-th/9905111].

7. T. Gherghetta, arXiv:1008.2570 [hep-ph].

8. A. Ahmed, A. Mariotti and S. Najjari, arXiv:1912.06645 [hep-ph].

ELEMENTARY PARTICLE MASSES FROM A NON–PERTURBATIVE ANOMALY

Roberto Frezzotti

Univ. of Roma Tor Vergata and INFN, via della Ricerca Scientifica 1, I-00173, Rome – Italy

Giancarlo Rossi

Centro Fermi - Compendio del Viminale, Piazza del Viminale 1, I-00184, Rome, Italy

Univ. of Roma Tor Vergata and INFN, via della Ricerca Scientifica 1, I-00173, Rome – Italy

Abstract

A novel dynamical mechanism of elementary particle mass generation has recently been conjectured and numerically demonstrated by lattice simulations in a simple SU(3) gauge model where a SU(2) doublet of strongly interacting fermions is coupled to a complex scalar field doublet through a Yukawa and a Wilson-like term. As a first step towards building a natural (à la 't-Hooft) extension of the Standard Model, we argue that in the presence of weak gauge interactions the mechanism above, acting as a kind of non-perturbative anomaly, yields for both elementary fermions and weak gauge bosons effective masses proportional to the Λ–parameter of the theory, with particle–specific gauge coupling dependent prefactors.

1 Introduction

The Standard Model (SM) of elementary particles, in spite of its very impressive successes, is widely believed to be only an effective low energy theory because it can not account for quantum gravity and dark matter and has not enough CP-violation for baryogenesis. Moreover, by construction the SM is unable to shed light on the puzzling problems of EW scale naturalness [1] and fermion mass hierarchy [2]. Apart from these open problems, it has been noted [3] that, if a dynamical mechanism based on non-SM interactions gives rise to the mass of the known elementary fermions, one also obtains massive $W^\pm$, Z^0 gauge bosons and a composite Higgs particle in the W^+W^-, Z^0Z^0, and/or $t\bar{t}$ channel.

Here we consider a new non-perturbative (NP) mechanism for the dynamical generation of elementary fermion masses [4]. This mechanism is conjectured to be at work in non-Abelian gauge models with fermions and scalars where A) (as usual) chiral transformations acting on fermions and scalars are exact symmetries, but B) (deviating from common assumptions) purely fermionic chiral symmetries are explicitly broken by the UV regularization. We focus on the "natural" model where the bare parameters are

tuned so as to minimize the breaking of fermionic chiral symmetries. In its quantum effective Lagrangian (EL) [5] operators of NP origin violating fermionic chiral symmetries, among which a fermion mass term, are expected to appear, if the scalar potential is such that the theory lives in its Nambu–Goldstone (NG) phase. Recently lattice simulations have provided good evidence in favor of this phenomenon, which (for reasons we explain below) is referred to as a "NP anomaly" of fermionic chiral symmetries [6].

2   The simplest gauge model with NP fermion mass generation

We start by reviewing the renormalizable $d = 4$ toy (yet highly non-trivial) model where the mechanism of interest has been numerically demonstrated – lacking analytical methods – by first principle simulations. The classical Lagrangian is a gauge–invariant ultraviolet (UV) regularization of

$$\mathcal{L}_{\text{toy}} = \mathcal{L}_k(Q, A, \Phi) + \mathcal{V}(\Phi) + \mathcal{L}_{Wil}(Q, A, \Phi) + \mathcal{L}_{Yuk}(Q, \Phi) \tag{1}$$

with $\mathcal{L}_k(Q, A, \Phi)$ and $\mathcal{V}(\Phi)$ standing for the standard kinetic terms and scalar potential (with quartic coupling λ_0 and subtracted scalar mass μ_Φ^2). $\mathcal{L}_{\text{toy}}$ includes an SU(3) gauge field, A_μ, with bare coupling g_0, a Dirac doublet, $Q = (u, d)^T$, transforming as a triplet under SU(3) and a complex scalar doublet, $\varphi = (\varphi_0 + i\varphi_3, -\varphi_2 + i\varphi_1)^T$, invariant under SU(3). For the latter we use the 2×2 matrix notation $\Phi = [\varphi | - i\tau^2 \varphi^*]$. The model has a hard UV cutoff $\Lambda_{UV} \sim b^{-1}$ and its Lagrangian contains a Yukawa term, $\mathcal{L}_{Yuk}(Q, \Phi) = \eta(\bar{Q}_L \Phi Q_R + \bar{Q}_R \Phi^\dagger Q_L)$, as well as a non-standard (so called "Wilson–like") term

$$\mathcal{L}_{Wil}(Q, A, \Phi) = \frac{b^2}{2} \rho (\bar{Q}_L \overleftarrow{\mathcal{D}}_\mu \Phi \mathcal{D}_\mu Q_R + \bar{Q}_R \overleftarrow{\mathcal{D}}_\mu \Phi^\dagger \mathcal{D}_\mu Q_L) . \tag{2}$$

The latter is a $\Lambda_{UV}^{-2} \times d = 6$ operator that leaves the model power-counting renormalizable [4], like it happens for the Wilson term in lattice QCD [7]. Among other symmetries, the Lagrangian (1) is invariant under the (global) chiral transformations involving fermions and scalars ($\Omega_{L/R} \in$ SU(2))

$$\chi_L \times \chi_R = [\tilde{\chi}_L \times (\Phi \to \Omega_L \Phi)] \times [\tilde{\chi}_R \times (\Phi \to \Phi \Omega_R^\dagger)], \tag{3}$$

$$\tilde{\chi}_{L/R} : Q_{L/R} \to \Omega_{L/R} Q_{L/R}, \quad \bar{Q}_{L/R} \to \bar{Q}_{L/R} \Omega_{L/R}^\dagger. \tag{4}$$

No power divergent fermion mass can be generated by quantum corrections as a term like $\Lambda_{UV}(\bar{Q}_L Q_R + \bar{Q}_R Q_L)$ is not $\chi_L \times \chi_R$ invariant. For generic non-zero values of the bare parameters ρ and η neither $\mathcal{L}_{Wil}$ nor $\mathcal{L}_{Yuk}$ are invariant under the purely fermionic chiral SU(2) transformations, which we call $\tilde{\chi}_L \times \tilde{\chi}_R$.

The term $\mathcal{L}_{Wil}$ is a typical representative of the $d > 4$ terms in the UV regulated Lagrangian that yield $\tilde{\chi}_L \times \tilde{\chi}_R$ breaking. Whatever their form, one expects that their effects at momentum scales $\ll \Lambda_{UV}$ are equivalent to those of $\mathcal{L}_{Wil}$ with an appropriate value of ρ. This would end the discussion of $\tilde{\chi}_L \times \tilde{\chi}_R$ breaking for a Lagrangian with no $\mathcal{L}_{Yuk}$ term. In the presence of a $\mathcal{L}_{Yuk}$ term, which has $d = 4$, its coefficient η can be tuned to a *critical* value, $\eta_{cr} = \eta_{cr}(\rho, g_0^2, \lambda_0)$, where the quantum EL has a *vanishing* effective Yukawa term [4]. In such a *critical model* we investigate whether the quantum EL contains any $\tilde{\chi}_L \times \tilde{\chi}_R$ breaking operators with $d \leq 4$, describing $\tilde{\chi}$ breaking effects down to momentum scales $\ll \Lambda_{UV}$.

The answer to this question is obviously negative only in the phase where the exact $\chi_L \times \chi_R$ invariance is realized à la Wigner, i.e. when $\hat{\mu}_\phi^2 > 0$[1]. In the Wigner phase there is only one $\tilde{\chi}$ breaking, $d \leq 4$ operator allowed by the field content and symmetries of the model: the Yukawa term, which by definition of η_{cr} is absent in the EL of the critical model. Its $d \leq 4$ sector is thus given by

$$\Gamma_4^{Wig} \equiv \Gamma_{\hat{\mu}_\Phi^2 > 0} = \frac{1}{4}(FF) + \bar{Q}_L \slashed{\mathcal{P}} Q_L + \bar{Q}_R \slashed{\mathcal{P}} Q_R + \frac{1}{2} \text{Tr}[\partial_\mu \Phi^\dagger \partial_\mu \Phi] + \mathcal{V}_{\hat{\mu}_\Phi^2 > 0}^{eff}(\Phi). \tag{5}$$

---

[1] Due to the hard UV cutoff $\hat{\mu}_\Phi^2 = Z_{\mu_\Phi^2} \mu_\Phi^2 = Z_{\mu_\Phi^2}(m_{0,\Phi}^2 - \Lambda_{UV}^2 \tau_{cr})$, with τ_{cr} a computable coefficient.

For $\hat{\mu}_\Phi^2 < 0$ the $\chi_L \times \chi_R$ invariance is realized à la NG already at the classical level and three massless Goldstone bosons appear in the spectrum. Owing to the non-zero vacuum expectation value (v) of the scalar field, in the quantum EL the (effective) Φ field can now be written in polar form

$$\Phi = RU\,, \quad R = (v + \zeta_0)\,, \quad U = \exp[iv^{-1}\tau^k\zeta_k]\,, \quad \langle\Phi\rangle = v > 0\,, \qquad (6)$$

in terms of Goldstone ($\zeta_{1,2,3}$) and massive (ζ_0) scalars. The dimensionless field U transforms as $U \to \Omega_L U \Omega_R^\dagger$ under $\chi_L \times \chi_R$ and only makes sense if $v^2 > 0$, i.e. for $\hat{\mu}_\Phi^2 < 0$. In the NG phase the existence of U combined with the emergence (dimensional transmutation) of the intrinsic NP scale Λ_S allows for further $\tilde{\chi}$ breaking operators to appear in the quantum EL. For the critical model its $d \leq 4$ piece reads

$$\Gamma_4^{NG} = c_2\Lambda_S^2 \text{Tr}[\partial_\mu U^\dagger \partial_\mu U] + c_1\Lambda_S[\bar{Q}_L U Q_R + \text{h.c.}] + \tilde{c}\,\Lambda_S R\,\text{Tr}[\partial_\mu U^\dagger \partial_\mu U] + \Gamma_{\hat{\mu}_\Phi^2 < 0} + \text{O}(1/v^2)\,, \quad (7)$$

where $\Gamma_{\hat{\mu}_\Phi^2}$ is given in Eq. (5). The term $\propto c_1$ describes a kind of NP $\tilde{\chi}_L \times \tilde{\chi}_R$ anomaly in the quantum EL, as it was conjectured few years ago [4]. When U is expanded around the identity this terms yields

$$c_1\Lambda_S[\bar{Q}_L U Q_R + \bar{Q}_R U^\dagger Q_L] = c_1\Lambda_S \bar{Q}Q\,[1 + \text{O}(\tau^k\zeta_k/v)] = M_Q^{eff}\bar{Q}Q\,[1 + \text{O}(\tau^k\zeta^k/v)]\,, \qquad (8)$$

thus a fermion mass term, $M_Q^{eff} = c_1\Lambda_S$, plus a host of complicated, non-polynomial $\bar{Q} - \zeta_{1,2,3}\,'s - Q$ effective vertices. One can argue that in the critical model NP corrections on top of the $\tilde{\chi}$ breaking terms in the correlators, which arise from residual $\text{O}(v\,\Lambda_{UV}^{-2}\,\text{momentum}^2)$ fermion bilinear Lagrangian terms, are responsible for all the NP $\tilde{\chi}$ breaking terms appearing in the quantum EL. In particular $c_1 = \text{O}(g_0^4)$.

The critical model which we focused on is "natural" because it is defined by the criterion of maximally restoring at low energy the fermionic chiral symmetries ($\tilde{\chi}$) that are anyway broken in the far UV. The role of the other two terms involving Λ_S in Eq.(7) is clarified in Sect. 4.2.

3 Lattice evidence for NP fermion mass in the $\mathcal{L}_{\text{toy}}$ model

Omitting technical details, our lattice study [6] of the model with classical Lagrangian (1) can be summarized as follows. In the Wigner phase by *setting to zero* a suitably chosen and normalized matrix element, called r_{AWI}, of the divergence of the Noether current $\tilde{J}_R^i - \tilde{J}_L^i \equiv \tilde{J}_A^i$ associated to the would-be $\tilde{\chi}_L \times \tilde{\chi}_R$ symmetries we *determine* η_{cr} (at nearly fixed renormalization conditions) for three different values of the UV cutoff b^{-1}. Data for r_{AWI} at different η are interpolated to find η_{cr} at each $\beta = 6/g_0^2$ value, as shown in Fig. 1a. Having made sure that the quantum EL can have no Yukawa term, we switch to the NG phase, where we take the continuum limit of the critical model at fixed renormalization conditions – now with a renormalized squared scalar mass $\hat{\mu}_\Phi^2 < 0$. We study the pseudoscalar meson mass (M_{PS}) and the ratio ($2m_{AWI}^R$) of the renormalized matrix elements of $(\partial \cdot \tilde{J}_A^i)$ and $P^i = \bar{Q}\gamma_5\frac{\tau^i}{2}Q$ between the vacuum and one pseudoscalar meson state. The results for M_{PS} and $2m_{AWI}^R$ (in a convenient hadronic scheme R) are shown in Fig. 1b,c in units of the Sommer scale [8] r_0 as a function of the squared lattice spacing² b^2. The continuum limit ($b \to 0$) results are non-zero within conservative error estimates.

This lattice investigation, involving simultaneously gauge, fermion and scalar fields, was numerically quite challenging and thus carried out within the quenched (or valence fermion) approximation, which has been widely used in lattice QCD and is known to preserve locality and renormalizability of the model. Quenched results in the continuum limit are in fact enough to establish the presence of NP terms violating the would-be $\tilde{\chi}_L \times \tilde{\chi}_R$ symmetries in the quantum EL (7), even if quenching is likely to obscure their

---

²No $\text{O}(b^{2n+1})$ cutoff effects occur in our model, as it follows from standard symmetry arguments [6].
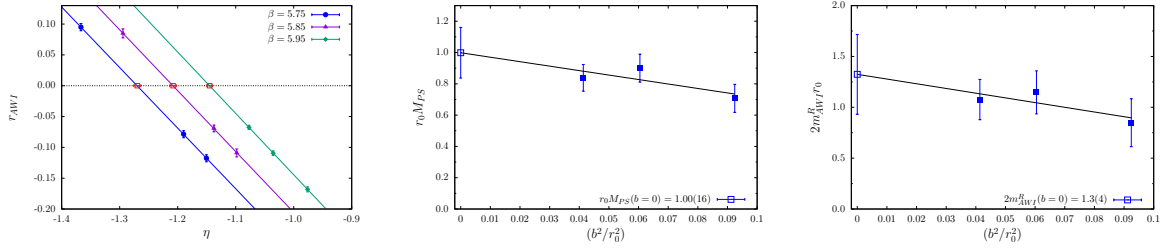
Figure 1: *a) r_{AWI} at various values of η for the lattice resolutions corresponding to $\beta = 6/g_0^2 = (5.75, 5.85, 5.95)$ and $\rho = 1.96$: straight lines show the linear interpolations in η; b) and c) $M_{PS}r_0$ and $2m_{AWI}^R r_0$ (renormalized in an hadronic scheme) versus b^2, with their linear extrapolation to $b^2 = 0$.*

universality properties (a point beyond the scope of the study). In particular, the non-vanishing result for $2m_{AWI}^R$ implies the occurrence in the quantum EL of the NP term $c_1\Lambda_S[\bar{Q}_L U Q_R + \text{h.c.}]$, plus possible higher dimensional ones with equal quantum numbers. The non-zero result for the pseudoscalar meson mass M_{PS} nicely fits with $2m_{AWI}^R \neq 0$ in view of the (explicitly verified) spontaneous breaking of the would-be $\tilde{\chi}_L \times \tilde{\chi}_R$ symmetries owing to strong interaction dynamics – just as it happens in QCD.

4 Fermion and weak gauge boson NP mass generation

The toy model discussed above can be extended to encompass weak interactions by gauging its exact χ_L-symmetry. Besides a chiral weak $\text{SU}(2)_L$ gauge force, we consider two vector gauge interactions, which we call strong (gauge group $\text{SU}(3)_S$) and "Tera-strong" (gauge group $\text{SU}(3)_T$), together with two sets of Dirac fermions: quarks $q_R \in (1_T, 3_S, 1_L)$, $q_L \in (1_T, 3_S, 2_L)$ and "Tera-quarks" $Q_R \in (3_T, 3_S, 1_L)$, $Q_L \in (3_T, 3_S, 2_L)$. Ignoring leptons, possible Tera-leptons and hypercharge effects, we consider here the (yet unrealistic) model with basic classical Lagrangian

$$\mathcal{L}_{\text{basic}}(Q, q, G, A, \Phi, W) = \mathcal{L}_{kin}(Q, q, G, A, \Phi, W) + \mathcal{V}(\Phi) + \mathcal{L}_{Wil}(Q, q, G, A, \Phi, W) + \mathcal{L}_{Yuk}(Q, q, \Phi) , \quad (9)$$

where G_μ, A_μ and W_μ denote $\text{SU}(3)_T$, $\text{SU}(3)_S$ and the weak $\text{SU}(2)L$ gauge bosons and we have

$$\mathcal{L}_{kin} = \frac{1}{4}F^G \cdot F^G + \frac{1}{4}F^A \cdot F^A + \frac{1}{4}F^W \cdot F^W + \bar{Q}_L\gamma_\mu\mathcal{D}_\mu^{G,A,W}Q_L + \bar{Q}_R\gamma_\mu\mathcal{D}_\mu^{G,A}Q_R +$$

$$+\bar{q}_L\gamma_\mu\mathcal{D}_\mu^{A,W}q_L + \bar{q}_R\gamma_\mu\mathcal{D}_\mu^A q_R + \kappa\frac{1}{2}\text{Tr}\left[(\mathcal{D}_\mu^W\Phi)^\dagger\mathcal{D}_\mu^W\Phi\right] \quad (10)$$

$$\mathcal{L}_{Wil} = \frac{b^2}{2}\rho_Q\left(\bar{Q}_L\overleftarrow{\mathcal{D}}_\mu^{G,A,W}\Phi\mathcal{D}_\mu^{G,A}Q_R + \text{h.c.}\right) + \rho_q\left(\bar{q}_L\overleftarrow{\mathcal{D}}_\mu^{A,W}\Phi\mathcal{D}_\mu^A q_R + \text{h.c.}\right) \quad (11)$$

$$\mathcal{L}_{Yuk} = \eta_Q\left(\bar{Q}_L\Phi Q_R + \text{h.c.}\right) + \eta_q\left(\bar{q}_L\Phi R + \text{h.c.}\right) , \quad (12)$$

with standard gauge covariant derivatives, e.g. $\bar{Q}_L\overleftarrow{\mathcal{D}}_\mu^{G,A,W} = \bar{Q}_L(\overleftarrow{\partial}_\mu + ig_T\lambda^a G_\mu^a + ig_S\lambda^c A_\mu^c + ig_w\frac{\tau^i}{2}W_\mu^i)$.

As both quarks and Tera-quarks couple to gluons, while only Tera-quarks are coupled to Tera-gluons, the Tera-strong coupling g_T will have a significantly faster running than the strong coupling g_S. For three quark generations the ratio of the LO coefficients of the β functions is $\beta_0^T/\beta_0^S = 7/3$, while for the "toy" case of just one quark generation, which for simplicity is considered here, one has $\beta_0^T/\beta_0^S = 21/17$. The renormalization group invariant (RGI) dynamical scale of the theory is denoted by Λ_T, with the idea that if the two gauge couplings are similarly small at energy scales close to the UV cutoff, moving towards low energy g_T gets O(1) at a scale of order Λ_T where still $g_S \ll 1$.

The model, among other symmetries, such as the UV regulated version of translation and Lorentz invariance, CP, time-reversal and the $\mathrm{SU(3)}_T \times \mathrm{SU(3)}_S$ vector gauge symmetry, is invariant under a global $\mathrm{SU(2)}_L \times \mathrm{SU(2)}_R$ symmetry group, which we call $\chi_L \times \chi_R$, with $\chi_{L,R} \equiv \tilde{\chi}_{L,R} \times \chi^{\Phi}_{L,R}$ and

$$\tilde{\chi}_L: \ Q[q]_L \to \Omega_L Q[q]_L, \ \bar{Q}[q]_L \to \bar{Q}[q]_L \Omega_L^{\dagger}, \ W_\mu \to \Omega_L W_\mu \Omega_L^{\dagger}, \qquad \chi^{\Phi}_L: \ \Phi \to \Omega_L \Phi, \quad \Omega_L \in \mathrm{SU(2)}_L, \ (13)$$

$$\tilde{\chi}_R: \ Q[q]_R \to \Omega_R Q[q]_R, \ \bar{Q}[q]_R \to \bar{Q}[q]_R \Omega_R^{\dagger}, \qquad\qquad\qquad \chi^{\Phi}_R: \ \Phi \to \Phi \Omega_R^{\dagger}, \quad \Omega_R \in \mathrm{SU(2)}_R, \ (14)$$

as well as under the corresponding local $\mathrm{SU(2)}_L$ gauge subgroup. The global $\chi_L \times \chi_R$ invariance is realized à la NG, i.e. spontaneously broken, already at the classical level if $\hat{\mu}_\Phi^2 < 0$ in the scalar potential $\mathcal{V}(\Phi)$.

4.1 The critical model for $g_w > 0$

The critical model is again defined as the one where the $\tilde{\chi}_L \times \tilde{\chi}_R$ symmetries, which are explicitly broken in the generic UV regulated model (9), are maximally restored in the quantum EL. Noting that W_μ transforms in the adjoint representation of the $\mathrm{SU(2)}_L$ group, maximal restoring $\tilde{\chi}_L$ at low energy corresponds to eliminating from the $d = 4$ sector of the quantum EL the effective $\tilde{\chi}$ breaking terms, i.e.

$$\Gamma^{Wig\,/\,NG}_{4,\,\tilde{\chi}\,\mathrm{breaking}} = \kappa_{eff} \frac{1}{2} \mathrm{Tr}\big[(\mathcal{D}^W_\mu \Phi)^\dagger \mathcal{D}^W_\mu \Phi \big] + y_{Q,eff}\big(\bar{Q}_L \Phi Q_R + \mathrm{h.c.} \big) + y_{q,eff}\big(\bar{q}_L \Phi q_R + \mathrm{h.c.} \big) . \qquad (15)$$

Taking into account the mixing of the Wilson–like terms with coefficients $\rho_{Q,q}$ in the Lagrangian (9) – which are the typical representatives for all $d > 4$ $\tilde{\chi}$ breaking operators – with the $d = 4$ Yukawa and scalar kinetic terms, one proves that critical values of the bare coefficients of the latter, namely $\eta_{Q,cr}$, $\eta_{q,cr}$ and κ_{cr}, exist for which the criticality conditions [3] on the effective $\tilde{\chi}$–violating couplings, v.i.z.

$$\kappa_{eff} \to 0^+ , \quad y_{Q,eff} = 0 , \quad y_{q,eff} = 0 , \qquad (16)$$

are realized for each g_T, g_S, g_w, λ_0, ρ_Q and ρ_q independently of the squared scalar mass (μ_Φ^2) value.

4.2 $\tilde{\chi}$ violating universal NP terms in the quantum EL (NG phase)

In the NG phase of the *critical model* defined above NP corrections to $\tilde{\chi}$ breaking effects (due to $\mathcal{L}_{Wil,Yuk}$) are expected to produce a number of $\tilde{\chi}$–violating terms in the quantum EL, according to a mechanism closely analogous to the one we discussed in Sections 2 and 3. The quantum EL should thus read $\Gamma^{NG} = \Gamma_{d\leq4,\,\hat{\mu}_\Phi^2} + \Delta\Gamma^{NG}_{d\leq4,\,\hat{\mu}_\Phi^2} + \Gamma_{d>4,\,\hat{\mu}_\Phi^2}$, where, with U as in Eq. (6), the $d \leq 4$ sector is given by

$$\Gamma_{d\leq4,\,\hat{\mu}_\Phi^2} = \frac{1}{4} \sum_{X=G,A,W} (F^X \cdot F^X) + \bar{Q}_L \slashed{\mathcal{D}}^W Q_L + \bar{Q}_R \slashed{\mathcal{D}} Q_R + \bar{q}_L \slashed{\mathcal{D}}^W q_L + \bar{q}_R \slashed{\mathcal{D}} q_R + \frac{\hat{\mu}_\Phi^2}{2} \mathrm{Tr}\big[\Phi^\dagger \Phi\big] + \frac{\hat{\lambda}}{4} \mathrm{Tr}\big[\Phi^\dagger \Phi\big]^2$$

$$(17)$$

plus, noting that ζ_0 decoupling implies $(C_2 \Lambda_T^2 + \tilde{C}\Lambda_T R) \to C_2 \Lambda_T^2$ as $\kappa_{eff} \to 0^+$, the NP terms

$$\Delta\Gamma^{NG}_{d\leq4,\,\hat{\mu}_\Phi^2} = \theta(-\hat{\mu}_\Phi^2)\Big[\sum_{\psi=Q,q} C_{1,\psi}\Lambda_T(\bar{\psi}_L U \psi_R + \mathrm{h.c.}) + C_2 \Lambda_T^2 \frac{1}{2}\mathrm{Tr}[(\mathcal{D}^W_\mu U)^\dagger \mathcal{D}^W_\mu U] \Big] . \qquad (18)$$

At quantum level the would-be $\tilde{\chi}$ symmetries are thus broken by fermion and weak boson mass terms and further $\tilde{\chi}$ violating NP vertices that involve U but are independent of $v^2 \sim \hat{\mu}_\Phi^2/\hat{\lambda}$. The W boson mass is $M_W^{eff} = g_w \sqrt{C_2}\Lambda_T$, while the Tera-quark and quark masses read $M_Q^{eff} = C_{1,Q}\Lambda_T$ and $M_q^{eff} = C_{1,q}\Lambda_T$. One can show [9] that $\sqrt{C_2} = \mathrm{O}(g_T^4)$, $C_{1,Q} = \mathrm{O}(g_T^4)$, $C_{1,q} = \mathrm{O}(g_S^4)$ and, owing to renormalizability of the basic Lagrangian (9), ratios of masses (such as W boson, Tera-hadron or hadron masses) are expected to be independent of UV regularization details (universality). Elementary fermion and weak gauge boson masses hence arise as a kind of *NP anomaly*. Based on dynamical properties of the basic model one can also argue, and check by numerical simulations, that $C_2 \ll 1$, i.e. $M_W^{eff} \ll \Lambda_T$ (*little hierarchy*).

4.3 Mass interpretation of the $\tilde{\chi}$ violating NP terms

To make contact with the standard phenomenological description of elementary particle mass effects, one can imagine to describe the physics of the critical model (9) with NP-ly anomalous $\tilde{\chi}$ symmetries in terms of an effective Lagrangian where the UV regularization preserves the $\tilde{\chi}$ symmetries and explicit terms $m_Q \bar{Q}_L U Q_R$, $m_q \bar{q}_L U q_R$ and $\frac{F^2}{2}\text{Tr}[(\mathcal{D}_\mu^W U)^\dagger \mathcal{D}_\mu^W U]$ are explicitly included. Owing to ζ_0 decoupling, the dimensionless Goldstone boson field $U = \exp(iF^{-1}\tau^k \zeta_k)$ is necessary to guarantee $\chi_L \times \chi_R$ invariance, which makes this effective Lagrangian description renormalizable only order by order in a $1/F$ expansion. The many finite low energy parameters associated with all the necessary UV counterterms are in principle fixed by using the info coming from Γ^{NG} of the basic model. Among these effective parameters we now find the *running masses* $\hat{m}_Q(\mu)$, $\hat{m}_q(\mu)$ and $\hat{m}_W(\mu)$, which at leading order are just m_Q, m_q and $g_w F$ and whose RG evolution is given by the anomalous dimension of the associated Lagrangian densities. It should also be noted that for particles (like q and possibly W) with effective mass much smaller than Λ_T the $d = 4$ soft mass terms are sufficient to describe the dominant effects of $\tilde{\chi}$ breaking, whereas for particles (like Q) with mass of order Λ_T all the $d \geq 4$ operators violating $\tilde{\chi}$ are equally important.

5 Outlook and conclusions

To proceed towards realistic models with "natural" elementary particle mass one must of course introduce hypercharge effects, leptons and possibly Tera-leptons (which can play a key role in gauge coupling unification [10]), while keeping the (gauged) $\text{SU}(2)_L \times \text{U}(1)_Y$ symmetry exact and maximally restoring the would-be fermionic chiral symmetries. From the discussion above it is clear that, if the observed top, $W^\pm$ and Z^0 masses have to be reproduced, a realistic model must include a new strong interaction with an intrinsic RGI scale Λ_T in the few TeV range and Tera-hadrons having masses of the same order, which is also crucial to pass electroweak precision tests. Owing to unitarity one can expect the low energy description that is valid for momenta well below Λ_T to be, even quantitatively, very similar to the SM if (as it is suggested by non-relativistic arguments [9]) the Higgs particle is given by a single bound state in the $WW + ZZ$ channel arising from the new strong interaction.

References

1. G. 't Hooft, NATO Sci. Ser. B, **59**, 135-157 (1980).

2. C.D. Froggatt and H. Nielsen, Nucl. Phys. B **147**, 277 (1979).

3. W.A. Bardeen *et al*, Phys. Rev. D **41**, 1647 (1990).

4. R. Frezzotti and G.C. Rossi, Phys. Rev. D **92**, 054505 (2015).

5. S.R. Coleman and E.J. Weinberg, Phys. Rev. D **7**, 1888-1910 (1973).

6. S. Capitani *et al*, Phys .Rev. Lett. **123** 061802 (2019).

7. K.G. Wilson, Phys. Rev. D **10**, 2445 (1974).

8. R. Sommer, Nucl. Phys. B **411**, 839-854 (1994)

9. R. Frezzotti *et al*, work in preparation

10. R. Frezzotti *et al*, Phys. Rev. D **93**, 105030 (2016).

STRONG DYNAMICS & DARK MATTER: INVESTIGATING A MINIMAL SETUP

Benjamin Fuks
Laboratoire de Physique Théorique et Hautes Energies (LPTHE), UMR 7589,
Sorbonne Université et CNRS, 4 place Jussieu, 75252 Paris Cedex 05, France
Institut Universitaire de France, 103 boulevard Saint-Michel, 75005 Paris, France

Federica Giacchino
INFN, Laboratori Nazionali di Frascati, C.P. 13, 100044, Frascati, Italy

Laura Lopez-Honorez
Service de Physique Théorique, CP225, Université Libre de Bruxelles,
Bld du Triomphe, 1050 Brussels, Belgium
Vrije Universiteit Brussel and The International Solvay Institutes,
Pleinlaan 2, 1050 Brussels, Belgium

Michel H.G. Tytgat and Jérôme Vandecasteele
Service de Physique Théorique, CP225, Université Libre de Bruxelles,
Bld du Triomphe, 1050 Brussels, Belgium

Abstract

We discuss the phenomenology of a dark matter scenario in which we extend the Standard Model by a real scalar particle and a vector-like heavy quark. Such a model can be seen as a simplified version of a composite setup in which the scalar field, that couples to the top quark via a Yukawa interaction with the new heavy quark, is a viable dark matter candidate. We emphasize that QCD corrections are important not only for predictions at colliders but also for direct and indirect dark matter searches and the relic abundance. We moreover show that a large fraction of the model parameter space remains unconstrained.

1 Introduction

There is a large experimental effort worldwide that aims at deciphering the nature of the dark matter. A much studied scenario assumes that the dark matter (DM) is made of a stable and neutral particle species, with a relic abundance fixed by chemical freeze-out in the early universe. As the required annihilation cross section is in the 1 pb range, such particles are collectively called weakly interacting massive particles (WIMPs). A generic feature of any DM candidate with an abundance originating from freeze-out is that they can be complementarily searched for directly, indirectly and at colliders. We report on a phenomenological analysis of a simple, yet rich, WIMP model in which DM is a real scalar particle that couples dominantly to the top quark [1]. Such a simplified scenario could seen as the dark sector of more ambitious theories beyond the Standard Model (SM), like non-minimal composite models [2].

2 Theoretical context

The Lagrangian describing our simplified model takes the form

$$\mathcal{L} = \mathcal{L}_{\mathrm{SM}} + i\bar{T}\slashed{D}T - m_T\bar{T}T + \frac{1}{2}\partial_\mu S\partial^\mu S - \frac{1}{2}m_S S^2 + \left[\tilde{y}_t\, S\, \bar{T}\, t_R + \mathrm{h.c.}\right], \qquad (1)$$
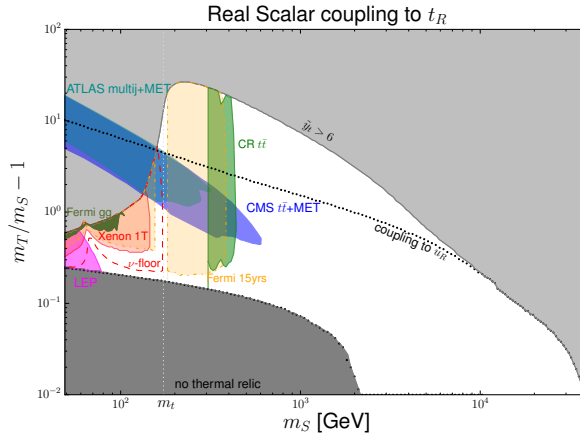
Figure 1: *Top-philic DM model parameter space shown in the DM mass (m_S) and spectrum compression factor ($m_T/m_S - 1$) plane. In the gray regions, the observed DM relic density cannot be accommodated, whilst in the region in between, there exists a specific $\tilde{y}_t$ value leading to the right DM abundance. We refer to the text for the description of the different experimental constraints, that each corresponds to a given colored region. We moreover impose $\tilde{y}_t < 6$ to allow for a perturbative treatment in our calculations (upper gray region). In the lower gray region, DM is under-abundant assuming thermal freeze-out.*

where S denotes the scalar dark matter candidate, T is a vector-like color triplet fermion and t_R stands for the right-handed top quark. Other terms are forbidden by imposing that both S and T are odd under a Z_2 symmetry whereas the SM fields are set to be even. This ensures the stability of the dark matter and forbids the mixing of the T-quark with the SM quarks. Whilst in practice the quantum numbers of the T particle also allow for couplings with S and the first and second generation quarks, we set these to zero (the associated phenomenology having been worked out in the past [3]), thus assuming that DM dominantly interacts with the top quark. Non-minimal composite models, in which the top quark plays a special role [2], could yield the Lagrangian of eq. (1). While such a possibility is very much worth further investigating, we consider in the meantime this Lagrangian as a simplified model [4]. We so assume that only 3 parameters are needed to study its phenomenology, namely the two new physics masses m_S and m_T, and the Yukawa coupling $\tilde{y}_t$.

In the sequel, we first summarize our determination of the relic abundance and then discuss the resulting experimental constraints on the model parameters. We put a special emphasis on the role of the QCD radiative corrections, which are particularly important in our model. The results of our analysis including DM direct and indirect detection, as well as the bounds stemming from LHC searches, are collected in figure 1. This exhibits the complementarity between the experimental searches, and that heavy DM configurations are untested.

3   Relic density

Assuming thermal freeze-out, all viable setups for which the DM relic abundance can match the Planck collaboration results correspond to the area in between the gray regions in figure 1, or equivalently, to the colored region in the left panel of figure 2. Both results are depicted in the plane ($m_S, m_T/m_S - 1$) where we coin $m_T/m_S - 1$ the spectrum compression factor as it shows how close are the mediator and DM masses. It turns out that a viable DM candidate can be continuously obtained from masses ranging
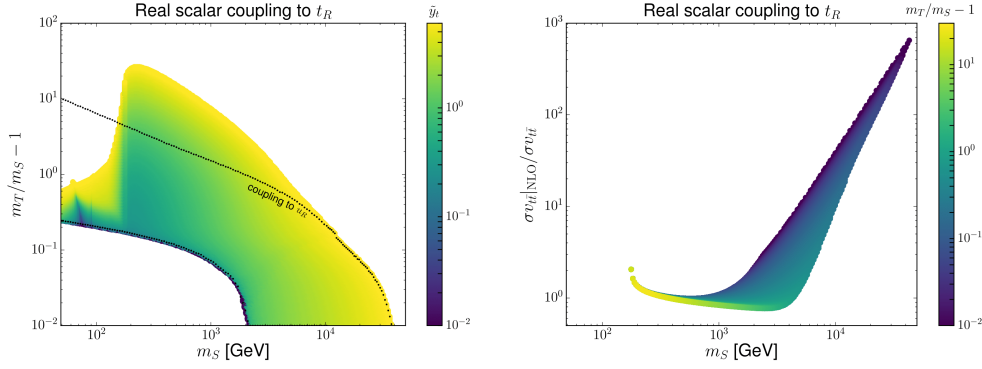
Figure 2: *Left: Parameter space region in which the observed DM abundance, $\Omega h^2 = 0.12$, can be accommodated. The results are presented in the $(m_S, m_T/m_S - 1)$ plane and the color gradient refers to the corresponding $\tilde{y}_t$ value. The dashed line refers to the bound obtained when neglecting the top-quark mass. Right: Ratio of the thermally-averaged NLO annihilation cross section to the LO one for each viable scenario. The color gradient represents the compression parameter.*

from a few GeV to up to 40 TeV. While not unexpected for WIMP candidates, this parameter range is quite large, owing to the various possible annihilation channels. For $m_S \gtrsim 5$ TeV (*i.e.*, $m_S \gg m_t$), the dominant annihilation channel involves additional QCD radiation, $SS \to t\bar{t}g$. This originates from the d-wave suppression of annihilations into fermion pairs in the $m_S \gg m_f$ limit and from a strong enhancement of the so-called virtual internal bremsstrahlung contributions [5, 6]. The latter is illustrated in the right panel of figure 2 in which we present the ratio of the next-to-leading-order (NLO) annihilation cross section into a $t\bar{t}$ pair (including extra gluon emission) to the leading-order (LO) one at freeze-out time. For $m_S \gg m_t$, this enhancement is significant and the NLO contributions clearly dominate. As m_S decreases the top quark mass becomes less negligible, and, while NLO effects remain important, the ratio between the NLO and LO predictions gets closer to 1. Finally, the apparent increase at $m_S \sim m_t$ is spurious and should be removed by a proper treatment of the threshold effects [7, 8]. On the left panel of figure 2, the impact of a non-negligible top quark mass can be seen by comparing the colored region associated with an S coupling to t_R to the viable parameter space region when S couples to the right-handed up quark u_R [3] (shown in between the dotted black lines). For $m_S \leq m_t$, the relic density could arise from loop-induced $SS \to gg$ annihilations [3, 9], a process that is also unexpectedly large if the mediator is not too heavy ($m_T \gtrsim m_S$) and the compression factor close to 1.

The abundance may also originate from co-annihilations (*e.g.*, $ST \to gt$) or even from mediator annihilation $T\bar{T} \to gg/q\bar{q}$ if the mass spectrum is sufficiently compressed (typically in the dark blue region of the left panel of figure 2 for $m_S \lesssim 3$ TeV), provided the S and T particles are in chemical equilibrium ($\Gamma(S \leftrightarrow T) \gtrsim H$ with H being the Hubble rate). The rationale for such a compressed mass spectrum in which a DM particle is degenerate with colored states in a natural way may stem from extra-dimensional [10] or grand unified [11] theories. In addition, departures from thermal equilibrium are known to potentially affect the results [12], and while we could expect that Sommerfeld corrections strongly impact the $T\bar{T} \to gg/q\bar{q}$ annihilation cross sections, the existence of both attractive and repulsive channels tame those effects that are at most of $\mathcal{O}(15\%)$ [1, 3].
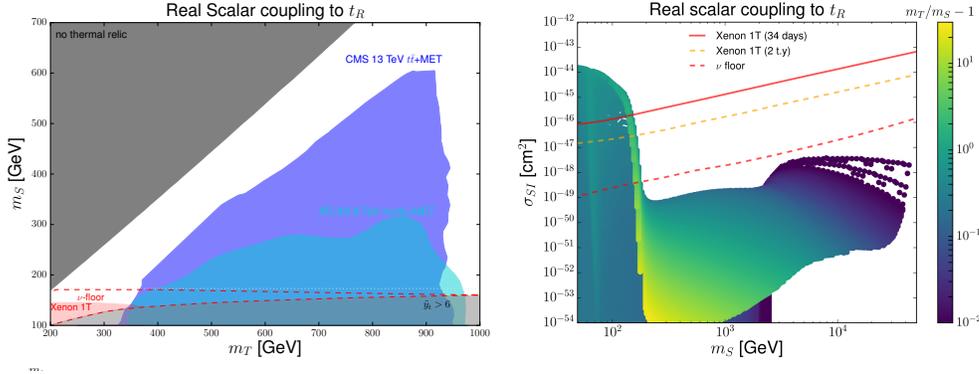
Figure 3: *Left: LHC constraints on the model expressed in the (m_S, m_T) mass plane, together with the DM relic density and direct detection bounds. Right: Spin-independent DM-nucleon scattering cross section as a function of m_S, for each scenario accommodating Planck data. The compression factor is depicted by the color code, and we superimpose current (solid red) and future (dashed orange) 90% confidence level exclusions from Xenon 1T.*

4   Experimental and observational constraints

4.1   LHC searches

Like for any WIMP-like DM, our model can be probed at the LHC through signatures comprised of missing transverse energy (MET) produced in association with either jets (mono-X-like probes) or a $t\bar{t}$ pair. We reinterpret the results of a typical DM search in the $t\bar{t}$ plus MET mode using 35.9 fb^{-1} of CMS data [13], increasing sensitivity to compressed scenarios by additionally considering a dedicated CMS search [14]. We moreover reinterpret the results of two early Run 2 ATLAS DM searches in the monojet and multijet plus MET modes [15, 16]. Those searches being limited by systematics, any constraint they could lead to is not expected to get more severe with more data [17]. Our results are presented in the left panel of figure 3. The colored regions correspond to scenarios excluded at the 95% confidence level by at least one of the considered $t\bar{t}$ plus MET (dark blue) or multijet plus MET (light blue) analyses, considering NLO simulations for the DM signal. The latter dominantly stems from the production of a pair of T-quarks decaying into top quarks and missing energy ($pp \to T\bar{T} \to tS\bar{t}S$) and is excluded for m_T values lying in the 300–1000 GeV range, provided there is enough phase space to guarantee the mediator decay. No constraint arises if the $T \to tS$ decay channel is closed, as the T-quark turns out to be long-lived. Those results are reported according to the same color code in figure 1.

4.2   Direct detection

DM being scalar, direct detection constraints can only originate from spin-independent exclusion limits imposed by ton-size liquid Xenon experiments (currently Xenon 1T [18, 19]). DM-nucleon scattering occurring at one loop through the exchange of virtual top quarks, the coupling between S and nucleons boils down to an $SSgg$ effective operator. This contrasts with models in which DM couples to light quarks, where higher-twist operators and long-range interactions are important [3]. The constraints on the scattering cross-section are presented in the right panel of figure 3, the strongest bounds arising for light DM candidates. In this case, the relic density is typically driven by annihilations into gluons ($SS \to gg$) mediated by a large $\tilde{y}_t$ Yukawa coupling. This suggests a potentially large value for the DM-
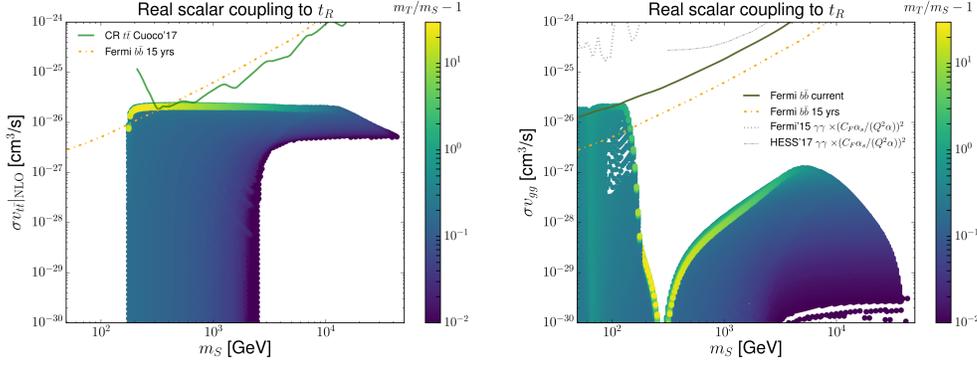
Figure 4: *NLO $SS \to t\bar{t}$ (left) and loop-induced LO $SS \to gg$ (right) annihilation cross sections at zero velocity, relevant for indirect searches. We superimpose limits from antiproton cosmic rays (solid light green) and from current (solid dark green) and future (dot-dashed orange) Fermi-LAT dwarf spheroidal galaxy data in the $b\bar{b}$ channel (after an appropriate recasting).*

nucleon scattering cross section. For heavier dark matter, however the scattering cross section typically lies below the neutrino floor (red dashed). This severely limits the relevance of DM direct detection searches for setups like the one of eq. (1). The state of affair is reported as the red colored area in figure 1.

4.3   Indirect detection

DM annihilations into gg or $t\bar{t}(g)$ systems would produce a continuum of gamma rays and cosmic rays (in particular antiprotons). Of particular relevance for indirect detection is the effect of bremsstrahlung of gluons, related to the issue of disentangling hard and soft gluon emission to control the associated infrared divergences [7, 8]. As shown in figure 4, some model configurations are excluded by current indirect detection searches [20, 21, 22]. In the right panel of the figure, we present the constraints arising from annihilations into gluons pairs, while in the left panel, we consider annihilations into a $t\bar{t}(g)$ final state. The former is most relevant for lighter DM, $m_S \lesssim 100$ GeV, some scenarios being excluded. Annihilations into the $t\bar{t}(g)$ mode can yield constraints from Fermi-LAT dwarf galaxy results. While assuming a $b\bar{b}$ final state, the latter can be recasted [1]. Some model configurations for which $m_t < m_S < 500$ GeV turn out to be excluded. Finally, DM annihilations can feature gamma-ray-line topologies to which experiments like Fermi-LAT are very sensitive to. These turn out to be subdominant compared with the gamma-ray continuum generated by the hadronization of the $t\bar{t}$ decay products and gluons (right panel). All indirect detection constraints are reported in figure 1 following the same color coding as in figure 4.

5   Summary

WIMP dark matter is being tested in various experiments in astrophysics, cosmology and at colliders. In this work, we have extensively investigated a simplified top-philic scalar DM scenario that could find its origin in composite setups. We have studied various existing constraints on the model and shown that although there is a complementarity between the different searches, only a small fraction of the viable parameter space is currently tested. The most fruitful long-term strategy therefore consists in an increase of the energy reach at colliders.

6   Acknowledgements

References

1. S. Colucci, B. Fuks, F. Giacchino, L. Lopez Honorez, M. H. G. Tytgat and J. Vandecasteele, Phys. Rev. D **98** (2018) 035002.

2. G. Cacciapaglia, H. Cai, A. Deandrea and A. Kushwaha, JHEP **1910** (2019) 035.

3. F. Giacchino, A. Ibarra, L. Lopez Honorez, M. H. G. Tytgat and S. Wild, JCAP **1602** (2016) 002.

4. J. Abdallah *et al.*, Phys. Dark Univ. **9-10** (2015) 8.

5. T. Toma, Phys. Rev. Lett. **111** (2013) 091301.

6. F. Giacchino, L. Lopez-Honorez and M. H. G. Tytgat, JCAP **1310** (2013) 025.

7. S. Colucci, F. Giacchino, M. H. G. Tytgat and J. Vandecasteele, Phys. Rev. D **98** (2018) 115029.

8. T. Bringmann, A. J. Galea and P. Walia, Phys. Rev. D **93** (2016) 043529.

9. F. Giacchino, L. Lopez-Honorez and M. H. G. Tytgat, JCAP **1408** (2014) 046.

10. D. Hooper and S. Profumo, Phys. Rept. **453** (2007) 29.

11. S. Ferrari, T. Hambye, J. Heeck and M. H. G. Tytgat, Phys. Rev. D **99** (2019) 055032.

12. M. Garny, J. Heisig, M. Hufnagel and B. Llf, Phys. Rev. D **97** (2018) 075002.

13. A. M. Sirunyan *et al.* [CMS Collaboration], Phys. Rev. D **97** (2018) no.3, 032009.

14. CMS Collaboration, CMS-PAS-SUS-16-052.

15. M. Aaboud *et al.* [ATLAS Collaboration], Phys. Rev. D **94** (2016) 032005.

16. M. Aaboud *et al.* [ATLAS Collaboration], Eur. Phys. J. C **76** (2016) 392.

17. S. Banerjee, D. Barducci, G. Blanger, B. Fuks, A. Goudelis and B. Zaldivar, JHEP **1707** (2017) 080.

18. E. Aprile *et al.* [XENON Collaboration], JCAP **1604** (2016) 027.

19. E. Aprile *et al.* [XENON Collaboration], Phys. Rev. Lett. **119** (2017) 181301.

20. A. Cuoco, J. Heisig, M. Korsmeier and M. Krmer, JCAP **1804** (2018) 004.

21. E. Charles *et al.* [Fermi-LAT Collaboration], Phys. Rept. **636** (2016) 1.

22. L. Rinchiuso *et al.* [HESS Collaboration], PoS ICRC **2017** (2018) 893.

BOTTOM-QUARK CONTRIBUTIONS TO COMPOSITE PSEUDO-SCALAR COUPLINGS AT LHC

Lara Mason

Department of Physics, University of Johannesburg, PO Box 524, Auckland Park 2006, South Africa

Université de Lyon, F-69622 Lyon, France: Université Lyon 1, Villeurbanne CNRS/IN2P3, UMR5822, Institut de Physique des 2 Infinis de Lyon

Alan S Cornell

Department of Physics, University of Johannesburg, PO Box 524, Auckland Park 2006, South Africa

Aldo Deandrea

Université de Lyon, F-69622 Lyon, France: Université Lyon 1, Villeurbanne CNRS/IN2P3, UMR5822, Institut de Physique des 2 Infinis de Lyon

Benjamin Fuks

Laboratoire de Physique Théorique et Hautes Energies (LPTHE), UMR 7589, Sorbonne Université et CNRS, 4 place Jussieu, 75252 Paris Cedex 05, France

Institut Universitaire de France, 103 boulevard Saint-Michel, 75005 Paris, France

Abstract

Composite Higgs models which describe the Higgs boson as a bound state emerging as pseudo-Nambu-Goldstone boson (pNGB) of a broken global symmetry are expected to be accompanied by additional resonances, some of which will occur ubiquitously. The subject of this work, a light pseudo-scalar which is the pNGB of a broken $U(1)$ symmetry, is one such state, and may provide evidence of a composite Higgs model, should it be detected. We study the phenomenology of the scalar, examining its production and decay, with particular emphasis on its interaction with gauge bosons, which proceed via triangle diagrams in which run Standard Model quarks. Previously, only the top quark has been considered to contribute; however, we show that, particularly for low mass of the scalar, the bottom quark loop in fact provides a dominant contribution to the production cross section and modifies decay modes in a manner which should not be neglected. If targeted low mass searches for such a resonance are to be performed, it is crucial that the associated phenomenology be accurately modelled, in both the analysis of existing LHC data and for future high energy analyses.

1 Introduction

The presence of light scalars in composite Higgs models, arising as pseudo-Nambu Goldstone bosons (pNGBs) of broken global symmetries, is a feature which may be valuable in searches at colliders. At present, the Large Hadron Collider (LHC) at CERN is in a long shut-down period, as it prepares for runs at its design energy of 14 TeV, as well as for high luminosity runs (HL-LHC). Many searches at the LHC are focused on the high energy regime, where theories such as supersymmetry promise new physics will appear. However, there may also be new physics hiding at low energies, where resonances such as the pseudo-scalar, which is the topic of this work, may be awaiting discovery [1]. It is for this reason that it

is crucial that targeted low energy searches be performed, for which the current long shut-down period is a perfect opportunity.

Composite Higgs models seek to extend the Standard Model (SM) and address questions in its scalar sector by postulating that the Higgs boson is a composite state emerging as a consequence of a broken global symmetry. One light state which results from a composite Higgs model, accompanying the Higgs boson in occurring ubiquitously, is a pseudo-scalar a, resulting from the breaking of a global $U(1)$ symmetry. In this work we have implemented a modelling of a using FeynRules [2] in conjunction with MadGraph [3] to leading order, making a case for targeted searches in the low mass region at the LHC. In coupling to gauge bosons, a is subject to both a SM and Beyond the Standard Model (BSM) contribution, where the SM component is a triangle diagram containing loops of SM quarks. In contrast to previous studies, we have included not only top quarks in these loops, but bottom quarks as well, which we show to have a non-negligible impact, particularly in targeted searches for lower masses of a.

2 Composite Higgs theories

We consider a class of composite Higgs models which are described by a fermion-gauge underlying description, confining at energies below some symmetry breaking scale, which we will consider to be of the order of 1 TeV. The Higgs boson can be identified as a pNGB if there is a breaking of a global symmetry G to some subgroup H, which occurs at the compositeness scale. The theory is defined by an unbroken gauge group G_{HC} [4]. While gauge bosons obtain their masses in the usual way, we include the mechanism of partial compositeness for fermion mass generation, for which we require underlying fundamental fermions in (at least) two different irreducible representations of the unbroken gauge group [1]. We will consider 12 models in this work, each described by different group structures, but all featuring at least two species of underlying fermions, ψ (carrying electroweak charge) and χ (carrying QCD colour and hypercharge, and responsible for partial compositeness), each subject to a global flavour symmetry which breaks due to the fermion condensate. The pattern of chiral symmetry breaking leading to these cosets depends on underlying gauge dynamics, governed by the dimension of the gauge group (number of fermionic matter fields) and on the subgroup to which the symmetry breaks [5]. Once the underlying fermion dynamics are specified, we may only have certain breaking patterns [1].

Global symmetries in the effective low-energy model are completely determined, allowing us to describe the nature of the theory and the expected particle content completely. We find that, in addition to the global flavour symmetries of the underlying fermions, there always exists a non-anomalous U(1) charge acting on both species of fermions [1]. This $U(1)$ symmetry will also break as a result of the fermion condensate, resulting in two U(1) singlet mass eigenstates, a and η', singlets under all SM gauge symmetries. There exists some non-trivial mixing between the two states, which depends on the characteristics of the underlying fermions. The presence of two types of underlying fermions in the theory, both of which condense, means that we are always able to construct anomaly-free combinations of the two $U(1)$s [4], $\tilde{a}$ and $\tilde{\eta}'$. We will consider here the case in which a is light, as the gauge eigenstate $\tilde{a}$ is typically lighter than the confinement scale. In this case, the other state decouples, and anomaly-free $\tilde{a}$ corresponds to the light mass eigenstate a [6].

This work builds from previous studies of a [1, 6], wherein the specifics of the models and theory are discussed in greater depth. We will focus predominantly on the phenomenology in this short article.

M	HC	Coset	ψ	χ	$-q_\chi/q_\psi$
1	$SO(7)$	$\frac{SU(5)}{SO(5)} \times \frac{SU(6)}{SO(6)}$	$5\times\mathbf{F}$	$6\times\mathbf{Sp}$	$5/6$
2	$SO(9)$				$5/12$
3	$SO(7)$	$\frac{SU(5)}{SO(5)} \times \frac{SU(6)}{SO(6)}$	$5\times\mathbf{Sp}$	$6\times\mathbf{F}$	$5/6$
4	$SO(9)$				$5/3$
5	$Sp(4)$	$\frac{SU(5)}{SO(5)} \times \frac{SU(6)}{SO(6)}$	$5\times\mathbf{A}_2$	$6\times\mathbf{F}$	$5/3$
6	$SU(4)$	$\frac{SU(5)}{SO(5)} \times \frac{SU(3)^2}{SU(3)}$	$5\times\mathbf{A}_2$	$3\times(\mathbf{F},\overline{\mathbf{F}})$	$5/3$
7	$SO(10)$		$5\times\mathbf{F}$	$3\times(\mathbf{Sp},\overline{\mathbf{Sp}})$	$5/12$
8	$Sp(4)$	$\frac{SU(4)}{Sp(4)} \times \frac{SU(6)}{SO(6)}$	$4\times\mathbf{F}_2$	$6\times\mathbf{A}_2$	$1/3$
9	$SO(11)$		$4\times\mathbf{Sp}$	$6\times\mathbf{F},$	$8/3$
10	$SO(10)$	$\frac{SU(4)^2}{SU(4)} \times \frac{SU(6)}{SO(6)}$	$4\times(\mathbf{Sp},\overline{\mathbf{Sp}})$	$6\times\mathbf{F}$	$8/3$
11	$SU(4)$		$4\times(\mathbf{F},\overline{\mathbf{F}})$	$6\times\mathbf{A}_2$	$2/3$
12	$SU(5)$	$\frac{SU(4)^2}{SU(4)} \times \frac{SU(3)^2}{SU(3)}$	$4\times(\mathbf{F},\overline{\mathbf{F}})$	$3\times(\mathbf{A}_2,\overline{\mathbf{A}}_2)$	$4/9$

Table 1: *Key definitions for models M1-M12, including (from left to right) the naming convention, the hypercolour gauge group, the EW and QCD cosets, the irreducible representations of fermions ψ and χ, and the charges of the fundamental fermions under the non-anomalous $U(1)$ charge in each sector* [1, 6].

3 Models

We have chosen to study twelve possible models, labelled M1-M12, all of which include partial compositeness for the top such that asymptotic freedom is not lost. The models enjoy varying group structures, each subject to a confining gauge group G_{HC} and two types of underlying fundamental fermions. The coefficients which govern the Lagrangian are computable and determined by the dimension of the underlying fermionic representation, allowing for a wealth of phenomenology. The features of each model which allow for the computation of the coefficients include $q_{\psi(\chi)}$, the charge of the fermion $\psi(\chi)$ under the non-anomalous $U(1)$, $N_{\psi(\chi)}$, the multiplicity of $\psi(\chi)$, and $f_{\psi(\chi)}$, the decay constant in each sector [1]. The ingredients for each model are then the choice of hypercolour group and the choice of fermion representations, which then govern the EW and QCD cosets, where key details are given in tab. 1.

The pNGB is considered in this implementation to be light, where $10 < M_a < 100$ GeV, with small couplings to SM particles. In order to describe it, the SM Lagrangian is augmented with the effective Lagrangian [6]

$$\mathcal{L} = \frac{1}{2}\left(\partial_\mu a\right)^2 - \frac{1}{2}M_a^2 a^2 - \Sigma_f \frac{iC_f m_f}{f_a}a\bar{\Psi}_f\gamma^5\Psi_f + \frac{g_s^2\kappa_g a}{16\pi^2 f_a}G_{\mu\nu}^a\tilde{G}^{a\mu\nu} + \frac{g^2\kappa_W a}{16\pi^2 f_a}W_{\mu\nu}^i\tilde{W}^{i\mu\nu} + \frac{g'^2\kappa_B a}{16\pi^2 f_a}B_{\mu\nu}\tilde{B}^{\mu\nu}.$$
(1)

The pseudo-scalar couples directly to fermions, and its couplings to gauge bosons take the form aXX' (where X, X' are gauge bosons which may or may not be different), which may be broken into a BSM component (effective vertex) and a SM component (loop of SM fermions). The BSM component is modelled in Lagrangian 1, and the SM component is modelled separately, including both top and bottom quarks running in the loops.

The pseudo-scalar is produced predominantly via gluon-fusion at the LHC, plotted in fig. 1, where models M1 and M9 have been chosen as examples due to their contrasting group structures. Additional, albeit less dominant, gluon fusion production may proceed via pair production and production in asso-
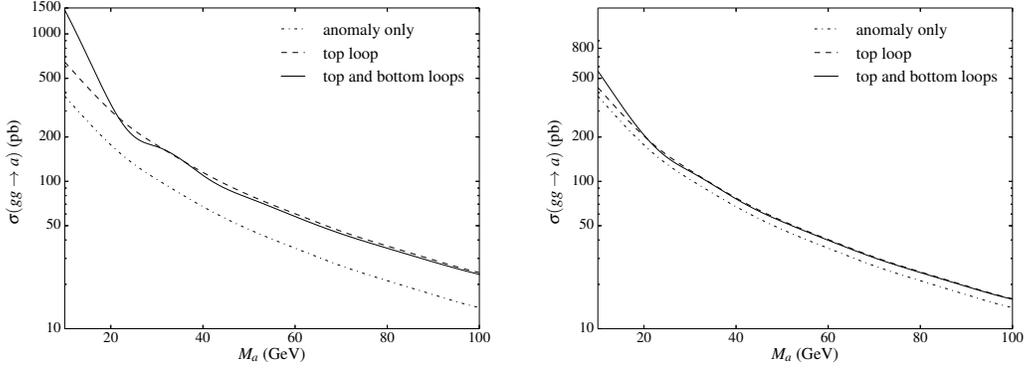
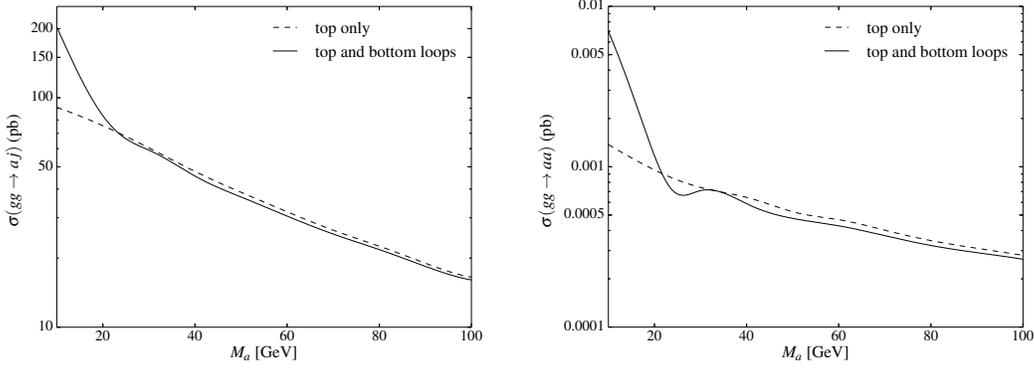Figure 1: *Gluon fusion production for model M1 (left) and model M9 (right).*

Figure 2: *Gluon fusion production in association with a jet (left) and pair production (right) for M1.*

ciation with a jet, plotted in fig. 2 for model M1. The effect of the inclusion of the b quark is clearly visible in both figures, particularly at lower masses of a. In particular, we see an increase in cross section for lower masses, with a destructive interference between the top and bottom contributions at higher masses. The undulating shape of the bottom contribution visible in figs. 1 and 2 arises from the form of the three point scalar function emerging from the triangle vertex propagator in the case of $2m_q < M_a$, which is always the case for the bottom quark in our chosen pseudo-scalar mass range. The integral over the propagator evaluates to the form $\tau f(\tau)$, where

$$f(\tau) = \begin{cases} -\frac{1}{4}\left[\log\left(\frac{1+\sqrt{1-\tau}}{1-\sqrt{1-\tau}}\right)\right]^2 & \text{if } \tau < 1 \\ \arcsin^2\left(\frac{1}{\sqrt{\tau}}\right) & \text{if } \tau \geq 1, \end{cases} \qquad \tau_f = \frac{4m_f^2}{M_a^2}. \tag{2}$$

Here, m_f is the mass of the SM quark running through the loop, and M_a is the mass of the pseudo-scalar. Given that we consider a mass range of $M_a \in [10, 100]$ GeV, $\tau_t > 1$ and $\tau_b < 1$ always. We find that $\tau f(\tau) \approx 1$ for tops, but the function is less stable due to the presence of the logarithms in the case of bottoms, as is visible in the figures.

Fig. 3 displays the full proton proton production cross section at the LHC for a variety of energies, including the upcoming 14 TeV run, for which we expect copious a production. In an attempt at model independence, we have normalised each cross section by the square of the anomaly coefficient κ_g.
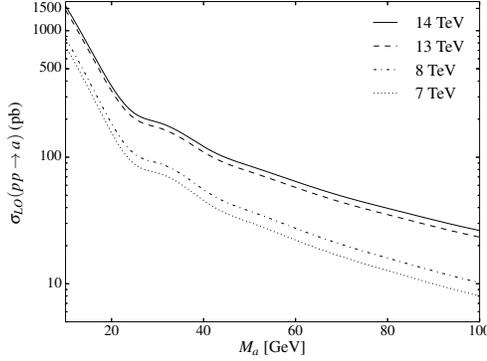
Figure 3: *Production cross section at the LHC for 7, 8, 13 and 14 TeV.*

We can make a further case for the inclusion of b quarks through the examination of the branching ratios of a to gauge bosons, plotted for hadrons in fig. 4. Similar magnitudes of modifications are observed in the case of photons, not shown here, which then modifies the remaining branching ratios by association. The upwards "flick" for low masses of a which is visible in the branching ratio plots results as a function of proximity to the $B\bar{B}$ threshold, producing a minimum in the branching ratios which is accentuated in the second plot. In planning a targeted low energy search one should consider the various possible
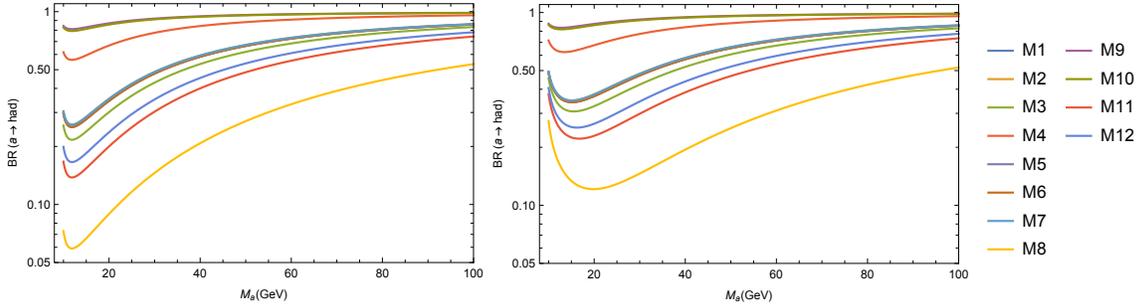

Figure 4: *Branching ratios of $a \rightarrow$ hadrons for each model without b quarks (left) and with both t and b quarks (right).*

decay modes, which are shown for models M8 and M9 in fig. 5. It is notable that even in comparing these two models, which have the same EW coset structure, we see a large variation across branching ratios, displaying the variety of possibilities generated by the models M1-M12. The largest branching ratios are to quarks and hadrons, which are very difficult to use for a robust analysis due to the large QCD background at low energies. Di-tau decays, although less copious, would provide a more achievable signal, and a promising low mass search for a pseudo-scalar boosted off an initial state radiation jet and decaying into a $\tau^+\tau^-$ pair has been proposed [6].

4 Conclusion

Light states which appear alongside the Higgs boson in composite Higgs models may provide the first signs of compositeness at colliders. One such state, the pNGB a, appears ubiquitously, and is a good candidate for low mass searches. The models presented in this work provide a range of interesting phenomenology
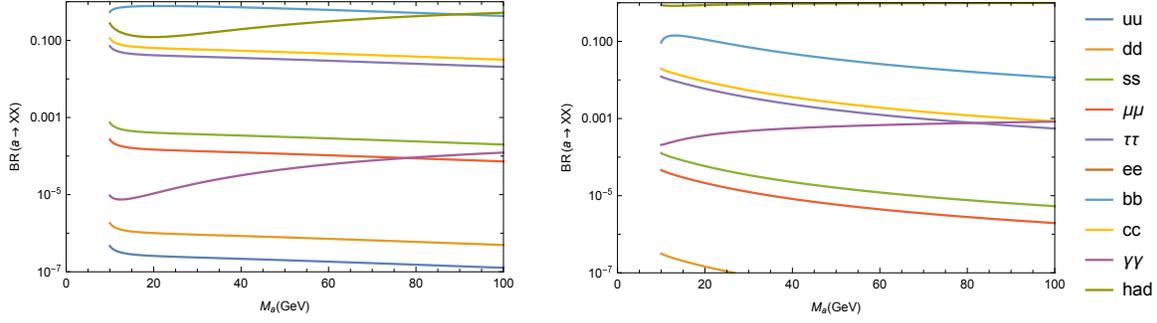
Figure 5: *Branching ratios of a for M8 (left) and M9 (right), which both have the $SU(4)/Sp(4)$ coset.*

for the pseudo-scalar, showing copious production at the LHC for past and future runs, and a range of decay modes. We have shown that in order to properly model this light state, it is crucial that the bottom quark be included in the loop of SM quarks contributing to the aXX' interaction vertex, as this significantly modifies the associated phenomenology.

5   Acknowledgements

References

1. G. Cacciapaglia, G. Ferretti, T. Flacke, and H. Serôdio, "Light scalars in composite Higgs models," *Front.in Phys.*, vol. 7, p. 22, 2019.

2. A. Alloul, N. D. Christensen, C. Degrande, C. Duhr, and B. Fuks, "FeynRules 2.0 - A complete toolbox for tree-level phenomenology," *Comput. Phys. Commun.*, vol. 185, pp. 2250–2300, 2014.

3. J. Alwall, R. Frederix, S. Frixione, V. Hirschi, F. Maltoni, O. Mattelaer, H. S. Shao, T. Stelzer, P. Torrielli, and M. Zaro, "The automated computation of tree-level and next-to-leading order differential cross sections, and their matching to parton shower simulations," *JHEP*, vol. 07, p. 079, 2014.

4. A. Belyaev, G. Cacciapaglia, H. Cai, G. Ferretti, T. Flacke, A. Parolini, and H. Serôdio, "Di-boson signatures as Standard Candles for Partial Compositeness," *JHEP*, vol. 01, p. 094, 2017. [Erratum: JHEP12,088(2017)].

5. G. Cacciapaglia and F. Sannino, "Fundamental Composite (Goldstone) Higgs Dynamics," *JHEP*, vol. 04, p. 111, 2014. [Erratum: JHEP12,088(2017)].

6. G. Cacciapaglia, G. Ferretti, T. Flacke, and H. Serodio, "Revealing timid pseudo-scalars with taus at the LHC," *Eur. Phys. J.*, vol. C78, no. 9, p. 724, 2018.

FLAVOUR PHYSICS FROM PRESENT TO FUTURE COLLIDERS

Monika Blanke

*Institute for Nuclear Physics (IKP) and Institute for Theoretical Particle Physics (TTP),
Karlsruhe Institute of Technology (KIT), D-76128 Karlsruhe, Germany*

Abstract

In these proceedings we provide a brief overview of the status of flavour physics, with focus on opportunities to discover New Physics in flavour-violating decays at current and future colliders.

1 Introduction

At the end of run 2 of the Large Hadron Collider (LHC), still no evidence for the production of new particles has been found. The resulting limits on the mass scale of New Physics (NP) in many cases reach beyond 1 TeV, and we have to face the possibility that the energy reached at the LHC might not be sufficient for a direct NP discovery. Although it is certainly too early to draw such depressing conclusions, the alternative indirect probes of NP in low-energy precision observables become increasingly relevant. While the reach of precision tests of the electroweak sector is limited to about 10 TeV, flavour-changing neutral current (FCNC) processes are sensitive to much higher scales, 1000 TeV and beyond [1]. In these proceedings we recapitulate the opportunities to discover NP in flavour observables, paying particular attention to some tensions in the data that arose over the past years.

2 New Physics Opportunities with the Unitarity Triangle

Consistency checks of the CKM mechanism in terms of Unitarity Triangle (UT) fits have a long tradition [2] and tell a story of success of the Standard Model (SM). A drawback of these global analyses is, however, that emerging tensions in particular channels remain hidden due to the large number of observables entering the fit. A good alternative hence is to compare the data on a few specific FCNC observables with their predictions using the CKM matrix elements determined from tree-level charged-current decays.
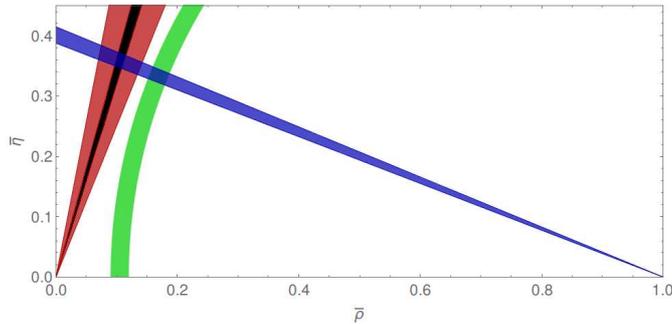
Figure 1: Constraints on the Unitarity Triangle from the measurement of $\sin 2\beta$ (blue), the ratio $\Delta M_d/\Delta M_s$ (green), and the tree-level determination of the angle γ (red). The future expected $1°$ sensitivity for γ by LHCb and Belle II is shown in black. Figure taken from Ref. [3].

Unfortunately a precise determination of the full reference unitarity triangle [4] is still impeded due to the persisting $|V_{ub}|$ problem [5]; yet an interesting tension arises already in the current data, shown in Figure 1. The red area displays the LHCb measurement [6] of the UT angle γ in tree-level $B \to DK$ decays, and the expected future $1°$ precision [7] by both LHCb and Belle II is indicated by the black line. One can see that such large values for $\gamma > 70°$ are inconsistent with its indirect determination through the ratio of mass differences $\Delta M_d/\Delta M_s$ in $B_{d,s} - \bar{B}_{d,s}$ mixings [3, 8], shown by the green band, irresepective of the size of $|V_{ub}|$. Such tension, if confirmed by future more accurate data would be an unambiguous sign of NP contributions to ΔM_d and/or ΔM_s.

In addition to the reduced uncertainty in the measurement of γ, a crucial ingredient to unravelling this potential anomaly is the impressive improvement made in the theoretical determination of the $SU(3)_F$-violating ratio ξ of the hadronic matrix elements entering $B_{d,s} - \bar{B}_{d,s}$ mixing both by lattice QCD [9] and QCD sum rule [10] calculations. The ball is now in the field of LHCb and Belle II to improve the tree-level determination of γ and thereby confirm whether indeed the ratio $\Delta M_d/\Delta M_s$ is affected by NP contributions.

3 Lepton Flavour Universality Violating Anomalies

Over the past years, several anomalies in both charged and neutral current semileptonic B meson decays emerged in the data. Interestingly, both of these sets of "B anomalies" are related to the violation of lepton flavour universality (LFU).

3.1 The Charged Current $b \to c\tau\nu$ Transitions

The ratios

$$R(D^{(*)}) = \frac{\text{BR}(B \to D^{(*)}\tau\nu)}{\text{BR}(B \to D^{(*)}\ell\nu)} \qquad (\ell = e, \mu) \tag{1}$$

provide a clean test of LFU in charged current $b \to c$ transitions, mediated in the SM by tree-level $W^{\pm}$ boson exchange. Various measurements by BaBar [11], Belle [12] and LHCb [13] indicate an enhancement with respect to the SM prediction, with the current HFLAV combination [14] finding a 3.1σ anomaly. An experimental consistency check of this result will be provided by a measurement of the corresponding baryonic ratio

$$R(\Lambda_c) = \frac{\text{BR}(\Lambda_b \to \Lambda_c\tau\nu)}{\text{BR}(\Lambda_b \to \Lambda_c\ell\nu)} \qquad (\ell = e, \mu) \tag{2}$$

which is predicted model-independently to be [15]

$$R(\Lambda_c) \simeq R(\Lambda_c)_{\text{SM}} \left(0.262 \frac{R(D)}{R_{\text{SM}}(D)} + 0.738 \frac{R(D^*)}{R_{\text{SM}}(D^*)}\right) = 0.38 \pm 0.01 \pm 0.01 \,. \tag{3}$$

Potential NP contributions at the origin of this anomaly can be systematically described by the effective Hamiltonian

$$\mathcal{H}_{\text{eff}}(b \to c\tau\nu) = 2\sqrt{2}G_F V_{cb} \left[(1 + C_V^L)O_V^L + C_S^R O_S^R + C_S^L O_S^L + C_T O_T\right]. \tag{4}$$

Several groups [15, 16, 17] have fitted the Wilson coefficients C_i to the available data.

Matching the effective Hamiltonian to simplified NP models in which the $b \to c\tau\nu$ transition arises from the tree-level exchange of a single mediator, a number of different scenarios emerges. Relevant contributions from a heavy charged W' gauge boson [18] are challenged both by electroweak precision constraints [19] and by high-p_T di-τ data at the LHC [20]. Charged Higgs contributions [21] generate a large branching ratio $\text{BR}(B_c \to \tau\nu) > 50\%$ and are put under pressure by mono-τ searches [22]. The best option for a NP explanation of the anomaly hence remains a scalar or vector leptoquark, see e.g. Refs. [23, 24, 25, 26].

Further insight on the underlying NP can be obtained by measuring differential and angular observables [15, 27] which can discriminate between the different scenarios. Additionally, decay modes related to $b \to c\tau\nu$ by $SU(2)_L$ symmetry, like $B \to K^{(*)}\nu\bar{\nu}$, $B_s \to \tau^+\tau^-$, $B \to K^{(*)}\tau^+\tau^-$, $\Upsilon \to \tau^+\tau^-$ and $\psi \to \tau^+\tau^-$ can receive significant NP contributions [26, 28, 29], depending on the NP model at work, and already now challenge some of the existing models. Overall, due to the large number of complementary observables, a NP origin of the anomaly can unambiguously be tested in both high-p_T and low-energy flavour data.

3.2 The Neutral Current $b \to s\ell\ell$ Modes

An equally interesting set of anomalies has appeared in measurements of B decays mediated by $b \to s\ell\ell$. The most relevant deviations from the SM are seen in the angular distribution of $B \to K^*\mu^+\mu^-$ [30], as well as in the LFU ratios [31]

$$R_{K^{(*)}} = \frac{\text{BR}(B \to K^{(*)}\mu^+\mu^-)}{\text{BR}(B \to K^{(*)}e^+e^-)} \,. \tag{5}$$

Again, potential NP effects can conveniently be described as contributions to the Wilson coefficients in

$$\mathcal{H}_{\text{eff}}(b \to s\ell\ell) = -\frac{4G_F}{\sqrt{2}} V_{tb}^* V_{ts} \frac{e^2}{16\pi^2} \sum_i (C_i \mathcal{O}_i + C_i' \mathcal{O}_i') + h.c. \,. \tag{6}$$

Here, the terms most sensitive to NP are the magnetic dipole operators $\mathcal{O}_7^{(\prime)}$ and the four-fermion operators $\mathcal{O}_{9,10}^{(\prime)}$. Note that the latter can be generated at tree level by Z' [32] or leptoquark [24, 26, 33] exchanges but are loop-suppressed in the SM, turning them into sensitive probes of NP.

Currently, one of the most promising solutions to the anomaly is a NP scenario with purely left-handed couplings, generating [17] (see also Ref. [34] for recent global fits)

$$\delta C_9^{bs\mu\mu} = -\delta C_{10}^{bs\mu\mu} \simeq -0.53 \,. \tag{7}$$

This scenario can accomodate a suppression of $\text{BR}(B_s \to \mu^+\mu^-)$ with respect to its SM value, and is easy to realise in concrete NP scenarios.

Among the most popular NP models for this anomaly is a TeV-scale $SU(2)_L$ singlet vector leptoquark coupling dominantly to left-handed quarks and leptons. Not only can it generate the required NP contribution in (7) without generating unwelcome effects in $B_s - \bar{B}_s$ mixing, but it can simultaneously also accomodate the required NP effect in the charged current transition $b \to c\tau\nu$. Interestingly such a particle arises from the Pati-Salam gauge symmetry unifying quarks and leptons [35]. Following this observation various model-building attempts [36, 37] have been undertaken to construct a viable UV-complete model for the B decay anomalies.

Instead of dwelling further on the model-building challenges, we turn our attention to complementary probes of such a NP explanation of the anomalies. In B physics, important tests are given by LFU violating angular observables in $B \to K^*\ell^+\ell^-$ [38], the $SU(2)_L$-related modes $B \to K^{(*)}\nu\bar{\nu}$, $B_s \to \tau^+\tau^-$, $B \to K^{(*)}\tau^+\tau^-$ [26, 28], and the lepton flavour violating meson decays $B \to K^{(*)}\tau^\pm\mu^\mp$ and $B_s \to \tau^\pm\mu^\mp$ [39]. In the lepton sector, these NP scenarios and their flavour structure are probed by lepton flavour violating μ and τ decays [28, 37, 39, 40]. Last but not least, also the high-energy frontier places important constraints on these scenarios, both in terms of the direct production of the vector leptoquark and its partner states [41] and in high-p_T di-lepton tails [42].

4 High-p_T Routes to Flavour

In addition to high-precision measurements of flavour-violating meson decays, the NP flavour structure can also be explored at the high-energy frontier, with ample opportunities at the High Luminosity phase of the LHC (HL-LHC) and future lepton or hadron colliders.

With the current hints for anomalies in flavour-violating B decays, it is conceivable that the underlying NP, coupling dominantly to the third generation, also leaves an observable imprint on flavour-violating top quark couplings. While the current bounds on transitions like $t \to (c, u)h$, $t \to (c, u)\gamma$ and $t \to (c, u)Z$ are too weak to put relevant limits on concrete NP models, the situation will significantly improve at the HL-LHC and in particular at a future high-energy hadron collider, due to the large number of top quarks produced [43].

If the scale of NP is low enough that the new particles can directly be produced, then their flavour structure has an immediate impact on their decay products. For instance, in the case of supersymmetric (SUSY) models, the presence of flavour mixing affects the accessible final states for squark pair production and therefore alters the corresponding phenomenology: The presence of mixing between the top and the charm squark significantly weakens the constraints from squark searches assuming flavour conservation [44, 45]. At the same time, the flavour-violating final state $tc + \slashed{E}_T$ becomes relevant [44, 45, 46], for which a dedicated search would be a promising way to discover scenarios with a large stop-scharm mixing angle, see Figure 2. Note that the $tc + \slashed{E}_T$ signature can arise also in other NP scenarios, like top-flavoured dark matter with a non-minimal flavour structure [47]. Interestingly in the latter case the cross-section can be large even if the relevant flavour mixing angles are zero.

5 Summary and Outlook

In these proceedings we provided a brief overview of the opportunities to discover NP in flavour-violating observables at present and future collider experiments. We did not cover charm decays here which, while experimentally a very interesting and rich field, still constitute a major problem for precise theoretical predictions due to the dominance of long-distance effects. We did not discuss kaon decays either, despite their unique sensitivity to NP contributions from very high energy scales, as the exploration of this
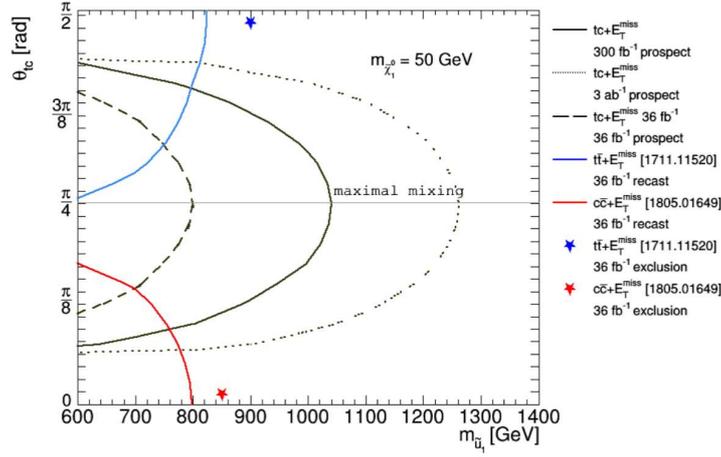
Figure 2: Bounds on the mass of the lightest squark, assuming it to be a mixture of stop and scharm flavour eigenstates. The blue and red curves display the constraints from $t\bar{t}+\not{E}_T$ and $c\bar{c}+\not{E}_T$, respectively, as a function of the mixing angle θ_{tc}. The black curves indicate the expected reach of a dedicated search for $tc+\not{E}_T$. Figure taken from Ref. [45].

exciting field does mostly not involve collider experiments. Recent reviews of the status of kaon physics, including the discussion of a potential anomaly in ϵ'/ϵ, can be found in Ref. [48].

6 Acknowledgements

References

1. A. J. Buras, D. Buttazzo, J. Girrbach-Noe and R. Knegjens, JHEP **1411** (2014) 121 [arXiv:1408.0728 [hep-ph]]. M. Bona [UTfit Collaboration], PoS CKM **2016** (2017) 096.

2. J. Charles *et al.* [CKMfitter Group], Eur. Phys. J. C **41** (2005) no.1, 1 [hep-ph/0406184]; updated results and plots available at `http://ckmfitter.in2p3.fr`. M. Bona *et al.* [UTfit Collaboration], JHEP **0610** (2006) 081 [hep-ph/0606167]; updated results and plots available at `http://www.utfit.org/UTfit/`.

3. M. Blanke and A. J. Buras, Eur. Phys. J. C **79** (2019) no.2, 159 [arXiv:1812.06963 [hep-ph]].

4. Y. Grossman, Y. Nir and M. P. Worah, Phys. Lett. B **407** (1997) 307 [hep-ph/9704287].

5. C. Bouchard, L. Cao and P. Owen, arXiv:1902.09412 [hep-ex].

6. LHCb Collaboration, M. W. Kenzie and M. P. Whitehead, LHCb-CONF-2018-002.

7. A. Cerri *et al.*, arXiv:1812.07638 [hep-ph]. E. Kou *et al.* [Belle-II Collaboration], arXiv:1808.10567 [hep-ex].

8. M. Blanke and A. J. Buras, Eur. Phys. J. C **76** (2016) no.4, 197 [arXiv:1602.04020 [hep-ph]].

9. A. Bazavov *et al.* [Fermilab Lattice and MILC Collaborations], Phys. Rev. D **93** (2016) no.11, 113016 [arXiv:1602.03560 [hep-lat]]. P. A. Boyle *et al.* [RBC/UKQCD Collaboration], arXiv:1812.08791 [hep-lat]. R. J. Dowdall, C. T. H. Davies, R. R. Horgan, G. P. Lepage, C. J. Monahan, J. Shigemitsu and M. Wingate, arXiv:1907.01025 [hep-lat].

10. A. G. Grozin, R. Klein, T. Mannel and A. A. Pivovarov, Phys. Rev. D **94** (2016) no.3, 034024 [arXiv:1606.06054 [hep-ph]]. A. G. Grozin, T. Mannel and A. A. Pivovarov, Phys. Rev. D **96** (2017) no.7, 074032 [arXiv:1706.05910 [hep-ph]]. M. Kirk, A. Lenz and T. Rauh, JHEP **1712** (2017) 068 [arXiv:1711.02100 [hep-ph]]. A. G. Grozin, T. Mannel and A. A. Pivovarov, Phys. Rev. D **98** (2018) no.5, 054020 [arXiv:1806.00253 [hep-ph]]. D. King, A. Lenz and T. Rauh, JHEP **1905** (2019) 034 [arXiv:1904.00940 [hep-ph]].

11. J. P. Lees *et al.* [BaBar Collaboration], Phys. Rev. Lett. **109** (2012) 101802 [arXiv:1205.5442 [hep-ex]]. J. P. Lees *et al.* [BaBar Collaboration], Phys. Rev. D **88** (2013) no.7, 072012 [arXiv:1303.0571 [hep-ex]].

12. M. Huschle *et al.* [Belle Collaboration], Phys. Rev. D **92** (2015) no.7, 072014 [arXiv:1507.03233 [hep-ex]]. S. Hirose *et al.* [Belle Collaboration], Phys. Rev. Lett. **118** (2017) no.21, 211801 [arXiv:1612.00529 [hep-ex]]. S. Hirose *et al.* [Belle Collaboration], Phys. Rev. D **97** (2018) no.1, 012004 [arXiv:1709.00129 [hep-ex]]. A. Abdesselam *et al.* [Belle Collaboration], arXiv:1904.08794 [hep-ex].

13. R. Aaij *et al.* [LHCb Collaboration], Phys. Rev. Lett. **115** (2015) no.11, 111803 Erratum: [Phys. Rev. Lett. **115** (2015) no.15, 159901] [arXiv:1506.08614 [hep-ex]]. R. Aaij *et al.* [LHCb Collaboration], Phys. Rev. Lett. **120** (2018) no.17, 171802 [arXiv:1708.08856 [hep-ex]]. R. Aaij *et al.* [LHCb Collaboration], Phys. Rev. D **97** (2018) no.7, 072013 [arXiv:1711.02505 [hep-ex]].

14. Y. Amhis *et al.* [HFLAV Collaboration], Eur. Phys. J. C **77** (2017) no.12, 895 [arXiv:1612.07233 [hep-ex]]. Updates available at `https://hflav.web.cern.ch/`.

15. M. Blanke, A. Crivellin, S. de Boer, T. Kitahara, M. Moscati, U. Nierste and I. Niandi, Phys. Rev. D **99** (2019) no.7, 075006 [arXiv:1811.09603 [hep-ph]]. M. Blanke, A. Crivellin, T. Kitahara, M. Moscati, U. Nierste and I. Niandi, Phys. Rev. D **100** (2019) no.3, 035035 [arXiv:1905.08253 [hep-ph]].

16. C. Murgui, A. Peuelas, M. Jung and A. Pich, JHEP **1909** (2019) 103 [arXiv:1904.09311 [hep-ph]]. R. X. Shi, L. S. Geng, B. Grinstein, S. Jäger and J. Martin Camalich, arXiv:1905.08498 [hep-ph]. S. Sahoo and R. Mohanta, arXiv:1910.09269 [hep-ph].

17. J. Aebischer, W. Altmannshofer, D. Guadagnoli, M. Reboud, P. Stangl and D. M. Straub, arXiv:1903.10434 [hep-ph].

18. X. G. He and G. Valencia, Phys. Rev. D **87** (2013) no.1, 014014 [arXiv:1211.0348 [hep-ph]]. A. Greljo, G. Isidori and D. Marzocca, JHEP **1507** (2015) 142 [arXiv:1506.01705 [hep-ph]].

19. F. Feruglio, P. Paradisi and A. Pattori, JHEP **1709** (2017) 061 [arXiv:1705.00929 [hep-ph]].

20. D. A. Faroughy, A. Greljo and J. F. Kamenik, Phys. Lett. B **764** (2017) 126 [arXiv:1609.07138 [hep-ph]].

21. J. Kalinowski, Phys. Lett. B **245** (1990) 201. W. S. Hou, Phys. Rev. D **48** (1993) 2342. A. Crivellin, C. Greub and A. Kokulu, Phys. Rev. D **86** (2012) 054014 [arXiv:1206.2634 [hep-ph]].

22. A. Greljo, J. Martin Camalich and J. D. Ruiz-Alvarez, Phys. Rev. Lett. **122** (2019) no.13, 131803 [arXiv:1811.07920 [hep-ph]].

23. M. Freytsis, Z. Ligeti and J. T. Ruderman, Phys. Rev. D **92** (2015) no.5, 054018 [arXiv:1506.08896 [hep-ph]]. N. G. Deshpande and A. Menon, JHEP **1301** (2013) 025 [arXiv:1208.4134 [hep-ph]]. M. Tanaka and R. Watanabe, Phys. Rev. D **87** (2013) no.3, 034028 [arXiv:1212.1878 [hep-ph]]. Y. Sakaki, M. Tanaka, A. Tayduganov and R. Watanabe, Phys. Rev. D **88** (2013) no.9, 094012 [arXiv:1309.0301 [hep-ph]]. D. Becirevic, I. Dorsner, S. Fajfer, N. Kosnik, D. A. Faroughy and O. Sumensari, Phys. Rev. D **98** (2018) no.5, 055003 [arXiv:1806.05689 [hep-ph]].

24. R. Alonso, B. Grinstein and J. Martin Camalich, JHEP **1510** (2015) 184 [arXiv:1505.05164 [hep-ph]]. S. Fajfer and N. Kosnik, Phys. Lett. B **755** (2016) 270 [arXiv:1511.06024 [hep-ph]].

25. M. Bordone, C. Cornella, J. Fuentes-Martin and G. Isidori, Phys. Lett. B **779** (2018) 317 [arXiv:1712.01368 [hep-ph]].

26. L. Calibbi, A. Crivellin and T. Ota, Phys. Rev. Lett. **115** (2015) 181801 [arXiv:1506.02661 [hep-ph]].

27. U. Nierste, S. Trine and S. Westhoff, Phys. Rev. D **78** (2008) 015006 [arXiv:0801.4938 [hep-ph]]. D. Becirevic, S. Fajfer, I. Nisandzic and A. Tayduganov, arXiv:1602.03030 [hep-ph]. A. Celis, M. Jung, X. Q. Li and A. Pich, Phys. Lett. B **771** (2017) 168 [arXiv:1612.07757 [hep-ph]]. S. Iguro, T. Kitahara, Y. Omura, R. Watanabe and K. Yamamoto, JHEP **1902** (2019) 194 [arXiv:1811.08899 [hep-ph]]. D. Becirevic, M. Fedele, I. Nisandzic and A. Tayduganov, arXiv:1907.02257 [hep-ph].

28. A. Crivellin, D. Mueller and T. Ota, JHEP **1709** (2017) 040 [arXiv:1703.09226 [hep-ph]].

29. D. Aloni, A. Efrati, Y. Grossman and Y. Nir, JHEP **1706** (2017) 019 [arXiv:1702.07356 [hep-ph]].

30. R. Aaij *et al.* [LHCb Collaboration], JHEP **1602** (2016) 104 [arXiv:1512.04442 [hep-ex]].

31. R. Aaij *et al.* [LHCb Collaboration], JHEP **1708** (2017) 055 [arXiv:1705.05802 [hep-ex]]. R. Aaij *et al.* [LHCb Collaboration], Phys. Rev. Lett. **122** (2019) no.19, 191801 [arXiv:1903.09252 [hep-ex]].

32. W. Altmannshofer and D. M. Straub, Eur. Phys. J. C **73** (2013) 2646 [arXiv:1308.1501 [hep-ph]]. R. Gauld, F. Goertz and U. Haisch, JHEP **1401** (2014) 069 [arXiv:1310.1082 [hep-ph]]. W. Altmannshofer, S. Gori, M. Pospelov and I. Yavin, Phys. Rev. D **89** (2014) 095033 [arXiv:1403.1269 [hep-ph]]. A. Crivellin, G. D'Ambrosio and J. Heeck, Phys. Rev. D **91** (2015) no.7, 075006 [arXiv:1503.03477 [hep-ph]]. S. Descotes-Genon, M. Moscati and G. Ricciardi, Phys. Rev. D **98** (2018) no.11, 115030 [arXiv:1711.03101 [hep-ph]].

33. G. Hiller and M. Schmaltz, JHEP **1502** (2015) 055 [arXiv:1411.4773 [hep-ph]]. D. Becirevic, S. Fajfer, N. Kosnik and O. Sumensari, Phys. Rev. D **94** (2016) no.11, 115021 [arXiv:1608.08501 [hep-ph]].

34. M. Alguero, B. Capdevila, A. Crivellin, S. Descotes-Genon, P. Masjuan, J. Matias and J. Virto, arXiv:1903.09578 [hep-ph]. A. Arbey, T. Hurth, F. Mahmoudi, D. M. Santos and S. Neshatpour, Phys. Rev. D **100** (2019) no.1, 015045 [arXiv:1904.08399 [hep-ph]]. K. Kowalska, D. Kumar and E. M. Sessolo, arXiv:1903.10932 [hep-ph].

35. J. C. Pati and A. Salam, Phys. Rev. D **10** (1974) 275 Erratum: [Phys. Rev. D **11** (1975) 703].

36. L. Di Luzio, A. Greljo and M. Nardecchia, Phys. Rev. D **96** (2017) no.11, 115011 [arXiv:1708.08450 [hep-ph]]. L. Calibbi, A. Crivellin and T. Li, Phys. Rev. D **98** (2018) no.11, 115002 [arXiv:1709.00692 [hep-ph]]. A. Greljo and B. A. Stefanek, Phys. Lett. B **782** (2018) 131 [arXiv:1802.04274 [hep-ph]]. S. Balaji, R. Foot and M. A. Schmidt, Phys. Rev. D **99** (2019) no.1, 015029 [arXiv:1809.07562 [hep-ph]]. R. Barbieri, C. W. Murphy and F. Senia, Eur. Phys. J. C **77** (2017) no.1, 8 [arXiv:1611.04930 [hep-ph]].

37. M. Blanke and A. Crivellin, Phys. Rev. Lett. **121** (2018) no.1, 011801 [arXiv:1801.07256 [hep-ph]].

38. B. Capdevila, S. Descotes-Genon, J. Matias and J. Virto, JHEP **1610** (2016) 075 [arXiv:1605.03156 [hep-ph]].

39. M. Bordone, C. Cornella, J. Fuentes-Martn and G. Isidori, JHEP **1810** (2018) 148 [arXiv:1805.09328 [hep-ph]].

40. R. Barbieri and R. Ziegler, JHEP **1907** (2019) 023 [arXiv:1904.04121 [hep-ph]].

41. M. J. Baker, J. Fuentes-Martn, G. Isidori and M. Knig, Eur. Phys. J. C **79** (2019) no.4, 334 [arXiv:1901.10480 [hep-ph]].

42. A. Greljo and D. Marzocca, Eur. Phys. J. C **77** (2017) no.8, 548 [arXiv:1704.09015 [hep-ph]].

43. P. Mandrik [FCC study Group], arXiv:1812.00902 [hep-ex].

44. M. Blanke, G. F. Giudice, P. Paradisi, G. Perez and J. Zupan, JHEP **1306** (2013) 022 [arXiv:1302.7232 [hep-ph]]. M. Blanke, B. Fuks, I. Galon and G. Perez, JHEP **1604** (2016) 044 [arXiv:1512.03813 [hep-ph]].

45. A. Chakraborty, M. Endo, B. Fuks, B. Herrmann, M. M. Nojiri, P. Pani and G. Polesello, Eur. Phys. J. C **78** (2018) no.10, 844 [arXiv:1808.07488 [hep-ph]].

46. T. Han, K. i. Hikasa, J. M. Yang and X. m. Zhang, Phys. Rev. D **70** (2004) 055001 [hep-ph/0312129]. A. Bartl, H. Eberl, B. Herrmann, K. Hidaka, W. Majerotto and W. Porod, Phys. Lett. B **698** (2011) 380 Erratum: [Phys. Lett. B **700** (2011) 390] [arXiv:1007.5483 [hep-ph]]. T. Hurth and W. Porod, JHEP **0908** (2009) 087 [arXiv:0904.4574 [hep-ph]].

47. M. Blanke and S. Kast, JHEP **1705** (2017) 162 [arXiv:1702.08457 [hep-ph]]. M. Blanke, S. Das and S. Kast, JHEP **1802** (2018) 105 [arXiv:1711.10493 [hep-ph]].

48. A. J. Buras, Acta Phys. Polon. B **49** (2018) 1043 [arXiv:1805.11096 [hep-ph]]. M. Blanke, arXiv:1908.09713 [hep-ph].

HIGH-ENERGY LEPTON COLLIDERS:
HIGGS-BOSON, TOP-QUARK AND BSM PHYSICS

Roberto Franceschini
Universitá degli Studi and INFN Roma Tre, Via della Vasca Navale 84, I-00146, Rome

Abstract

We discuss the physics opportunities and challenges presented by high energy lepton collider in the range of center of mass energy between few and several tens of TeV. The focus is on the progress attainable on the study of weak and Higgs interactions in connection with new physics scenarios motivated by the shortcomings of the Standard Model.

1   Introduction

A large activity for the update of the European Strategy for Particle Physics is presently underway to aim community efforts towards making progress in the understanding of fundamental interactions at the micro-scale investigated by particle physics. In this talk we will present some thoughts on the medium and long term application of high energy leptonic colliders towards this ambitious goal.

Presently considered high energy leptonic colliders vary widely in achievable center of mass energy, degree of technical maturity, and many other practical aspects. However the high energy leptonic colliders considered here all share the capability to explore fundamental interactions in a deeply novel way compared to the previous generation "then high energy" colliders such as LEP and SLC, or the machines dedicated to high intensity studies such as the flavor factories. For this reason the discussion of this talk is centered around projects such as the International Linear Collider (ILC) [1], the Compact Linear Collider (CLIC) [2], and more futuristic machines based on muons beams [3] and high-gradient acceleration in plasmas [4, 5].

We will take the Compact Linear Collider (CLIC) and muon colliders as reference points for the more mature and more technically challenging options, respectively. The choice is motivated by the highest energies considered by these projects in their own category and by their consideration in the

Update of the European Strategy for Particle Physics. Still it is worth stressing that the development of novel acceleration techniques is uncertain in nature, hence we do not exclude progress that will make this choice obsolete. As a matter of fact, even relatively well established techniques such as those employed to make the accelerating structures of the ILC can be substantially improved [6]. Therefore, as often in research, *"time will tell"*.

High energy lepton collider projects emerge as unique proposals, as they promise to deliver collisions between beams of point-like particles at energies well above the TeV scale. However, each project has its own challenges and peculiarities, and they differ in quite a number of aspects. Even restricting the focus to CLIC and muon colliders, one is immediately struck by their diversity, first of all the fact that CLIC is a linear collider whereas muon colliders presently considered would be circular machines. Nevertheless, the capability to probe short-distance physics with clean probes as leptons (as opposed to "dirty" protons), is a very strong common point between all the proposals, and it is the key which helps us to put in perspective the role that lepton machines, if run at sufficiently large energies, may play in the future of high energy physics.

The impact of these machines on our understanding of fundamental interactions at the micro-scale can be gauged on the improvements that these machines will bring on our knowledge of the recently discovered Higgs boson, the top quark, and searches for various kinds of new physics. The Higgs boson is the cornerstone of the spontaneous breaking of the symmetry related to weak interactions, it originates the masses of the fundamental particles, of which the top quark is heaviest. Due to its large mass the top quark is also the Standard Model particle more strongly coupled to the Higgs boson. Both the top quark and the Higgs boson are presently studied in current experiments, but the measurements of their properties are not yet very precise. In general the precision of measurements of Standard Model quantities at the LHC (and the HL-LHC) ranges between few and tens of percent, rarely is possible to get reliable measurements below the percent level. These levels of precision are roughly comparable to the effects expected from phenomena beyond the Standard Model taking place at an energy scale no larger than roughly 1 TeV. Therefore the top quark and the Higgs boson are natural targets for an in-depth study at future colliders, especially if they can cleanly probe phenomena happening at distances well below TeV^{-1}, too short to be visible at the Large Hadron Collider.

High energy lepton colliders such as CLIC or a muon collider offer unique opportunities in this exploration, as they allow to copiously produce Higgs bosons and top quarks, as well as they have a sufficient kinematic reach to directly produce and discover the new physics states responsible for deviations from the SM prediction in the properties of SM particles. The possibility to probe new physics both directly, through the search for new particles, and indirectly, through high-precision measurements, is a key strong point among the physics capabilities of high energy lepton colliders. In the following we will discuss how these two strategies complement and support each other. We will also highlight how, thanks the increasing importance of underlying weak boson scattering processes in high-energy $\ell^+\ell^-$ collisions, the copious production of SM particles for "high intensity" studies is synergistic with the direct exploration of the highest energy scales.

The possibility to pursue simultaneously "high energy" and "high intensity" studies has the important practical consequence of allowing these projects to attain the desired results in relatively short periods of data taking. This should be contrasted with the approach pursued in more "specialized" projects in which "dedicated" runs each of several years are foreseen to study each specific target, e.g. a stage for the production of copious number of top quarks, another stage for the copious production of Higgs bosons, and so on. While in principle the two approaches can lead to equally good results,

we find more sustainable to pursue projects which are already now designed to deliver their full load of results in the time-frame of one human generation (or less), that is to say two or three decades at most. According to presented schedules [7] both the *full* program of CLIC and a, somewhat less established, physics program at a muon collider may be carried out within this time-frame[1]. This further adds to the motivation to consider very seriously these machines for a future large facility in which the high energy physics community can put resources and efforts and expect physics results of prime importance in a reasonable time.

We have already mentioned the possibility to directly search for new physics at high energy lepton colliders. It is worth giving more details on this aspect as to show how a lepton collider running at a fraction of the center of mass energy of an hadron collider can still be enormously useful to extend our reach in searches for motivated new physics. A key fact to be noted is the motivation why we search for new physics in the first place. This motivation lies in many observations of phenomena that do not find an explanation in the Standard Model, such as the nature of the Dark Matter of the Universe, or that seem to involve a very special arrangement of parameters of the Standard Model to produce the observed properties of SM particles, such as masses and mixing angles of quarks and leptons, or some even more peculiar choice of parameters of the, SM such as those behind the discrimination between matter and anti-matter in the SM dynamics and the effective absence of strong force gauge interactions that break the CP symmetry. A remarkable common aspect of all these issues, except maybe the CP symmetry breaking in strong gauge interactions, is that they all have to do with the electro-weak interactions. In fact these are the only interactions that Dark Matter particles can carry consistently with observations. The weak interactions are related to symmetries and upon their breaking the masses and mixing angles of quarks and leptons become non-vanishing physical observables, as well as a physical CP phase in the SM is generated[2].

These considerations clearly show that the most urgent exploration in the search for new physics is an exploration of the electro-weak interactions, hence a search for new electro-weak charged states beyond the known particles of the Standard Model, and of course a more thorough understanding of the Higgs boson and its interactions. We will discuss more in detail the prospects for exploration in these directions in later Sections 2, 3 and 4.

The above mentioned practical need to pursue searches for new physics in a reasonable time-frame and the motivation just reminded for a bigger emphasis on searches for departure from the SM in electro-weak interactions and Higgs boson interactions altogether provide a very strong case for pursuing high energy lepton colliders, offering, for the first time, a road to discovery alternative to the classic pattern in which hadron machines make discovery and leptonic ones make precision studies. In the following we will describe a few concrete studies in which the power of high energy lepton colliders has been studied in detail. We will find very promising results for a large class of BSM scenarios motivated by the shortcomings of the SM reminded above.

---

[1]Of course the actual length of data taking will depend crucially on meeting the expectations on design luminosity of each project. As a matter of fact, such "make it or break it" luminosity challenge is a common trait of all future collider projects, each with its own peculiarities, but all bound to yield results only as valuable as how much they pushed the luminosity bar further up .

[2]The CP breaking strong interactions terms are a non-redundant interaction in the action only after SM quarks acquire a mass upon electro-weak symmetry breaking, possibly relating this problem as well to weak interaction and the breaking of their related symmetries.

2 The size of the Higgs boson

The Higgs boson is a "first". In fact it is the first spinless fundamental particle ever observed and this implies that it may be the beginning of a new era in the exploration of fundamental interactions. The great phenomenological success of the Standard Model is deeply rooted in the stucture of quantum gauge field theories and the Higgs boson is a peculiar object in this theoretical context. In fact it can be embedded in the SM in a theoretically consistent way only if it is a point-like particle. This fact, coupled with its spinless nature, makes the Higgs boson in principle sensitive to very short-distance physics. Therefore testing the spin and size of the Higgs boson is a very deep test of the picture underlying the Standard Model.

The spin of the Higgs boson is already under the grasp of current LHC experiments and the spinless nature of the Higgs boson has been quite conclusively proven since the beginning of the study of Higgs boson properties [12]. The study of the size of the Higgs boson instead is only at the beginning, hence future experiments will play a major role in this investigation. The finite size of the Higgs boson can manifest in gauge and Yukawa interactions of the Higgs boson as well as in interactions of the longitudinal degrees of freedom contained in W and Z bosons. To capture these effects it is best to study SM extensions via a suitable effective field theory [13] in which the Higgs boson is thought as a composite state of size $\ell_H \equiv 1/m_\star$. The mass scale $m_\star$ can be thought as the physical scale at which new degrees of freedom emerge and the SM is superseded by a more fundamental theory. Thanks to the direct searches at LHC for new particles, we can be guaranteed that the scale $m_\star$ is not too close to the Higgs boson mass, hence we can safely consider the EFT as a perturbation around the SM and observables can be computed schematically as

$$O = O_{SM} + \delta O_{BSM}$$

where the BSM part provides a small correction to the SM prediction.

As the BSM part is generated by dimensionful couplings (dim $\leq$ -2) for the new contact interactions of the EFT, generically we expect

$$\delta O_{BSM} = \left(\frac{\mu}{\Lambda}\right)^2 C,$$

where μ is a characteristic mass scale probed in the measurement in question and Λ is the effective scale of the new contact interaction ($\Lambda = v$=246 GeV if this was the Fermi effective theory of weak interactions at low energy). Clearly the size of the correction induced by the new contact interactions is controlled by the scale μ, which represents the momentum exchanged in the process under measurement. In simple cases, such as the measurement of a property of an on-shell particle, this is readily identified with the mass of the particles studied. Thus if we study the partial decay widths or the branching fractions of the Higgs boson we can expect

$$\delta\Gamma_{BSM}^{(h \to XX)} = \left(\frac{m_h}{\Lambda}\right)^2 C, \tag{1}$$

for some numerical coefficient C suitable for the specific case. The relative size of the effect of the new physics compared to the prediction of the SM is therefore of order

$$\frac{\delta O}{O} \sim \frac{m_h^2}{\Lambda^2}. \tag{2}$$

In a useful experiment we must be able to carry out the measurement with both statistical and systematic uncertainties below this level. As we consider probing larger Λ values of course the effect will become eventually too small to be observable and the experiment will no longer be a useful probe of such large new physics scale.

In cases in which the measurement is sensitive to larger momentum transfer we may still recover sensitivity to these large new physics scale. For instance if we were to probe the rate and transverse momentum of the h produced in a $2 \to 2$ process such as $e^+e^- \to Zh$ we would expect a correction

$$\frac{\delta O}{O} \sim \frac{p_{T,h}^2}{\Lambda^2}. \tag{3}$$

This makes large momentum transfer processes an ideal probe of heavy new physics, hence a powerful tool to test the size of the Higgs boson at the shortest distances. It is important to stress that one must insist on measuring properties that are truly sensitive to the p_T of the Higgs. In fact, measurements of "pole properties" , e.g. branching ratios, would be screened from short-distance effects, as the relevant decay phenomena take a "long time", not shorter than order $1/m_h$ to happen, hence the short time scale effects of heavy new physics are drowned in a too large "sampling time window" and little visible.

For this reason we can distinguish probes of new contact interactions in two categories:

- "High energy" probes (HEP) in which large momentum transfer is probed, possibly with large statistics, but with no great emphasis on the collection of large amount of data

- "High intensity" probes (HIP) in which we try to leverage the availability of a large amount of particles with no emphasis on the momentum transfer involved

By their very nature the HIP observables become more sensitive to heavy new physics when the statistical uncertainties can be reduced. The challenge in HIP observables is the control of the systematic effects to the same level of precision. In contrast HEP observables become more sensitive to heavier new physics when larger momentum transfer is attained, even keeping fixed the statistical error of the measurement in question. That is to say that 100 events of Zh production at $p_{T,h} \sim 100$ GeV are far less a powerful probe of heavy new physics than 100 events of Zh at $p_{T,h} \sim 1$ TeV. Of course energy limits the momentum transfer at which a measurement can be sensitive and HEP observables are inevitably limited by attainable beam energy. This makes a great case for pursuing the highest possible energies at lepton colliders.

Studying reactions such as

$$e^+e^- \to f\bar{f} \quad \text{and} \quad e^+e^- \to Zh, WW, hh$$

at 3 TeV CLIC it is possible to constrain the size of the Higgs boson ℓ_H at a level around

$$\ell_H < (20 \text{ TeV})^{-1}.$$

Remarkably this reach is comparable with the excellent results attainable with a 100 TeV pp collider [7]. Going to higher center of mass energies a "very" high energy collider at 14 or 30 TeV realized with plasma acceleration or muon beams can probe even smaller size of the Higgs boson. If one keeps the statistical uncertainty fixed, the reach on ℓ_H grows linearly with the center of mass of the collider, therefore easily going in the hundreds of TeV [16] for $m_\star \sim 1/\ell_H$ for futuristic plasma and muon colliders[3].

---

[3]It should be stressed that it is not trivial to collect a sample of $2 \to 2$ scattering events at ever higher energies. In fact the short-distance cross-section for events at high-momentum transfer decreases for geometrical reasons $\sigma \sim 1/p_{T,h}^2$. For this reason it is mandatory to develop muon beams and plasma acceleration with a guaranteed growth in the instantaneous luminosity of the machine as the beam energies become larger. The MAP program for the study of muon beams has already found results that confirm the $\mathcal{L} \sim E^2$ growth necessary to counterbalance the shrinking of the short-distance cross-section may be attainable [14].

3 SM Higgs boson and Top quark production

The exploration of physics beyond the Standard Model through measurements of Higgs boson and top quark properties at high energy lepton colliders can be carried out thanks to the large number of Higgs bosons and top quarks that these machines are able to produce. The major element of novelty here is the dominance of electro-weak boson fusion dominance in the production of both top quarks and Higgs bosons

$$WW \to h \quad \text{and} \quad WW \to t\bar{t}$$

among the several possible production mechanisms available. As these processes are essentially dominated by collisions of W bosons collinear with the beam forming a center of mass at the threshold of the reaction, their cross-sections are slowly growing with energy (due to the logarithmic growth of the flux of W bosons, and of size around 1 pb for $WW \to h$ and 10 fb for $WW \to t\bar{t}$. As such it is foreseen that CLIC 3 TeV will produce more than 1 million Higgs boson and tens of thousand top quark pairs, enabling precision studies for the Higgs boson pole properties with reach comparable to that of dedicated Higgs factories. For top quarks the energy is still not large enough to compete with $e^+e^- \to t\bar{t}$ production and the lower energies stages of CLIC at 1.5 TeV and 350-380 GeV are going to be in general better probes of top quark pole properties [15].

As the energy is increased to tens of TeV, as imaginable with plasma-based acceleration and muon beams, the top quark production is dominated by $WW \to t\bar{t}$ and alike subprocesses as the $\ell^+\ell^-$ center of mass energy is greater than about 20 TeV. In this scenario it is possible to imagine carrying out a top quark physics program exploiting top quarks pairs produced at largest momentum transfer via $\ell^+\ell^- \to t\bar{t}$ as well as the very copious low-momentum transfer production of $WW \to t\bar{t}$, thus allowing excellent and complementary results for both HIP and HEP observables. Very remarkably all these processes involve top quark production via electro-weak interactions, hence allowing to progress the knowledge of electro-weak interactions in a domain so far very little constrained (e.g. the measurement of SM quantities such as V_{tb} could be improved by orders of magnitude) [16]. The production of Higgs bosons will also be greatly enhanced and it would reach a fraction of a billion Higgs boson produced in $WW \to h$ sub-processes at a 30 TeV $\ell^+\ell^-$ collider with 100/ab integrated luminosity. Such a large sample of Higgs bosons would enable the precision study of rare Higgs boson decay modes, e.g. the one into leptons, and the loop-level decays in gauge bosons [16] as well as improve measurements of the most abundant decay modes [19].

4 Direct reach

The great mysteries around the origin of the scale of weak interactions, and the key role played by these interactions in the formulation of a number of theoretical and experimental puzzles that lead us to conclude new physics beyond the Standard Model must exists are a tremendous motivation to search for new particles carrying weak charge or new force carriers that may be related to those of the weak interactions in a bigger picture of fundamental interactions. Searches for these states at the LHC suffer from the large amount of background rate they receive from look-alike SM processes and the progress made in the search of new electro-weak particles at the LHC has so far been quite limited because of these difficulties. The search for new force carriers, when they are coupled to quarks, has improved significantly over the pre-LHC results. However, it remains difficult to probe force carriers that are not coupled to quarks, or are too light or too broad (or both) to distinguish them from ordinary SM events in the feature-less differential distributions they give rise to (e.g. see Ref [8]). Improvements will come as more data will be accumulated in the forthcoming Run3 and beyond, up to the HL-LHC epoch. However, the

search for new electro-weak particles and elusive force carriers remains a weak point in the new physics coverage at hadron colliders and even the final HL-LHC results will leave a lot of ground uncovered in this area. In concrete examples one can see that the mass reach for pair-produced new electro-weak charged scalars or boson is in the range of few hundreds GeV - very far from the desired sensitivity at TeV scale and possibly above. A striking instance of a search in which the LHC coverage is quite limited is the search for a new fermionic weak doublet. Such a new particle is a potential Dark Matter particle and can even be a WIMP thermal relic candidate if its mass is around 1000 GeV. Notably, this is a Dark Matter candidate with very elusive signatures in direct detection experiments [9, 10] and colliders are in principle a very promising way to discover this Dark Matter candidate. Unfortunately the LHC is not able to cover this scenario, and even the HL-LHC will not come close to cover it, with a mass reach only up to 400 GeV [7].

High energy lepton colliders will be extremely powerful probes for the search of new electro-weak particles and force carriers. As a matter of fact several complementary approaches can be pursued at high energy lepton collider to highlight the existence of these new physics states. A relatively large and comprehensive collection of studies of this sort is contained in a recent report [11] and we refer to reader to that reference for more details. The upshot of these studies is that running a high energy lepton collider at 3 TeV as foreseen in the CLIC project would enable us to probe, in some cases in a conclusive manner, several interesting scenarios of new physics. For instance it would be possible to rule out the existence of WIMP Dark Matter candidates such as a Higgsino-like fermionic weak doublet, probe conclusively the nature of the phase transition from the unbroken to broken phase of electro-weak interactions, rule out the presence of other Higgs bosons part of the electro-weak sector or other scalars related to the Higgs boson but not charged under electro-weak interactions. Furthermore a 3 TeV lepton collider as foreseen in the CLIC project would be able to probe other possible Dark Matter candidates, such as scalar weak triplets, and a number of "Dark Sector" scenarios in which new physics signatures emerge with a systematic displacement from the main interaction point. In addition, a high energy lepton collider has great potential to reveal the existence of new force carriers as they can be observed directly when light enough to be produced with the available center of mass energy, or through the precision measurement of differential rates of SM processes, where they show up as new contact interactions.

In general these results hold, in a even tighter form, at colliders with center of mass energy larger than 3 TeV as foreseen in projects with muon beams or plasma acceleration [16]. One obvious point of improvement is the kinematically accessible mass of new electroweak states. When we consider tens of TeV center of mass energy we go closer to the direct probe of perturbative unitarity for thermal dark matter [17] and already around 30 TeV center of mass energy we would be able to probe directly and conclusively a large class of WIMPs thermal Dark Matter candidates whose stability on cosmological time-scales follows "accidentally" from their electro-weak charges [18]. These DM candidates emerge as viable and elegant DM candidates when the WIMP paradigm is disentangled from supersymmetry. Therefore the conclusions of lower energies lepton colliders on "classic" WIMPs such as the Higgsino, can be further extended to a much broader class of WIMPs.

5 Conclusions

The technical developments of novel acceleration techniques enables us today to realistically imagine particle colliders capable of lepton-antilepton center of mass energies above the TeV. The CLIC project aims at colliding e^+e^- with 3 TeV center of mass energy and has come to maturity for a concrete implementation as soon as logistically and financially possible. For the first time it is thinkable to carry

out experiments at an e^+e^- collider and have reach for the most motivated models of new physics, both directly and indirectly, overall comparable to that of an equally challenging future hadron machine. This result motivates the investigation of the physics case of even higher energy leptonic machines, which may be realized exploiting muons beams or plasma acceleration. These machines are not yet technically feasible, but they look very promising. The machine requirements, especially on the instantaneous luminosity, appear tight, but attainable. The physics results that could be obtained fully justify the effort of a serious and well funded R&D program for these machines. The preliminary exploration of their physics potential show enormous possible progress in the understanding of fundamental interactions. High energy lepton colliders enable us to put SM particles under the microscope of permil high intensity studies and under the pressure of TeV momentum transfer high energy probes, obtaining extremely valuable information on the SM and its possible extensions.

The availability of such large center of mass energies makes these machines also capable of directly discovering new particles featured in the most motivated new physics scenarios. Therefore high energy lepton colliders emerge as fully capable to deliver both precision and mass reach necessary to get to a dramatic increase in our understanding of fundamental interactions at the micro-scale.

The necessity for novel challenging particle acceleration techniques to become a reality and the possible results to be reaped motivate to think big about the future of particle physics experiments. Large community efforts are necessary and must be put in place to pursue these ambitious goals in particle acceleration as to soon put them at work in physics studies about experiments to be built around these challenging machines.

6 Acknowledgements

References

1. **Linear Collider** Collaboration, Bambade et al., "The International Linear Collider: A Global Project," *arXiv e-prints* (Mar., 2019) , arXiv:1903.01629 [hep-ex].

2. P. Roloff, R. Franceschini, U. Schnoor, and A. Wulzer, "The Compact Linear e$^+$e$^-$ Collider (CLIC): Physics Potential," *Input to the European Particle Physics Strategy Update on behalf of the CLIC and CLICdp Collaborations - arXiv e-prints* (Dec., 2018) , arXiv:1812.07986 [hep-ex].

3. J. P. Delahaye, M. Diemoz, K. Long, B. Mansoulié, N. Pastrone, L. Rivkin, D. Schulte, A. Skrinsky, and A. Wulzer, "Muon Colliders," *arXiv e-prints* (Jan., 2019) , arXiv:1901.06150 [physics.acc-ph].

4. B. Cros and P. Muggli, "Alegro input for the 2020 update of the european strategy," arXiv:1901.08436v2 [physics.acc-ph].

5. J.-P. Delahaye, E. Adli, S. Gessner, M. Hogan, T. Raubenheimer, W. An, C. Joshi, and W. Mori, "A Beam Driven Plasma-wakefield Linear Collider from Higgs Factory to Multi-TeV," in *Proceedings, 5th International Particle Accelerator Conference (IPAC 2014)*, p. THPRI013. 2014. http://jacow.org/IPAC2014/papers/thpri013.pdf.

6. Grassellino et al., "Unprecedented quality factors at accelerating gradients up to 45 mv/m in niobium superconducting resonators via low temperature nitrogen infusion," `arXiv:1701.06077v1 [physics.acc-ph]`.

7. Richard Keith Ellis et al., "Physics Briefing Book,". `https://cds.cern.ch/record/2691414`. Physics Briefing Book - Input for the European Strategy for Particle Physics Update 2020.

8. A. Mariotti, D. Redigolo, F. Sala, and K. Tobioka, "New lhc bound on low-mass diphoton resonances," `arXiv:1710.01743v1 [hep-ph]`.

9. J. Hisano, K. Ishiwata, N. Nagata, and T. Takesako, "Direct detection of electroweak-interacting dark matter," *Journal of High Energy Physics* **7** (July, 2011) 5, `arXiv:1104.0228 [hep-ph]`.

10. R. J. Hill and M. P. Solon, "WIMP-nucleon scattering with heavy WIMP effective theory," *arXiv e-prints* (Sept., 2013) , `arXiv:1309.4092 [hep-ph]`.

11. J. de Blas et al. , "The CLIC Potential for New Physics," *CERN Yellow Rep. Monogr. Vol. 3 (2018)* (Dec., 2018) , `arXiv:1812.02093 [hep-ph]`.

12. ATLAS Collaboration, "Evidence for the spin-0 nature of the Higgs boson using ATLAS data," *ArXiv e-prints* (July, 2013) , `arXiv:1307.1432 [hep-ex]`.

13. G. F. Giudice, C. Grojean, A. Pomarol, and R. Rattazzi, "The strongly-interacting light Higgs," *Journal of High Energy Physics* **6** (June, 2007) 045, `hep-ph/0703164`.

14. J.-P. Delahaye, C. Ankenbrandt, S. Brice, A. D. Bross, D. Denisov, E. Eichten, S. Holmes, R. Lipton, D. Neuffer, M. A. Palmer, S. A. Bogacz, P. Huber, D. M. Kaplan, P. Snopok, H. G. Kirk, R. B. Palmer, and R. D. Ryne, "A Staged Muon Accelerator Facility For Neutrino and Collider Physics," *ArXiv e-prints* (Feb., 2015) , `arXiv:1502.01647 [physics.acc-ph]`.

15. Abramowicz et al., "Top-quark physics at the clic electron-positron linear collider," `arXiv:1807.02441v1 [hep-ex]`. `https://cds.cern.ch/record/2210491`.

16. D. Buttazzo, R. Franceschini, A. Wulzer, *in preparation*

17. K. Griest and M. Kamionkowski, "Unitarity Limits on the Mass and Radius of Dark Matter Particles," *Phys.Rev.Lett.* **64** (1990) 615.

18. L. Di Luzio, R. Gröber, and G. Panico, "Probing new electroweak states via precision measurements at the LHC and future colliders," *ArXiv e-prints* (Oct., 2018) , `arXiv:1810.10993 [hep-ph]`.

19. N. Bartosik, A. Bertolin, L. Buonincontri, M. Casarsa, F. Collamati, A. Ferrari, A. Ferrari, A. Gianelle, D. Lucchesi, N. Mokhov, M. Palmer, N. Pastrone, P. Sala, L. Sestini, and S. Striganov, "Detector and physics performance at a muon collider," `arXiv:2001.04431v1 [hep-ex]`.